Photothermal ionisation spectroscopy studies on shallow impurities in silicon

Griffin, Jennifer Anne

Award date:
1987

Awarding institution:
University of Bath

Photothermal Ionisation Spectroscopy studies on shallow impurities in silicon.

submitted by Jennifer Anne Griffin
for the degree of PhD
of the University of Bath
1987

ProQuest LLC
789 East Eisenhower Parkway
P.O. Box 1346
Ann Arbor, MI 48106-1346

Abstract

Photothermal ionisation spectroscopy is a highly sensitive technique for the study of shallow impurities in semiconductors and can detect individual concentrations of impurities as low as $10^7 cm^{-3}$. This technique is based on the two stage ionisation of a donor (acceptor). The absorption of a photon lifts the bound carrier into an excited state where by the absorption of a phonon it is lifted into the conduction (valence) band. Two photothermal ionisation spectroscopy systems have been developed based on a stepping and fast-scan Fourier Transform spectrometer. Experimental results on ultra-pure germanium demonstrate that both systems match the sensitivity achieved by other groups. Photothermal ionisation spectroscopy has been used to study the Thermal Donors in oxygen-rich Cz-silicon annealed at 450°. A new series of seven shallow donors called the Shallow Thermal Donors present at concentrations up to $\sim 10^{13} cm^{-3}$ are identified with ionisation energies 34.7-37.4meV. The spectra of oxygen-rich undoped and boron-doped samples are presented and discussed. The experimental results show that these donors are effective mass-like oxygen-related single donors. The dependence of the Shallow Thermal Donor growth and development on annealing temperature and annealing time is studied. Model calculations allow an estimate of the concentrations of the impurity species observed in the photothermal ionisation spectra. The dependence of the intensity of the Shallow Thermal Donor transitions on the temperature at which the photothermal ionisation spectroscopy measurement is made is studied. It is demonstrated that a simple Boltzmann factor is not sufficient to describe the thermal ionisation of a bound carrier from an excited state in photothermal ionisation spectroscopy, a more precise expression must be used.

Contents

List of Figures

List of Tables

Chapter 1

Introduction

1.1 Scope of the thesis

The work described in this thesis falls into two areas. Firstly two experimental systems have been established and developed which allow Photothermal Ionisation Spectroscopy (PTIS) to be carried out on a stepping-type Fourier Transform (FT) spectrometer and a commercial fast-scan FT spectrometer. PTIS is a highly sensitive spectroscopic method for the investigation of electrically active impurities and impurity complexes in semiconductors. The detection limit of this method lies below 10^7 impurities per cubic centimeter which is far superior to that offered by the conventional characterisation methods for semiconductors such as infrared FT spectroscopy, DLTS, EPR, or photoluminescence. This spectroscopic method can be combined to advantage with the techniques of FT spectroscopy. Test measurements have been carried out which show that these PTIS systems match the standard achieved by other groups.

Secondly, stimulated by the interest in the Thermal Donor (TD) problem in silicon, an investigation of Czochralski(Cz) -silicon containing these heat-treatment donors was carried out by PTIS on the fast-scan FT spectrometer.

A new species of donors, referred to as the Shallow Thermal Donors, was determined from this study. The Shallow Thermal Donors appear at very low concentrations ($\leq 10^{13}cm^{-3}$) making PTIS the ideal tool for their investigation. The Shallow Thermal Donors have been extensively studied using PTIS and the results of those studies are presented here.

In Chapter 1 the role of PTIS in the study of impurities and impurity complexes in semiconductors is discussed and the basic theory of this spectroscopic method is presented. The effective mass theory description of an impurity in a semiconductor is described as this is the basis for the analysis of the PTIS spectra. Finally a summary of the properties of the Thermal Donors in silicon, as understood at the present time, is given.

The experimental method is discussed in Chapter 2. This chapter includes a brief review of FT spectroscopy. A description of the Double Beam FT spectrometer (stepping-type) and the Bruker IFS 113v spectrometer (fast-scan) are given. The experimental arrangement necessary to achieve a highly sensitive PTIS system is given in detail in each case. The performance of these two systems is evaluated in comparison to that of E.E. Haller an established expert in the field of PTIS on ultra-pure germanium. The spectra of an ultra-pure p-type germanium sample with a net carrier concentration of $10^{10}cm^{-3}$ measured on all three systems are compared.

The establishment and development of the PTIS system for the Double Beam FT spectrometer and initial analysis of the Shallow Thermal Donor results was carried out in collaboration with Dr. H. Navarro at the Max-Planck Institute in Stuttgart. The adaptation of the software to incorporate a micro-processor stepper motor controller for the interferometer moveable mirror was the sole responsibility of the author. The development of the PTIS system on the

Bruker IFS 113v spectrometer and subsequent measurements made therewith were primarily the responsibility of the author.

Chapter 3 is a presentation of the experimental results obtained when heat-treated Cz-silicon containing the Thermal Donors is investigated by PTIS. These measurements serve to make the reader familiar with the features of the PTIS spectra of these samples. The results obtained for the Thermal Donors from infrared transmission measurements are compared to those obtained from PTIS and the reproducibility of the spectra is discussed. The existence of the Shallow Thermal Donors is established and their ionisation energies and central cell corrections are determined. Different origins for the hydrogenic series of transitions observed are critically evaluated and the single donor nature of the Shallow Thermal Donors is established.

In Chapter 4 the role of phosphorus, boron and oxygen in the growth and development of the Shallow Thermal Donors is considered. The interaction of the different donor species and the importance of such considerations in interpreting the PTIS spectra are discussed and the link to interstitial oxygen is established. It is shown that a model based on that of Bambakidis and Brown (1986) is extremely useful in understanding the PTIS spectra and may be used to obtain a good estimate of the concentration of the Shallow Thermal Donors.

In Chapter 5 the results of a controlled study of the dependence of the Shallow Thermal Donor concentration on annealing temperature and annealing duration are presented and discussed. Chapter 6 deals with a study of the temperature dependence of the PTIS spectra. The value of this study is two-fold. It provides an opportunity to study the PTIS process itself in more detail and allows an estimation of the thermal activation energies of the Shal-

low Thermal Donors. It is shown that the thermal activation energies are not given by the slope of an Arrhenius plot which assumes a Boltzmann probability for the thermal ionisation from an excited state. If a more detailed expression for the thermal ionisation probability from an excited state is used the observed temperature dependence may be interpreted using the thermal activation energies predicted by the effective mass theory.

A summary of the experimental results presented in this thesis is given in Chapter 7 and their significance as regards the Thermal Donor problem in silicon is discussed. An interpretation of the future role of PTIS completes the thesis.

With regard to the interpretation of the experimental results and the development of the ideas presented in this thesis the author benefited from many discussion with colleagues.

1.2 The role of Photothermal Ionisation Spectroscopy in the study of impurities in semiconductors

The growth of high-purity semiconductors has always been an area of paramount importance in both science and technology. The reduction of the residual impurity concentrations has been a major factor in achieving this goal. Ultra-pure germanium can now be grown with an impurity concentration as low as $10^{9}cm^{-3}$ and many other materials can be grown with impurity concentrations of the order of $10^{13}cm^{-3}$. The characterisation of ultra-pure semiconductors and the identification of the residual impurities is vital if materials are to be further improved. The most commonly used spectroscopic techniques for the identification and study of shallow impurities in semiconductors are

infrared transmission spectroscopy (Fan, 1967) and photoluminescence (Fan, 1967, Pankove, 1971, Smith, 1981). For both these techniques the absolute detection limit is reached at a net impurity concentration of approximately $10^{10}cm^{-3}$ under ideal conditions. However, the practical detection limit for routine samples and experimental methods may be said to lie in the region of $10^{13}cm^{-3}$. PTIS is a highly sensitive spectroscopic technique for the investigation of shallow impurities and can detect individual concentrations of impurities as low as $10^{7}cm^{-3}$ (Haller, 1975). The measurement of samples with a net impurity concentration $10^{10}cm^{-3}$ is routine.

PTIS was first developed at the Institute of Radio Engineering and Electronics of the USSR in 1964 (Lifshits and Nad, 1965). During experiments on photoconductivity in Ge it was observed that distinct structure, related to the residual impurities, appeared in the photoconductivity spectrum at photon energies well below the impurity ionisation energy. This technique is still referred to as photoelectric spectroscopy by some Soviet authors.

A comprehensive review of early PTIS is given by Kogan and Lifshits (1977). Much of the initial experimental work on PTIS was carried out at the Clarendon Laboratory, University of Oxford, G.B. by Kirkman and Stradling. They were concerned with the study of impurities in GaAs (Kirkman and Stradling, 1973; Cooke et al, 1978) and impurities in silicon and germanium (Skolnick et al, 1974). At the same time Stillman also began to look at impurities in epitaxial GaAs using PTIS (Stillman et al, 1972; Wolfe et al, 1974, 1977). Meanwhile Haller at the Lawrence Berkeley Laboratory , University of California, USA began to study ultra-pure germanium by PTIS (Haller and Hansen, 1974a, 1974b, Haller et al, 1975, 1977).

PTIS was first applied to the study of impurities in silicon by Skolnick et al

(1974). They studied high-purity n-type ($N_D - N_A \sim 5 \times 10^{13}\text{cm}^{-3}$) and p-type ($N_A - N_D \sim 10^{13}\text{cm}^{-3}$) silicon in order to determine the residual donors and residual acceptors in the material. Using the technique of band-gap illumination (see section 4.2.1) to reveal both the minority and majority carriers simultaneously, phosphorus was determined to be the main residual donor and boron the main residual acceptor in both cases.

Interest in the investigation of defects in silicon by PTIS grew in the early 1980's. Humphreys et al (1981) and Chandler et al (1982) used PTIS in the study of the S donor and the In acceptor respectively. PTIS has also been applied to the study of S, Se and Te and their pairs by Janzén et al (1984).

In GaAs epitaxial layers the presence of many impurities have been identified. Acceptors C, Zn, Si, Ge and Mg and donors Sn, S, Se, Te, Pb and Ge have been studied by several authors. Stillman and Low, now at the Materials Research Laboratory at the University of Illinois, USA are particularly active in the investigation of impurities in epitaxial GaAs (Low et al, 1982; Skromme et al, 1982, 1983; Stillman et al, 1985).

Germanium is still the main research topic of Haller's group. After the presence of elemental donors such as As, P and Sb and acceptors such as B, Al and Ga were established interest moved towards the study of hydrogen centre acceptors (Haller et al, 1980) and novel acceptors (Haller et al, 1983a, 1983b). Darken has also studied shallow impurities in Ge (Darken, 1982, 1983, Darken and Hyder, 1983).

Other semiconducting materials which have been studied using PTIS include InP and CdTe (Bajaj et al, 1975), InGaAsP and InGaAs (Cook et al, 1982), and semiconducting diamond (Collins and Lightowlers, 1968).

1.3 The principle of Photothermal Ionisation Spectroscopy

PTIS is based on the two stage ionisation of an impurity in a semiconductor. The bound carrier (electron or hole) is lifted into an excited state by the absorption of a photon, a phonon is then absorbed completing the ionisation and lifting the electron (hole) into the conduction (valence) band as shown in Fig 1.1. Before discussing PTIS in detail it is necessary to form a model for an impurity in a semiconductor.

1.3.1 The hydrogenic approximation for an impurity

Firstly, the case of a semiconductor containing a single residual donor species is considered. A donor may be considered analogous to a hydrogen atom, in that one electron can be ionised through a series of excited states to leave a ion of single positive charge. The hydrogen-like excited states of a donor may be described as an effective Rydberg equation which accounts for the host lattice through the use of the effective mass and the dielectric constant (effective mass theory) as

$$E_n = \frac{-m^* Z^2 e^4}{(4\pi\epsilon_0\epsilon_r)^2 2\hbar^2}\frac{1}{n^2} \qquad n = 1, 2, 3... \qquad (1.1)$$

where E_n is the energy of the nth level below the conduction band, and the conduction band minimum is taken as zero. The effective mass ground state is given by n=1. m^* is the electronic effective mass and Z and e are the hydrogenic nuclear charge and the elecronic charge respectively. $\epsilon_0\epsilon_r$ is the dielectric constant of the host material and $\hbar = h/2\pi$, where h is Planck's constant. The energy level scheme calculated for a donor in silicon from the effective Rydberg equation (1.1) is shown in Fig 1.2.

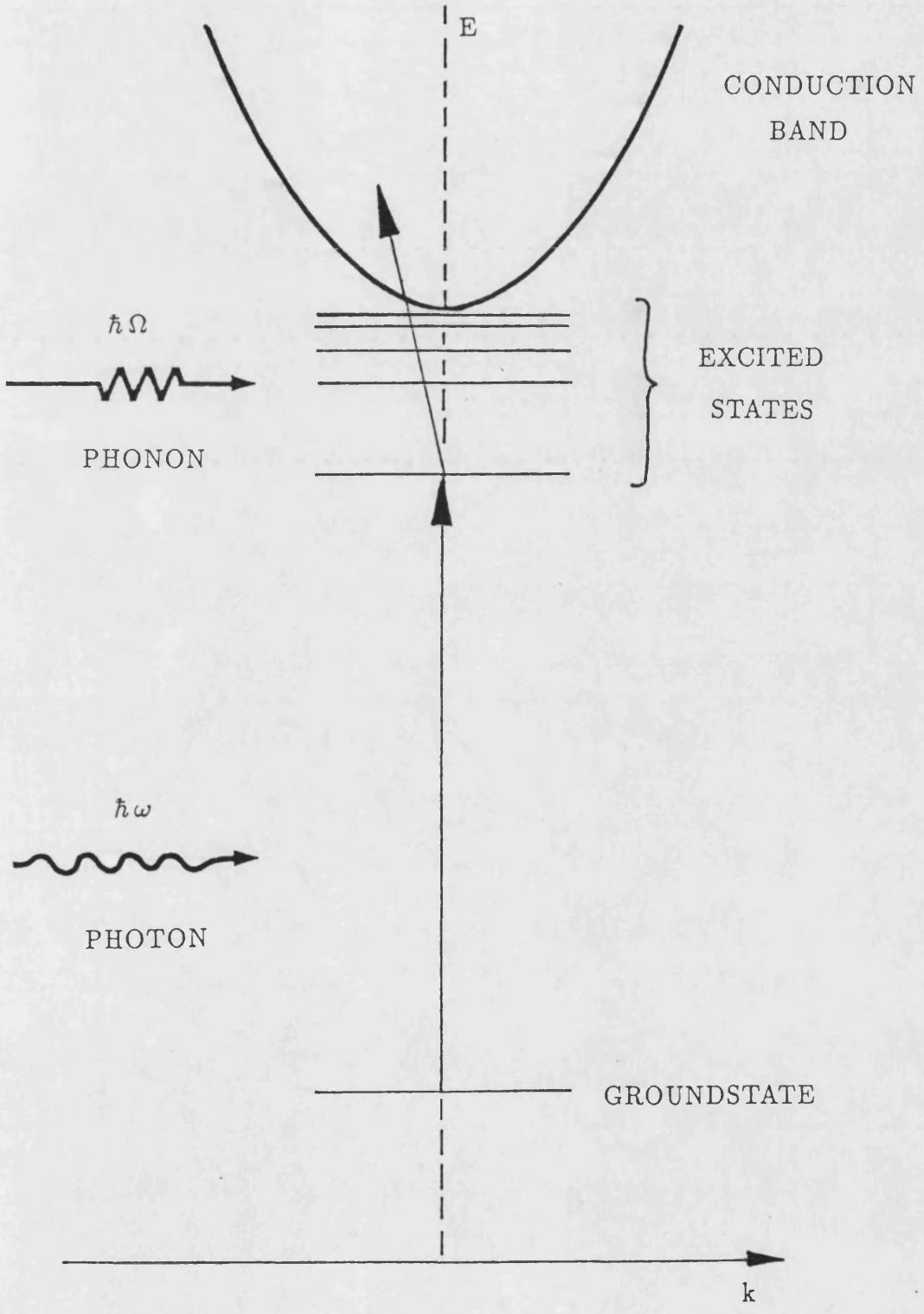

Fig 1.1: The photothermal ionisation of a donor impurity.

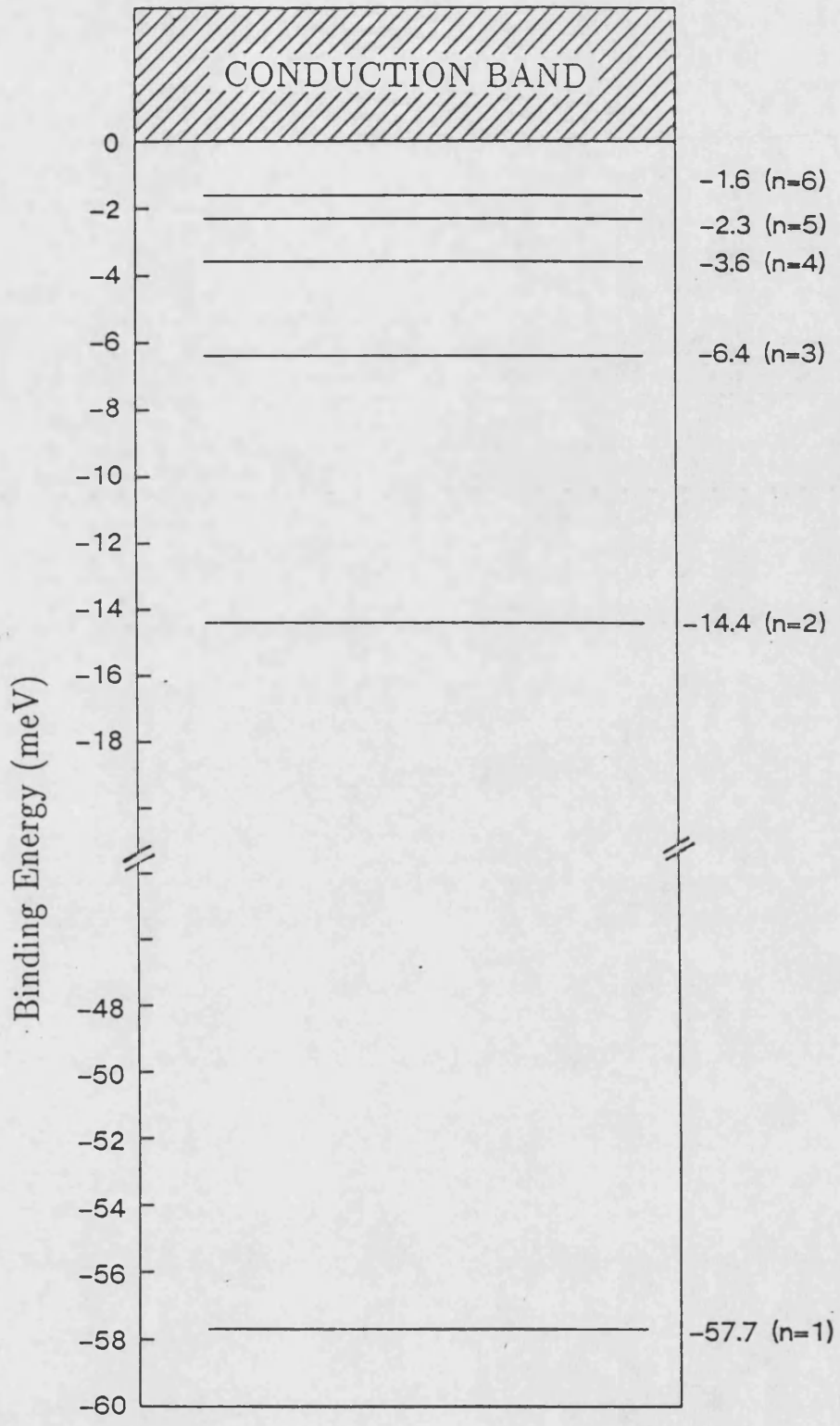

Fig 1.2: The energy level scheme for a donor in silicon according to the effective mass Rydberg equation.

A further refinement is required to the effective mass theory (EMT) however. The EMT assumes that the radius, r of the electron wavefunction is large and therefore does not interact with the impurity potential at the impurity site at r=0. However the probability density of the 1s hydrogenic groundstate wavefunction is non-zero at r=0. The interaction of the wavefunction with the potential due to the impurity itself has the effect of shifting the groundstate from its predicted EMT position. The magnitude of the shift depends on the chemical nature of the impurity and so is called the central cell correction or chemical shift. Each different donor type gives rise to a different central cell correction.

In PTIS the donor electron is lifted into an excited state by the absorption of a photon corresponding to the energy between the groundstate and the excited state. While in the excited state the electron absorbs a phonon and is lifted into the conduction band. Once in the conduction band the photothermally generated electrons can be detected by the application of an electric field across the semiconductor. The presence of these carriers proportionally changes the photoconductivity relative to the equilibrium state. This will clearly result in a peak in the photoconductivity at photon energies corresponding to the excitation of an electron into an excited state when the sample is illuminated by a broadband source. These sharp features in the photoconductivity spectrum always lie at energies below the onset of the ionisation continuum due to direct photo-ionisation from the impurity groundstate. Hence we see that a donor impurity in a semiconductor gives rise to a characteristic series of transitions in PTIS.

Referring to Fig 1.2, the transitions from the groundstate to the first excited state and from the groundstate to the second excited state occur at energies

$\hbar\omega = E_2 - E_1$ and $\hbar\omega = E_3 - E_1$ respectively. Their energy seperation is given by

$$(E_{n+1} - E_1) - (E_n - E_1) = E_{n+1} - E_n$$

which is independent of the groundstate energy and therefore the same for all donors. However the position of the series of transitions on the energy scale is dependent on E_1 and is therefore different for each donor species. These two facts have strong implications for the analysis of PTIS spectra. From PTIS it is possible to detect the presence of effective-mass like shallow donors and acceptors by their EMT "fingerprint" i.e. the characteristic spacing between transitions. The case for acceptors is exactly analogous to that of donors. Also the ionisation energy and central cell correction of each donor may be calculated from the absolute energies of the transitions. Thus the presence of a known impurity such as P or B can be determined or the impurity may be revealed as a previously unknown impurity centre.

1.4 The role of the sample temperature in Photothermal Ionisation Spectroscopy

The temperature of the semiconductor sample is extremely important in PTIS since it determines the probability of thermal ionisation from an excited state. If the temperature is too high depopulation of the groundstate by direct thermal ionisation occurs. If the temperature is too low the thermal ionisation of electrons from the excited states into the conduction band is inefficient. The optimum temperature range for PTIS lies between these two limits and depends on the depth of the groundstate and excited states below the conduciton band. The usual temperature range for PTIS is 4.2 - 10K in Ge and 14 - 28K in Si.

1.5 Generation of the PTIS signal

An analytical description of the generation of a PTIS signal is given by Kogan and Sedunov (1966), Van de Steeg (1982) and by Bambakidis and Brown (1986). Bambakidis and Brown developed a model for calculating the photoconductive response in a multiply doped semiconductor illuminated by the modulated far infrared light used in FT spectroscopy and were able to successfully simulate the PTIS spectra obtained for silicon doped with In and Al and with Ga and B acceptors.

PTIS is generally combined with the techniques of far infrared FT spectroscopy which will be discussed fully in the next chapter. For the following discussion of the generation of the PTIS spectrum certain equations will be stated without definition.

Bambakidis and Brown showed that for acceptors in silicon the magnitude of the generated excess photocurrent is modulated in the same way as the exciting modulated far infrared illumination and is in phase with it. They determined that the photoconductivity response, as represented by the cosine FT of the excess photocurrent, can be written in terms of the generated excess hole concentration. Finally the PTIS response function was defined. This analysis is also applicable to donor impurities as follows.

Firstly the rate equations for ionised donor and electron generation must be set up. Since a far infrared modulated source is being considered the PTIS response is a non-equilibrium situation. The excess photoconductivity $\Delta\xi(t)$ at a time t is given by

$$\Delta\xi(t) = \xi(t) - \xi(0) = e(\mu_n \Delta n(t) + \mu_h \Delta p(t)) \qquad (1.2)$$

where ξ is the photoconductivity, μ_n and μ_h are the electron and hole mobilities and $\Delta n(t)$ and $\Delta p(t)$ are the excess electron and hole concentrations at time t respectively. It is assumed that in the case of n-type silicon $\Delta p \ll \Delta n$.

The ionisation rate of the jth donor species is given by

$$\frac{dN_j^+(t)}{dt} = -\frac{dN_j^0(t)}{dt} \tag{1.3}$$

where N_j^+ is the ionised donor concentration and N_j^0 is the neutral donor concentration. The rate of loss of neutral donors can be written

$$-\frac{dN_j^0(t)}{dt} = N_j^0(t)\,P_j^0 + N_j^0(t)\int_0^\infty I(\omega,t)\,\sigma_{jm}(\omega)\,P_{jm}\,d\omega - C_j\,g_j\,n(t)\,N_j^+(t) \tag{1.4}$$

the first term of the equation gives the rate of direct thermal ionisation, where P_j^0 is the temperature dependent probability of thermal ionization per unit time of the jth donor.

The second term is the rate of photothermal ionisation where $\sigma_{jm}(\omega)$ is the frequency dependent photo-absorption cross-section for the mth excited state of the jth donor (in this sense complete ionisation is regarded as an excited state) and P_{jm} is the temperature dependent probability of thermal ionization from the mth excited state of the jth donor. $I(\omega,t)$ is the intensity spectrum of the modulated far infrared source, defined by

$$I(\omega,t) = I_0(\omega)\,(1+\cos\Omega t) \tag{1.5}$$

given

$$\Omega = \frac{2\nu\omega}{c} \quad ,$$

where ω is the angular frequency of the radiation, ν is the speed of the moveable mirror (see section 2.1) and c is the speed of light. Ωt is related to the interferometric path difference, δ through

$$\Omega t = \frac{2\pi\delta}{\lambda} \quad ,$$

where λ is the wavelength of the radiation.

The third term in equation (1.4) is the rate of neutralisation of ionised donors by electron capture. C_j is the capture coefficient for electrons, g_j is the state degeneracy and $n(t)$ is the free electron concentration at time t.

The net generation of electrons is limited by the number undergoing recombination. In silicon the time constant for electron capture is τ_C=10^{-11}s compared to a time constant of τ_R=10^{-5}s for surface recombination (Bambakidis and Brown, 1986). On this time scale, determined by τ_C, the recombination term only determines the long-term approach to equilibrium and may be omitted.

Then for excess electron generation

$$\frac{\Delta n(t)}{dt} \approx \sum_j \frac{dN_j^+(t)}{dt} = -\sum_j \frac{dN_j^0(t)}{dt} \quad . \tag{1.6}$$

It is now necessary to derive an expression for the excess electron concentration. It will be assumed that $N_j^0(t) = N_j^0(0)$ at all t. Just before the sample is illuminated the system is in equilibrium and from equation (1.4) at t=0

$$N_j^0(0)\, P_j^0(0) = C_j\, g_j\, n(0)\, (N_j - N_j^0(0)) \tag{1.7}$$

since $N_j^+(0) = N_j - N_j^0(0)$. Then for the jth donor at t>0 with the sample illuminated the rate of loss of neutral donors is

$$-\frac{dN_j^0}{dt} = N_j^0(0) \int_0^\infty I(\omega,t)\, \sigma_{jm}(\omega)\, P_{jm}\, d\omega + C_j\, g_j\, \Delta n(t)\, (N_j - N_j^0(0)) \tag{1.8}$$

where the first term in equation (1.4) has been replaced by the right-hand side of equation (1.7) and the second term in equation (1.8) represents the net excess electron production not due to photothermal ionisation. Equation (1.8) is also the rate of generation of electrons from the jth donor and summed over all donors can be written in the form

$$\frac{d\Delta n(t)}{dt} = \int_0^\infty G(\omega,t)\, d\omega - \frac{1}{\tau_{av}}\, \Delta n(t) \tag{1.9}$$

where $G(\omega,t)$ is the net generation rate of electrons by photothermal ionisation per unit ω

$$G(\omega,t) = I(\omega,t)\sum_{jm}\sigma_{jm}(\omega)\,P_{jm}\,N_j^0(0) \tag{1.10}$$

and τ_{av} is the average electron recombination time

$$\tau_{av}^{-1} = \sum_{j} C_j\,g_j\,\Delta n(t)\,(N_j - N_j^0(0)) \tag{1.11}$$

The FT spectrometer takes the cosine FT of the excess photocurrent, $\Delta i(t) - \Delta i(\infty)$ where $\Delta i(t)$ is the excess photocurrent at time t and $\Delta i(\infty)$ is the limit of the excess photocurrent at large interferometric path differences when the beams are no longer coherent. The photocurrent is proportional to the excess electron concentration so the cosine FT of $\Delta n(t) - \Delta n(\infty)$ is required. Considering the excess electron concentration generated at each frequency, ω then equation (1.9) can be written

$$\frac{d\Delta n(\omega,t)}{dt} = G(\omega,t) - \frac{1}{\tau_{av}}\Delta n(\omega,t) \tag{1.12}$$

In the limit

$$\Omega\,\tau_{av} \ll 1 \quad ,$$

such that one cycle of the far infrared modulated illumination (see equation (1.5)) is several times greater than the time constant for recombination, τ_{av} then equilibrium is established such that

$$\frac{d\Delta n(\omega,t)}{dt} = 0$$

so

$$G(\omega,t) = \frac{1}{\tau_{av}}\Delta n(\omega,t)$$

that is the excess electron concentration is given by

$$\Delta n(\omega,t) = G_0\,\tau_{av}\,(1+\cos\Omega t) \tag{1.13}$$

where

$$G_0(\omega)\,(1+\cos\Omega t) = G(\omega,t) \quad .$$

This tells us that the excess photocurrent is inphase with the modulated far infrared radiation.

The time origin is now moved to $-\infty$ with $\Delta n(-\infty) = 0$. The time regime is now $-\infty > t > \infty$. Then it follows that

$$\Delta n(t) = \int_0^\infty G_0(\omega)\,\tau_{av}\,(1+\cos\Omega t)\,d\omega \tag{1.14}$$

which in the limit $t \to \infty$ gives

$$\Delta n(\infty) = \int_0^\infty G_0(\omega)\,\tau_{av}\,d\omega$$

Thus we can write

$$\Delta n(t) - \Delta n(\infty) = \int_0^\infty G_0\,\tau_{av}\,\cos\Omega t\,d\omega \tag{1.15}$$

or, converting to the variable Ω

$$\Delta n(t) - \Delta n(\infty) = \frac{c}{2\nu}\,\tau_{av}\int_0^\infty G_0(\omega)\,\cos\Omega t\,d\Omega \tag{1.16}$$

The physical meaning of equation (1.16) is that the PTIS signal $\Delta n(t) - \Delta n(\infty)$ can be constructed from cosine profiles of frequency $\Omega = (2\nu\omega/c)$ that is

$$\Delta n(t) - \Delta n(\infty) = \frac{2}{\pi}\int_0^\infty \Delta n(\Omega)\,\cos\Omega t\,d\Omega \tag{1.17}$$

where $\Delta n(\Omega)$ is the amplitude of the waveform

$$\Delta n(\Omega) = \frac{\pi c}{4\nu}\,\tau_{av}\,G_0(\omega) \tag{1.18}$$

The spectrum of the excess photoconductivity, $\Delta i(\Omega)$ is proportional to the excess electron concentration $\Delta n(\Omega)$ and from equation (1.18)

$$\Delta n(\Omega) \propto G_0(\omega) \quad .$$

Considering $G_0(\omega)$ more closely

$$G_0(\omega) = I_0(\omega) \sum_{jm} \sigma_{jm}(\omega)\, P_{jm}\, N_j^0(0) \quad . \tag{1.19}$$

It is clear that it is not sufficient to represent the available photons through $I_0(\omega)$ in the form given in equation (1.5). The total sample response is given by the response in a layer dZ at a depth Z in the sample, summed over the whole sample thickness,d (Szmulowicz and Baron, 1980). Therefore, the total response of the system, including multiple reflections at the air to sample interfaces, is given by

$$\text{Total response}(\omega) = I_0(\omega) \frac{(1-R)(1-e^{-\alpha(\omega)d})}{\alpha(\omega)\,(1-Re^{-\alpha(\omega)d})} \sum_{jm} \sigma_{jm}(\omega)\, P_{jm}\, N_j^0(0) \tag{1.20}$$

where

$$\alpha(\omega) = \sum_{jm} \sigma_{jm}(\omega)\, N_j^0(0) + \alpha_0(\omega) \tag{1.21}$$

where the first term is the absorption due to direct photo-ionisation of impurities from the ground state and α_0 is absorption due to all other processes, for example Breit-Wigner-Fano resonances, localized vibrational excitations of electrically inactive impurities etc. R is the reflectivity (~ 0.3 for silicon) (Szmulowicz and Baron, 1980).

Hence the PTIS response function in the general case is given by

$$R.F. = \frac{G_0(\omega)}{\alpha(\omega)} \frac{(1-R)(1-e^{-\alpha(\omega)d})}{(1-Re^{-\alpha(\omega)d})}. \tag{1.22}$$

The proportional response of a semiconductor to illumination by modulated far infrared light under conditions optimum for photothermal ionization process is described by equation (1.22).

1.5.1 Model calculation

In a system containing a single donor species the PTIS response function always gives rise to a peak in the photoconductivity spectrum at the transition frequencies corresponding to the excitation of an electron into an excited state. However, when more than one donor species is present the resultant PTIS response at a given transition frequency depends on the concentrations of the donor species and the temperature. Also the direct photo-ionisation and photothermal ionisation processes compete for the available photons. The effect of such interaction on the PTIS spectrum is demonstrated by the following model calculation.

Consider a system containing one shallow donor A and phosphorus. Let the ionisation energy of A be 35meV. The ionisation energy of P is 45meV. The $1s \rightarrow 2p_{\pm}$ transition of P occurs at $1/\lambda$=316cm^{-1}. At this frequency a photon can

- be absorbed by donor A and cause a direct ionisation into the conduction band,
- be absorbed by phosphorus and lift an electron into the 2p± state, where by the subsequent absorption of a phonon ionisation may occur.

These two processes compete for the available photons.

The resultant PTIS response of this system may be calculated using equation (1.22). It is assumed that in the spectral region around 316cm^{-1} the only absorptions arise from the excitation or ionisation of the bound carriers of the impurities A and P. Values of d=0.2cm and R=0.3 are used in the calculation.

The PTIS response, R_p is given by

$$R_p(\omega) = I(\omega)\frac{(1-R)(1-e^{-\alpha(\omega)\,d})}{(1-Re^{-\alpha(\omega)\,d})}\left[\frac{N_A\,\sigma_A(\omega)+N_P\,\sigma_P(\omega)\,P_P}{N_A\,\sigma_A(\omega)+N_P\,\sigma_P(\omega)}\right] \tag{1.23}$$

and

$$\alpha(\omega) = \sigma_A(\omega)\,N_A + \sigma_P(\omega)\,N_P \tag{1.24}$$

where σ_A and σ_P are the optical absorption cross-sections, and N_A and N_P are the concentrations, of donors species A and P. P_P is the thermal ionisation probability from the 2p± excited state of donor P into the conduction band.

The dependence of the absorption cross-section on frequency for the excitation of an electron into an excited state from the ground state may be described by a simple Lorentzian lineshape

$$\sigma(\omega) = \frac{\sigma_0}{1+\left(\frac{\omega-\omega_0}{\Gamma}\right)^2} \tag{1.25}$$

where σ_0 is the photo-absorption cross-section at the centre frequency, ω_0 and 2Γ is the full linewidth at half-height. The optical absorption cross-section of P is represented by equation (1.25) with $\sigma_{P0} = 3\times10^{-14}\text{cm}^2$, $2\Gamma_P = 3\text{cm}^{-1}$ and $N_P = 5\times10^{13}\text{cm}^{-3}$. The absorption cross-section of donor A is assumed to be constant over the small spectral region under consideration. The value $\sigma_A = 3\times10^{-14}\text{cm}^2$ was used in this calculation. Both transitions are strong and therefore this assumption that $\sigma_A \approx \sigma_P$ is not unrealistic.

The thermal ionisation probability of an electron in the mth excited state of a donor is given by the general formula

$$P_{jm} = \left(1+\frac{\Delta E_m}{kT}\right)exp\left(\frac{\Delta E_m}{kT}\right) \tag{1.26}$$

after Abakumov and Yassievich (1976) where ΔE_m is the thermal activation energy of the mth excited state of the jth donor, k is the Boltzmann constant and T is the temperature. An alternative expression has been determined by

Janzén et al but the two approaches give very similar results in the temperature range of interest. For the $1s \rightarrow 2p_{\pm}$ transition of P ΔE=6.4meV holds.

Using this model with the given parameters the expected PTIS response for this system, containing two donor species with competing absorption processes, may be calculated. The joint effects of temperature and relative concentration may be observed by calculating the ratio of the PTIS response at the transition frequency, R_p against the background response, R_0 at a frequency slightly removed where

$$R_0(\omega) = I(\omega)\frac{(1-R)(1-e^{-\sigma_A(\omega)N_A d})}{(1-Re^{-\sigma_A(\omega)N_A d})} \tag{1.27}$$

In Fig 1.3 the predicted PTIS response at 316cm^{-1}, relative to the continuum, is shown at a constant temperature of 15K for different relative concentrations of the two donor species. The P concentration is kept constant at 5×10^{13}cm^{-3} and the concentration of donor A is varied between 2.5×10^{12}cm^{-3} and 5×10^{13}cm^{-3}. The temperature dependence of the PTIS response is shown in Fig 1.4 with constant donor concentrations of $N_p = 5 \times 10^{13}$cm^{-3} and $N_A = 1 \times 10^{13}$cm^{-3}.

It is clear that where more than one donor species is present either a peak, a minimum or no discernable feature may be observed in the photoconductivity spectrum at the transition frequency corresponding to the excitation of an electron from the groundstate of a donor into an excited state. The intensities of the transitions observed in PTIS result from a complex interplay of the efficiencies of the various ionization processes and the concentrations of the different donor species and great care must be taken in the interpretation of experimental spectra.

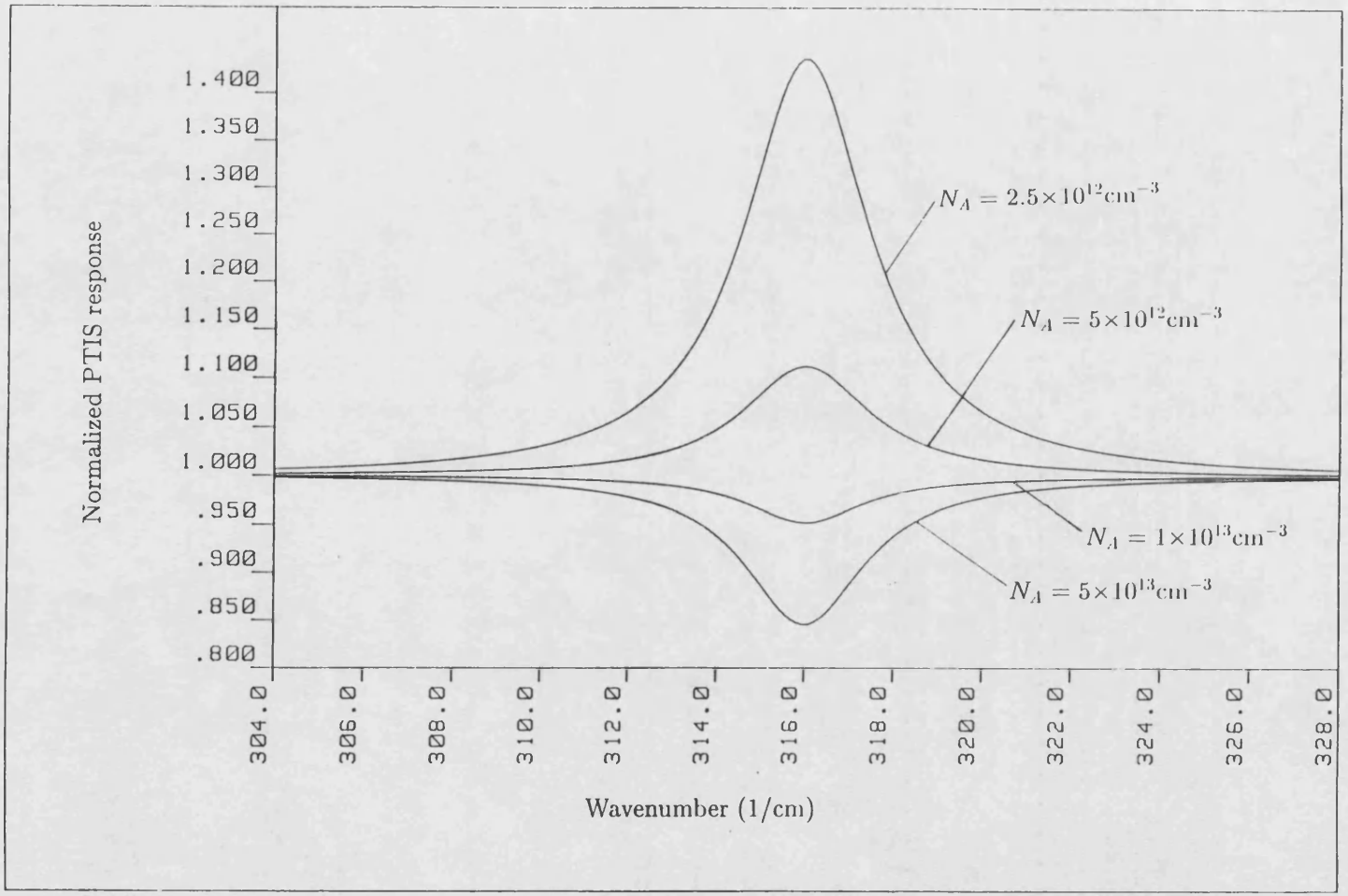

Fig 1.3: The calculated PTIS spectrum at the $1s \rightarrow 2p_{\pm}$ transition of P, normalized against the continuum, for different concentrations of the shallower donor A. $N_p = 5 \times 10^{13}\text{cm}^{-3}$, R=0.3, d=0.2cm and $\sigma_A = \sigma_{P0} = 3 \times 10^{-14}\text{cm}^2$. A temperature of 15K was used.

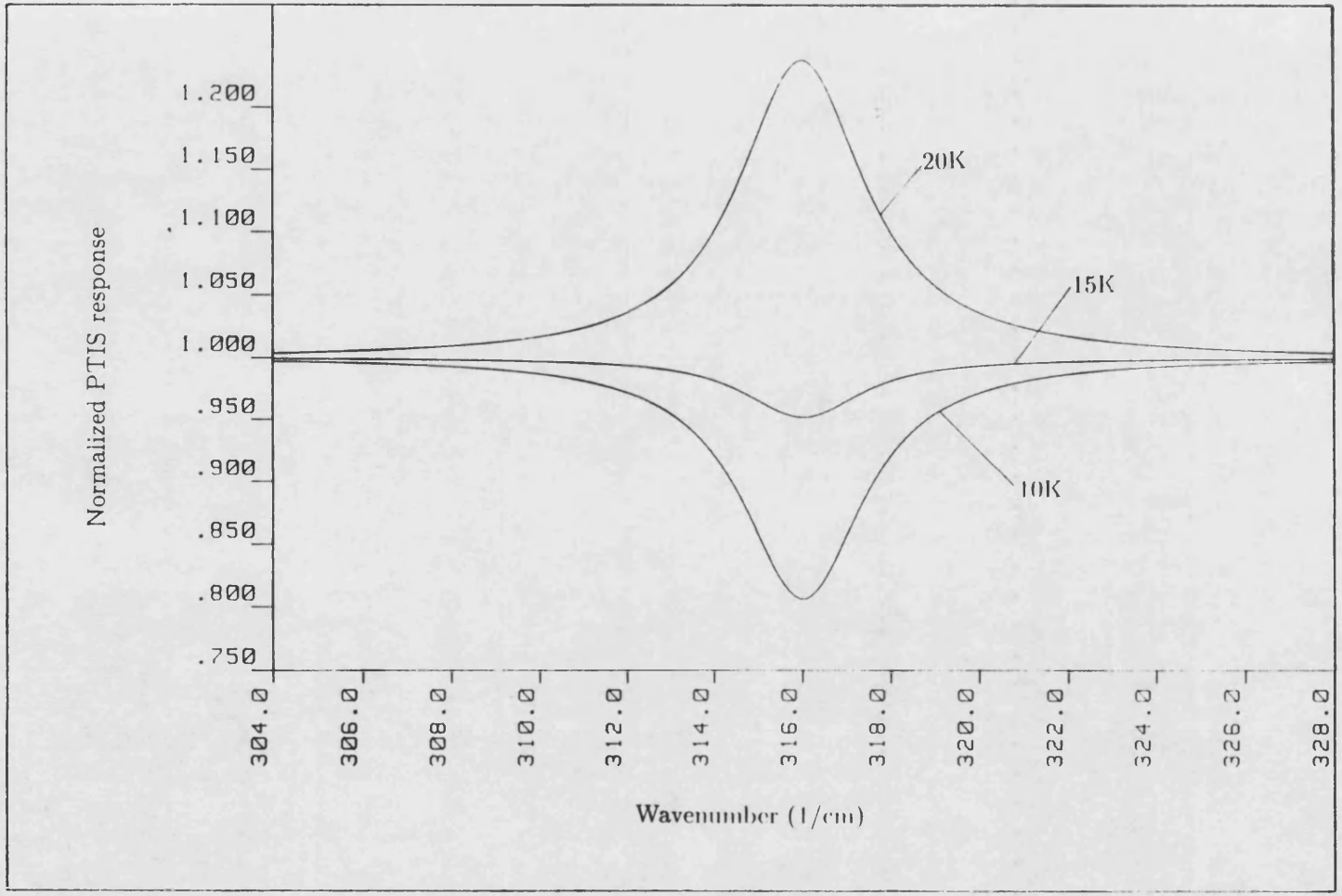

Fig 1.4: The calculated temperature dependence of the PTIS spectrum at the $1s \rightarrow 2p_{\pm}$ transition of P, normalized against the continuum. $N_A = 1 \times 10^{13}\text{cm}^{-3}$, $N_p = 5 \times 10^{13}\text{cm}^{-3}$, R=0.3, d=0.2cm and $\sigma_A = \sigma_{P0} = 3 \times 10^{-14}\text{cm}^2$.

1.6 Effective Mass Theory

The description of the energy levels of a donor in silicon given in section 1.3 is based on a very simple model. The problem of donor and acceptor impurities has been of great interest to many theoretical physicists. The energy level scheme of an effective-mass like impurity has been very accurately calculated from the effective-mass Hamiltonian. An accurate knowledge of the energy level scheme is necessary in order that the correct ionisation energy of the impurity may be calculated and the central cell correction accurately deduced.

1.6.1 Donors in silicon

Faulkner (1969) calculated the energy levels of the donor effective-mass Hamiltonian for a series of values of the effective mass ratio, $\gamma = m_t/m_l$. m_t is the transverse (short axis) effective mass and m_l the longitudinal effective mass (long axis) in a semiconductor with an ellipsoidal Fermi surface. For silicon $\gamma = 0.2079$, taking values of m_t and m_l from the cyclotron resonance measurements of Hensel et al (1965) as $m_t/m_0 = 0.1905$ and $m_l/m_0 = 0.9163$ where m_0 is the electron rest mass. The energy level scheme for donors in silicon was then interpolated from the theoretical data at $\gamma = 0.2079$ as shown in Fig 1.5. Comparing his predictions to the experimental data of P and Li impurities in silicon Faulkner calculated the ratio $E(2p_\pm) - E(2p_0)/E(3p_\pm) - E(2p_\pm)$, where $E(2p_\pm)$ is the energy required for a transition into the $2p_\pm$ excited state from the groundstate for example. This value, which is independent of the dielectric constant ε, was in excellent agreement with the theoretically predicted value, while the separation $E(3p_\pm) - E(2p_\pm)$ differed considerably from the experimental value. Therefore Faulkner used the theory to exactly determine the dielectric constant obtaining a value of $\varepsilon_r = 11.40 \pm 0.05$.

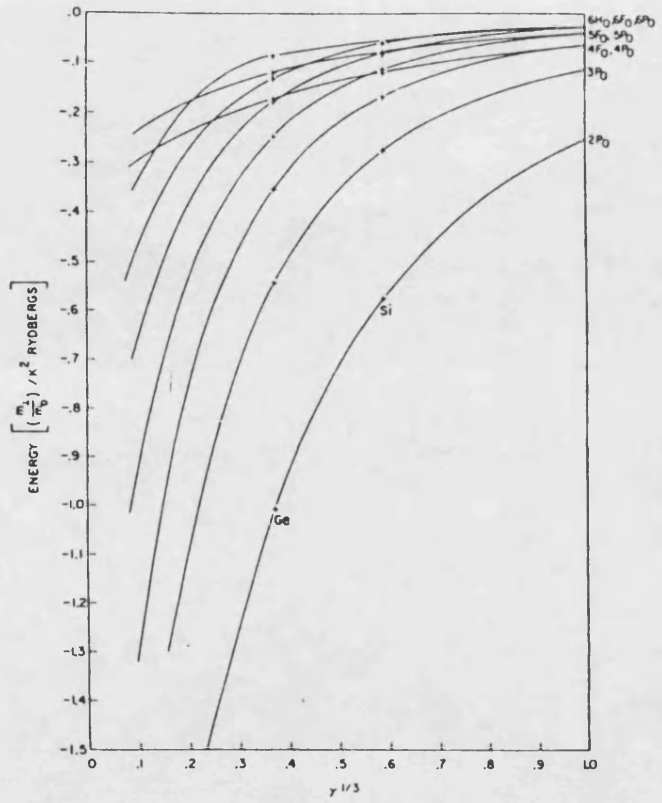

Fig 1.5(a): P_0-like donor energy levels calculated in the effective mass approximation as a function of the mass ratio $\gamma = m_t/m_l$. The energy unit is $m_t\, e^4/2\,\hbar\, K^2$. (Faulkner, 1969)

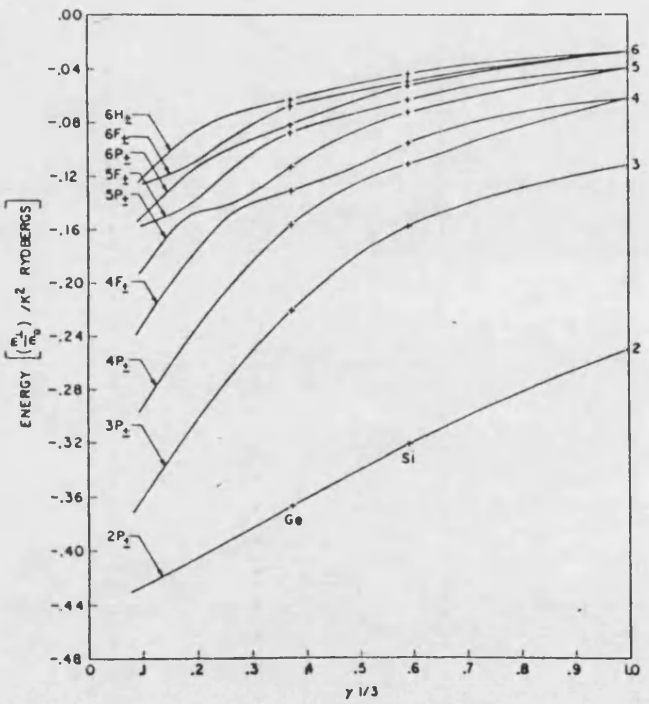

Fig 1.5(b): $P_\pm$-like donor energy levels calculated in the effective mass approximation as a function of the mass ratio $\gamma = m_t/m_l$. The energy unit is $m_t\, e^4/2\,\hbar\, K^2$. (Faulkner, 1969)

Recently Janzén et al (1984) recalculated the energy levels using the same variational method as Faulkner but using a far larger set of basis functions in order to bring the accuracy of the theory above the accuracy at present experimentally achievable. Also Janzén et al performed the calculation at $\gamma = 0.2079$ of silicon exactly, taking the dielectric constant as determined by Faulkner. An improvement of less than 0.1meV was achieved but was found to be in significantly better agreement with experiment where EMT could be expected to be valid. The calculated energy levels for a donor impurity after Janzén are shown in Fig 1.6.

Now the ground state of a donor in silicon will be considered. An impurity on a substitutional site in a silicon lattice belongs to the T_d symmetry group. From point group considerations Kohn and Luttinger (1955) showed that the irreducible representation of the 1s ground state consists of

$$1s = A_1 + E + T_2$$

which are one, two and three dimensional functions respectively. The six functions arise from the six equivalent valleys of silicon and are degenerate in EMT theory. However intervalley coupling, which depends on the amplitude of the EMT wavefunction close to the cell centre, is strong for s-states. The EMT is not valid for the 1s groundstate and due to coupling via the impurity potential it splits into three levels, the A_1, E and T_2 with degeneracy 1, 2 and 3 respectively.

The A_1 state is the only component which has amplitude at the centre of the cell and is therefore strongly affected by the local impurity potential in comparison to the other two states. Hence in the case of a substitutional donor in silicon the A_1 state is the deepest ground state. The other two groundstates are less affected and their energy may be calculated once the $1_s(A_1)$ has been

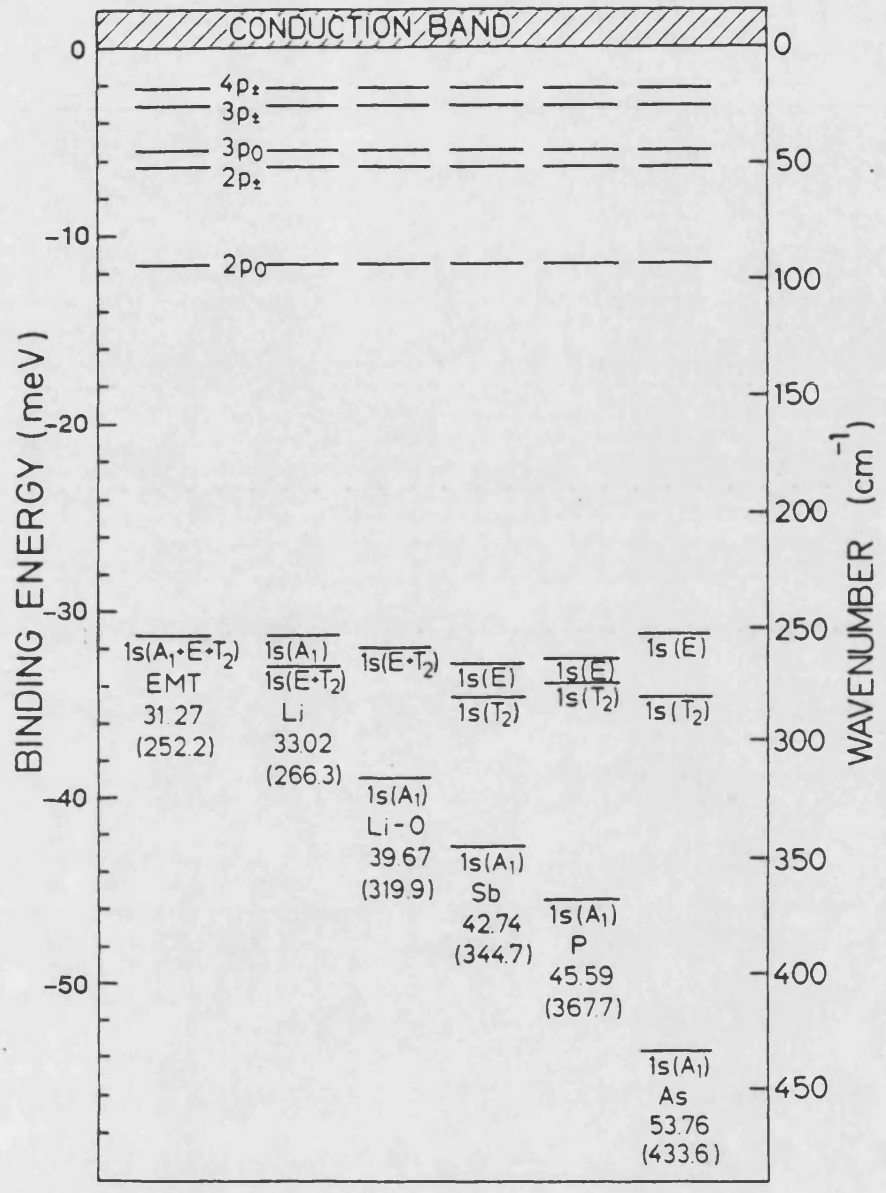

Fig 1.6: The donor energy levels in silicon calculated in the effective mass approximation (EMT) after Janzén et al (1984) and the experimentally observed energy levels for the most common shallow donor impurities in silicon. The ionisation energy of each donor is given in meV and wavenumber, 1/cm (in brackets).

experimentally determined. The splitting between the E and T_2 states was measured by Aggarwal (1964) as 1.35meV. In general at low temperatures only the deepest groundstate is occupied. Only under particular circumstances do the higher groundstates become populated.

Considering the excited states, higher s-states are also expected to split into three levels due to inter-valley coupling. Transitions from the $1s(A_1)$ ground state to $ns(E)$ and $ns(A_1)$ states are symmetry forbidden and have only been observed indirectly as Fano resonances. Transitions to the $ns(T_2)$ higher excited states, EMT forbidden but symmetry allowed, have been observed for Se^0 and S^0 centres (Janzén et al, 1984).

All transitions to p-states are allowed. The p-states have the property that their EMT wave function vanishes at the donor nucleus and therefore no valley-orbit splitting or central cell correction is expected for these states. It is observed that p-states are usually in excellent agreement with EMT. The energy level diagrams of the most common shallow donors in silicon are shown in Fig 1.6.

1.6.2 Acceptors in silicon

The theoretical description of acceptors in silicon is far more complex than for donors since while the conduction band has a simple minimum the valence band maximum is degenerate. This problem has been studied extensively by Baldereschi and Lipari (1974, Lipari et al, 1978, 1980a) who have successively refined the effective-mass Hamiltonian for shallow acceptor states. The basic Hamiltonian is (Lipari et al, 1980b)

$$H = H_{kin} + V_{spc} + V_{sr}$$

where H_{kin} describes the valence bands including the split-off band, V_{spc} describes the potential of the point charge screened by the dielectric constant of the host lattice and V_{sr} is the short range potential which accounts for the electronic structure of the ionic core of the impurity and the surrounding lattice relaxation i.e. those effects giving rise to the central cell correction. V_{sr} is empirically determined. In this way the binding energies of the ground and excited states of acceptors in silicon have been semi-empirically determined within the effective-mass approximation.

1.7 Thermal Donors in silicon

When Cz-silicon is annealed between 300°C and 500°C donor impurities are created. The presence of these donors was determined from resistivity measurements some 30 years ago and has since grown to be an extremely active area of research.

Cz-silicon contains high concentrations of oxygen, up to $10^{18}cm^{-3}$. The oxygen is absorbed from the quartz crucibles into the melt during growth. Float-zone silicon contains very little oxygen, of the order of $10^{16}cm^{-3}$ and no donors are formed in this material after heat treatment at 450°C. It has been shown that these donors known as the "Thermal Donors" (TD) which are typically produced at a temperature of 450°C, are oxygen related.

In 1958 Kaiser et al reviewed the available experimental data on the TD which establish the link with oxygen and show that the initial rate of donor formation is proportional to the fourth power of the oxygen concentration and the maximum attained donor concentration is proportional to the third power of the oxygen concentration. The oxygen concentration is determined from the 9μm

infrared absorption band of interstitial oxygen. It has been observed that the intensity of the interstitial oxygen band and the formation of TD are related, however no direct evidence for the presence of oxygen in the TD structure has yet been found (Tan et al, 1986, Newman, 1986).

1.7.1 Optical transitions

A complete description of the TD has remains tantilisingly elusive despite recent increased interest in the field. A comprehensive wealth of data on the optical transitions has been gathered by experimental methods such as infrared absorption spectroscopy, DLTS, and photoluminescence.

Infrared absorption spectroscopy has perhaps provided the most important information concerning the TD. In the infrared transmission spectra of Cz-silicon samples annealed for different times at 450°C many optical transitions arising from the TD are observed. These features have been identified as the transitions from the groundstate to the excited states of several different donors (Wruck and Gaworzewski, 1979, Oeder and Wagner,1983, Pajot et al, 1983). It has also been determined that the donors are double donors. Two groups of optical transitions are observed arising from the neutral (TD^0) and singly-ionised (TD^+) donor centres respectively.

The effective mass theory as described in section 1.6 has been applied to analyse the spectroscopic data and it was found that the TD centres are effective-mass like. The appropriate model is in this case however a helium-like system as opposed to a hydrogen-like system. The first electron sees a screened core potential and the second electron the core potential arising from a charge Z=2.

The binding energy for a double donor may therefore simply be estimated as

$$E(TD^0) = E(EMT)\,[E(He^0)/E(H^0)] \tag{1.28}$$

and

$$E(TD^+) = 4 \times E(EMT) \tag{1.29}$$

where $E(He^0)$ is the binding energy of the neutral He atom and $E(H^0)$ the binding energy of the H atom. $E(EMT)$ is the predicted EMT binding energy for a H-like donor (Ho and Ramdas, 1972). Hence one expects $E(TD^0)$ to be 56.5meV and $E(TD^+)$ to be 125meV.

The spectroscopic data and conclusions formed from it are summarized by Wagner et al (1984). Transitions arising from nine separate TD (TD1 - TD9) have been observed in Cz-silicon annealed at 450°C. The deeper donors are formed first and with longer annealing times at 450°C successively shallower donors become apparent. The observed ionisation energies are in the range 69.3meV (TD1) - 53.0meV (TD9) for the neutral donor centres. Transitions arising from the singly ionised donor centres have been observed for centres TD1 to TD6 in the range 156.3meV (TD1) - 127.9meV (TD6). The assignments of the observed transitions and the ionisation energies of the TD are shown in Table 1.1.

The excited p-state binding energies of the TD agree well with those predicted, as for the elemental donors in silicon, but the 1s ground state suffers a central cell correction due to the local potential at the impurity. In Table 1.2 a comparison is made between the EMT predictions (Faulkner, 1969, Janzén et al, 1984) and the experimental data.

It is believed that the TD are oxygen containing complexes of increasing size. The spectroscopic data supports this view which was already proposed by

TD-Nr.	1	2	3	4	5	6	7	8	9
TD_i^0-transitions/cm^{-1}									
$2p_0$	461	442	423	405	388	372	357	343	330
$2p_\pm$	507	488	470	451	434	417	404	385	376
$3p_0$	–	494	475	456	441	–	–	–	–
$3p_\pm$	533	514	496	477	–	443	–	–	–
E_B/meV	69.3	66.9	64.7	62.3	60.2	58.1	56.5	54.1	53.0
TD_i^+-transitions/cm^{-1}									
$2p_0$	854	806	762	713	678	645	(614)	(584)	
$2p_\pm$	1044 1048	991 998	945 951	889 904	846 862	(804) 825	(782) (793)	(769)	
$3p_\pm$	1156 1160	1105 1107	1057 1059	1011 1014	968 972	– –			
$4p_\pm$	1187	–	–	–	–				
E_B/meV	156.3	149.7	143.8	138.2	132.5	127.9			

Table 1.1: Energies of the infrared absorption lines at 8K and the optical binding energies E_B for the oxygen-related Thermal Donors in oxygen-rich silicon annealed at 450°C TD_i^0 refers to the neutral donor and TD_i^+ to the singly ionised donor (P. Wagner, C. Holm, E. Sirtl, R. Oeder, W. Zulehner, Advances in Solid State Physics "Festköperprobleme XXIV" (Vieweg, Braunschweig) 1984).

Donor	EMT[1]	EMT[2]	TD1	TD2	TD3	TD4	TD5	TD6	TD7	TD8	TD9
TD_i° transitions/cm^{-1}											
$1s \rightarrow 2p_\pm - 1s \rightarrow 2p_0$	51.61	51.632	46	46	47	46	46	45	47	42	46
$1s \rightarrow 3p_0 - 1s \rightarrow 2p_\pm$	7.42	7.392	-	6	5	5	7	-	-	-	-
$1s \rightarrow 3p_\pm - 1s \rightarrow 2p_\pm$	26.45	26.469	26	26	26	26	-	26	-	-	-
TD_i^+ transitions/cm^{-1}											
$1s \rightarrow 2p_\pm - 1s \rightarrow 2po$	206.44	206.528	192	188	186	174	176	(170)	(173)	(185)	-
$1s \rightarrow 3p_\pm - 1s \rightarrow 2p_\pm$	105.80	105.876	112	112	110	118	-	-	-	-	-
$1s \rightarrow 4p_\pm - 1s \rightarrow 3p_\pm$	30.00	30.098	29	-	-	-	-	-	-	-	-

1. R. A. Faulkner, Phys. Rev. 184 (3) 1969.
2. E. Janzén, R. Stedman, G. Grossman, H. G. Grimmeiss, Phys. Rev. B 29 (4) 1984.

Table 1.2 Comparison of the experimentally observed binding energies of the excited states of the Thermal Donors to those predicted by effective mass theory.

Kaiser et al in 1958 and as it will be shown, the formation kinetics also conform with this hypothesis.

The dependence of the infrared transmission spectra on the presence of other impurities has been studied. It is observed that the presence of carbon retards the growth of the TD (Kaiser et al, 1958, Bean and Newman, 1972, Helmreich and Sirtl, 1977). It is possible that carbon forms electrically inactive complexes with the oxygen hence competing with the growth of Si-O complexes. Wagner et al (1984) report no dependence on the presence of other impurity species such as P, Sb, B or Al.

DLTS measurements on Cz-silicon annealed at 450°C have revealed two levels at E_c-0.07eV and E_c-0.150eV respectively (Kimerling and Benton, 1981), where E_c represents the conduction band minimum. These values are in agreement with the predicted effective mass values confirming the double donor nature of the centres. However the individual donors are not resolved.

Photoluminescence measurements of samples annealed up to 100 hours have revealed the presence of new luminescence lines. The new lines labelled the O-lines appear to arise from shallow donors and free holes (D^0, h). Weber and Queisser (1986) determine four ionisation energies from the photoluminescence data which correspond to the ionisation energies of the neutral TD9 to TD6. This recombination is only possible assuming an inhomogeneous distribution of the TD. This is also indicated by infrared transmission spectra. After long annealing times boron is also observed in the spectra of n-type material showing the TD. Normally the boron would be completely compensated and undetectable, only if regions of the sample are p-type is it possible to observe the donors and acceptors simultaneously.

1.7.2 Structure

The first model of the TD was the SiO_4 model of Kaiser, Frisch and Reiss (KFR model) and subsequently many models have been put forward. Some of the most important models are: an interstitial Si-O molecule (Pajot et al, 1982); the oxygen interstitial pair (Oeherlein and Corbett, 1983), an extension of the SiO_4 model; the Helmreich-Sirtl model (1977) based on a substitutional oxygen stabilized by nearby acceptors; the Y-lid configuration (Stavola and Snyder, 1983) which takes the silicon atom as the electrically active element; the Ourmazd-Bourret-Schröter model (OBS model, 1984) in which a substitutional silicon is displaced to an interstitial site by at least three nearby oxygen interstitials.

Recent measurements and results of uniaxial stress measurements in EPR, DLTS and infrared transmission spectroscopy have contributed factual data concerning the symmetry of the TD defects. The EPR centre NL8 has been shown to be related to the TD (Lee et al, 1985), although the individual TD are not resolved. This centre has C_{2v} symmetry. ENDOR measurements have not been able to confirm the presence of oxygen in the donor core. From DLTS under uniaxial stress (Benton et al, 1985) C_{2v} symmetry is also deduced for the TD through the observed stress splitting and the anisotropy of the electric field interaction. Again however the individual TD are not resolved.

Infrared absorption measurements under uniaxial stress (Stavola et al 1985a, 1985b, Stavola and Lee, 1986) allow the study of the individual donor centres in detail. The excited states and the conduction band split due to the application of uniaxial stress according to the EMT. In this case the components split by the same amount and therefore the transition frequencies remain as

before. Small non-effective mass splittings are observed and are attributed to orientational degeneracy due to an anisotropic central cell along the < 110 > direction. A C_{2v} symmetry is deduced for the individual donors TD1→TD5 studied to date.

Of the proposed models the Y-lid model shown in Fig 1.7c) appears to be the simplest model which satisfies the observed symmetry of the TD and can explain the electrical activity of the centres. The central trivalently bound silicon of the Y-lid which has one unbound electron can acquire a second electron from the neighbouring trivalently bound oxygen giving rise to double donor behaviour. The silicon Y-lid is stabilized by two or more interstitial oxygen atoms, lying along the < 100 > direction.

The OBS model, shown in Fig 1.7d), also explains a large body of the experimental data. The electrical activity arises from two silicon broken bonds at the cluster centre. The model also assumes the addition of one oxygen from TD_n to TD_{n+1}. Further, the model agrees with experiment on the following points: double donor activity is predicted, symmetry is C_{2v}(mm2) as required from EPR data and infrared uniaxial stress measurements and it is predicted that no hyperfine interaction should be observable. The donors grow preferentially in the < 110 > direction. The termination of electrical activity is explained by the ejection of the central silicon which at the same time provides a stress relaxation mechanism, this property of the model is of importance in reproducing the kinetics of the donors. The remaining structure is similar to that of coesite. Coesite rod-like defects are observed by electron microscopy in Cz-silicon annealed for long times at 450°C.

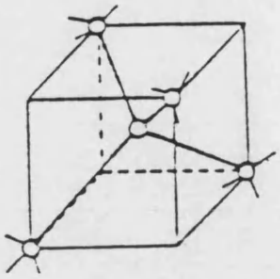

a) silicon lattice

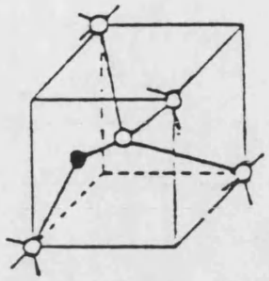

b) oxygen intersitial

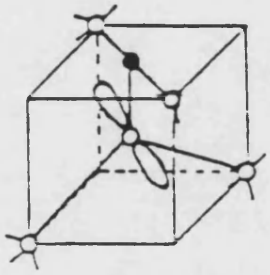

c) Y-lid model

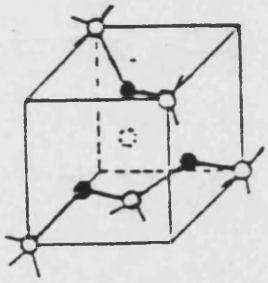

d) OBS model

Fig 1.7: A schematic outline of the proposed Y-lid model and OBS model for the Thermal Donor in comparison to the unperturbed silicon lattice and the electrically inactive oxygen interstitial. • oxygen atom ∘ silicon atom

1.7.3 Formation Kinetics

The formation kinetics of the TD has also been a topic of interest. The experimental data has been made available principally from infrared transmission spectroscopy, although some early work was based on Hall measurements.

The diffusion of oxygen has been a key problem in understanding the formation kinetics of the TD. The interstitial oxygen (O_i) is believed to diffuse and agglomerate to form Si-O complexes. However, the measured rates of formation require an oxygen diffusivity 10-100 times higher than the accepted value. For this reason O_2 molecule diffusion has been proposed as an alternative to O_i diffusion (Gösele and Tan, 1982). However, it has been shown that the temperature dependence at room temperature for O_2 is unreasonable therefore discounting this proposal.

A further problem is that the rate of formation of the donors also depends on the thermal history of the sample, which determines the initial concentration of interstitial oxygen and also whether TD (or smaller seed complexes) are already present. For example TD are created during cooling in the growth process. For this reason a ten minute anneal at either 700°C or at 1000°C is used to disperse any existing TD. The TD are destroyed by annealing above 500°C but the "New Thermal Donors" (Cazarra and Zunino, 1980) are formed at 600-800°C and therefore a 1000°C anneal is sometimes preferred to the 700°C anneal.

A recent comprehensive study of the formation kinetics of the TD has been carried out by infrared absorption spectroscopy (Wagner et al, 1984) on low carbon Cz-silicon samples pre-annealed for 10 minutes at 770°C. The detected concentrations of the individual TD were monitored after annealing times bet-

ween 10 minutes and greater than 10 hours at 460°C. The observed behaviour is indicative of the growth of successively larger complexes. At short annealing times deeper donors, which are believed to represent the first electrically active stages of clustering are dominant, as the annealing time is increased shallower donors corresponding to larger complexes begin to dominate. After approximately ten hours the donor formation saturates and then starts to decay. There is no indication that more than the nine observed donors exist. It is supposed that the next stage of clustering is no longer electrically active and hence no longer detectable by infrared spectroscopy. However the resistivity does not saturate until approximately 100 hours. This can possibly be accounted for as the formation of donor interface states or the "New Thermal Donors" which although normally formed after heat treatment between 600°C and 800°C may form slowly at these lower temperatures.

It was found that there is a distinct difference between the annealing time dependence of the absorption coefficients of the individual donors and the net concentration of donors.

A model which describes the formation kinetics of the TD must incorporate this fact and the known dependency of the growth on the oxygen concentration. The formation kinetics have only been calculated for the KFR model, the Oehrlein model and the OBS model which make a best fit to the data. Borenstein et al (1986a) have extended the kinetic model of Suezawa and Sumino (1984). Here the core is not defined, rather the parameters of the deepest donor (TD1) are the starting point upon which the calculations are based.

The KFR model predicts the SiO_4 unit as the major electrically active donor and its formation kinetics can qualitatively explain the experimental data. Re-examining the KFR model Oehrlein showed that in the general case of

samples with different oxygen concentrations the formation kinetics could be better described assuming a SiO_3 complex as the major donor species. It was noted however, that after longer annealing times the SiO_3 complex alone is not sufficient and higher complexes SiO_4, SiO_5 etc. must be included in the calculations.

Although the Oehrlein model addresses such features as the origin of electrical activity and the change to electrically inactive clusters after the ninth donor stage (Oehrlein and Corbett, 1983) there are still many experimental facts which are not well explained by this model, for example the known defect symmetry.

The OBS model presents a very comprehensive picture of the formation kinetics of the TD and is able to explain the most important experimental data and many significant details. The decay in the donor concentration after longer annealing times and the transition to electrically inactive clusters is achieved by allowing the ejection of the central electrically active silicon self-interstitial which also results in stress relaxation of the cluster. It is assumed that each donor species differs from the next by the addition of one oxygen, an effective diffusion rate for the interstitial oxygen is assumed. Constructing a series of forward and reverse reactions from this basis Ourmazd, Bourret and Schröter were able to fit the formation kinetics of the individual donor species obtained from infrared spectroscopy measurements. Fits were achieved for a set of stabilities such that a cluster containing five oxygens is the first electrically active donor and is most stable, smaller clusters are electrically inactive and unstable, larger clusters are progressively more unstable. The average kinetic information obtained from resistivity measurements is easily reproduced.

Suezawa and Sumino (1984) analysed their own infrared absorption measure-

ments using a similar scheme to Kaiser, Reiss and Frisch. The rate constants and cluster species of the first donor are regarded as parameters. From their data they concluded that the first TD should contain three oxygens. Borenstein et al (1986a) extended this empirical approach based on the infrared data of Oeder and Wagner (1983) and Suezawa and Sumino. Here the approach was to analyse the general features of the TD annealing curves to determine the rate constants. Following this approach they were able to fit both sets of available infrared data. The fit does not uniquely define the number of oxygens in the first TD, between two and five oxygens would all give a reasonable fit. For this reason Borenstein et al also suggest that kinetic equations alone are not sufficient to determine the number of oxygens present in the different donor species.

1.7.4 Summary

The TD are formed during heat treatment between 300 and 500°C. They are series of nine oxygen aggregates of increasing size formed by the agglomeration of interstitial oxygen which is abundant in Cz-silicon. These clusters act as effective-mass like double donors. The initial electrically active cluster (TD1) is expected to contain between three and five oxygens. The addition of further oxygen to the cluster reduces the cluster binding energy. It is assumed that the addition of a single oxygen is required for the transition $TD_n \rightarrow TD_{n+1}$. The electrical activity of the TD is lost beyond a certain cluster size. The Y-lid model and the OBS model, which are very similar, describe a large body of the experimental data.

The growth of the TD is very sensitive to the thermal history of the sample and the initial dispersed oxygen concentration. The initial growth rate de-

pends on the oxygen concentration to approximately the fourth power and the maximum net donor concentration observed is approximately proportional to the third power of the oxygen concentration. The individual donor concentrations increase successively with annealing time, saturate and then begin to decay after approximately 10 hours.

The TD have C_{2v} (mm2) symmetry and an extended central cell in the $< 110 >$ direction. They are effective mass like double donors.

Chapter 2

Experimental Method

2..5 The Michelson Interferometer

Most Fourier Transform spectrometers for the spectral region 25cm^{-1} - 2000cm^{-1} are based on the Michelson Interferometer (Fig 2.1). Consider a monochromatic light source at S. At zero path difference between the reflected-transmitted (I_{rt}) and transmitted-reflected (I_{tr}) beams there is constructive interference. As the moveable mirror is moved from the zero path position the two beams alternatively fulfill the conditions for constructive and destructive interference. The phase difference ϕ between the two components is given by

$$\phi = 2\pi\sigma\delta \tag{2.1}$$

where σ is the wavenumber of the radiation and δ is the path difference.

2.1 Short derivation of the basic integral of Fourier Transform Spectroscopy

Now we consider a broad band source. Let the incident amplitude , E on the beamsplitter be

$$E(z,\sigma)d\sigma = E_0(\sigma)e^{i(\omega t - 2\pi z\sigma)}d\sigma \tag{2.2}$$

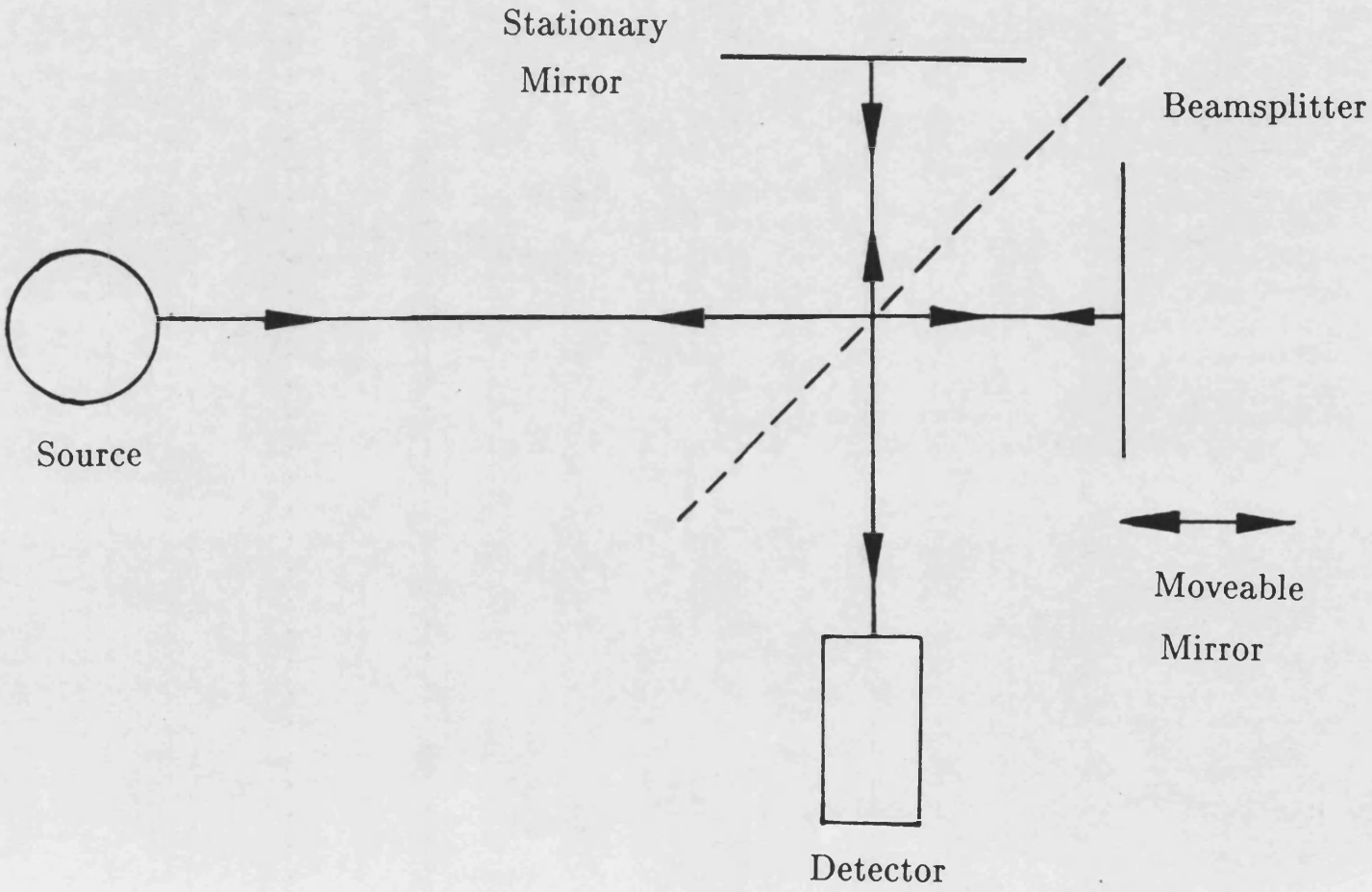

Fig 2.1: The Michelson interferometer.

where z is the path length travelled and ω is the frequency of the radiation. At the detector the observed amplitude is given by

$$E_D(z_1, z_2, \sigma)d\sigma = r\,t\,E_0[e^{i(\omega t - 2\pi z_1\sigma)} + e^{i(\omega t - 2\pi z_2\sigma)}]\,d\sigma \tag{2.3}$$

where z_1 and z_2 are the path lengths travelled by the two different beams and r and t are the reflection and transmission coefficients of the beamsplitter.

The flux for a spectral element $d\sigma$ is given by

$$\begin{aligned} I(z_1, z_2, \sigma)d\sigma &= E_D(z_1, z_2, \sigma)\,E_D^*(z_1, z_2, \sigma) \\ &= 2E_0^2(\sigma)|r\,t|^2\{1 + cos[2\pi(z_1 - z_2)\sigma]\}\,d\sigma \end{aligned} \tag{2.4}$$

For any path difference $\delta = z_1 - z_2$ the total flux is given by

$$\begin{aligned} I_D(\delta) &= \int_0^\infty E_0^2(\delta, \sigma)\,d\sigma \\ &= 2\,|r\,t|^2\left[\int_0^\infty E_0^2(\sigma)\,d\sigma + \int_0^\infty E_0^2(\sigma)\,cos(2\pi\delta\sigma)\,d\sigma\right] \end{aligned} \tag{2.5}$$

Therefore at $\delta = 0$

$$I_D(0) = 2\,|r\,t|^2\left[2\int_0^\infty E_0^2(\sigma)\,d\sigma\right] \tag{2.6}$$

Hence we can write

$$\left[I_D(\delta) - \frac{1}{2}I_D(0)\right] = 2\,|r\,t|^2\int_0^\infty E_0^2(\sigma)\,cos(2\pi\delta\sigma)\,d\sigma \tag{2.7}$$

where $I_D(\delta) - \frac{1}{2}I_D(0)$ is the interferogram as shown in Fig 2.2. Also $\frac{1}{2}I_D(0) = I_D(\infty)$ since at long path lengths the beams are no longer coherent.

The inverse Fourier Transform of this equation gives

$$B(\sigma) \propto E_0^2(\sigma) = (1/\pi\,|r\,t|^2)\int_0^\infty [I_D(\delta) - I_D(\infty)]\,cos(2\pi\delta\sigma)\,d\delta \tag{2.8}$$

That is the intensity as a function of wavenumber is given by the inverse Fourier Transform of the interferogram, equation (2.8) is the basic equation of FT spectroscopy (for general FT spectroscopy see Mertz, 1965, Bell, 1972 or Genzel and Sakai, 1977).

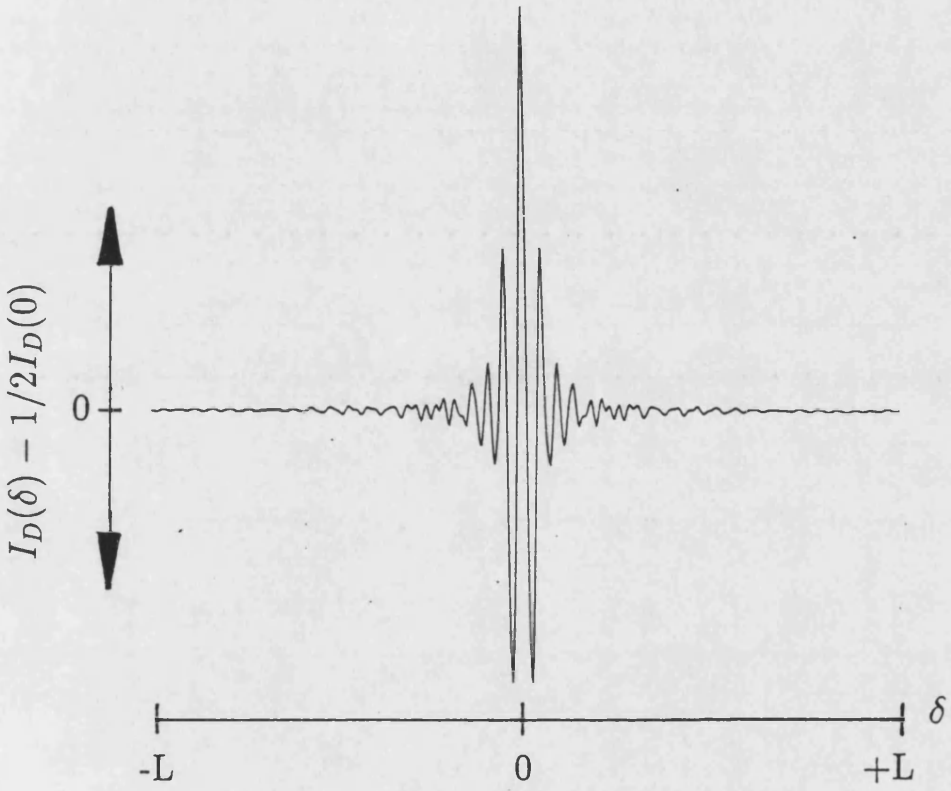

Fig 2.2: The interferogram measured on the Double Beam Fourier Transform Spectrometer using a mercury arc source and Ge bolometer with a quartz filter.

2.2 The advantages of Fourier Transform Spectroscopy

The two main advantages of FT spectroscopy are the Jaquinot advantage and the Fellgett advantage. The Jaquinot advantage or throughput advantage notes that in a dispersive spectrometer the radiation reaching the detector is determined by the slits of the monochromator whereas in an interferometer the circular input aperture and mirror size limit the throughput. Therefore the optical throughput is larger for an interferometer than for a monochromator. The Felgett advantage describes the fundamental advantage of an interferometer that a broad band of frequencies are measured simultaneously. In the time taken to measure one spectral element in a monochromator, the complete interferogram can be measured with the same signal-to-noise ratio.

2.3 Apodization

The basic Fourier Transform integral has infinite limits but in an experimental situation the distance travelled by the moveable mirror is only $\pm$L. In the frequency spectrum this inconsistency results in a finite linewidth instead of an infintely narrow linewidth and side-lobes or "feet" at adjacent frequencies. To account for the finite optical path difference the interferogram is multiplied by a mathematical function which weights the small path differences (with high signal-to-noise ratio) against the longer path differences e.g. a triangular function. This process is called apodization, other functions with a similar effect to the triangular function may also be used as appropriate. Apodization has the side-effect that the resolution is also reduced by approximately a factor of 2.

2.4 The double beam Fourier Transform Spectrometer

In a standard Michelson interferometer the twice reflected (I_{rr}) and twice transmitted (I_{tt}) components of the incoming radiation are not used. A modified arrangement which makes this second output available and also permits the use of a second input is shown in Fig 2.3. The second output contains the anti-interferogram, the complement of the interferogram.

For the initial PTIS measurements a stepping Fourier Transform spectrometer of the type shown schematically in Fig 2.4 was used. This double beam Fourier Transform spectrometer (DBFTS) was designed and constructed by L.Genzel and co-workers (Genzel et al, 1976, 1978, Chandrasekhar et al, 1976). A single source is split into two beams P_1 and P_2 which are chopped 90° out-of-phase by a two blade mechanical chopper(C). After incidence on the first beamsplitter the beams are divided, travel a path length determined by the position of the double-sided moveable mirror (DM) and are divided again at the second beamsplitter. Considering the recombined components in output 1 shown schematically in Fig 2.5 we find the interferogram from input 1, I_{11} and the anti-interferogram from input 2, A_{21}. Using lock-in techniques I_{11} and A_{21} are subtracted. The resultant interferogram in output 1 is the coherent addition of I_{11} and A_{21} giving a modulation approximately twice that of I_{11}. Similarly in output 2 one finds the interferogram of output 2, I_{22} and the anti-interferogram of output 1, A_{12} which may be treated in the same way. This spectrometer thus offers double modulation intensity in the outputs compared to a single beam instrument. This feature may be used to advantage in PTIS where only a single beam is required. The fact that r and t are not perfectly 0.5 leads to a departure of the background level from $\frac{1}{2}I_D(0)$. The backgrounds for the interferogram and anti-interferogram are different in magnitude. Combining

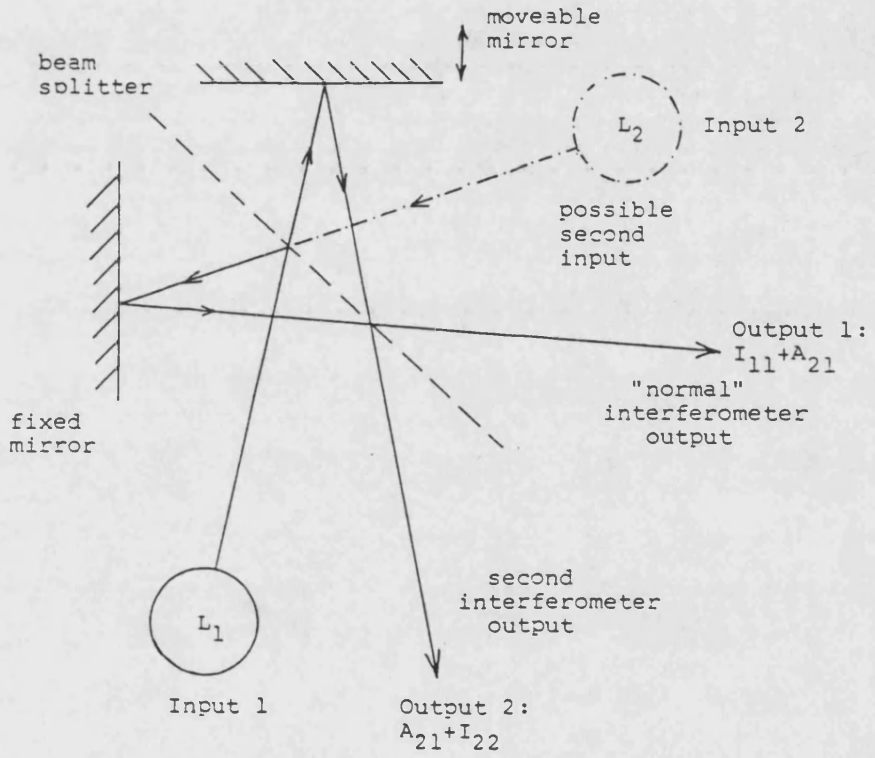

Fig 2.3: A modified Michelson interferometer which allows the use of the second output. A second input may be positioned at L_2.

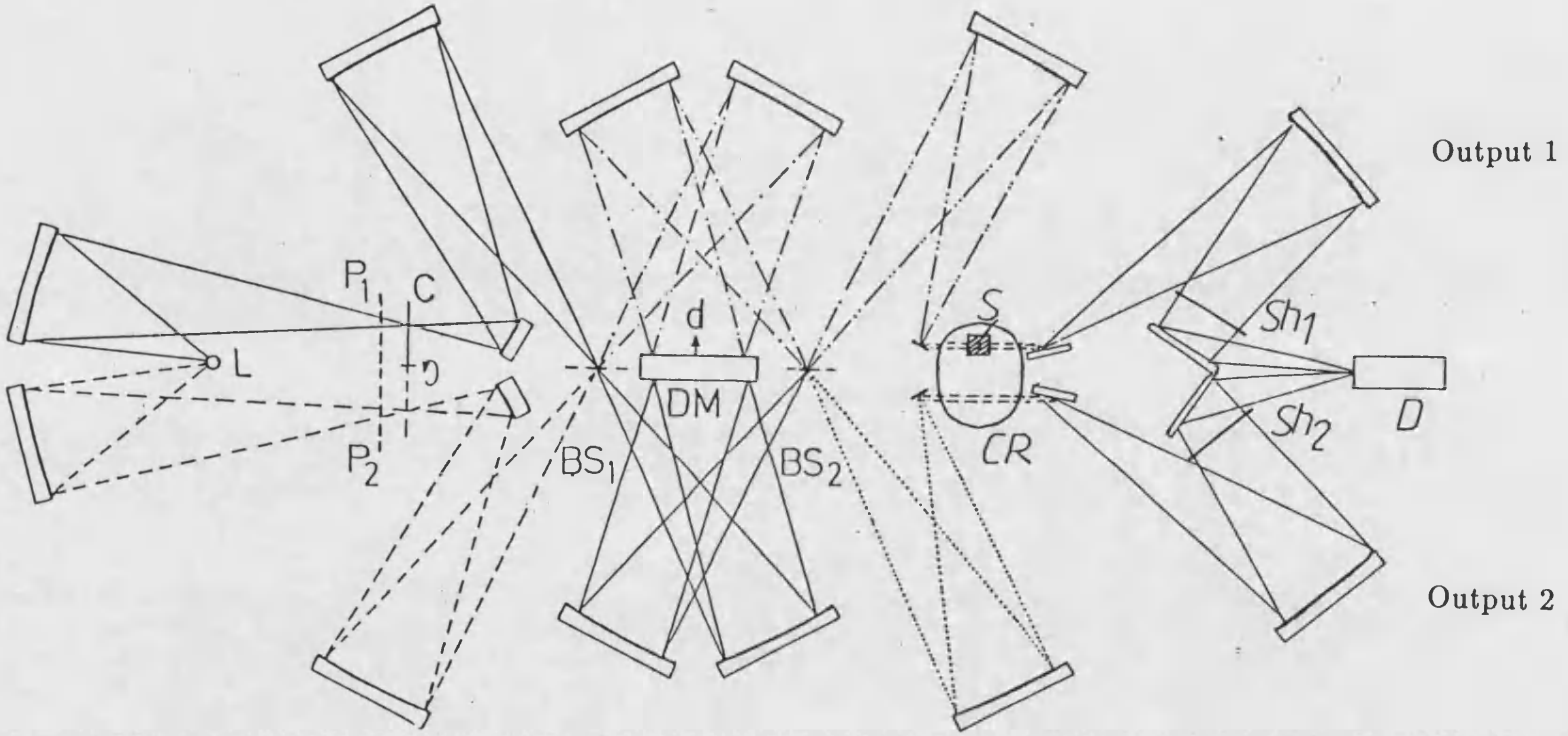

Fig 2.4: The Double Beam Fourier Transform Spectrometer (DBFTS) designed and constructed by L. Genzel and co-workers.

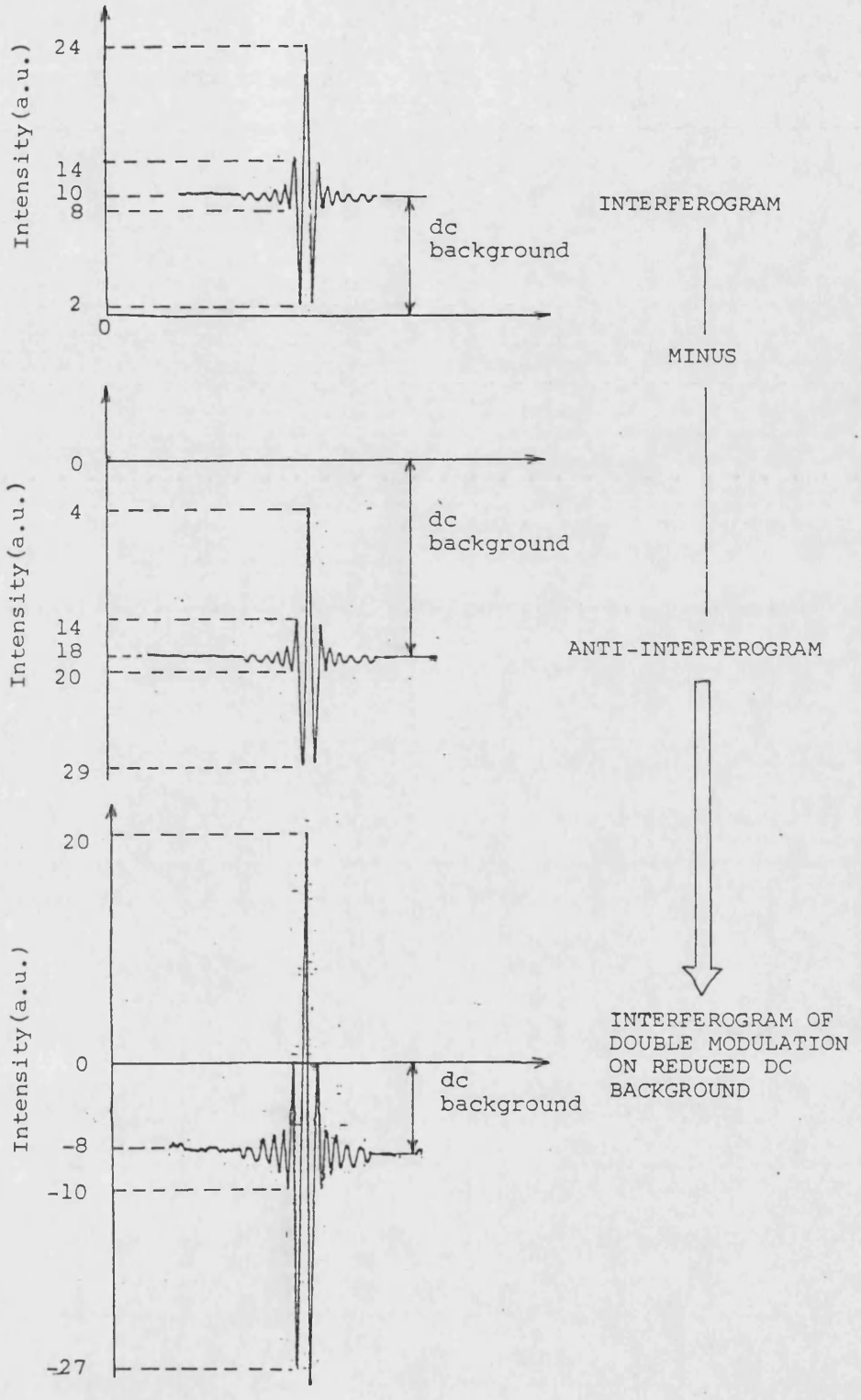

Fig 2.5: The subtraction of an interferogram and anti-interferogram using lock-in techniques results in an interferogram of approximately twice the modulation of the interferogram alone. Also the unmodulated background is reduced.

the two components has the advantage that the background is reduced.

It is also possible to make a simultaneous measurement of a sample (at S) and a reference (at R) (Fig 2.4). By combining the resultant interferograms the construction of a "difference" interferogram may be achieved allowing extremely sensitive transmission measurements to be made (Shen et al, 1980).

Further advantages of this design are that the beam is focused onto the beamsplitters so that the effective beamsplitter diameter is small and that a double-sided moveable mirror is used so that for a 1μm movement a path difference of $\sim$ 3.8μm is achieved (including the effect of angle of incidence). The optical chamber is filled with circulating dry air to avoid absorption by water vapour whose rotational lines occur in the far infrared region of the spectrum. Using either a mercury arc source or globar with metal mesh or mylar beamsplitters the spectral range of this instrument is 20cm^{-1} - 1000cm^{-1}.

The signal-to-noise ratio is dependent on the collection time at each mirror position which is four times the lock-in time constant (1 - 0.3 seconds) plus dead-time. For a typical measurement the total measurement time is of the order of one and a half to three hours.

2.5 The Fast-Scan Fourier Transform Spectrometer

The Bruker IFS 113v spectrometer has a spectral range of 10cm^{-1} - 4800cm^{-1}. A diagram of the optical system, designed by Prof. L. Genzel, is shown in Fig 2.6. This single beam system also allows a small effective beamsplitter diameter and uses a double-sided mirror as for the DBFTS.

The moveable mirror is moved with a constant velocity, v so that at any given

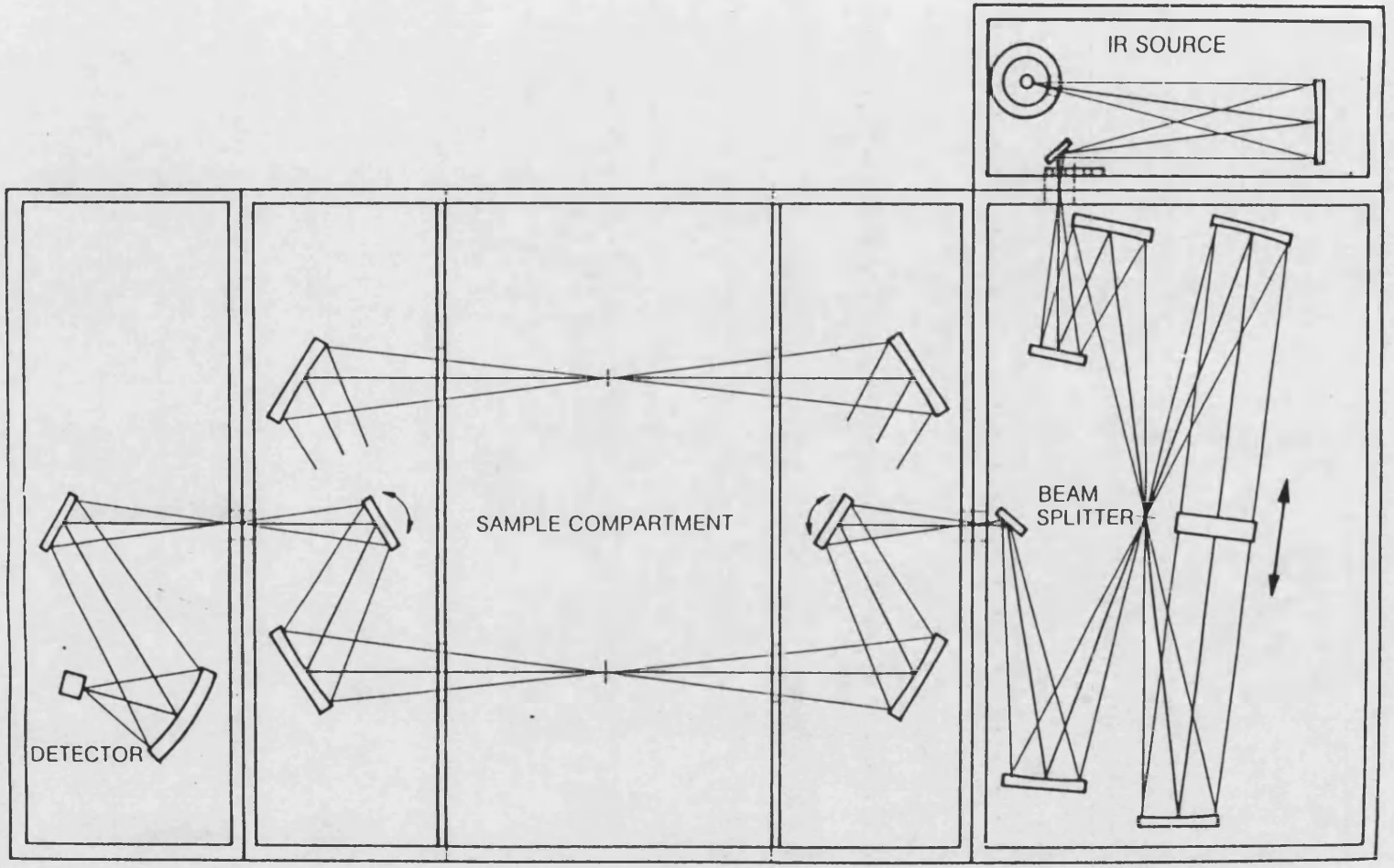

Fig 2.6: The optical arrangement of the Bruker IFS 113v spectrometer.

time the path difference (assuming zero time at zero path difference) is given by $v \times t$. Further, the velocities used are rapid (0.23-3.2cm/sec) so that there is a self-modulation, each spectral element being modulated at a frequency, ν, in the audio-frequency range such that

$$\nu = 2v\sigma. \tag{2.9}$$

Therefore, mechanical chopping of the input is not required in this case. The signal is electronically filtered using high-pass and low-pass filters with a variable cut-off so only those frequencies corresponding to the wavenumber range of interest are passed.

A mercury arc source and globar are available together with the option of six different beam splitters and six filters which are selected by computer control. The optical chamber is evacuated eliminating the problem of water vapour absorptions and beamsplitter vibration. A He-Ne laser interferometer determines the mirror position giving high frequency accuracy.

In a fast-scan spectrometer the complete interferogram is measured in a time of the order of one second. The signal-to-noise ratio is improved by co-adding many scans. A typical measurement requires the co-adding of 200 - 1000 scans giving rise to measurement times between three minutes and one and a half hours.

2.6 Light sources, beamsplitters and filters for the Far Infrared

Both spectrometers offer the option of a mercury arc lamp or globar source. A mercury arc lamp is best below 50cm^{-1} but provides sufficient radiation for measurements up to 1000cm^{-1}. The quartz envelope containing the gas is ran-

domly dimpled to avoid channel spectra. A globar source is more appropriate for the middle infrared >250cm^{-1}. However, all the studies presented here concerned impurities whose transitions were in the spectral region <300cm^{-1} and so the mercury arc lamp was always used.

For PTIS measurements on Ge in the wavenumber range 10 - 100cm^{-1}, carried out on the DBFTS, metal mesh beamsplitters with 400 copper wires per inch were used. A 6μm mylar beamsplitter (<100cm^{-1}) and a 3.5μm mylar beamsplitter (<1000cm^{-1}) were used with the Bruker IFS 113v. The characteristics of the mylar beamsplitters measured using a Ge bolometer are shown in Fig 2.7.

To eliminate high frequency radiation black polyethylene filters (70, 190 or 380μm warm or cold) were used in both spectrometers. Further filtering with either a warm capacitive filter (cut-off 100cm^{-1}) or a cold Yoshinaga filter (see Table 2.1) was used for measurements on Ge. It must be remembered that the cryostat window material also acts as a filter and must be considered in the analysis of the spectra. Table 2.1 lists the different filters and window materials and the spectral regions in which they transmit.

2.7 Resolution and maximum frequency

The resolution and maximum frequency are two parameters available to the experimentalist. Their maximum values depend on the maximum path difference achievable and therefore on the available scan length of the moveable mirror. In general the resolution before apodization, $\Delta\sigma$ is given by

$$\Delta\sigma = \frac{1}{2\delta} \tag{2.10}$$

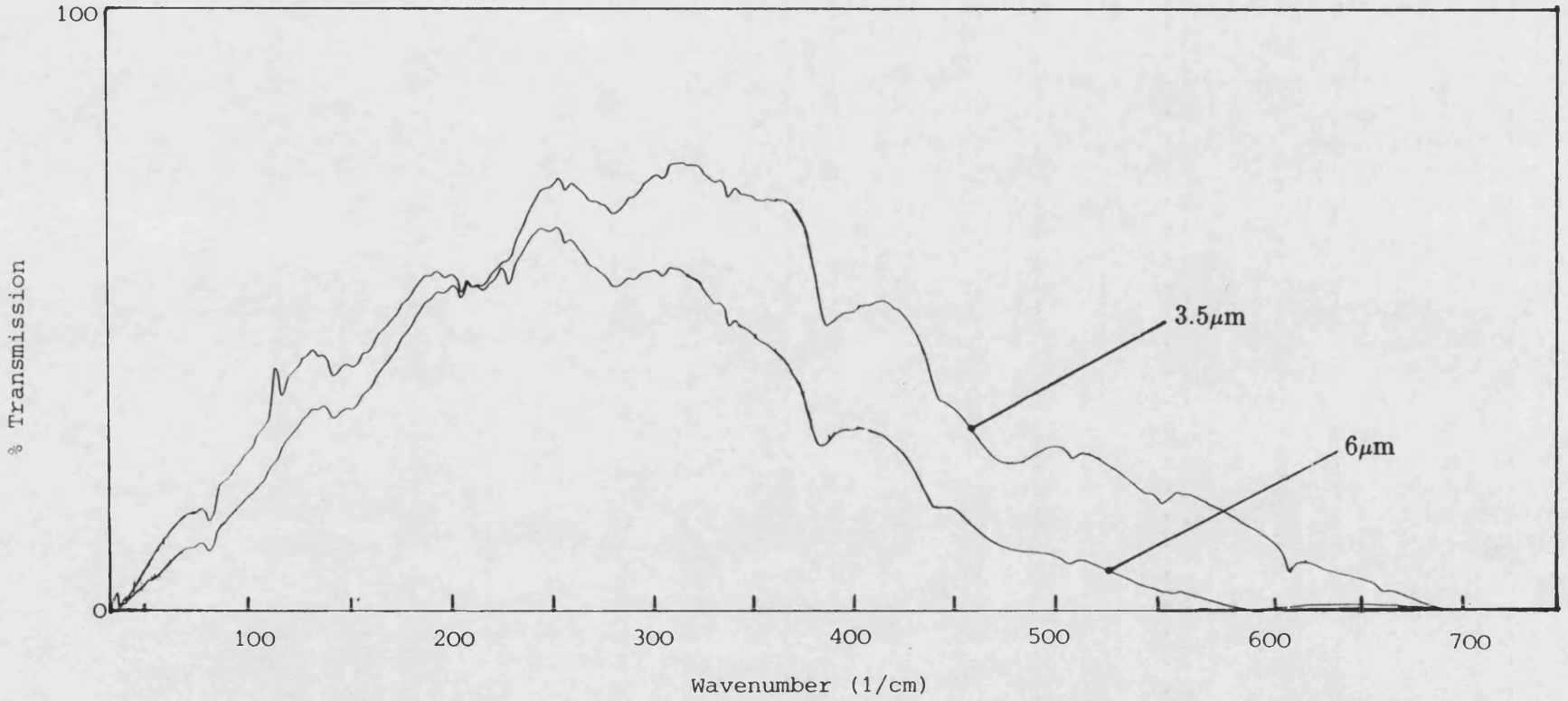

Fig 2.7: The transmission spectrum of the mercury arc source taken with different mylar beamsplitters used with the Bruker IFS 113v. A Ge bolometer (Infrared Labs. Inc. HD2) was used for the measurements.

MATERIAL	WAVENUMBER RANGE OF TRANSMISSION
1. Filters	
Capacitive Filter	$< 110 cm^{-1}$
	$< 150 cm^{-1}$
Yoshinaga Filter 1 BeO $4 mg/cm^2$ NaF $4 mg/cm^2$ ZnO $4 mg/cm^2$ KCl $3 mg/cm^2$	$< 42 cm^{-1}$ and $> 666 cm^{-1}$
Yoshinaga Filter 2 LiF $4 mg/cm^2$ CuF_2 $4 mg/cm^2$	$< 200 cm^{-1}$ and $> 666 cm^{-1}$
Yoshinaga Filter 3 LiF $4 mg/cm^2$ BaF_2 $6 mg/cm^2$ KBr $6 mg/cm^2$	$< 100 cm^{-1}$ and $> 500 cm^{-1}$
Yoshinaga Filter 4 TlF $8 mg/cm^2$ TlCl $8 mg/cm^2$ NaF $4 mg/cm^2$	$< 66.7 cm^{-1}$ and $> 666 cm^{-1}$
Black Polyethylene 190 m	$< 800 cm^{-1}$
2. Window materials	
White polyethylene 1-2mm	$< 700 cm^{-1}$
Plastic foil	$< 700 cm^{-1}$
KRS 5	$> 250 cm^{-1}$

Table 2.1: The transmission windows of common filter and window materials used in the far infrared.

In the DBFTS the maximum path length is 17.73cm giving a maximum resolution before apodization of 0.08cm^{-1}. In the Bruker IFS 113v the maximum resolution before apodization is 0.1cm^{-1}.

The maximum frequency, σ_{max} is determined in a stepping interferometer by

$$\sigma_{max} = \frac{1}{2\Delta z} \tag{2.11}$$

where Δz is the path difference between measurement points. If a spectrum containing intensity at frequencies greater than the allowed maximum frequency (according to the choice of Δz) is measured aliasing will occur in the spectrum. In the DBFTS the minimum available Δz is 3.8μm and therefore the maximum frequency is limited to 1315cm^{-1}. In a fast-scan instrument Δz is determined by the digitization of the analog signal but is usually very small.

2.8 Detection limiting factors and line broadening

The lower detection limit of PTIS has not yet been experimentally determined. The sensitivity of the method is greater than man's ability to produce ultra-pure semiconductor materials at the present time. The purest germanium which can be grown has a net impurity concentration of 10^9cm^{-3}. In this material individual impurities of concentrations 10^6-10^7cm^{-3} have been identified (Haller et al, 1975). This sensitivity arises from the fact that both the number of photothermally generated carriers and the number of carriers giving rise to the background without the presence of light, depend on the concentration of the majority and compensating impurities. If the concentration of impurities decreases the background level decreases correspondingly. However, in samples of higher net impurity concentration this background may be higher and therefore the sensitivity not as good.

PTIS is not a suitable method for investigating heavily doped semiconductors. "Concentration" broadening (White, 1967, Jagannath et al, 1981) of the transitions results in a smearing out of the spectrum such that the hydrogenic series are no longer resolveable. In n-type GaAs where the donors are very effective mass like and the central cell corrections are small this situation is reached at relatively low donor concentrations of the order of $10^{13}cm^{-3}$. Concentration broadening arises from the disturbance of the neutral donors due to the random electric fields of neighbouring ionised donors (Berman et al, 1974, Kogan et al, 1981). Also the wavefunctions of neighbouring impurities can overlap leading to a concentration dependent broadening of the energy levels. At higher impurity concentrations an impurity band exists rather than discrete levels. The actual upper detection limit of PTIS is determined by the magnitude of the central cell correction and the linewidths of the transitions and is therefore different in each material and for each different combination of impurity species.

Improper mounting of samples also leads to the broadening and splitting of transitions due to inhomogeneous stress. With careful mounting of the sample and an awareness of this problem such broadening can be avoided. Internal stress has been known to produce similar effects e.g. the splitting of the gallium transitions in germanium observed in the presence of barium impurities due to the lattice deformation caused by the latter (Artemenko et al, 1974).

2.9 Transmission measurements

Transmission measurements of silicon samples (net impurity concentration 10^{14} - $10^{17}cm^{-3}$ and filter materials were carried out on the Bruker IFS 113v using an Oxford cold-finger cryostat and an Infrared Labs. Inc. HD2 Ge bolometer.

2.10 The Photothermal Ionisation Spectroscopy system

A PTIS system which makes use of FT techniques consists of a far infrared FT spectrometer the output of which, directed to the sample, supplies the far infrared photons for the first stage of the photo-thermal ionisation process. The sample must be mounted electrically isolated and free from stress in a cryostat such that the sample temperature can be carefully controlled between 4.2K and 30K. Further a bias voltage must be applied to the sample and a data acquisition and signal processing chain are also required.

2.10.1 Temperature control

It is important that the area of the sample from which the PTIS response is generated is unstressed. For this reason cold finger cryostats are usually unsuitable for PTIS. In the present studies only helium evaporation contact gas cryostats have been used. With the DBFTS a custom built Cryovac cryostat is used (Fig 2.8a). This cryostat has two front windows and two rear windows to allow the simultaneous measurement of two samples, one in each output of the spectrometer (positioned at CR in Fig 2.4). For PTIS either one or two samples may be mounted on a bayonet holder. The sample temperature is monitored by a calibrated germanium resistor adjacent to the samples.

For measurements on the Bruker IFS 113v a Leybold-Heraeus cryostat with four mutually perpendicular windows was used (Fig 2.8b). Two samples can be mounted and alternatively brought into the interferometer output. The sample temperature is monitored by a calibrated Allan-Bradley 100Ω 1/8W carbon resistor adjacent to the sample.

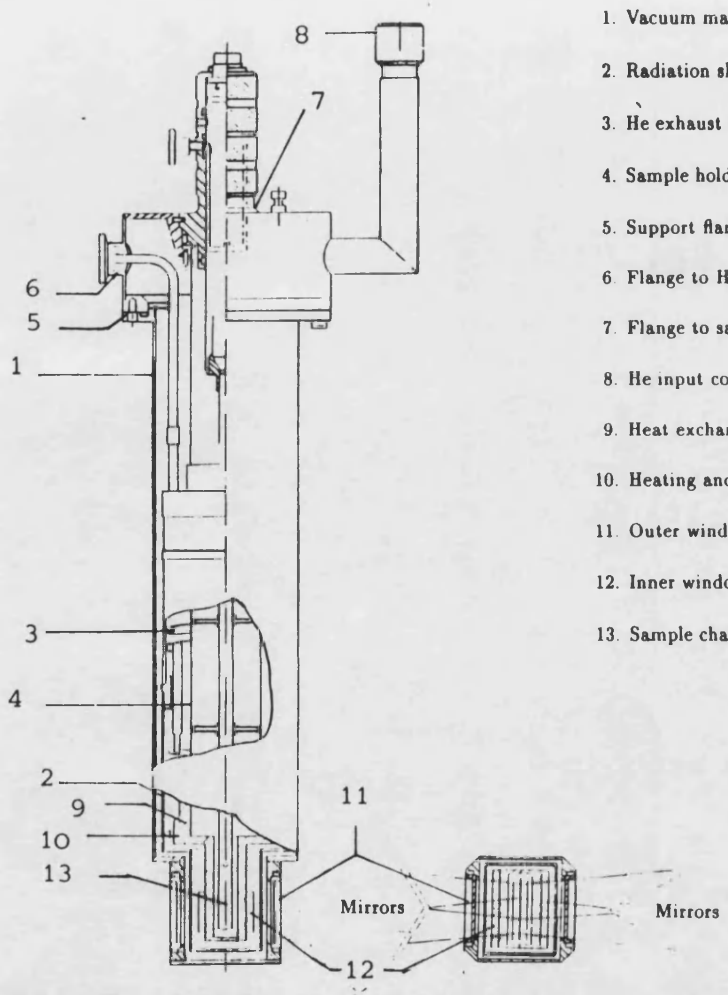

1. Vacuum mantel
2. Radiation shield
3. He exhaust spiral
4. Sample holder tube
5. Support flange
6. Flange to He pump
7. Flange to sample holder
8. He input connector
9. Heat exchanger
10. Heating and temperature sensor
11. Outer windows (warm)
12. Inner windows (cold)
13. Sample chamber

Fig 2.8a): The Cryovac evaporation cryostat used with the Double Beam Fourier Transform Spectrometer.

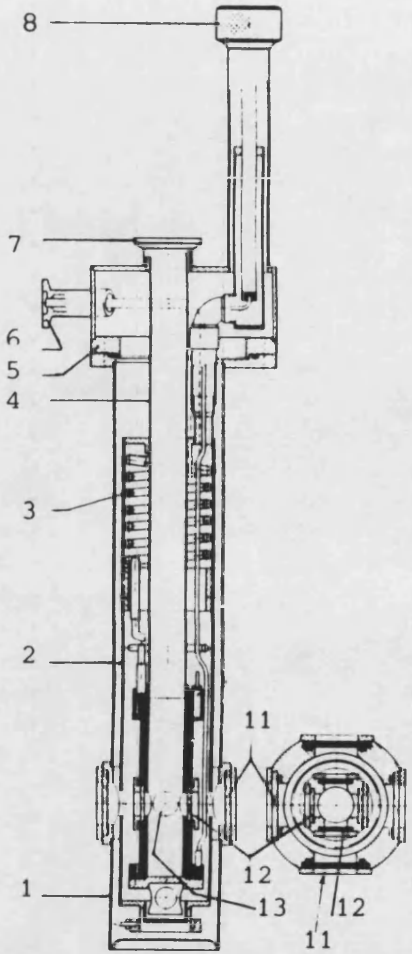

Fig 2.8b): The Leybold-Heraeus evaporation cryostat used with the Bruker IFS 113v spectrometer.

During the PTIS measurements careful control of the sample temperature is required. The arrangement of the cryostat and peripheral devices is shown in Fig 2.9. Initially both the isolation vacuum space and the exchange gas space are evacuated to a pressure of $\leq 10^{-5}$ Torr. The relevant inner cryostat windows for PTIS are thin polyethylene sealed with indium which can not withstand large pressure differentials or sudden pressure changes. The exchange gas space is flushed with helium and then filled with helium gas to a pressure of 200mbar and sealed. The isolation vacuum is pumped continuously during the measurement.

The liquid helium flows continuously from the reservoir through a transfer tube to the cryostat pumped by a helium pump. The sample is cooled through the helium exchange gas which has a high thermal conductivity. The complete cooling system is shown in Fig 2.10. As an alternative to pumping the helium, pressure may be applied to the helium reservoir using dry helium gas so that the helium is "pushed" through the system. As long as the pressure is applied through a safety relief valve this is inherently safer than the pumping method. If there is a leak in the system air can be sucked into the system by the pump where it will freeze. This can lead to the formation of dangerous blockages.

Coarse temperature control is achieved by adjusting the helium flow rate through a needle valve on the transfer tube. Fine control with a stability of ± 0.1K is achieved by a Cryovac TIC 201 PDI temperature controller. The controller monitors the cryostat temperature through a carbon resistor and thermistor.

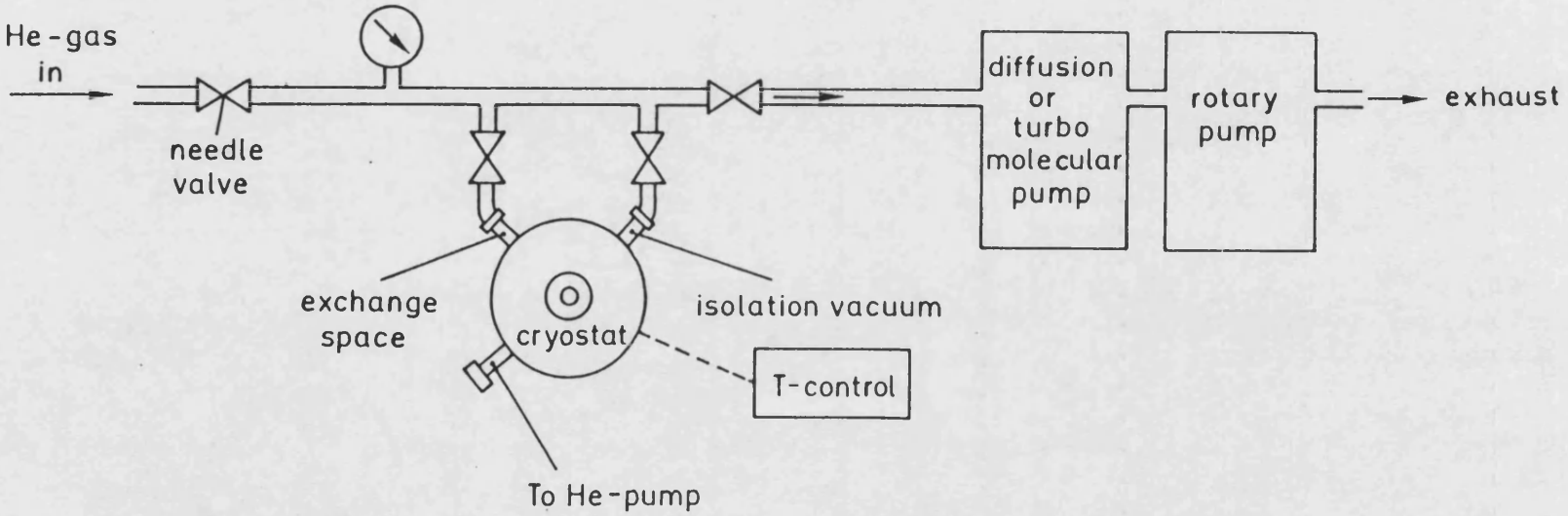

Fig 2.9: Arrangement of cryostat vacuum and He exchange gas lines.

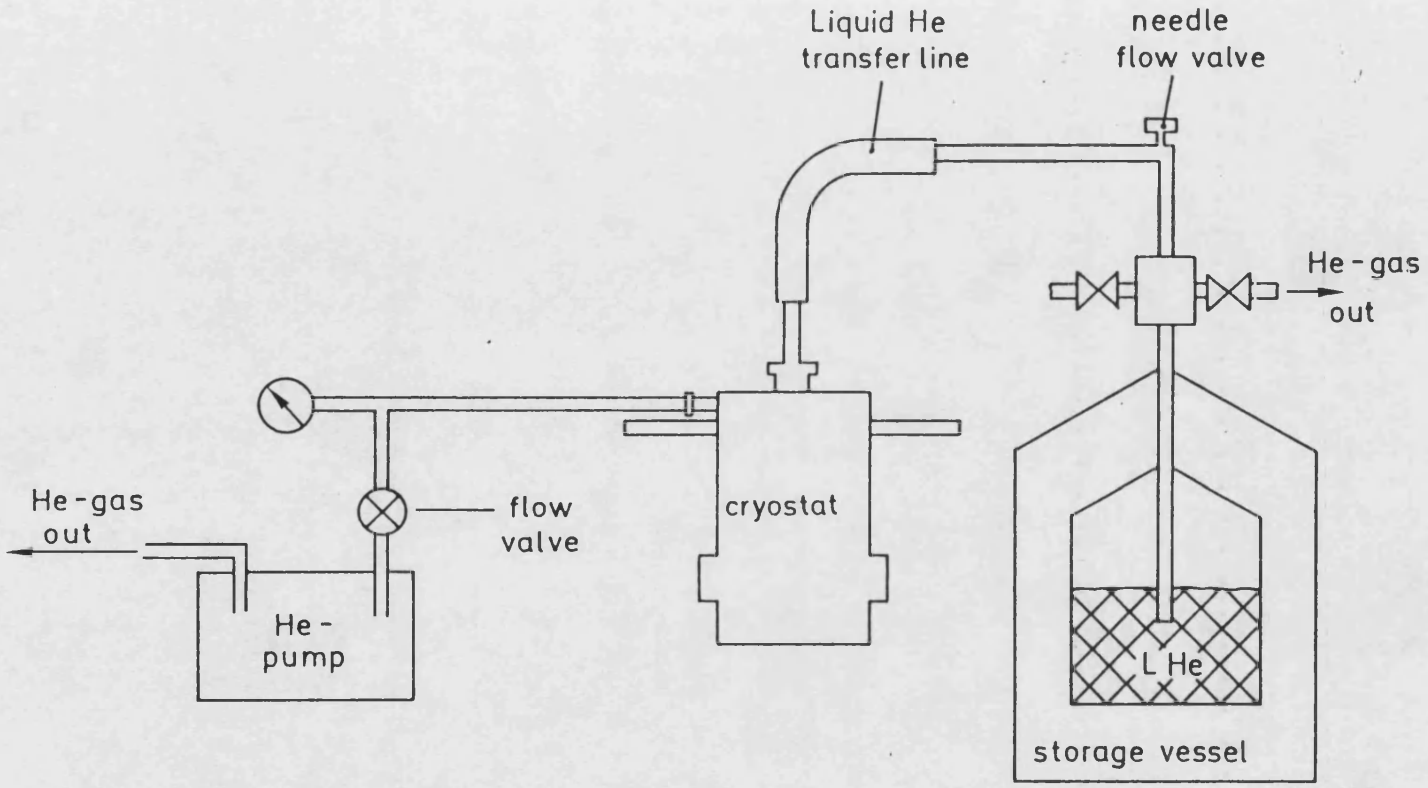

Fig 2.10: Arrangement of a He continuous flow cryostat.

2.10.2 Application of the bias voltage

The bias voltage is applied to the sample either by a simple resistor and battery arrangement (Fig 2.11) or a transconductance amplifier (McMurray, 1985). The transconductance amplifier (Fig 2.12) has the advantage that as well as applying the bias voltage this circuit also acts as a low noise amplifier of the PTIS response. The disadvantage of this circuit design is that that only a maximum of 2V can be applied to the sample, this is optimum for Ge and GaAs (bias voltage $\sim$ 1V) but not for silicon (bias voltage $\sim$ 6V). The sample is connected to the bias voltage circuit through fine insulated copper wires inside the cryostat and individually shielded cables outside the cryostat. Good earthing of the system and screening are paramount as the main source of signal disturbance is pick-up and 50Hz noise. The working current is often only of the order of 10^{-11}A and therefore a very clean electronic system is required.

Both circuits monitor the voltage across the sample. The PTIS response is seen as an a.c. voltage fluctuation mounted on the d.c. bias voltage.

2.10.3 Measurement control and signal processing with the Double Beam Fourier Transform Spectrometer

In the DBFTS the PTIS response is modulated at the same frequency as the chopped input radiation and is separated from the d.c. bias by a PAR 124 A lock-in amplifier whose reference is taken directly from the chopper (172 Hz) by a photodiode arrangement. A Hewlett-Packard 3455A digital voltmeter measures the amplified PTIS response in volts and is linked directly to a Hewlett-Packard 9358A microcomputer and a chart recorder.

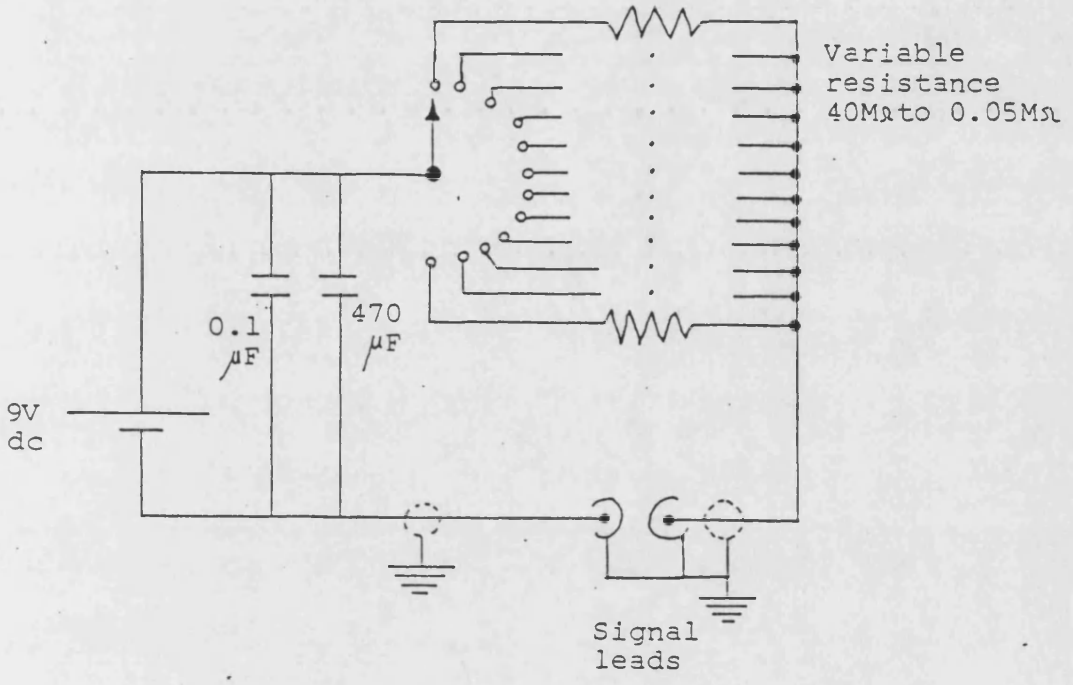

Fig 2.11: Simple battery and resistor arrangement for PTIS.

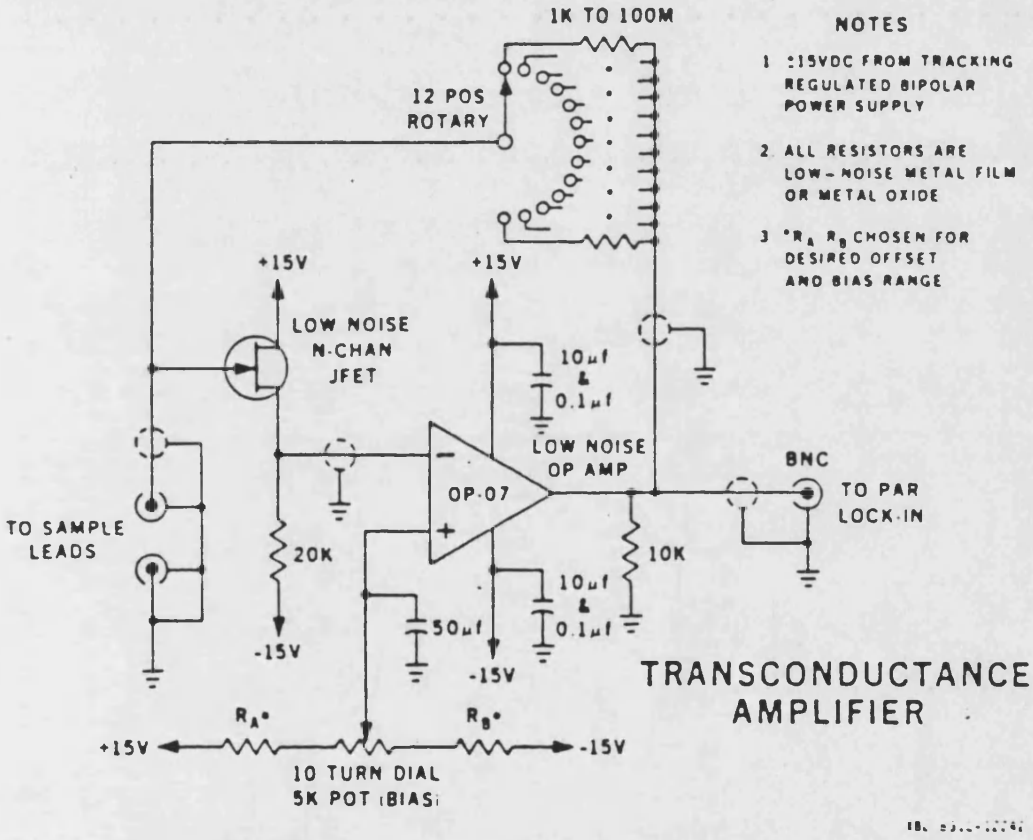

Fig 2.12: Transconductance amplifier after McMurray (1984).

The DBFTS is completely computer controlled. An overview of the system hardware is shown in Fig 2.13. The HP 9358A microcomputer controls the movement of the moveable mirror through an intelligent micro-processor unit, reads the data from the digital voltmeter and after processing it stores it on floppy disk as a raw interferogram data file and a spectrum file. Through the computer these may then be plotted in a variety of formats.

The use of a separate micro-processor unit for controlling the moveable mirror increases the speed with which commands concerning the mirror can be carried out. For example to bring the mirror to its initial position through the computer requires 5 minutes, through the controller a few seconds.

The measurement cycle showing the interaction between the computer, digital voltmeter and micro-processor mirror stepper motor controller is presented schematically in Fig 2.14. Firstly the measurement program is selected from a menu of programs. This program interactively asks for all the information required for the measurement which includes software parameters such as file names and apodization function and hardware parameters such as the lock-in amplifier time constant and sensitivity settings. The moveable mirror is then moved to its starting position far away from the white light position by the micro-processor motor controller. The main program then loads a complete program to the micro-processor. This program is in two parts. The first part is executed immediately and causes the micro-processor to send a high-low trigger to the digital voltmeter. This tells the digital voltmeter to send a service request to the computer. The service request initiates a software interrupt. In a service routine the data from the digital voltmeter is read and the necessary variables such as measurement point number etc. are updated. Before proceeding a check is conducted to see if the measurement cycle is complete. If

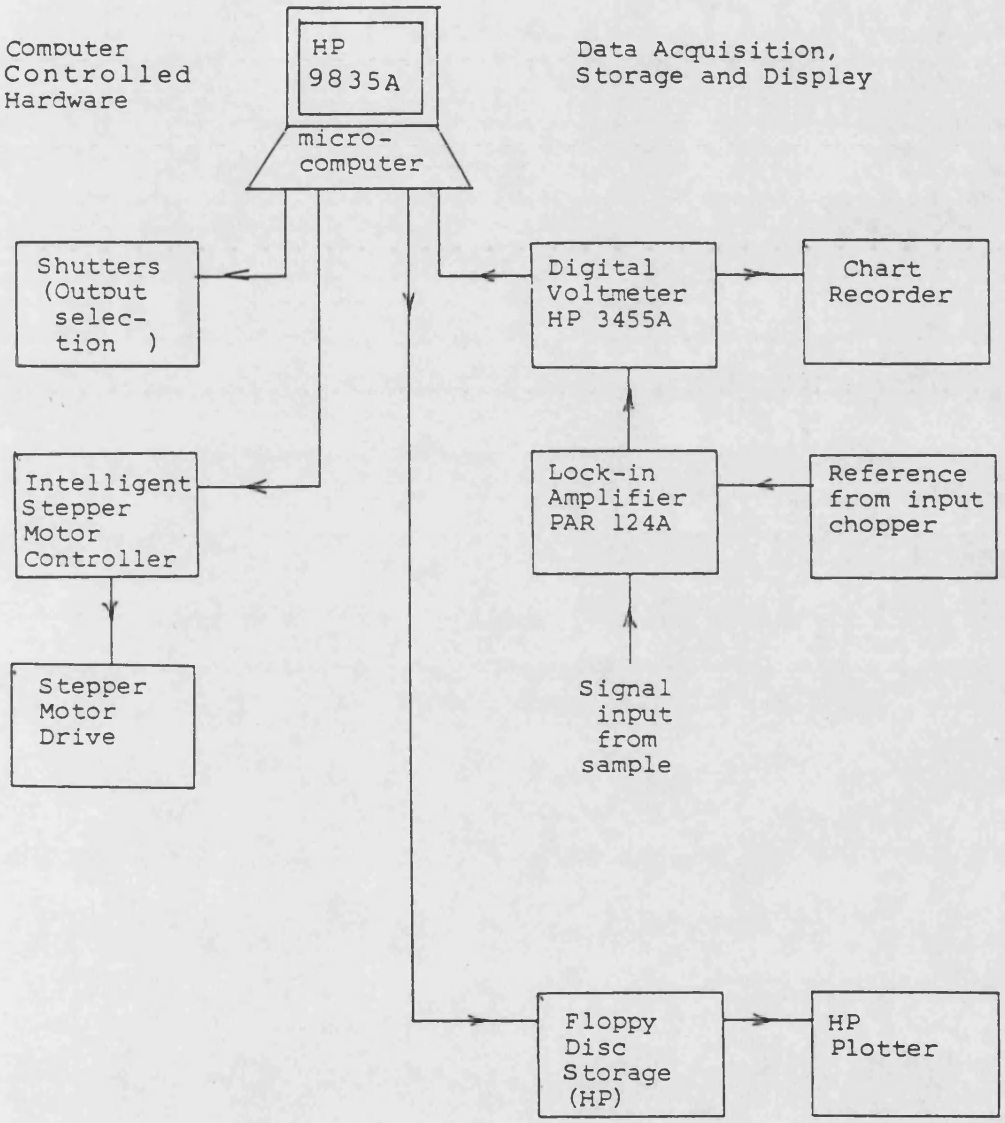

Fig 2.13: A schematic outline of the computer control of the DBFTS through a microcomputer and external devices.

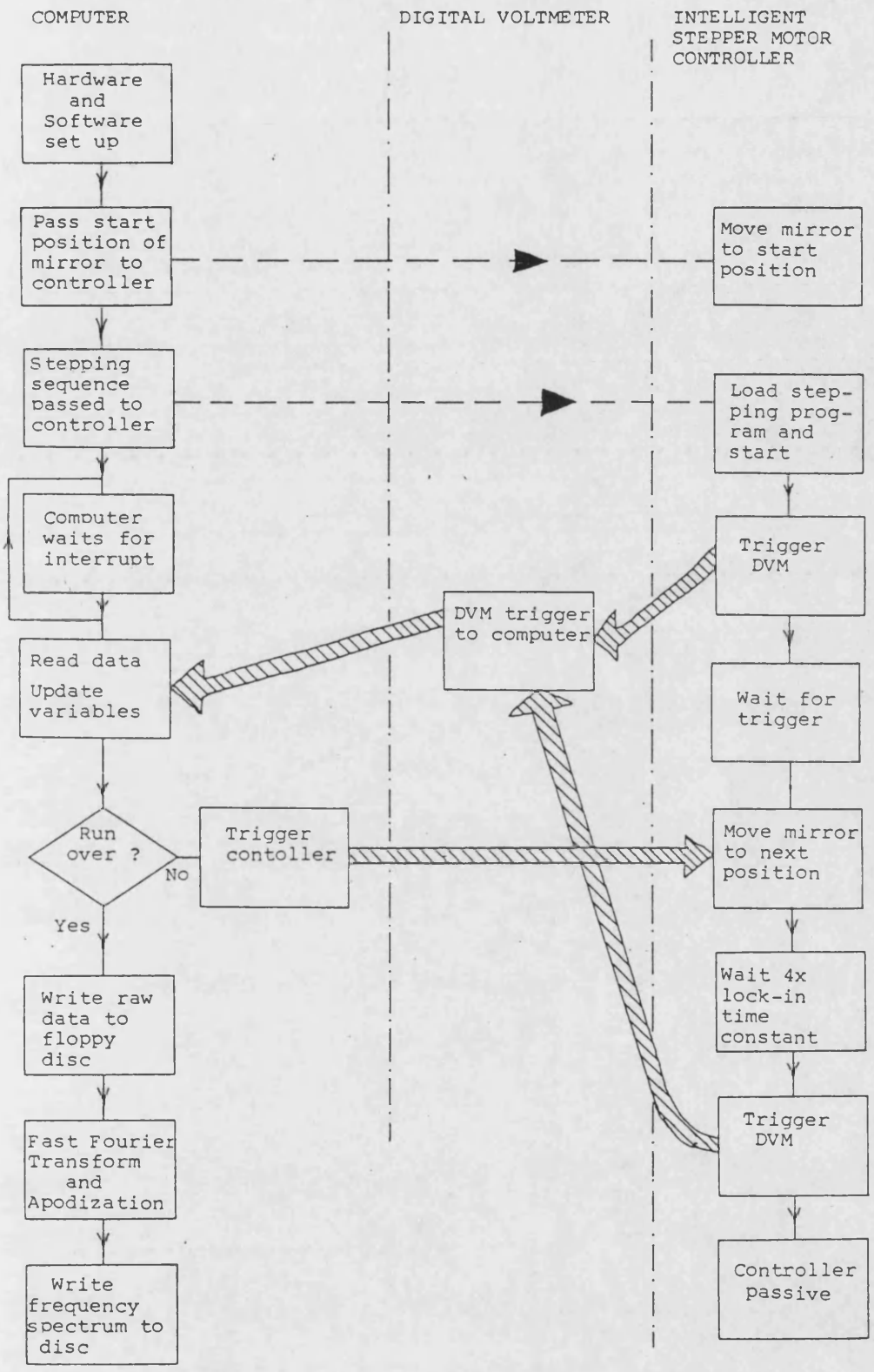

Fig 2.14: A schematic view of the DBFTS measurement program on the microcomputer and its interaction with the digital voltmeter and intelligent stepper motor controller.

there are more data points to be measured then a restart command is sent to the micro-processor which initiates the second part of the loaded program.

The micro-processor moves the mirror to the next measurement position, waits for a collection time of four times the lock-in amplifier time constant and then sends a trigger to the digital voltmeter. On this trigger the digital voltmeter and computer interact as before. Once the data has been read the computer triggers the mirco-processor controller to move the mirror to the next measurement position.

When all points have been taken the interrupt service routine returns control to the main program. The raw data is stored on disc. It is then corrected, manipulated into a file containing 2^n points, where n is any integer, with the white light position at the centre. The data is then apodized, Fourier transformed and phase corrected to obtain the frequency spectrum which is then also stored on disc. A Cooley-Tukey Fast Fourier Transform algorithm is used (Cooley and Tukey, 1965).

2.10.4 Measurement control and signal processing with a fast-scan Fourier Transform Spectrometer

In the case of a fast-scan FT spectrometer the PTIS response is modulated within a given band of frequencies according to the wavenumber range and the mirror velocity as discussed in section 2.5. The voltage across the sample is measured by a band-pass a.c. coupled EG & G (PARC) model 113 (battery powered) pre-amplifier which is set to pass only those modulation frequencies which are expected from the beamsplitter and filter characteristics e.g. for a measurement of a spectrum between 4000cm^{-1} and 400cm^{-1} with a mirror velocity of 0.2cm/sec the maximum modulation frequency is 1600Hz and the

minimum modulation frequency is 160Hz.

The amplification factor is set so that a signal of the order of 1V is given at the amplifier output. This signal is then fed directly to the Bruker IFS 113v detector input. It is then handled exactly as the normal detector input by the spectrometer.

The Bruker IFS 113v is a self-contained spectrometer. A diagram of the interaction between the Bruker computer and other apparatus is shown in Fig 2.15. From the keyboard the source, filter and beamsplitters may be selected. Also the speed of the mirror may be set and electrical filters are defined. A graphics screen allows the display of the interferogram in real time. After the completion of a user defined number of scans the interferogram is apodized and fast Fourier transformed. The interferogram or computed spectrum may then be displayed on the graphics terminal or plotter once data collection is complete. Data is stored internally on a Winchester disc from where files may be transferred to floppy disc for permanent storage.

2.11 The use of reference measurements in PTIS

In PTIS the sample is simultaneously the infrared detector. Effectively a detector characteristic is being observed. In far infrared reflection and transmission studies a sample and reference measurement is made. The reference measurement shows the intensity reaching the sample over a given spectral range. This spectrum is determined by the spectral content of the source, the effect of all filters in the system and the flatness of the detector response. By dividing the sample measurement by the reference measurement (these should be made consecutively) the effect of these parameters on the sample spectrum is

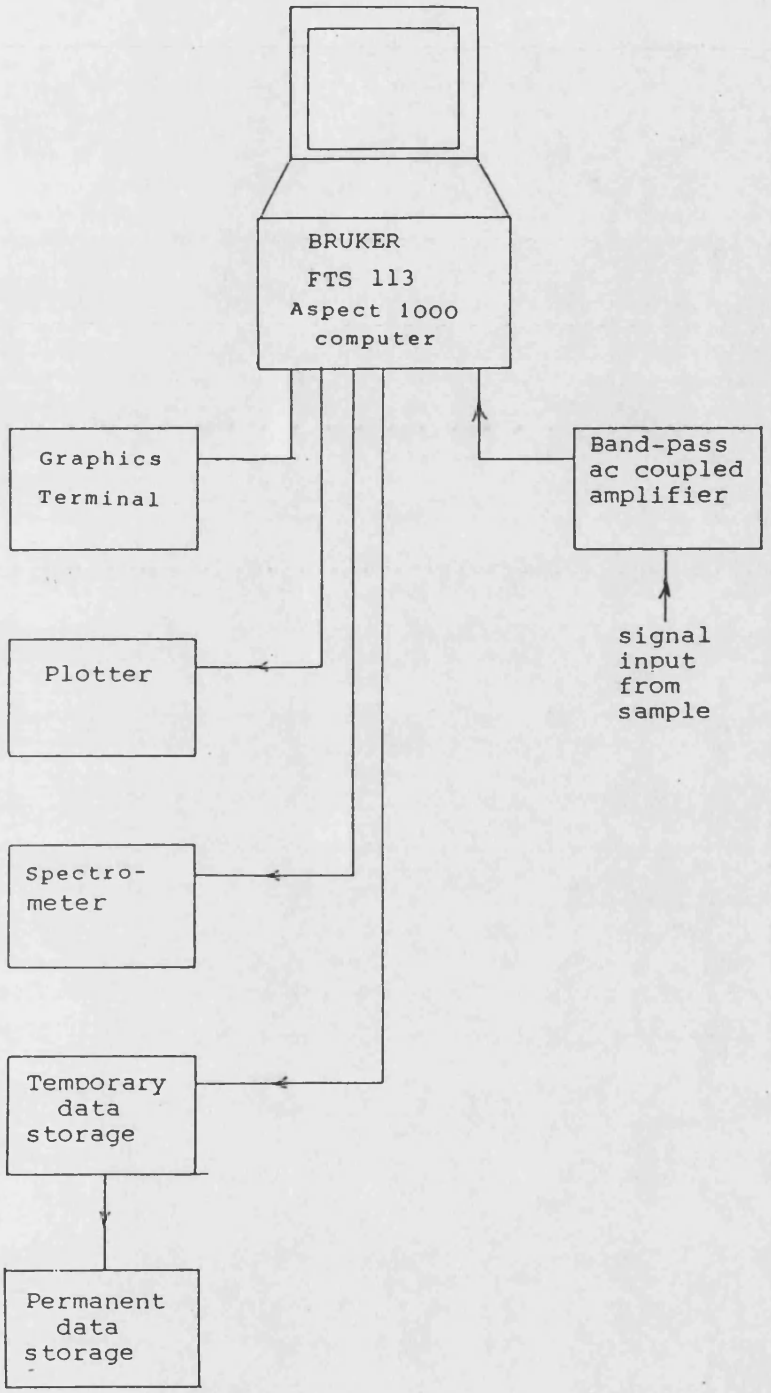

Fig 2.15: A schematic outline of the integrated computer system of the Bruker IFS 113v.

removed. Thus, the sample spectrum is normalized and the intensities of transitions in the spectrum may be compared with those of any other normalized spectrum.

In PTIS if the sample is removed it must be replaced by a detector. The reference measurement, made with a Ge bolometer for example, contains information of the spectral content of the source and filters but also of the detector itself. Dividing the PTIS spectrum by the reference gives rise to a spectrum which is in fact

$$\frac{\text{detector 1 (PTIS sample)}}{\text{detector 2 (Ge element in detector)}}$$

If the detector used to make the reference measurement were perfectly flat this would be more acceptable but practically this is not the case.

Most importantly the efficiency of the PTIS sample compared to a highly doped detector element is low and depends on the quality of the ohmic contacts, surface conditions etc. Therefore even if a perfectly flat detector were used it would not be justifable to compare the intensities in two normalized spectra.

One disadvantage of PTIS is the fact that no suitable reference exists. Each PTIS sample has its own detectivity, therefore absolute intensities in different spectra may only be compared after calibration (see section 5.3). A reference taken with a standard detector may be some assistance in identifying absorptions which result from the beamsplitter or filters but the limitation of the use of a reference should be recognized. The absolute intensities of transitions in the PTIS spectra from one sample taken within a short time period (thus excluding source fluctuations and degradation of contacts due to temperature cycling) may be compared with one another.

2.12 Mounting of samples

Measurements were made on p-type Ge and n-type Si. In each case, depending on the sample size and contacting arrangement different methods of mounting were used.

2.12.1 Germanium

A p-type Ge sample 7mm × 7mm × 3mm ($N_A - N_D = 10^{10}\text{cm}^{-3}$) was provided by E.E. Haller of the University of Berkeley, California, U.S.A.. The net impurity concentration was determined from Hall measurements. The 7mm × 3mm unpolished faces of the sample were implanted with boron, all other faces were polished. Good ohmic contacts were achieved by applying Ga-In eutectic and a thin pad of indium foil to the B implanted region. The sample was mounted on a mica sheet for electrical isolation. It was held against a copper contact embedded in teflon by a soft steel spring, the second contact, pressing the opposite face.

2.12.2 Silicon

The silicon samples used in these experiments were kindly provided by P. Wagner of Wacker Heliotronic, Burghausen, FRG. The samples were received after characterisation by infrared spectroscopy for oxygen (1106cm^{-1} local mode of O_i) and carbon (605cm^{-1} local mode). The net impurity concentration was determined from resistivity measurements.

The sample preparation and contacting for silicon samples is discussed at the beginning of each investigation. Those samples of dimensions ~ 10mm × 10mm × 2mm were mounted on a bayonet holder as shown in Fig 2.16 for the

Leybold-Heraeus cryostat. Electrical isolation was achieved by a sheet of mica between the sample and cryostat. The fine wires from the sample contacts were soldered to diagonally placed electrically isolated soldering points. A small amount of vacuum grease retained the sample in positon.

2.13 Photothermal Ionisation Spectroscopy of ultra-pure Germanium

In order to test and perfect the PTIS system an ultra-pure p-type Ge sample with a net carrier concentration, $N_A - N_D = 10^{10}\text{cm}^{-3}$ supplied by E. E. Haller, Lawrence Berkeley Laboratory, University of California, U.S.A. was measured. The PTIS spectrum obtained by Haller for this sample at 6.5K is shown in Fig 2.17. The notation of the transitions is after Jones and Fisher (1965). The hydrogenic series of transitions due to aluminium and a hydrogen-carbon acceptor complex are observed, weak transitions arising from the boron implanted region are also seen. The PTIS spectrum of this sample measured on the DBFTS at 4K, using two inputs and 0.1cm^{-1}, resolution is shown in Fig 2.18. All the transitions observed by Haller are observed in this spectrum and the signal-to-noise ratio is comparable. The linewidth of the transitions is 0.35cm^{-1} compared to 0.2cm^{-1} in Haller's spectrum. Also absorptions due to water vapour are observed in the spectrum indicating the spectrometer is not satisfactorily dried. The broader line width indicates some residual stressing of the sample possibly due to cooling the sample too quickly or due to an imperfect mounting of the sample.

The Ge sample was also measured on the Bruker IFS 113v. The PTIS spectrum measured using this spectrometer is shown in Fig 2.19 with 0.2cm^{-1} resolution at 10K. An additional capacitive filter with a cut-off of 100cm^{-1} was used

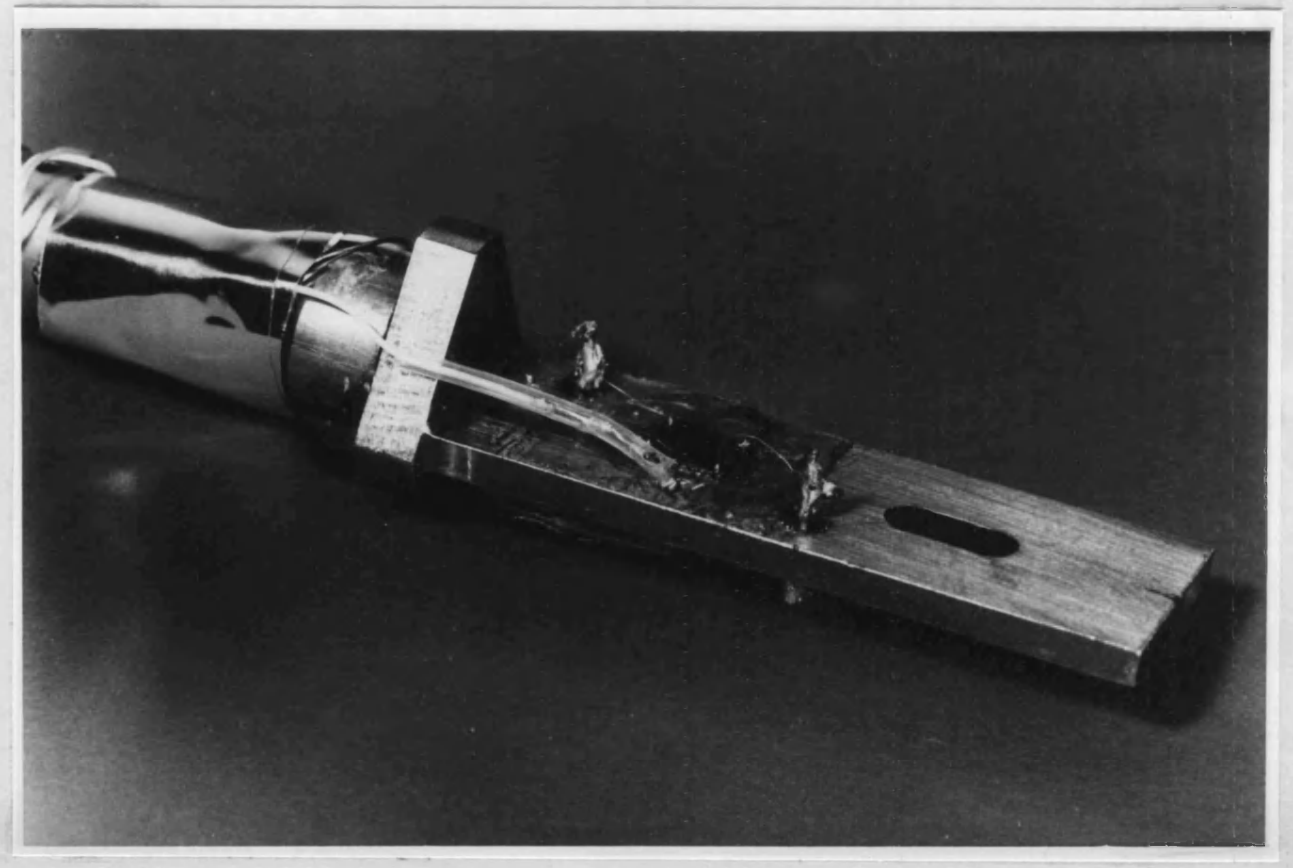

Fig 2.16: The bayonet sample holder of the Leybold-Heraeus evaporation cryostat showing a mounted sample.

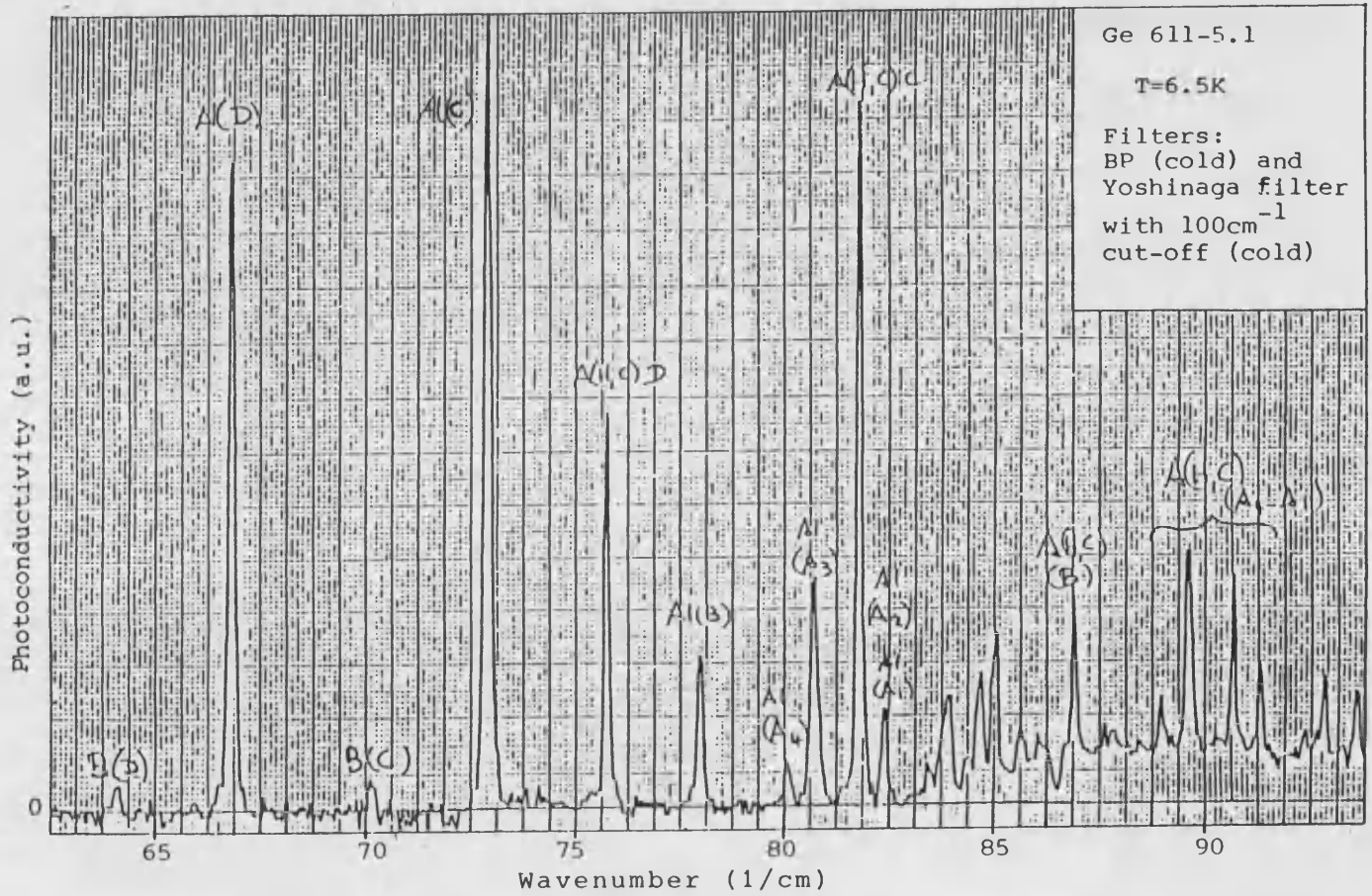

Fig 2.17: The PTIS spectrum of p-type Ge 611-5.1 ($N_A - N_D = 10^{10}\text{cm}^{-3}$) measured by E. E. Haller, Berkeley, University of California, U.S.A. showing Al and B acceptors and a hydrogen-carbon acceptor complex A(H,C). Notation after Jones and Fischer (1965). The spectrum is shown as received from E. E. Haller.

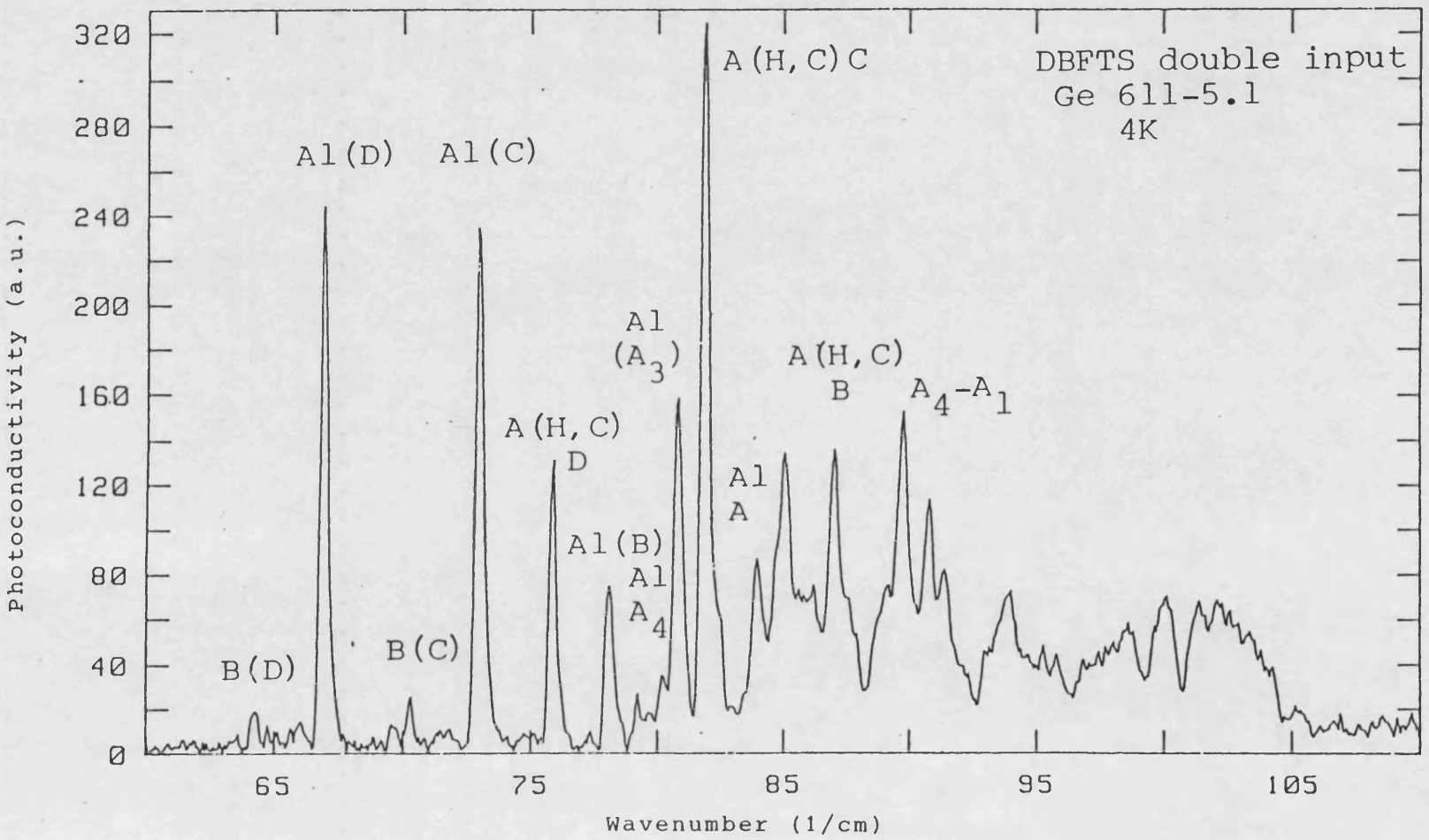

Fig 2.18: The PTIS spectrum of Ge 611-5.1 at 4K measured on the DBFTS in the double input mode.

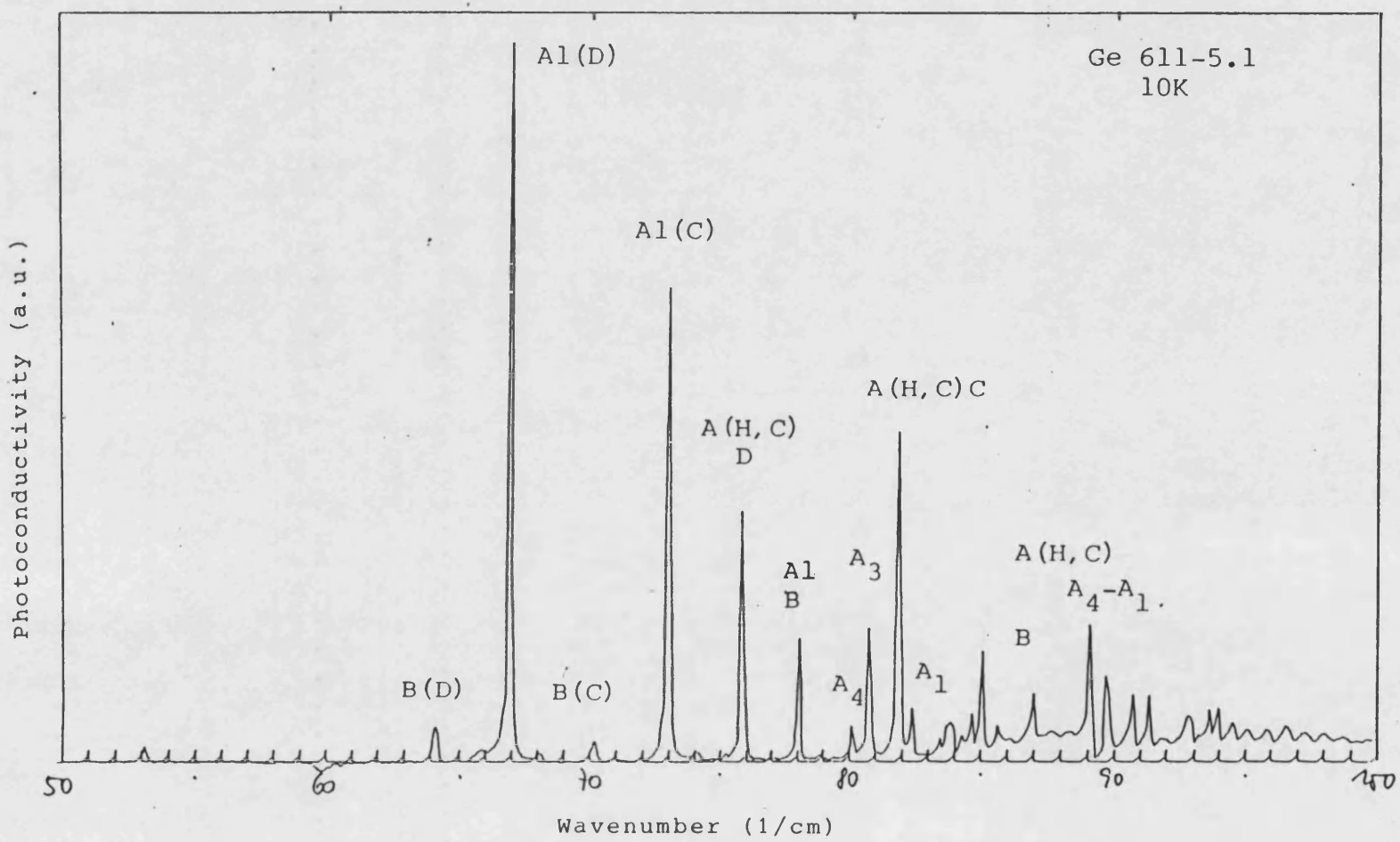

Fig 2.19: The PTIS spectrum of Ge 611-5.1 measured on the Bruker IFS 113v at 10K.

to limit the spectral range. In this spectrum all the transitions observed by Haller are clearly visible and the linewidth is determined by the instrumental linewidth. The signal-to-noise ratio in this spectrum is excellent and surpasses that of both Haller's system and the DBFTS. This may be attributed to a more simple and compact signal collection system. A summary of the peak positions observed by Haller, in the PTIS spectra measured in the single input and double input modes of the DBFTS and on the Bruker IFS 113v is given in Table 2.2. A very good level of agreement is achieved , particularly comparing Haller's data and that of the Bruker IFS 113v.

It can be concluded it is possible to carry out PTIS successfully on both the stepping and fast-scan spectrometers. Both systems have matched the sensitivity required to measure ultra-pure semiconductors achieved by other groups. Further experiments on ultra-pure Ge have been carried out in collaboration with E. E. Haller (see Appendix A).

Observed Transition		Haller 6.5K	Single Input DBFTS 4K	Double Input DBFTS 4K	Bruker FTS 113 10K
Notation		Peak position / cm^{-1}			
Boron:	B(D)	64.09	64.29±0.3	64.21±0.1	64.14±0.1
	B(C)	70.12	70.28	70.32	70.16
Aluminium:	Al(D)	66.80	66.98	66.93	66.98
	Al(C)	72.82	73.06	73.05	72.82
	Al(B)	77.96	78.03	78.08	78.00
	$Al(A_4)$	80.07	79.23	80.19	80.05
	$Al(A_3)$	80.67	80.82	80.84	80.65
	$Al(A_1)$	82.36	-	82.49	82.34
Hydrogen -Carbon Complex	A(H,C)D	75.76	75.90	75.88	75.71
	A(H,C)C	81.75	81.92	81.96	81.74
	A(H,C)B	86.85	87.00	87.09	86.92
	$A(H,C)A_4$	88.88	89.00	89.18	88.97
	$A(H,C)A_3$	89.56	89.69	89.76	89.58

Table 2.2: A comparison of the transition energies obtained from all measurements made by PTIS on the p-type Ge sample 611-5.1. The error for all transitions is indicated at the top of the column in each case.

Chapter 3

Investigation of the thermally formed donors present in undoped oxygen-rich silicon after a 450°C anneal

The Thermal Donors have been extensively characterised by photoluminescence, DLTS, EPR and infrared transmission measurements. In particular the ionisation energies of the excited states and the groundstate of nine distinct donors in the neutral and singly ionized state have been experimentally observed by infrared transmission measurements, line assignments being made by comparison to the theoretical predictions of the effective mass theory for shallow donors in silicon (section 1.6).

PTIS measurements on Cz-silicon annealed at 450°C should display all those features observed in infrared transmission measurements. However PTIS has greatly increased sensitivity compared to infrared transmission (factor 10^5) and therefore the potential exists to detect very weak transitions involving fewer carriers which are normally undetectable.

3.1 Sample preparation

The starting material was high-resistivity undoped n-type Cz-silicon. The net free carrier concentration was estimated from room temperature resistivity measurements to be $|N_D - N_A| \simeq 4 \times 10^{12}\text{cm}^{-3}$, where N_D and N_A denote the donor and acceptor concentrations respectively. Two identical discs 12mm in diameter and 2mm thick were cut from the material. The samples were pre-annealed in nitrogen at 770C for 10 minutes to destroy any TD formed during the growth process and bring the material to a common initial state. They were then heat treated in nitrogen at 450°C, sample 1 for 4.5 hours and sample 2 for 15 minutes. The final net donor concentrations were $\simeq 8 \times 10^{14}\text{cm}^{-3}$ for sample 1 and $\simeq 5 \times 10^{13}\text{cm}^{-3}$ for sample 2. These values were obtained from electrical resistivity measurements after annealing.

Electrical contacts with good ohmic properties were prepared by vapour deposition and laser annealing. The contacts are a 200$\mathring{A}$ layer of Sb capped by a 3000$\mathring{A}$ layer of Au laid down in parallel strips 1mm wide and 10mm apart on a circular polished face of the sample. As no further heat treatment of the samples was possible a Nd-YAG laser was used in the pulsed mode to laser anneal a series of points along each strip. Such contacts give satisfactory results even at low temperatures. It was found that contacts degenerate with time due to temperature cycling and they were therefore periodically renewed. A fine silver coated copper wire was bonded to each gold contact using silver conducting paint.

3.2 Far Infrared Transmission measurements

Both samples were measured in infrared transmission at 5K using a Bruker IFS 113v spectrometer.

The normalised transmission spectrum of sample 1 at 5K at a resolution of 0.25cm^{-1} is shown in Fig 3.1. In this sample, annnealed for 4.5 hours, transitions arising from all nine previously reported neutral TD are observed in the spectral region 330 - 550cm^{-1} with an intrinsic linewidth of 3-4cm^{-1}. This is consistent with the results on the Thermal Donor kinetics (Wagner et al, 1984) which predict the detectable presence of all species after such a length of time. No transitions arising from singly ionised TD centres are observed. At 5K in originally n-type material it is to be expected that the Fermi level is pinned to the neutral TD, or even shallower donors, the singly ionised state can only be observed by depopulating the neutral state thermally or with strong illumination. No previously unreported features are observed in this spectral region.

Transitions due to phosphorus, known to be the major residual donor impurity in silicon, are observed at 316.7, 343.7, 352.4 and 357.0cm^{-1} corresponding to the $1s(A_1) \rightarrow 2p_{\pm}$, $1s(A_1) \rightarrow 3p_{\pm}$, $1s(A_1) \rightarrow 4p_{\pm}$, and $1s(A_1) \rightarrow 5p_{\pm}$ transitions (Ramdas and Rodriquez, 1981) respectively. Using the calibration factor for phosphorus in silicon given by Baber (1980) the strength of the $1s \rightarrow 2p_{\pm}$ transition corresponds to a concentration of $\sim 1.9 \times 10^{13}$cm^{-3}.

Three very small features which could not be identified from the infrared transmission alone were observed at 241, 248, and 252cm^{-1} which were later assigned to transitions of the Shallow Thermal Donors observed in PTIS as will be discussed later.

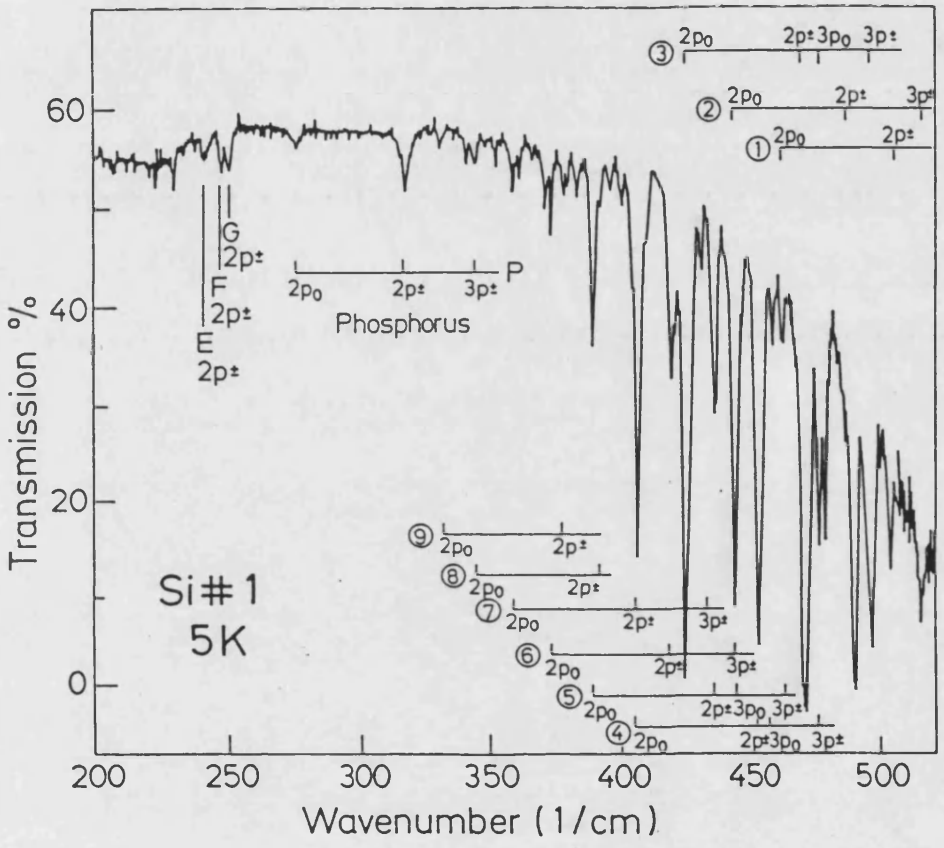

Fig 3.1: The transmission spectrum of Cz-silicon sample 1 annealed for 4.5 hours at 450°C at 0.25cm^{-1} resolution. The hydrogenic series of transitions associated with the TD (e.g. (1) =TD1), P and the $1 \rightarrow 2p_{\pm}$ transitions of STD E,F, and G are observed. All transitions are from the 1s groundstate into the given excited state.

The normalised transmission spectrum of sample 2 at 5K and 0.25cm^{-1} resolution is shown in Fig 3.2. Due to the shorter annealing time of only 15 minutes, Thermal Donors TD1, TD2 and TD3 are predominant in this sample. The intrinsic linewidth is 3-4cm^{-1}. The transitions of phosphorus are observed and the concentration is estimated to be $\sim 1.3 \times 10^{13}$cm^{-3}. Small features are also observed at 241, 247 and 250cm^{-1} which were assigned to the Shallow Thermal Donors.

3.3 PTIS measurements

The PTIS measurements of samples 1 and 2 are shown in Fig 3.3 and Fig 3.4 at 15.5K and a resolution of 0.5cm^{-1}. The experiment was conducted on the Bruker IFS 113v rapid scan spectrometer. The applied bias voltages were 6.8v and 6.5v respectively.

Both PTIS spectra show a broad continuum beginning at $\sim$ 210cm^{-1} (26meV) with broad minima at $\sim$ 370cm^{-1} and 620cm^{-1} due to the cryostat window material and at 545cm^{-1} in Fig 3.3 and 620cm^{-1} in Fig 3.4 due to the interferometer beamsplitter. The signal intensity is given in arbitrary units and is directly proportional to the measured photoconductivity without relation to any reference measurement. The problem of taking a suitable reference measurement was discussed in section 2.11.

The background continuum extending from 210cm^{-1} to 650cm^{-1} and beyond, results from the direct photo-ionisation of electrons from the groundstate into the conduction band. In the region below 400cm^{-1} several extremely sharp peaks resulting from the photothermal ionisation process are clearly visible in both samples. The experimental conditions have been optimized for the

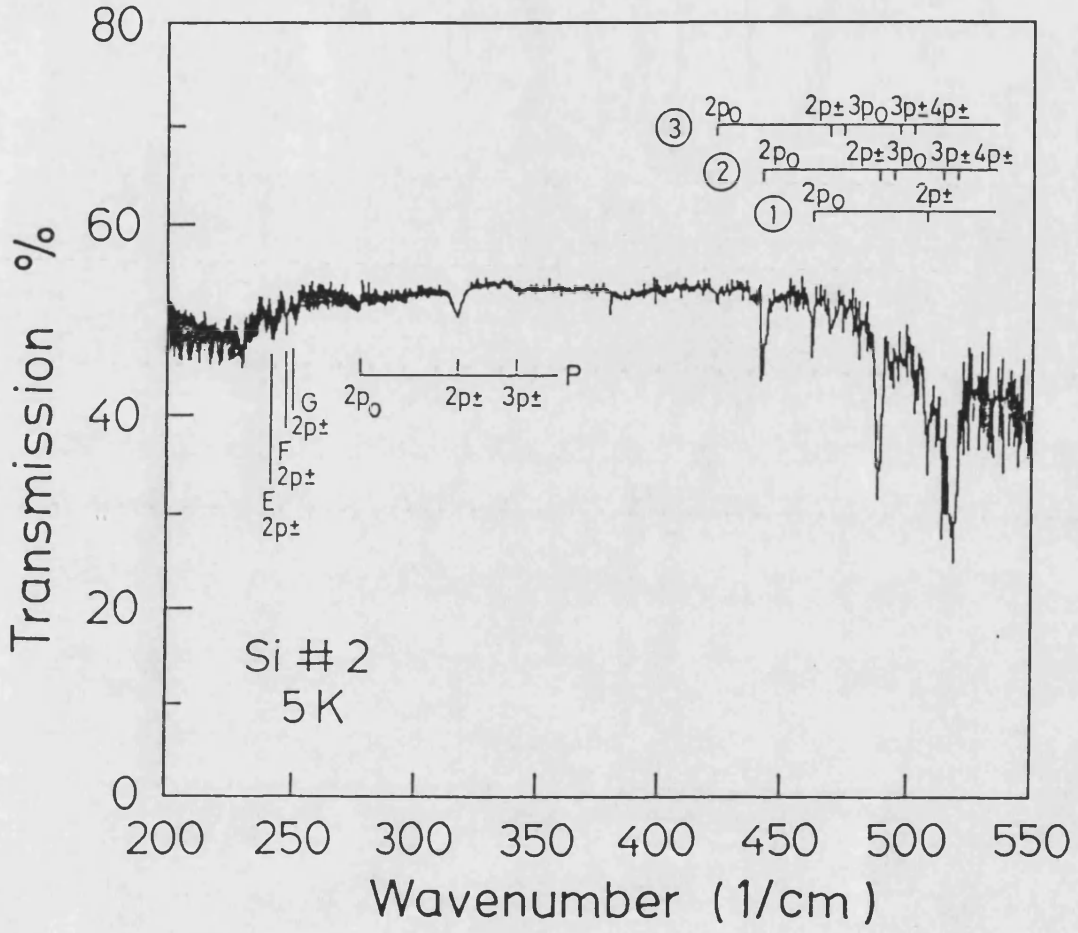

Fig 3.2: The transmission spectrum of Cz-silicon sample 2 annealed for 15 minutes at 450°C at 0.25cm^{-1} resolution. The hydrogenic series of transitions associated with the TD (e.g. ① =TD1), P and the $1s \rightarrow 2p_{\pm}$ transitions of STD E,F, and G are observed. All transitions are from the 1s groundstate into the given excited state.

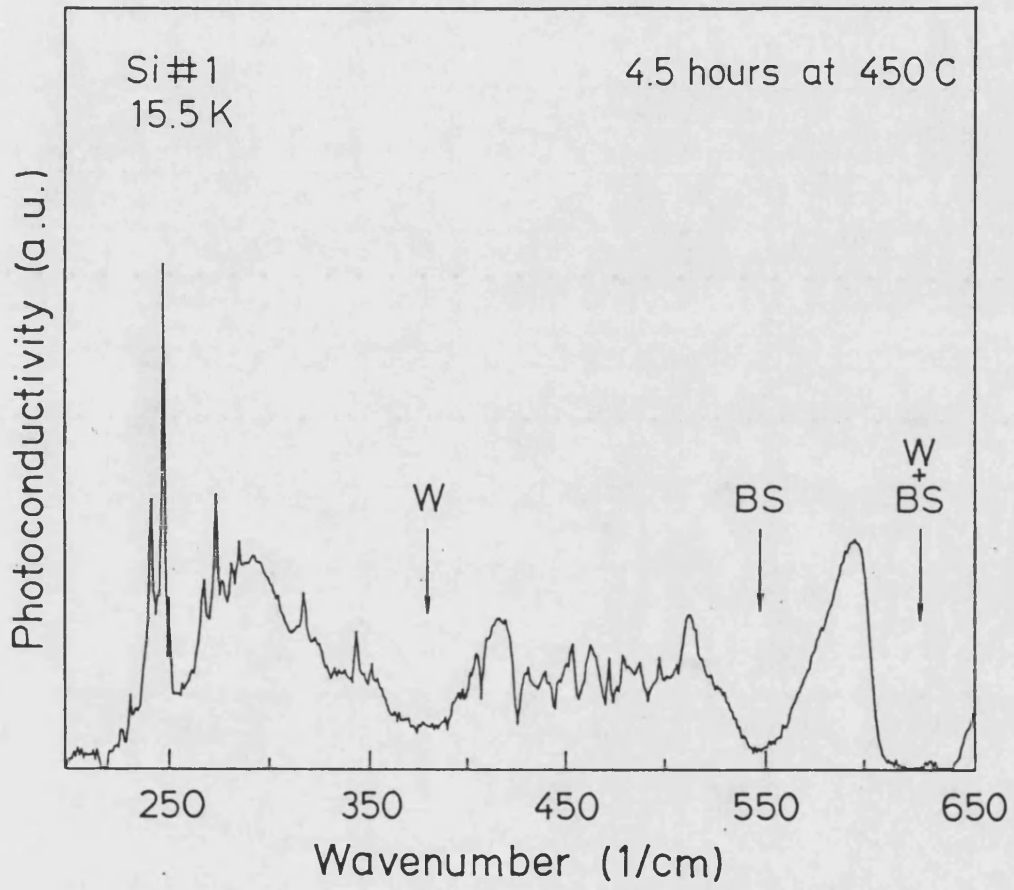

Fig 3.3: The PTIS spectrum of sample 1 at a resolution of $0.5cm^{-1}$. Broad minima due to absorptions by the window material (W) and the beamsplitter characteristic (BS) are indicated.

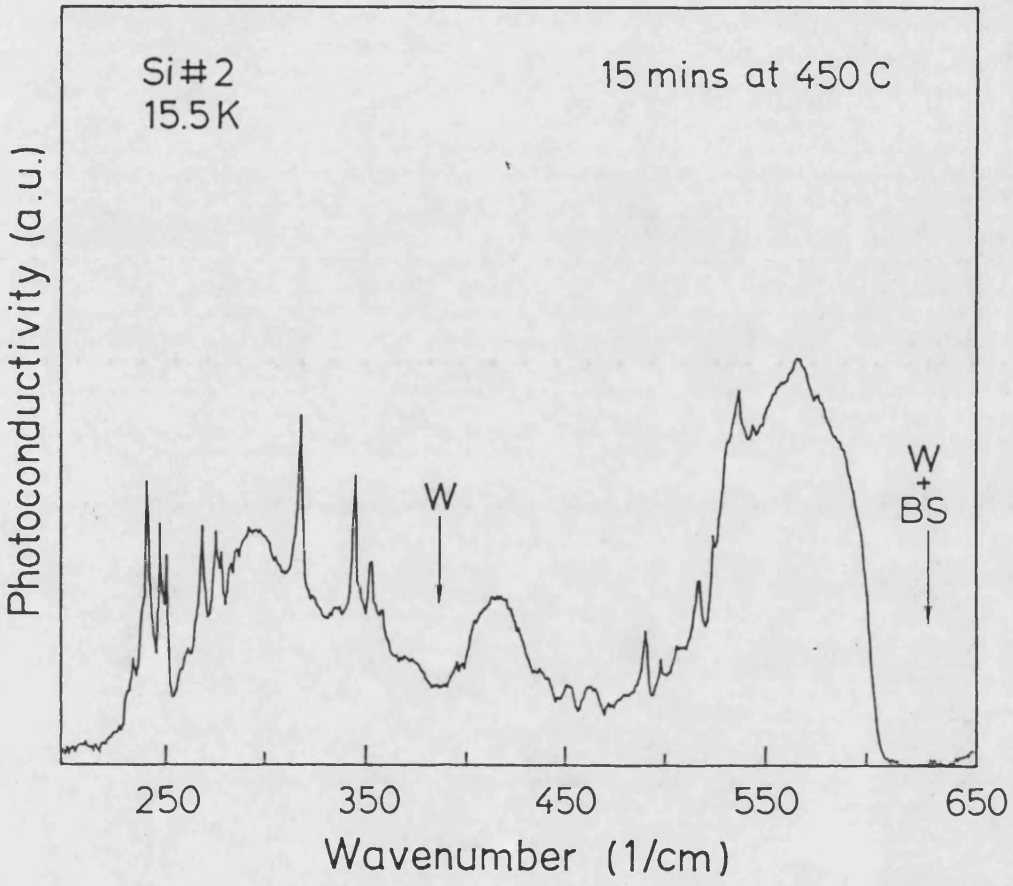

Fig 3.4: The PTIS spectrum of sample 2 at a resolution of $0.5cm^{-1}$. Broad minima due to absorptions by the window material (W) and the beamsplitter characteristic (BS) are indicated.

spectral region below 400cm^{-1}.

For sample 1 many sharp minima are observed in the continuum in the spectral region 400cm^{-1} - 500cm^{-1}. In contrast, for sample 2 peaks are seen in this region. These features also result from the photothermal ionisation process. The observed features in the spectral region above 400cm^{-1} arise from the TD. This region of the spectrum will be discussed in detail in the following section. The TD are observed clearly in infrared transmission and PTIS and therefore the information gained by the two methods may be compared. In this way the validity of the PTIS spectra may be experimentally established. Secondly, the region below 400cm^{-1} where the sensitivity of PTIS reveals many features only weakly observed or absent in the infrared transmission spectra is discussed.

3.3.1 Thermal Donors

Firstly the spectral region most significant in the infrared transmission measurements is analysed for the case of sample 1. Detail of the spectral region 360cm^{-1} - 580cm^{-1} from the spectrum in Fig 3.3 is presented in Fig 3.5. This spectrum has been corrected to remove the absorption of the window material. The background spectrum (excluding beamsplitter absorption) was measured using a germanium bolometer (Infrared Laboratories Inc. HD2).

The minima observed in the background continuum in this spectral region may be assigned to groundstate to excited state transitions arising from the photothermal ionisation of the nine TD. As discussed in section 1.5 the phenomena of photothermal ionisation giving rise to minima is predicted under certain conditions when more than one impurity is present and is dependent on the relative concentrations of the different impurity species and the sample temperature. The background is due to the sum of the photo-ionisation

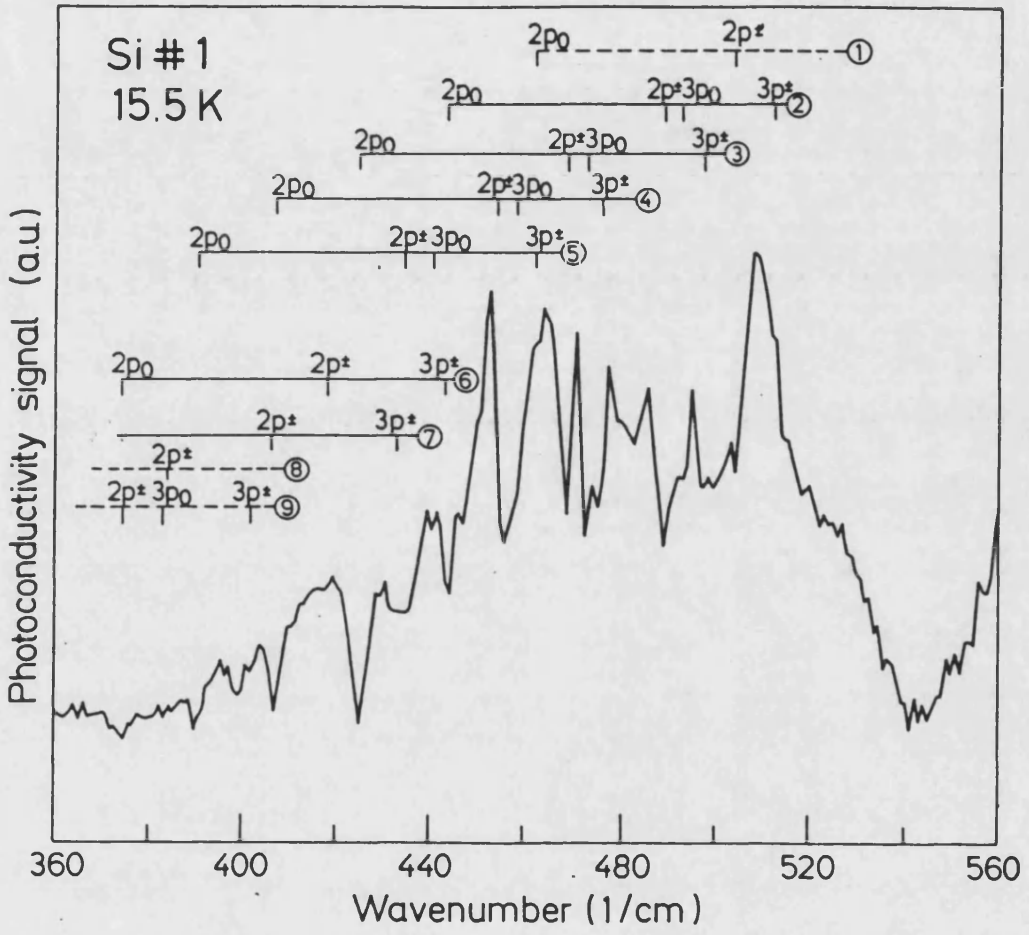

Fig 3.5: The PTIS spectrum of sample 1. The hydrogenic series of transitions of the TD are indicated. This spectrum has been corrected for the absorption of the window material.

continua of all the shallower donors present in the material. The efficiency of the thermal ionisation process for the TD at this temperature is very low such that at the frequencies corresponding to internal transitions of the TD the net photo-response is reduced. This behaviour has also been reported for the case of In and Ga acceptors in silicon (Bambakidis and Brown, 1986) and for the case of a positively charged acceptor in Ge (Herrmann et al, 1975). The transitions of the TD are observed as minima in this sample over the temperature range (4.2K - 25K) studied.

All those features observed in far infrared transmission are also observed in PTIS as expected. The transitions observed in the two spectra are summarized in Table 3.1. In PTIS the relative intensities of the transitions are different than in far infrared transmission spectra. This may be explained in that photothermal ionisation involves the probability of a photon being absorbed by an electron in the groundstate plus the thermal ionisation probability from the excited state. At any given temperature the thermal ionisation probability is increasingly large for excited states closer to the conduction band minimum. The combination of these two factors can lead to a different probability in PTIS for the transitions in comparison to far infrared transmission spectroscopy.

Further information may be won in PTIS by careful choice of window material, beamsplitter and light source to determine the photon spectrum and the choice of temperature to shape the phonon spectrum. Fig 3.6 shows a PTIS spectrum of sample 1 recorded at $0.5cm^{-1}$ resolution and $\sim$ 7K with a KRS5 window and 3.5μ beamsplitter. This optimizes the photon spectrum in the region of the TD transitions while reducing the probability of thermal ionisation from an excited state by keeping the sample very cold. As is to be expected the TD transitions now appear as far stronger minima in the photo-ionisation continuum and may

Sample 1		Sample 2		Donor species	Transition ($1s \rightarrow$)
PTIS (15.5K)	FIRT (5K)	PTIS (15.5K)	FIRT (5K)		
	275.0±0.25		275.0±0.25	P	$2p_0$
316.7±0.5	316.0	316.7±0.5	318.0	P	$2p_\pm$
	332.0	335.0		TD9	$2p_0$
343.7	341.0	343.7	345.0	P, TD8	$3p_\pm$, $2p_0$
353.4	351.5	352.4		P	$4p_\pm$
357.0	357.5	357.0		P, TD7	$5p_\pm$, $2p_0$
372.7	373.5			TD6	$2p_0$
378.5	377.5			TD9	$2p_\pm$
383.3	382.5			TD8, TD9	$2p_\pm$, $3p_0$
388.1	388.7			TD5	$2p_0$
394.8	394.5			TD8	$3p_\pm$
399.0	399.0		398.0	TD9	$3p_\pm$
405.5	405.7	403.6		TD4, TD7	$2p_0$, $2p_\pm$
416.1	417.0		416.0	TD6	$2p_\pm$
423.8	424.0	423.8		TD3	$2p_0$
428.7	429.0			TD7	$3p_\pm$
434.5	435.0	434.1		TD5	$2p_\pm$
440.3				TD5	$3p_0$
443.2	443.2	443.1	443.0	TD2, TD6	$2p_0$, $3p_\pm$
454.7	452.0			TD4	$2p_\pm$
457.6	456.0			TD4	$3p_0$
463.0	462.0	461.5		TD1, TD5	$2p_0$, $3p_\pm$
468.3	470.0	470.0	469.0	TD3	$2p_\pm$
475.0	476.0			TD3	$3p_0$
478.9	478.7	477.9	477.0	TD4	$3p_\pm$
482.7		480.8	480.0	TD4	$4p_\pm$
489.5	490.7	489.5	488.0	TD2	$2p_\pm$
497.2	497.5	496.3	496.0	TD3	$3p_\pm$
503.4	502.0	503.9	502.0	TD3	$4p_\pm$
507.0	507.0	507.8	508.0	TD1	$2p_\pm$
514.6	514.0	514.6	514.0	TD2	$3p_\pm$
		522.3	520	TD2	$4p_\pm$
		529.0		TD2	$5p_\pm$
		533.9		TD1	$4p_\pm$

Table 3.1: The electronic transitions observed in the PTIS spectra and far infrared transmission (FIRT) spectra of samples 1 and 2 annealed at 4.5 hours at 450°C and 15 minutes at 450°C respectively.

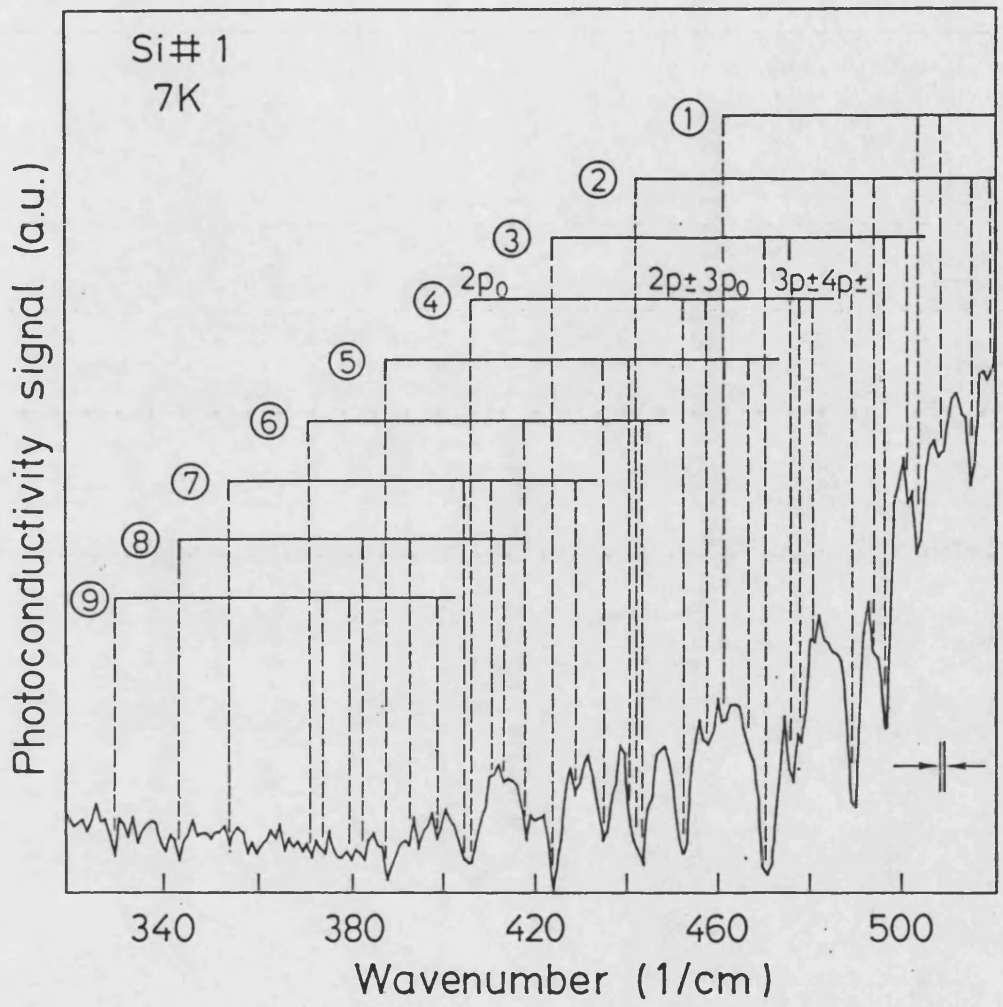

Fig 3.6: The PTIS spectrum of sample 1 at 0.5cm^{-1} resolution. The temperature, cryostat window material and beamsplitter have been chosen to enhance the depth of the minima associated with the TD transitions.

be easily assigned to the appropriate transitions. Transitions observed only weakly in Fig 3.5, for example those of TD1, emerge clearly and the $1s \rightarrow 4p_{\pm}$ transitions of the most intense series, TD1, TD2, TD3, TD4 and TD5 are now detected.

The spectral region 360cm^{-1} - 560cm^{-1} for sample 2 is presented in detail in Fig 3.7 without correction for beamsplitter and window absorptions. The PTIS spectrum of sample 2 shows little noise and the signal-to-noise ratio is comparable to that of sample 1 despite the lower donor concentration. Unlike the PTIS spectrum of sample 1 however the TD transitions appear predominantly as peaks against the continuum. From Wagner's studies of the TD growth kinetics (Wagner et al, 1984) and supported by the infrared transmission spectrum, the expected concentrations of the donors are TD1, TD2 and TD3 in decreasing order. In PTIS the transitions of TD1,TD2 and TD3 are observed and additionally TD4 is detectable consistent with this view. Here PTIS has already proved advantageous in that the TD4 transitions could be observed and the signal-to-noise ratio achieved was much improved compared to infrared transmission. The TD transitions observed by PTIS in this sample are summarized in Table 3.1 togther with those observed in infrared transmission for comparison.

In the case of sample 2 it is useful to increase the probability of PTIS, some transitions already being positive, by increasing the temperature. Hence this effect may be enhanced as shown in Fig 3.8 at 26K and 1cm^{-1} resolution. Now the transitions of TD1,TD2,TD3 and TD4 are far stronger. To improve the distinction of the shallower TD expected to be present in very small concentrations it would be necessary to reduce the temperature considerably causing their transitions to emerge as minima in the continuum.

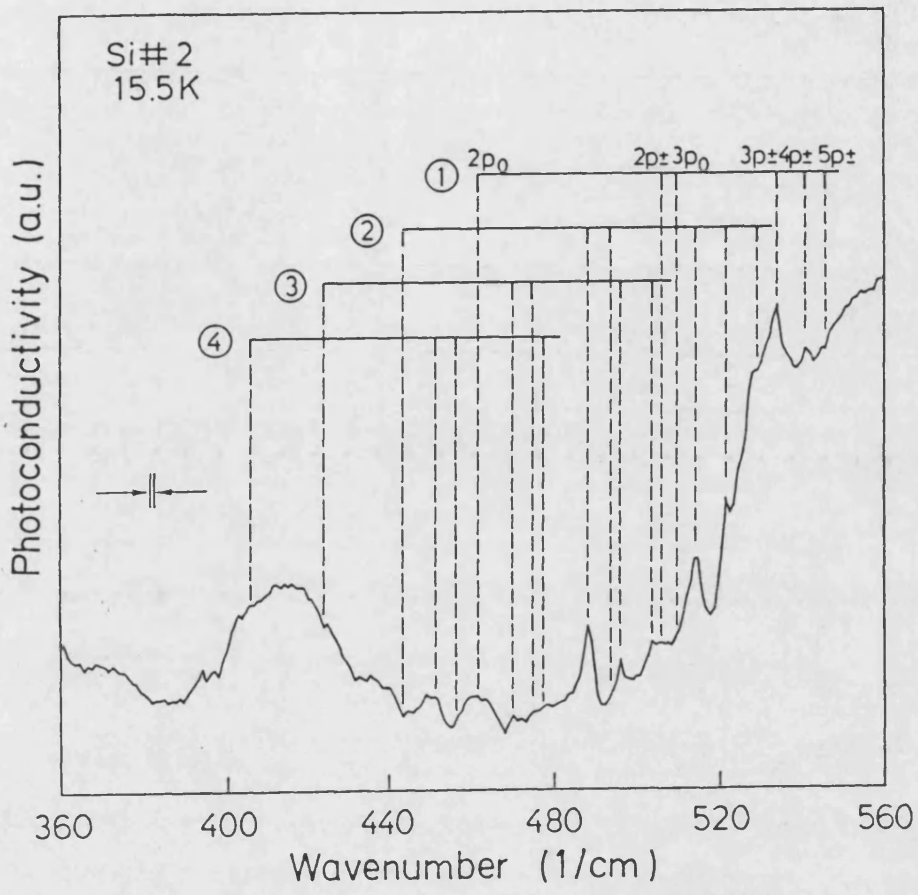

Fig 3.7: The PTIS spectrum of sample 2 at 0.5cm^{-1} resolution. The hydrogenic series of transitions of the TD are indicated.

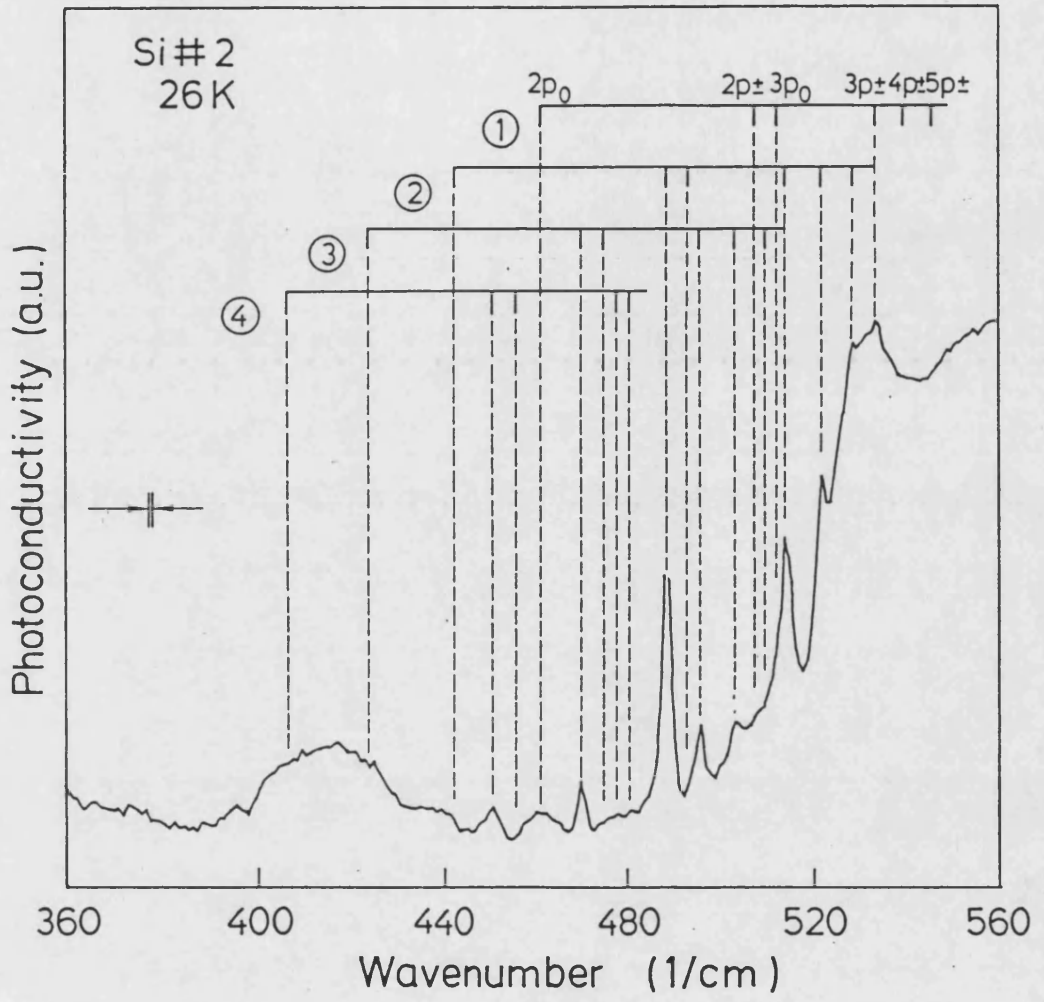

Fig 3.8: The PTIS spectrum of sample 2 at $1cm^{-1}$ resolution. The temperature has been chosen to enhance the transitions of the TD which appear mainly as peaks in this sample.

The experimental results presented above demonstrate that the technique of photothermal ionisation spectroscopy can successfully provide the same spectroscopic information about a sample as an infrared transmission measurement. The signal-to-noise ratio achieved for low concentrations of impurities is superior to that obtained in infrared spectroscopy. Further by tuning the temperature and spectral content of the illumination to optimize PTIS over a particular spectral range, even greater sensitivity is achieved. Due to this increased sensitivity the hydrogenic series of donor centres of lower concentrations may be detected and more transitions may be identified in each series.

3.3.2 Shallow Thermal Donors and Phosphorus

The spectral region below 380cm^{-1} in Fig 3.3 and Fig 3.4 is shown in detail in Fig 3.9 and Fig 3.10 for samples 1 and 2 respectively. The experimental conditions are optimized for this region of the spectrum. The transitions arising from phosphorus, already identified in the infrared transmission spectra, are observed as sharp peaks in the PTIS spectra in both cases. Most striking however are the very sharp peaks at lower energies which occur at the onset of the continuum. Only the very strongest of these transitions are to be detected, barely above the noise level, in the infrared transmission spectra.

Firstly considering the spectrum of sample 1, these new transitions appear to occur in two groups, one group at approximately 240cm^{-1}, the second at approximately 270cm^{-1}, that is a separation of the order of 30cm^{-1}. The effective mass theory predicts a separation of 26cm^{-1} between the $1s \rightarrow 2p_{\pm}$ and the $1s \rightarrow 3p_{\pm}$ transitions of a shallow donor. On closer inspection the new transitions may be assigned according to the effective mass theory as arising from five EMT-like shallow donors referred to as the Shallow Thermal Donors

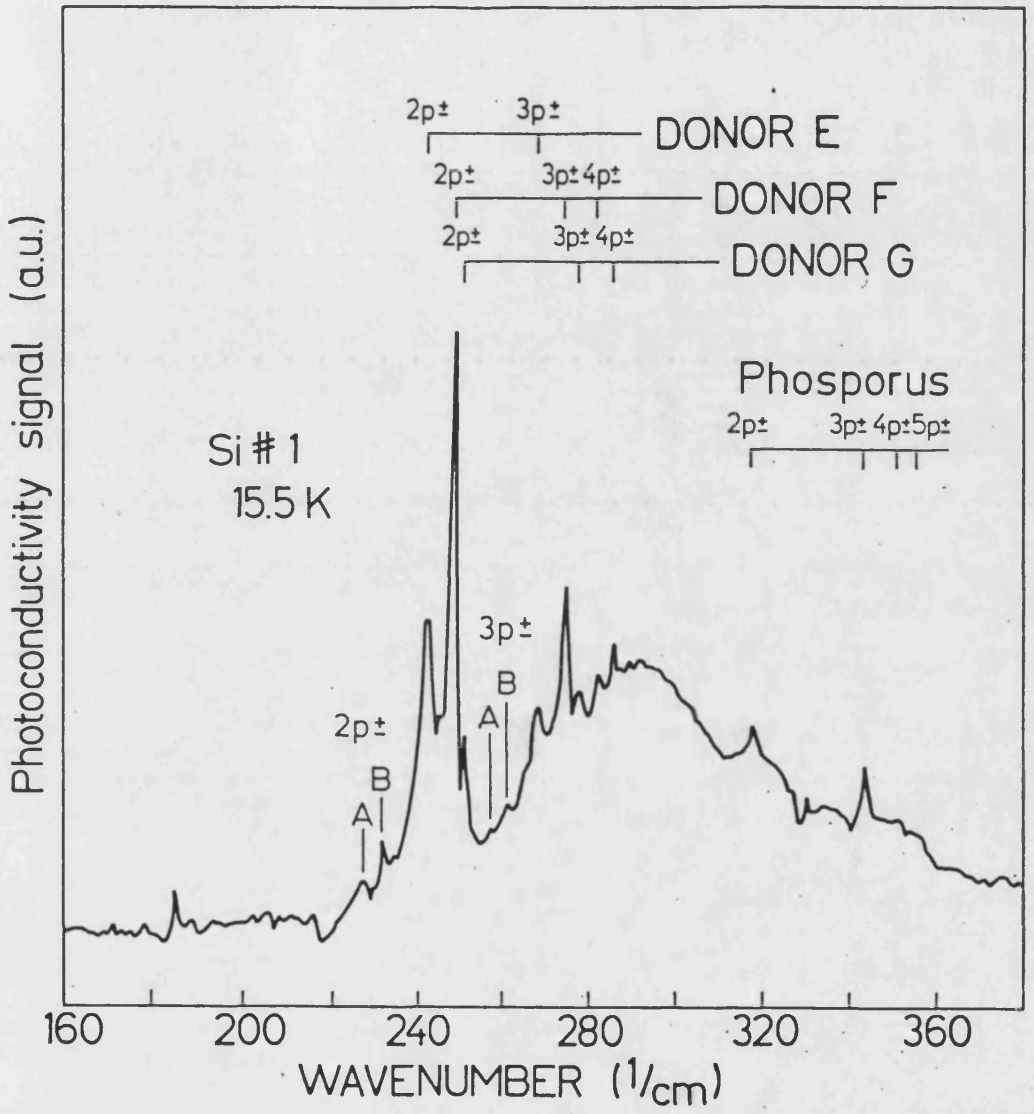

Fig 3.9: The PTIS spectrum of sample 1 showing the hydrogenic series of transitions assigned to the STD E,F and G (strong) and the STD A and B (weak). The hydrogenic series of transitions associated with P is also observed. All transitions are from the 1s groundstate into the given excited state.

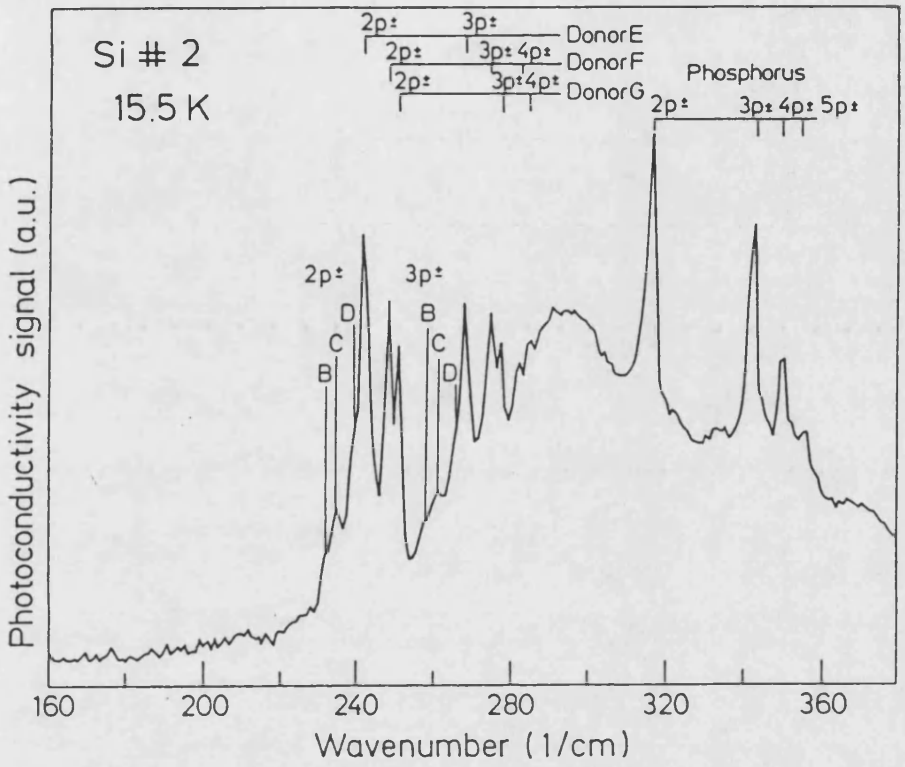

Fig 3.10: The PTIS spectrum of sample 2 showing the hydrogenic series of transitions assigned to the STD E, F and G (strong) and STD B,C and D (weak). The hydrogenic series of transitions associated with P is also observed. All transitions are from the 1s groundstate into the given excited state.

(STD). In the case of the strongest donors STD E, F and G, the $1s \rightarrow 2p_{\pm}$, $1s \rightarrow 3p_{\pm}$ and $1s \rightarrow 4p_{\pm}$ transitions are clearly distinguishable. The $1s \rightarrow 2p_{\pm}$ and $1s \rightarrow 3p_{\pm}$ transitions of two further, even shallower donors STD A and B, of low intensity are also identified.

The spectrum of sample 2 shows similar groups of transitions only varying in intensity relative to the phosphorus transitions. The donors STD E, F and G identified in sample 1 also give rise to the strongest transitions in this sample. Again the $1s \rightarrow 2p_{\pm}, 3p_{\pm}$ and $4p_{\pm}$ transitions are present. Three other donors of far less intensity are also observed, STD B, also present in sample 1 and two donors STD C and STD D which are not visible in sample 1. For these three donors only the $1s \rightarrow 2p_{\pm}$ and $1s \rightarrow 3p_{\pm}$ transitions are observed.

From a consideration of the difference in intensity of the P $1s \rightarrow 2p_{\pm}$ transition at 316cm^{-1} due to competition from the STD it can be shown (section 4.3) that the concentration of the STD is higher in sample 1 than in sample 2. This indicates that the STD develop with a given formation rate at 450°C as do the TD. The STD however develop at a much slower rate, even after a 4.5 hour anneal they remain at the detection limit of infrared transmission spectroscopy with an estimated concentration $\leq 10^{13}$cm^{-3}. A complete study of the formation of the STD is presented in Chapter 5.

The STD transitions lie on a continuum which has a local maximum at approximately 295cm^{-1}. This continuum may be attributed to the direct photoionisation of the STD whose ionisation energies lie between 279.8 and 301.6cm^{-1}. A point of interest is that there is an exponential tail before the ionisation edge where a far sharper edge would normally be expected. This has also been observed in GaAs (Stillmann et al, 1977). The continuum begins at ~210cm^{-1} (26meV) in both samples and is also visible at 4.2K, which excludes the con-

tinuum arising from thermal or photothermal processes. It is suggested that this residual photoconductivity continuum arises from the ionisation of donors which have a decreased ionisation energy due to a slightly different position in the lattice or slight differences in the clustering arrangement, assuming the new centres are not elemental donors. The inhomogeneous distribution of impurities and hence the creation of local electric and strain field could also contribute to this effect. It is known from photoluminescence and infrared transmission measurements (Weber, 1986) that the TD distribution is inhomogeneous for example. A further possibility is band bending at the contacts which could give rise to a small concentration of donors with reduced ionisation energies.

A summary of the STD donor transitions observed and the ionisation energies are given in Table 3.2 . The energy separations between the excited states are in close agreement with those predicted by effective mass theory (Janzén et al, 1984), indicating that these donors are well described by the EMT. The ionisation energies of the donors A→G from the groundstate were determined by adding the theoretically calculated ionisation energy from the $2p_{\pm}$ level to the optically measured energy of the $1s \rightarrow 2p_{\pm}$ transition. The central cell corrections, calculated by taking the difference between the calculated ionisation energy and the ionisation energy of a perfect EMT donor, are small (3.5-6.3meV) confirming the EMT nature of these donor centres.

3.4 Reproducibility

Photothermal ionisation spectroscopy is a rather complicated technique since the detection of the photo-thermally generated carriers is dependent on the temperature at which the measurement is carried out and the electric field

Donor Transitions	EMT[1]	STD A	STD B	STD C	STD D	STD E	STD F	STDG
$1s \rightarrow 2p_{\pm}$	200.49	228.7±0.5	232.5	234.0	239.5	241.1	247.5	250.5
$1s \rightarrow 3p_{\pm}$	226.96	255.0	257.8	260.0	265.0	267.4	274.2	277.1
$1s \rightarrow 4p_{\pm}$	234.49	-	-	-	-	277.1	282.5	285.0
$\Delta E(2p_{\pm} \rightarrow 3p_{\pm})$	26.4	26.3	25.4	26.0	25.5	26.0	26.7	26.6
$\Delta E(3p_{\pm} \rightarrow 4p_{\pm})$	7.53	-	-	-	-	9.7	8.3	7.9
E_i (cm^{-1})	252.1	279.9	283.9	285.5	291.1	292.7	298.4	301.6
E_i (meV)	31.262	34.7	35.2	35.4	36.1	36.3	37.0	37.4
Central cell correction (meV)	-	3.44	3.94	4.14	4.84	5.04	5.74	6.14

1. E. Janzén, R. Stedman, G. Grossman, H. G. Grimmeiss, Phys. Rev. B 29 (4) p1907 1984.

Table 3.2: A summary of the electronic transitions of the STD observed in the PTIS spectra of samples 1 and 2. The energy separations of the energy levels (ΔE) are compared to those predicted by effective mass theory (EMT). The ionisation energy (E_i) of each donor is calculated by adding the EMT predicted ionisation energy from the $2p_{\pm}$ level to the observed energy of the $1s \rightarrow 2p_{\pm}$ transition. The central cell correction is given by the difference between the ionisation energy and the ionisation energy of a perfect EMT donor.

applied to the sample. The ohmicity of the electrical contacts also plays a crucial role.

3.4.1 Temperature dependence

As discussed in section 1.4 the temperature plays a major role in PTIS. The photo-thermal ionisation probability which governs the probability of an electron being lifted from an excited state into the conduction band is strongly temperature dependent. Further, the number of electrons in the groundstate is temperature dependent. This strong temperature dependence of the photothermal ionisation process is observed experimentally and therefore it is an important criteria that when comparing different spectra the temperature at which the measurements are made is taken into account. A reproducibility of better than 2% was achieved under identical experimental conditions. The variation of the spectra with temperature is illustrated in Fig 3.11 and is treated fully in Chapter 6. The metamorphosis of the P $1s \rightarrow 2p_{\pm}$ transition at 316.1cm^{-1} from a peak at 17K to an minima at 12K is clearly observed.

3.4.2 Voltage dependence

The far infrared light intensity interferogram generated by the interferometer must be truly translated into an interferogram in the photocurrent dimension. If the electrical contacts on the sample are not ohmic the interferogram will be distorted by their response. The problem of consistently producing low temperature ohmic contacts is not trivial, especially in this case where heat treatment is not possible. Although the contacts used have been shown to be reliably ohmic, changes in the magnitude of the signal from sample to sample or after recontacting occur and may be due to differences in the contacts and

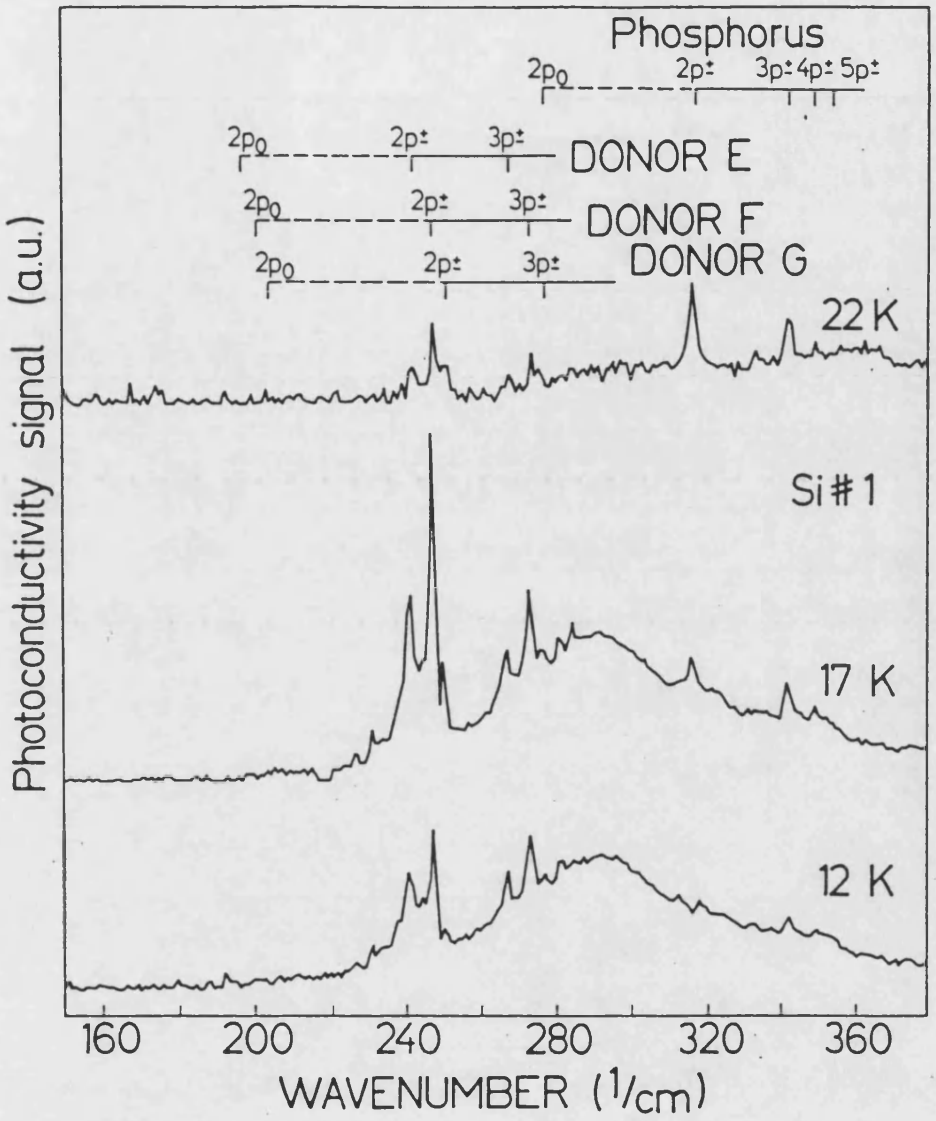

Fig 3.11: The temperature dependence of the PTIS spectra of sample 1. The P $1s \rightarrow 2p_{\pm}$ transition at 316cm^{-1} is observed as a minimum at 12K and a peak at 17K. At 22K the intensity of the peak is increased.

surface conditions. It was not found necessary to shield the contacts.

The distance between contacts and the applied bias voltage influence the probability that an electron recombines before reaching one of the contacts. In turn this influences the intensity of the photothermal transitions in the PTIS spectrum. This effect has been discussed in detail by Darken and Hyder (1983). For the measurements made here a profile of the PTIS response against voltage was routinely carried out as a preliminary to the measurements. It was determined that for the undoped n-type silicon used in the majority of these studies the optimum electric field was of the order of 6.5V/cm as generally used for high purity silicon (Skolnick et al, 1974). The voltage profile as shown in Fig 3.12 measured with sample 1 at 15.5K shows that variations of the order of $\pm$0.5V/cm only reduce the intensity slightly whereas a large deviation severely reduces the intensity measured.

3.5 Discussion of the experimental results

The PTIS spectra of undoped Cz-silicon samples annealed at 450°C have revealed the presence of seven hydrogenic series of transitions which may be assigned according to the EMT-model of shallow donors in silicon. However there are other alternative explanations of these transitions which must be considered and will be discussed here.

3.5.1 Lithium and Lithium-oxygen donors in silicon

The observed ionisation energies of the STD are shallower than for all known elemental donors (P, As , Sb etc.) in silicon with the exception of lithium which has an ionisation energy of 31.24 meV compared to STD A, the shallowest

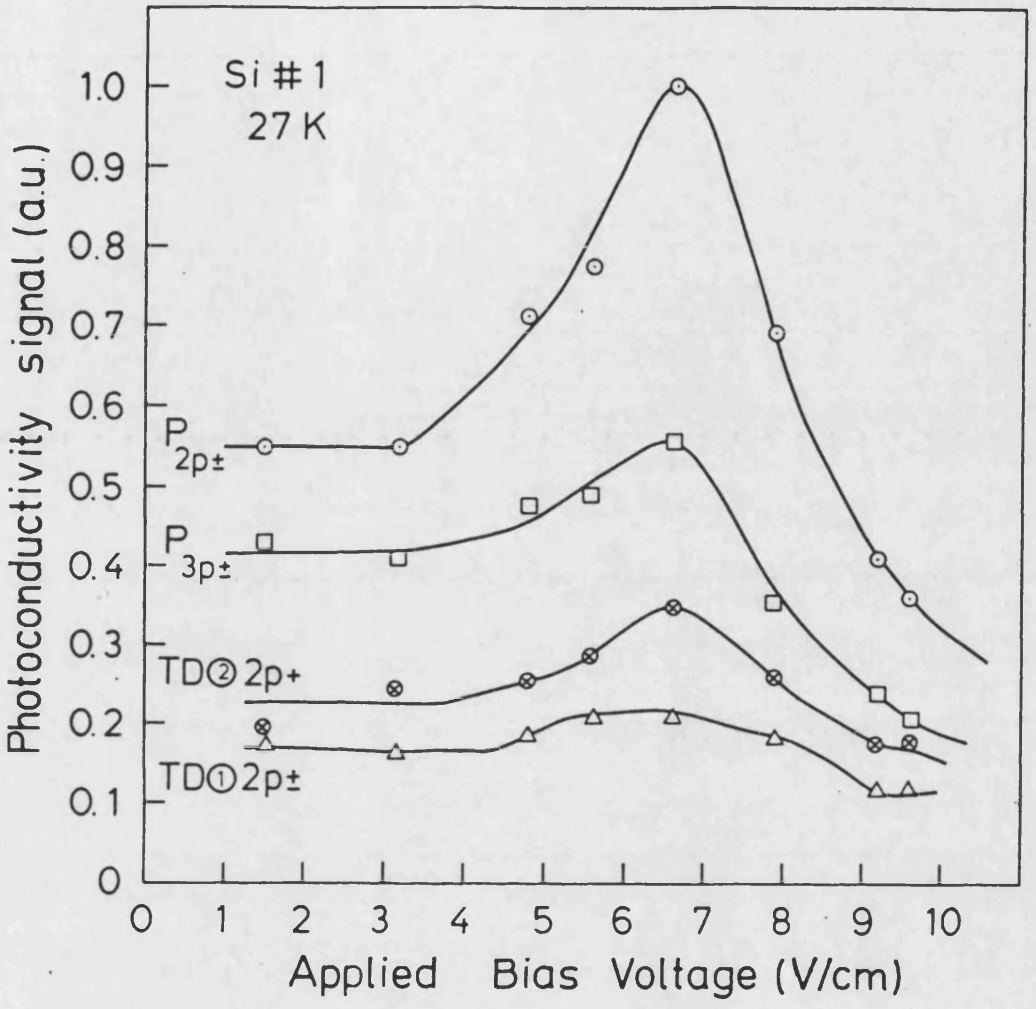

Fig 3.12: The intensity of the electronic transitions of the P and the TD1 and TD2 as a function of applied bias voltage. The experimental data is obtained from PTIS measurements on sample 1 at 27K.

STD, with an ionisation energy of 34.7 meV. Also, it is known that oxygen forms clusters with Li giving rise to six Li-O shallow donor complexes (Gilmer et al, 1965; Aggrawal et al, 1965). However neither the observed transitions of the different Li-O complexes nor their ionisation energies show a correlation to those of the STD as shown in Fig 3.13 and therefore they may be discounted as the origin of the STD.

3.5.2 The relationship of the Shallow Thermal Donors and Thermal Donors

Originally it was suspected that shallower donors in the TD series, present in concentrations below the detection limit of infrared transmission spectroscopy, might be revealed by PTIS. However, the observed STD are far shallower than the shallowest Thermal Donor, TD9. STD G, the deepest STD, has an ionisation energy 15.6meV lower than TD9 whereas TD9 lies only 1.1meV below TD8. The average change in ionisation energy between TD is -2.17meV ($TD_n \rightarrow TD_{n+1}$). It would therefore not seem reasonable to assume that the STD are a simple continuation of the TD clustering process.

3.5.3 Experimental evidence for the single donor nature of the Shallow Thermal Donors

It is proposed that the STD are single donors, where only one electron is available for excitation and ionisation in contrast to the TD which are double donors with two available electrons. In this case the core of the STD must be expected to be considerably different than the TD. The large gap between the shallowest TD and deepest STD is then a result of the difference in effective nuclear charge between a single donor and a double donor. Also, the ionisation energies of the STD are very close to the predicted EMT ionisation energy of

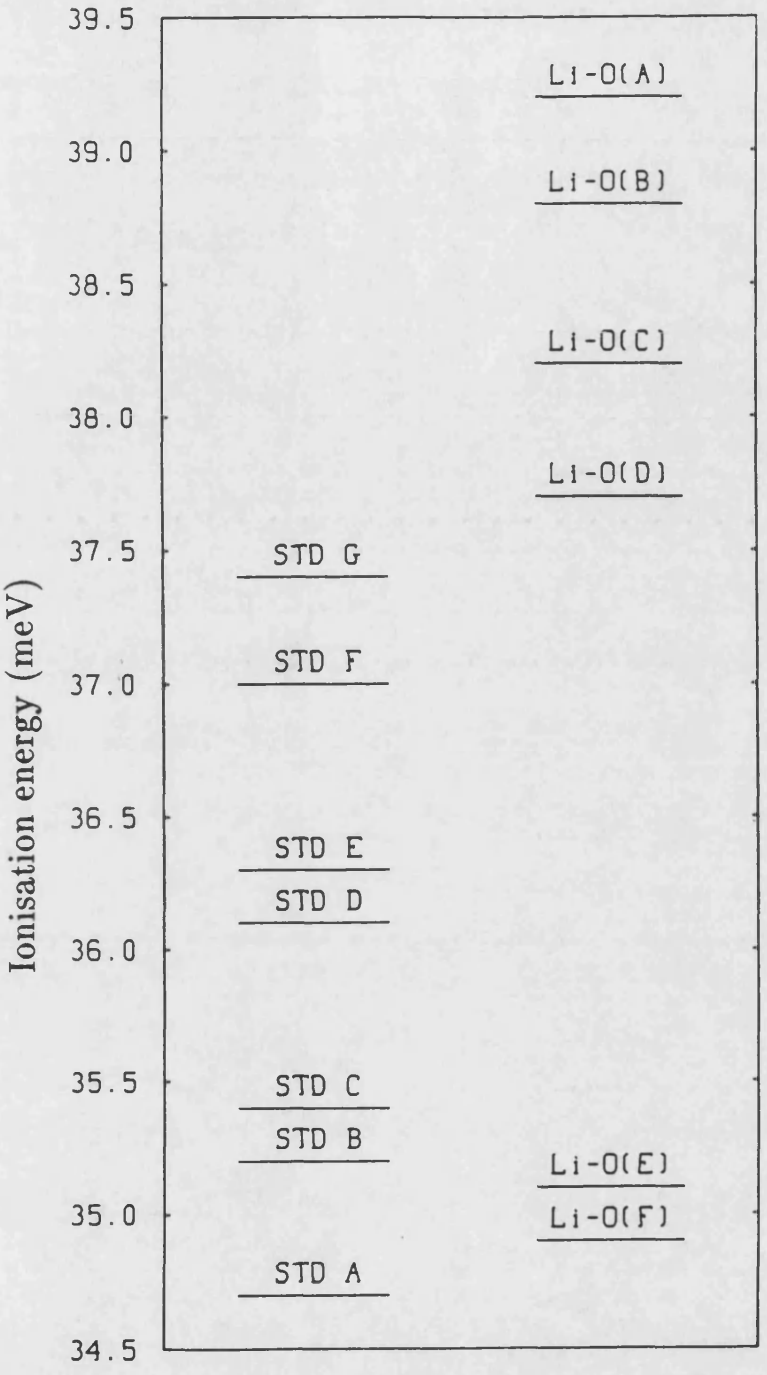

Fig 3.13: The ionisation energies of the STD are compared to the ionisation energies of the Li-O complexes (T. E. Gilmer, R. K. Franks, R. J. Bell, J. Phys. Chem. 26 p1195 1965).

31.3 meV (Janzén et al, 1984) for a single donor in silicon.

All double donors give rise to two series of hydrogenic transitions. Assuming the STD were double donors, a second series of transitions due to the singly ionised species would be expected in the spectral region up to 125 meV ($1000cm^{-1}$). However, despite a systematic search of the PTIS spectra at temperatures between 10K and 30K no features which could be assigned to such transitions were observed.

Due to these considerations, the assumption that the STD are single donors is strongly favoured. This conclusion again weighs against a direct correlation of the STD and TD.

3.5.4 Transitions from higher groundstates

It is known that hydrogenic series of transitions can also arise from the excitation of electrons in a higher groundstate of a donor to the excited states, if the higher groundstate is populated and transitions are allowed. The TD have recently been shown to have C_{2v} symmetry, a reduced T_d symmetry. The 1s groundstate is constructed only from a single pair of conduction band valleys and is non-degenerate. There exist two higher ground states, the 1s(E) and 1s(T_2) states (see section 1.6).

The STD cannot be associated with transitions from these higher groundstates for two independent reasons. Firstly, the relative populations of these states would be insignificant at 15.5K. Although EMT does not predict the energy of the 1s(E) and 1s(T_2) states, from the experimental data available on other shallow donors these states would be expected to lie approximately 32 meV below the conduction band (Ramdas and Rodriquez, 1981). Hence, the energy

separation $1s(A_1) \rightarrow 1s(E+T_2)$ would be approximately 20-40meV compared to the available thermal energy $k_B T = 1.33$meV at 15.5K. This gives a Boltzmann probability factor of the order of 10^{-8} for occupation of these higher groundstates.

Secondly, in sample 1 five STD are observed, STD E, F and G being most intense, and TD2, 3 and 4 are most abundant. In sample 2 six STD are observed, again STD E, F and G are dominant, but now only TD 1, 2 and 3 are detected. It must therefore be concluded that there is no simple correlation between the STD and the TD.

Phosphorus has T_d symmetry. The groundstate manifold consists of three components and transitions involving the higher $1s(E)$ and $1s(T_2)$ groundstates may occur. However, it is not possible that the STD may be attributed to such transitions. The ionisation energies of both groundstates are experimentally well known and lie at 32.28meV and 33.98 meV respectively, shallower than the observed ionisation energies of the STD. Also the Boltzmann occupation probability of these levels are only 4.7×10^{-5} and 1.6×10^{-4} respectively at 15.5K and therefore transitions as intense as those arising from the STD can not be associated with these levels.

3.5.5 Application of the perturbation model to the Shallow Thermal Donors.

Kinetic models have ascribed the TD in silicon to a series of oxygen aggregates as discussed in section 1.7. The ladder of ground state energies for the neutral and singly ionised TD have been explained by a perturbation model (Corbett et al, 1984, Borenstein et al, 1986b). The model assumes an unknown donor core and that the continued agglomeration of oxygen introduces an additional

repulsive potential at the core of the defect. This leads to a successive reduction in the agglomerate binding energy with reference to the deepest donor.

The repulsive interaction due to the addition of an oxygen atom may be treated as a small perturbation of the attractive Coulomb potential of the core. If the Coulomb potential is reduced the electron orbit increases and the binding energy is reduced. The simplest approximation for the repulsive interaction, V_p between the agglomerating oxygen atoms and the shallow electrons is a constant over the volume of the aggregate

$$V_p = \begin{cases} V_0 & r < Rn^{\frac{1}{3}} \\ 0 & r > Rn^{\frac{1}{3}} \end{cases}$$

where R is the radius of an oxygen atom (1.46 $\mathring{A}$ in silicon) and n represents the number of oxygens in the aggregate around the donor core. A spherical cluster is assumed and this has been shown not to change the qualitative success of the model (Borenstein et al, 1986c).

The binding energy changes $\Delta E(TD^0)$ and $\Delta E(TD^+)$ may be evaluated analytically and fit to the observed groundstate ladder. Borenstein et al (1986b) achieved a good fit to the experimental data for the TD in silicon using a repulsive potential of $V_0 = 1.90$V. Comparison between the experimental results and the model predictions reveal that excellent agreement is achieved assuming the ladder of donors proceeds with the addition of a single oxygen into the donor core.

Borenstein et al (1986b) were also able to achieve excellent agreement with the experimental data of the TD in Ge (Clauws and Vennik, 1984, 1986) using the same parameters when the depth of the repulsive potential is scaled according to the dielectric constant in Ge. The predictions of the model for both donor charge states in Si and Ge is presented in Fig 3.14 together with

the experimental results after Oeder and Wagner (1983) and Pajot et al (1983) for Si and Clauws et al (1984) for Ge.

3.5.6 Extension of the Thermal Donor series

The perturbation model argues that the TD groundstate energy is determined by the two opposing mechanisms of the attractive central cell correction and the repulsive perturbing potential due to the growing oxygen aggregate. The experimentally observed ionisation energies of the STD are approximately 37meV. If the STD are extensions of the TD series a repulsive potential far greater than the positive central cell correction of 13meV (obtained from TD^01) would be required. The necessary repulsive perturbing correction of $\sim$ 50 meV would correspond to the addition of the order of 18 oxygen atoms to the TD core. For clusters containing 16, 17 and 18 oxygens the model predicts binding energies of 38.3, 36.6 and 34.9 meV respectively. The spacing of these ionisation energies is far larger than experimentally observed for the STD. It can be concluded from these considerations that it is unlikely that the STD are an extension of the TD series.

3.5.7 Predictions for an independent Shallow Thermal Donor series related to oxygen

The deepest STD has an ionisation energy of 37.4 meV, that is a central cell correction of 6 meV compared to the EMT ionisation energy of a single donor. Based on this the perturbation model predicts the spacing between donors due to the addition of a single oxygen to the cluster to be of the order of 0.8 meV. Analysis of the ladder of ionisation energies experimentally observed reveals that the STD are not evenly spaced and the interval ranges between 0.2 and

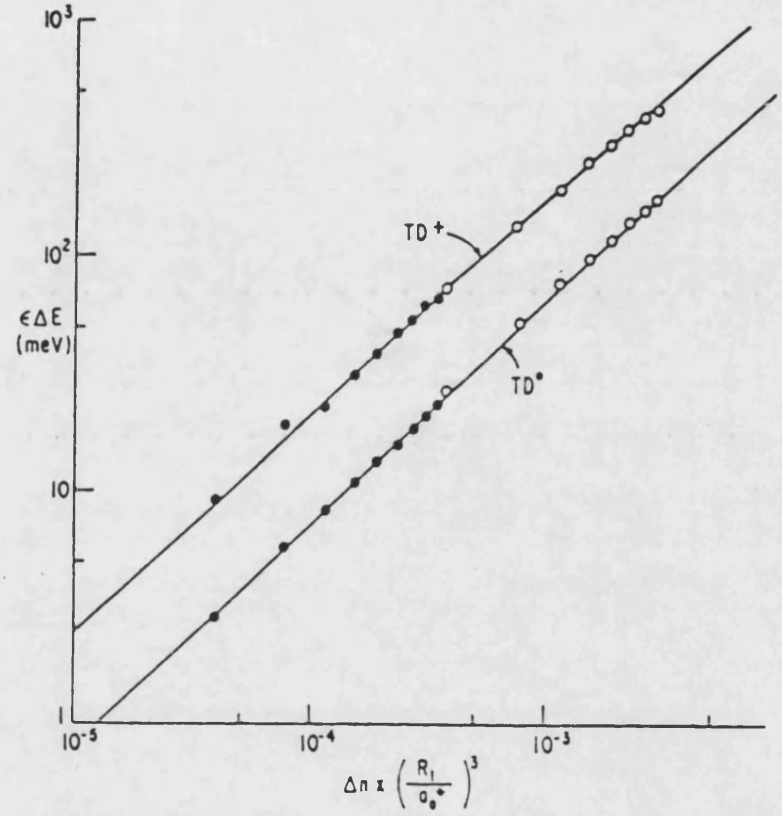

Fig 3.14: Predictions of the model (solid lines) for both thermal donor charge states versus experimental values for Si (o) and Ge (•). The ordinate is the product of the ionisation energy and the host dielectric constant, while the abscissa contains Δn the number of oxygens added to the cluster, multiplied by the cube of the oxygen-to Bohr- radius ratio. (J. T. Borenstein, J. W. Corbett, Oxygen, Carbon, Hydrogen and Nitrogen in crystalline silicon, MRS Symposia Proceedings 59 p159 1986.)

0.7 meV. It can not be excluded that the observed STD are members of more than one overlapping series, each with a different core. If it is assumed that two series exist one finds that the STD can be grouped into two approximate ladders with an average energy spacing of 0.9 meV as shown in Table 3.3. The predictions of the perturbation model for the STD (assuming two series exist) and for the two charge states of the TD are shown together with the experimental results in Fig 3.15. Further experiments are required to confirm the proposed assignment of the STD to two similar series of oxygen-related donor complexes.

3.6 Summary

Using the high sensistivity of PTIS under carefully controlled experimental conditions it has been possible to identify seven previously undiscovered donors present in Cz-silicon annealed at 450°C. The STD are shallower than the observed residual donor P and the TD and have ionisation energies 34.7meV, 35.2meV, 35.4meV, 36.1meV, 36.3meV, 37.0meV and 37.4meV, very close to the perfect EMT donor ionisation energy. The transitions show temperature dependence and voltage sensitivity as expected for transitions arising from a photo-thermal process detected through the generated photocurrent. A continuum, arising from direct ionisation processes of these donors is observed and exhibits an exponential tail beginning at 26meV with a maximum at $\sim$ 36.6meV.

The possibility that the transitions assigned to the STD may be associated to a known donor or to the transitions from a higher groundstate of a known donor into the excited states is excluded. No direct correlation to the TD is observed and this is shown to be unlikely from the perturbation model.

STD	ϵ_i(meV)	Interval	$\Delta\epsilon_i$(meV)
Series 1			
G	37.4±0.1	G-E	1.1±0.2
E	36.3	E-C	0.9
C	35.4	C-A	0.7
A	34.7		
Series 2			
F	37.0±0.1	F-D	0.9±0.2
D	36.1	D-B	0.9
B	35.2		

Table 3.3: Experimental values for the ionisation energies (ϵ_i) of the STD referenced to the conduction band and the increase in ground-state energy ($\Delta\epsilon_i$) from the nth to the (nth+1) donor assuming two overlapping series.

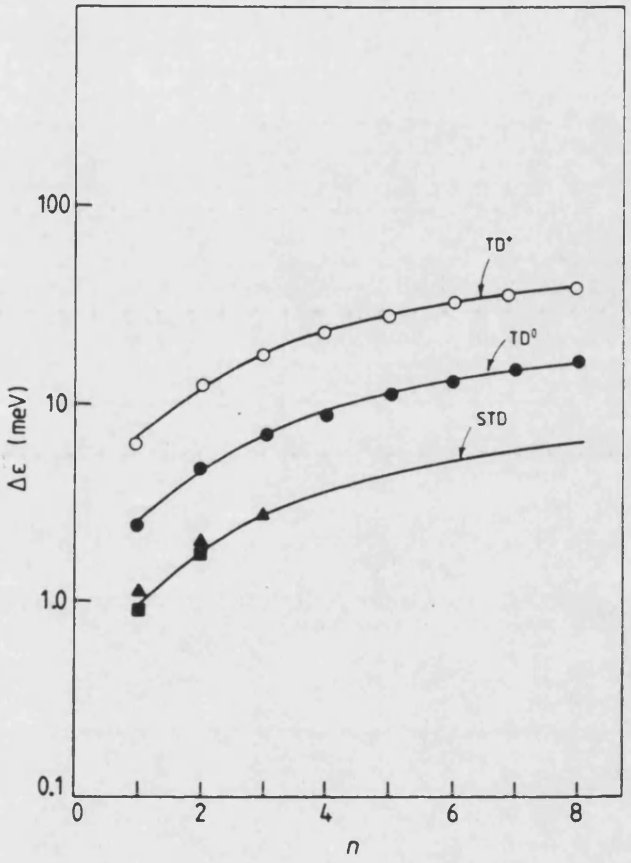

Fig 3.15: Shift ($\Delta\varepsilon$) in the groundstate energy for the nth thermal donor referenced to the deepest thermal donor (TD1) groundstate, versus the number of oxygen atoms added to TD1 (n) for both thermal donor charge states in silicon and for the STD. The experimental values are represented as follows: TD^+ (○), TD^0 (●), STD series 1 (▲), STD series 2 (■). The full curves indicate the predictions of the perturbation model.

It can be concluded from the experimental results that the STD are single donors. One possible structural model for the STD is given by the perturbation model which indicates that if grouped into two series the STD may be described as the successive agglomeration of oxygen around two slightly different unknown cores.

Chapter 4

The role of phosphorus, boron and oxygen in the formation and growth of the Shallow Thermal Donors.

Considering the nature of the STD, the occurrence of seven donors with only slight differences in ionisation energy is extremely reminiscent of the TD and suggests that the STD are also formed by the clustering of one or more elemental impurities to form donor complexes. The experimental results indicate that the STD are related to oxygen and may be oxygen complexes, possibly involving other impurities. Phosphorus and boron are probable candidates for complexing being residual impurities present in all silicon material. Both are present in concentrations of the order of $10^{13}cm^{-3}$ in undoped Cz-silicon which is comparable to the maximum achievable STD concentration (section 5.3) observed in these measurements.

4.1 The role of phosphorus

Phosphorus doped samples were not available for study, therefore the role of P was studied using n-type undoped Cz-silicon in which P is the major residual impurity. Samples cut from the same slice of undoped n-type Cz-silicon were annealed for different lengths of time at 450°C giving rise to different concentrations of the STD (see Chapter 5). Infrared transmission measurements indicate that the P concentration in these samples, as determined from the P $1s \rightarrow 2p_{\pm}$ transition, is not correlated to the STD growth. As shown in Fig 4.1 the P concentration remains constant. The small fluctuations in concentration can be explained as the expected variation of P over a single wafer.

The intensity of the P transitions in the PTIS spectra change with STD concentration. The net photo-response at energies corresponding to the P transitions is dependent on the STD concentration since there is competition between direct photo-ionisation of the STD and photo-thermal ionisation of the P. The observed changes in intensity of the P transitions may be explained assuming a constant P concentration and varying STD concentration. If the conditions are optimised for PTIS of the P then its transitions increase in intensity and dominate the spectrum. The P transitions observed in sample 2 at 21.5K are shown in Fig 4.2. The STD transitions appear very small in comparison.

It should also be noted that no enhancement of the STD due to the presence of higher concentrations of P has been observed. These observations indicated that P does not play a determining role in the growth and formation of the STD. However, further studies should be made on P-doped samples to conclusively evaluate the importance of P.

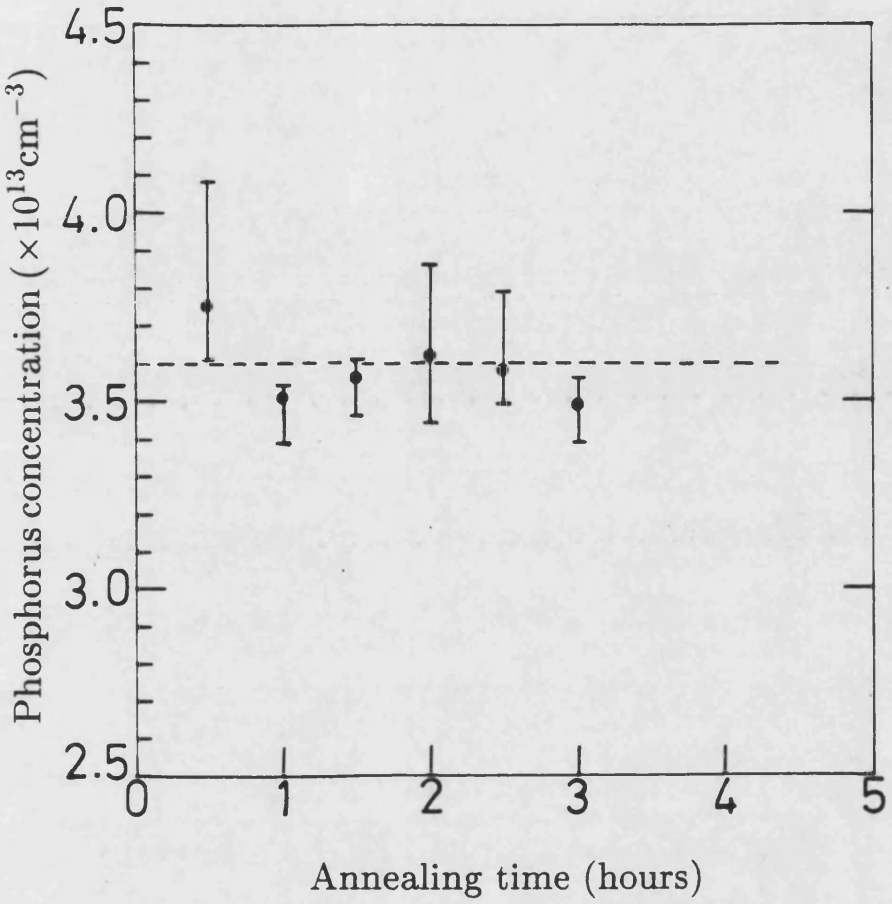

Fig 4.1: Phosphorus concentration determined from the transmission spectra of similar samples of undoped oxygen-rich Cz-silicon versus the duration of the 450°C anneal, which corresponds to different TD and STD concentrations. The error bars were determined from the signal-to-noise ratios in the individual spectra. The dashed line shows the mean value of the P concentration.

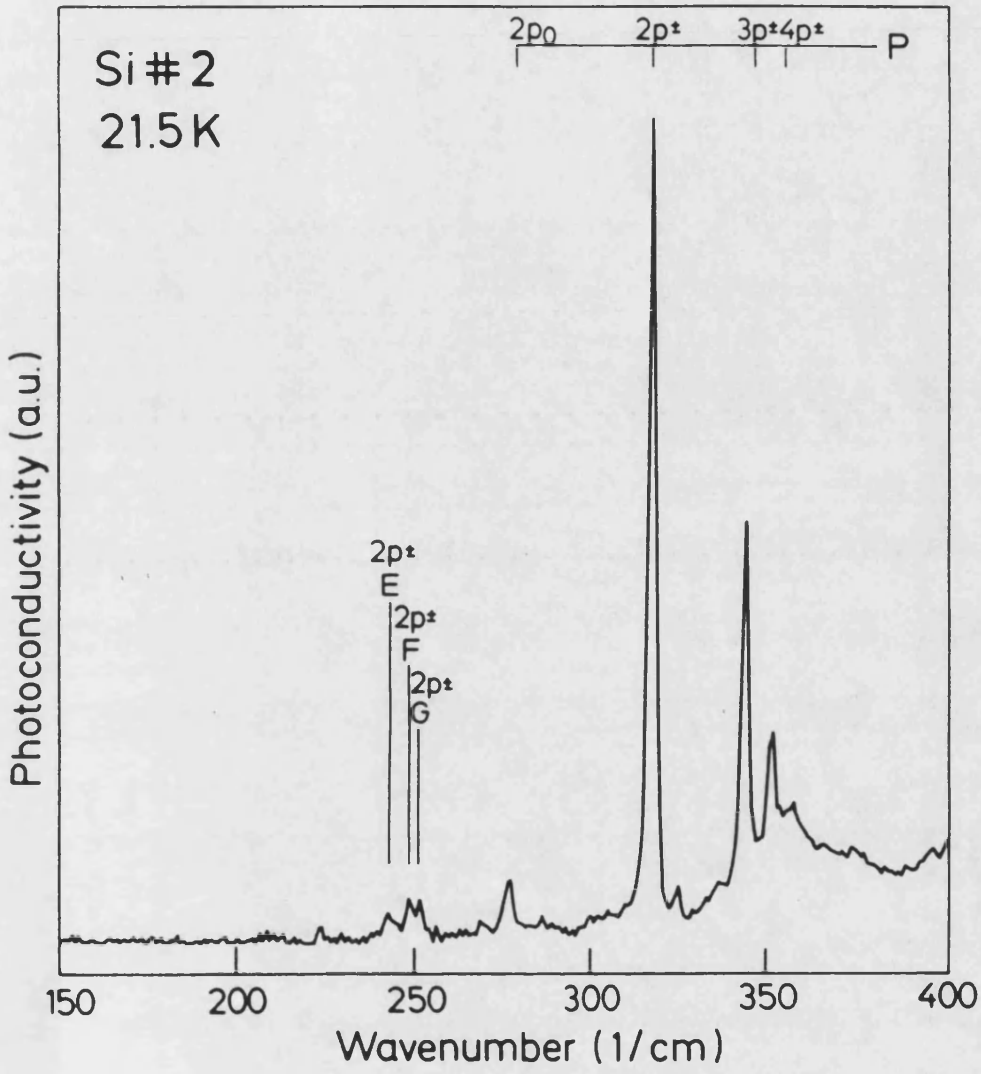

Fig 4.2: The PTIS spectrum of sample 2 at 21.5K. The experimental conditions are optimised for phosphorus. The $1s \rightarrow 2p_{\pm}$ transitions of STD E, F and G are still visible in this spectrum but their intensity is very weak compared to the P transitions.

4.2 The role of boron

The possibility that the STD are related to boron must also be considered. The PTIS spectrum of a typical boron-doped Cz-silicon sample is shown in Fig 4.3a. The boron sample used was 10mm× 10mm × 2mm and was polished on both faces. Multiple layer contacts of 100Å Ni, 500Å Au, 130Å Sb and 3870Å Au were deposited in two 1mm wide strips 7mm apart and laser annealed. The boron concentration in this sample, determined from resistivity measurements, is $4 \times 10^{15}cm^{-3}$. After heat treatment at 450°C for 15 hours the net donor concentration estimated from resistivity measurements was approximately $4 \times 10^{13}cm^{-3}$. The PTIS spectrum was recorded at 27.6K at $0.5cm^{-1}$ resolution with an applied bias voltage of 6V. The infrared transmission spectrum of the beamsplitter and a 2mm white polyethylene window is shown by the dashed curve for comparison.

In Fig 4.3a the typical continuum observed in undoped samples, beginning at approximately $200cm^{-1}$, is absent. The continuum begins at approximately $390cm^{-1}$ and increases sharply. Features are observed in the region below $600cm^{-1}$ which may be associated with the transitions of the neutral donors TD1,2,3 and 4. At $600cm^{-1}$ there is a broad strong minima band arising from the 3.5μm beamsplitter. Between $600cm^{-1}$ and $1000cm^{-1}$ many sharp minima are observed which may be assigned to the transitions of the singly ionised TD^+ centres. Transitions arising from TD^+7,6,5,4,3 and 2 are present. Through the sensitivity of PTIS some transitions are observed in addition to those reported by Wagner et al (1984) and it is possible to confirm some tentative assignments made by them with regard to the $1s \rightarrow 2p_{\pm}$ and $1s \rightarrow 3p_{\pm}$ transitions of TD^+6 and 7.

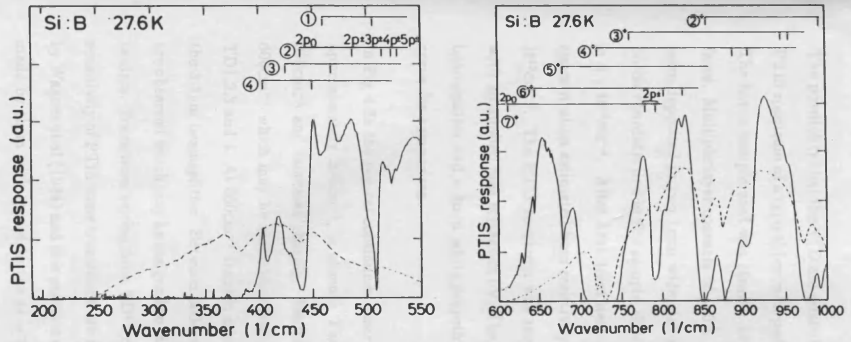

Fig 4.3a): The PTIS spectra of B-doped ($4 \times 10^{15}cm^{-3}$) Cz-silicon annealed for 15 hours at 450°C. In the spectral region 200-550cm^{-1} the observed TD^0 transitions are indicated. In the spectral region 600-1000cm^{-1} the observed TD^+ transitions are indicated. The beamsplitter transmission spectrum is shown by the dashed line for comparison.

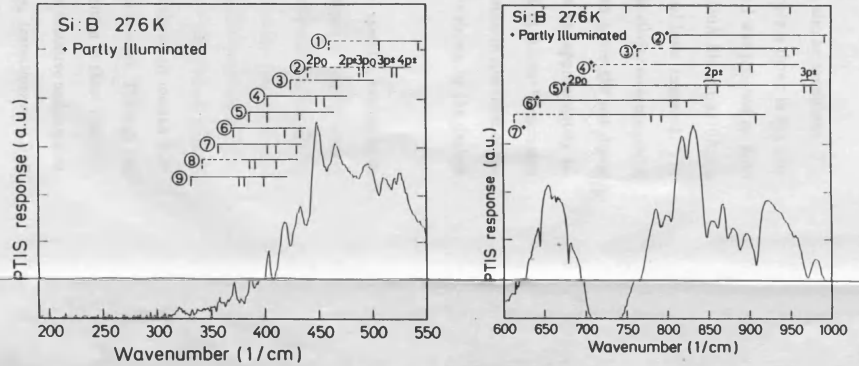

Fig 4.3b): Sample illuminated by stray band-edge light in the spectrometer.

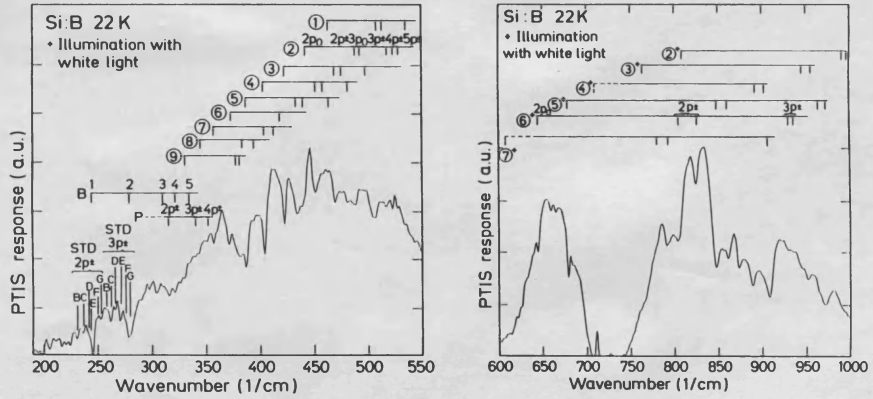

Fig 4.3c): Sample under illumination from band-edge light from a tungsten filament lamp. In the spectral region 200-550cm^{-1} transitions associated to B and weak minimia which are tentatively assigned to the STD are observed.

The absence of spectral features below 390cm^{-1} may be understood from a consideration of the Fermi level in this sample. Firstly, after 15 hours annealing the presence of all nine TD is expected. The concentration of residual phoshorus can be assumed to be of the order of 10^{13}cm^{-3} and the presence of the STD is speculated. However, due to the presence of the B the shallower donors are compensated. Transitions due to the STD, P and the neutral donor species $TD^0$9,8,7,6 and 5 are not observed in the PTIS spectra indicating they are compensated. Transitions are observed arising from $TD^0$4,3,2 and 1 indicating that they are not completely compensated. Further the transitions of the singly ionised species, TD^+7,6,5 and 4 are observed. This leads to the conclusion that the Fermi level must lie at approximately the level of $TD^0$4. Additionally, even though TD^+3, 2 and 1 are predicted as being present only as neutral donors the transitions of TD^+3 and 2 are observed. This probably indicates an inhomogeneous distribution of B in the sample such that some regions are more compensated than others, a smearing of the Fermi level due to the finite temperature at which the measurement is made is not sufficient to explain this phenomenon alone. The proposed system of compensated and uncompensated donors is portrayed schematically in Fig 4.4 and estimates of the relative concentrations of the different donors species support the assumption that the Fermi level lies in the region between $TD^0$4 and $TD^0$1. The ground-state energies of the donors (E_d) and acceptors (E_a) are given relative to the conduction band minimum (E_c) and valence band maximum (E_V) respectively.

4.2.1 The application of band-edge light to boron doped samples

The application of band-edge light, that is light of energy greater than the energy gap of the material, may be used to enable the observation of both majority and minority carriers simultaneously in infrared transmission (Kol-

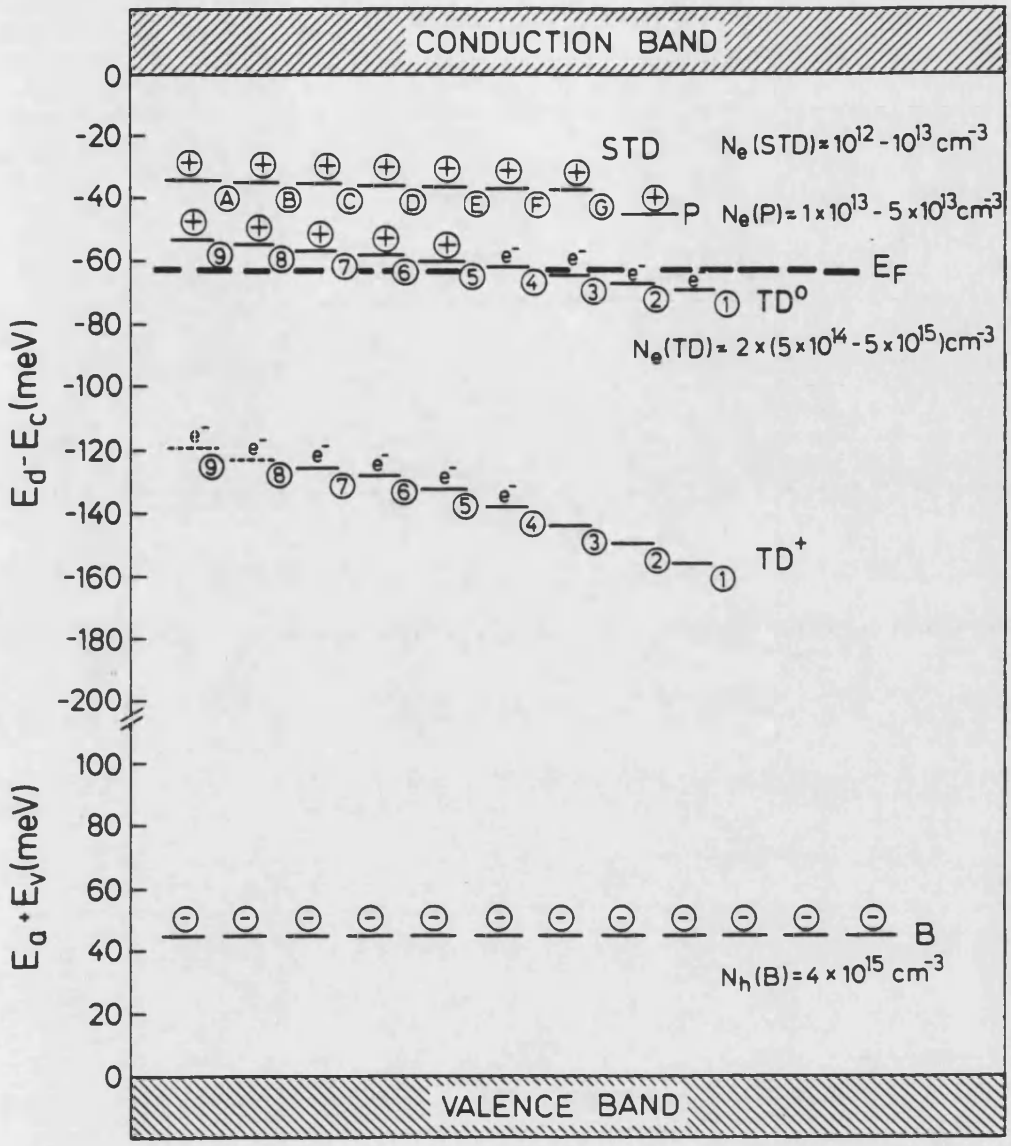

Fig 4.4: A schematic view of the position of the Fermi level (E_F) in the B-doped ($4 \times 10^{15}cm^{-3}$) oxygen-rich Cz-silicon sample annealed for 15 hours at 450°C showing the donor and acceptor species concerned, their estimated concentrations and the degree to which they are compensated. N_e represents the number of electrons made available by a given donor species (twice the donor concentration for the TD) and N_h represents the number of holes made available by an acceptor. ⊕ indicates a compensated donor and ⊖ indicates a compensated acceptor. e^- represents a neutral donor with its bound electron.

besen, 1975) or PTIS (Skolnik et al, 1974, Darken and Hyder, 1983). When the sample is illuminated with band-edge light a bath of electron-hole pairs is created. Recombination occurs between the electrons and ionised donors and holes and ionised acceptors. An equilibrium population of neutral donors and accepters is established and their internal transitions may be spectroscopically observed. The PTIS spectra shown in Fig 4.3b and Fig 4.3c were made using the same sample as in Fig 4.3a. The spectrum in Fig 4.3b was measured after the installation of a further KRS5 outer window and Suprasil inner window (absorbs below $250cm^{-1}$) to allow illumination by an outside source. Even before illumination changes are apparent in the spectrum; these were attributed to stray light from the interferometer mercury arc source. In comparison, the PTIS spectrum in Fig 4.3c shows the effect when light from a tungsten filament lamp is shone onto the sample.

Both Fig 4.3a and Fig 4.3b were recorded at 27.6K. The spectrum in Fig 4.3c was recorded at 22K since depopulation of the groundstates of the most shallow donors is already significant at the higher temperature. The resolution in Fig 4.3b is $0.5cm^{-1}$ and in Fig 4.3c $1cm^{-1}$. The spectra were taken with a bias voltage of 5.95V and 6.44V respectively.

At partial illumination in Fig 4.3b the continuum now begins at approximately $310cm^{-1}$ indicating that some neutralisation of shallower donors has been achieved. Also, the $1s \rightarrow 2p_0$ and $1s \rightarrow 2p_{\pm}$ transitions of $TD^0$5,6,7 and 8 and more transitions of the TD^+ are clearly visible in addition to those transitions observed in Fig 4.3a. In Fig 4.3c at full illumination the continuum begins at $200cm^{-1}$ as in undoped material indicating considerable neutralisation has been achieved. Indeed five transitions are observed as minima in this spectrum which may be assigned to boron, the first two at $245cm^{-1}$ and

278cm^{-1} are broad and strong, the remaining three at 304cm^{-1}, 320cm^{-1} and 334cm^{-1} are weaker. Now some higher $1s \rightarrow 3p_{\pm}$ and $1s \rightarrow 4p_{\pm}$ transitions of $TD^0 9$ to $TD^0 1$ and $1s \rightarrow 3p_{\pm}$ transitions of the TD^+ are observed in addition to the transitions observed in Fig 4.3a. A comparison of the TD^0 transitions and TD^+ transitions observed in the three figures is given in Table 4.1a and b respectively. The TD^0 transitions now all appear as minima in the continuum compared to Fig 4.3a and Fig 4.3b where the most shallow donors present gave rise to peaks.

The application of band-edge light also generates noise in the photoconductivity spectrum which increases with the light intensity. In both Fig 4.3b and Fig 4.3c this make it difficult to assign weak features in the low energy tail of the continuum with certainty. On the limit of the noise level minima are observed in Fig 4.3c which are tentatively assigned to P and to the $1s \rightarrow 2p_{\pm}$ and $1s \rightarrow 3p_{\pm}$ transitions of the STD B, C, D, E, F, and G.The proposed assignments are summarized in Table 4.2 together with those for boron. That the P and STD only appear very weakly may also indicated that the density of electron-hole pairs produced by the incoming light is insufficient to neutralise the majority of the ionised impurity centres. That the STD appear in these samples as minima may be associated with the fact that due to the presence of the electron-hole pairs the recombination is far higher than in unilluminated material.

The results presented here indicate that the technique of illumination with band-edge light is applicable to this problem. Illumination with light of a single frequency and the excitation of a high carrier density, for example by the use of a Nd-YAG laser, can be expected to improve the signal-to-noise ratio significantly.

a)Unilluminated	b)Part Illumination	c)Full Illumination	Donor Species	Transition (1s→)
		330	TD9	$2p_0$
		343	TD8	$2p_0$
	358	357	TD7	$2p_0$
	371	371	TD6	$2p_0$
	378	(376)	TD9	$2p_\pm$
	387	382	TD5,TD8	$2p_0$,$2p_\pm$
	392	393	TD8	$3p_0$
	398	(397)	TD9	$3p_\pm$
404	404	404	TD7,TD4	$2p_\pm$,$2p_0$
		412	TD8,TD7	$3p_\pm$,$3p_0$
418	418	(417)	TD6	$2p_\pm$
424		422	TD6,TD3	$3p_0$,$2p_0$
(434)	433	434	TD5	$2p_\pm$
441		439	TD5,TD2	$2p_0$,$2p_\pm$
	440	440	TD6	$3p_\pm$
451	448	451	TD4	$2p_\pm$
456	456	458	TD4	$3p_0$
461	460	463	TD5,TD1	$3p_\pm$,$2p_0$
467	468	469	TD3	$2p_\pm$
		475	TD3	$3p_0$
		480	TD4	$4p_\pm$
488		488	TD2	$2p_\pm$
	492	493	TD2	$2p_\pm$
	496	496	TD2	$3p_0$
508	506	506	TD1	$2p_\pm$
		512	TD1	$3p_0$
518	518	516	TD2	$3p_\pm$
523	522	522	TD2	$4p_\pm$
526	525	526	TD2	$5p_\pm$
		533	TD1	$3p_\pm$

Table 4.1a): The TD^0 transitions observed in the PTIS spectra of the B-doped ($4 \times 10^{15}cm^{-3}$) oxygen-rich silicon sample annealed for 15 hours at 450°C at different stages of illumination with band-edge light.

a)Unilluminated	b)Part Illumination	c)Full Illumination	Donor Species	Transition (1s→)
613			$TD7^+$	$2p_0$
632			?	
	645	645	$TD6^+$	$2p_0$
660	659	659	?	
665	664	664	?	
668	667		?	
679	679	679	$TD5^+$	$2p_0$
766	766		$TD8^+$	$2p_\pm$
790	792	792	$TD7^+$	$2p_\pm$
804	804	804	$TD6^+$,$TD2^+$	$2p_\pm$, $2p_0$
825	825	825	$TD6^+$	$2p_\pm$
	848	848	$TD5^+$	$2p_\pm$
	855	856	$TD1^+$	$2p_0$
	861	862	$TD5^+$	$2p_\pm$
	874	874	$TD8^+$	$3p_\pm$
887	889	887	$TD4^+$	$2p_\pm$
902		902	$TD4^+$	$2p_\pm$
	908	908	$TD7^+$	$3p_\pm$
		929	$TD6^+$	$3p_\pm$
		935	$TD6^+$	$3p_\pm$
945		946	$TD3^+$	$2p_\pm$
952	953	952	$TD3^+$	$2p_\pm$
		965	$TD5^+$	$3p_\pm$
	972	971	$TD5^+$	$3p_\pm$
992	991	992	$TD2^+$	$2p_\pm$

Table 4.1b): The TD^+ transitions observed in the PTIS spectra of the B-doped ($4 \times 10^{15}cm^{-3}$) oxygen-rich Cz-silicon sample annealed for 15 hours at 450°C at different stages of illumination with band-edge light. Not all features observed in the spectra in this region could be assigned.

Previous PTIS experiments	Full Illumination	Donor Species	Transition (1s→)
232.0	230	STD B	$2p_{\pm}$
234.0	236	STD C	$2p_{\pm}$
239.5	240*	STD D	$2p_{\pm}$
241.0	241*	STD E	$2p_{\pm}$
247.2	247*	STD F	$2p_{\pm}$
250.1	252	STD G	$2p_{\pm}$
257.5	257	STD B	$3p_{\pm}$
260.0	261	STD C	$3p_{\pm}$
265.0	265	STD D	$3p_{\pm}$
267.4	270	STD E	$3p_{\pm}$
274.2	274*	STD F	$3p_{\pm}$
277.1	277*	STD G	$3p_{\pm}$
Reported in+ the literature			
245.04	245	B	1
278.51	278	B	2
309.29	309	B	3
316.09	315	P	$2p_{\pm}$
320.05	320	B	4
334.86	334	B	5
342.55	340	P	$3p_{\pm}$
350.05	350	P	$4p_{\pm}$

+ A.K. Ramdas and S. Rodriguez, Rep. Prog. Phys. 44 p1297 1981.

Table 4.2: The transitions associated with the STD, B and P observed in the PTIS spectrum of the B-doped ($4 \times 10^{15} cm^{-3}$) oxygen-rich Cz-silicon sample under illumination with band-edge light from a tungstem filament lamp. Transitions marked by an asterisk coincide to some degree with the major boron transitions.

4.2.2 As-grown boron doped Cz-silicon

A sample of as-grown Cz-silicon containing $7\times10^{14}cm^{-3}$ boron has been studied by PTIS. This sample was cut from a slice taken from a B-doped Cz-silicon boule during the growth process before the final heat-treatment processing. At this stage the Cz-silicon is n-type since it contains TD formed during the growth. The net donor impurity concentration estimated from the room temperature resistance is $2.6\times10^{14}cm^{-3}$. The B concentration of the material was determined from resistivity measurements on the remainder of the boule after heat-treatment to disperse these donors. The sample dimensions were 3mm× 3mm× 10mm and all faces were polished. Multiple layer contacts consisting of 100Å Ni, 100Å Au, 100Å Sb and 3800Å Au were deposited on opposite 3mm× 10mm faces and laser annealed.

The PTIS spectrum of the as-grown B-doped material is shown in Fig 4.5 at 14.2K, a resolution of $1cm^{-1}$ and 2.3V bias voltage. In the wavenumber range 380-530cm^{-1} minima associated with the hydrogenic series of transitions of TD1 to TD4 are observed (Fig 4.5a). In the wavenumber range 200-300cm^{-1} two transitions of similar intensity are observed at 240.4cm^{-1} and 244.0cm^{-1} and two weaker transitions are observed at 266.7cm^{-1} and 270.5cm^{-1} (Fig 4.5b). Their separations correspond to the energy separation between EMT-like $1s \rightarrow 2p_{\pm}$ and $1s \rightarrow 3p_{\pm}$ transitions. The transitions occur in the same wavenumber region as the STD but are rather broad, probably due to concentration broadening. The transitions at 240.4cm^{-1} and 266.7cm^{-1} are tentatively assigned to STD D. The transitions at 244.0cm^{-1} and 270.5cm^{-1} possibly result from the overlap of STD E and F.

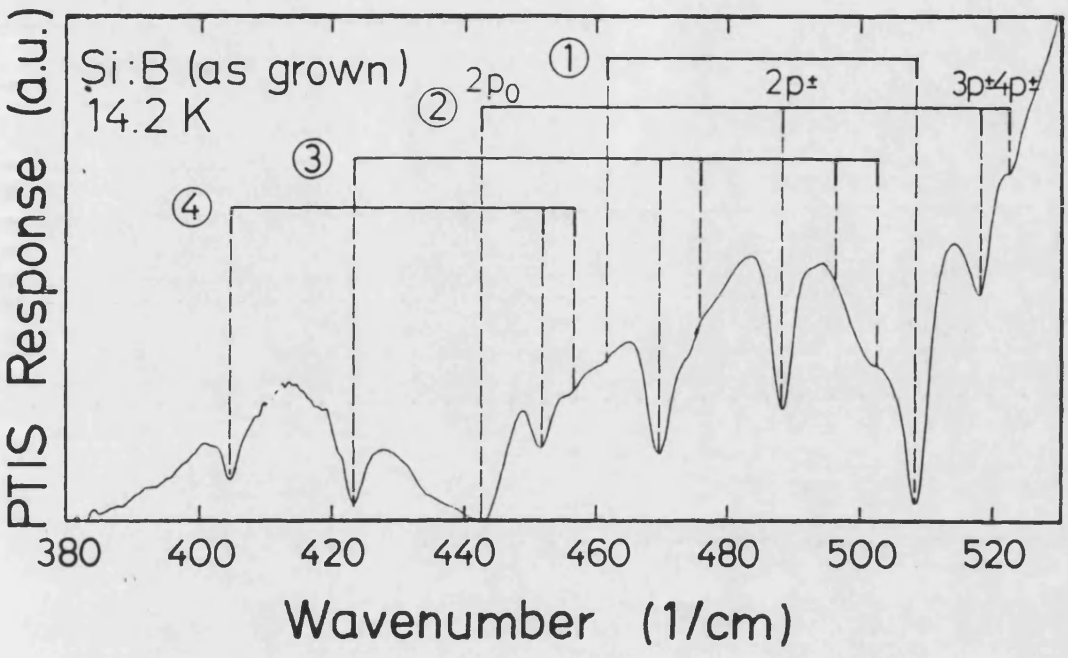

Fig 4.5a): The PTIS spectrum of as-grown B-doped ($7 \times 10^{14}cm^{-3}$) Cz-silicon. The TD^0 transitions are indicated.

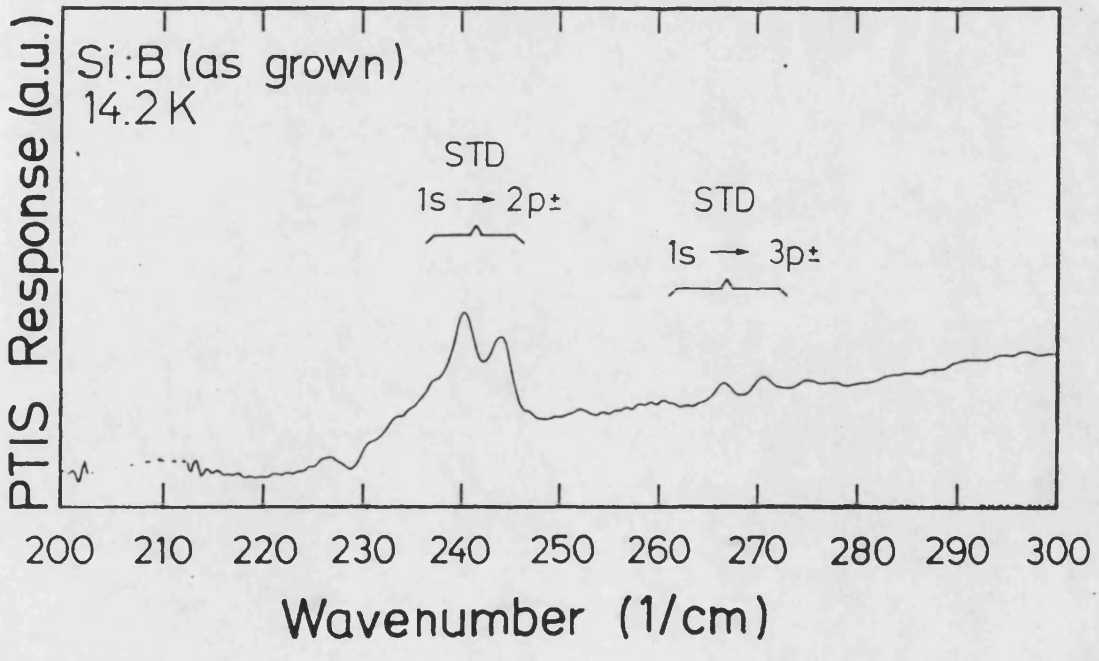

Fig 4.5b): The PTIS spectrum of as-grown B-doped ($7 \times 10^{14}cm^{-3}$) Cz-silicon showing features associated with the STD.

4.2.3 Conclusions

Weak minima which are tentatively assigned to the transitions of the STD are observed in a B-doped ($7 \times 10^{15}cm^{-3}$) Cz-silicon sample illuminated by band-edge light. Peaks observed in the PTIS spectra of as-grown B-doped ($7 \times 10^{14}cm^{-3}$) Cz-silicon also indicate the presence of the STD in this material. No evidence of enhancement of the STD formation due to the presence of the B was found.

4.3 The role of oxygen

The experimental data strongly suggest that the STD are oxygen related. The STD have only been observed in oxygen-rich Cz-silicon after heat treatment in the range 420-470°C. They have not been observed in float-zone silicon even after extended heat treatment at 450°C. Similar to the TD, according to the perturbation model the STD may possibly be assigned to two series of oxygen agglomerates each with an unknown donor core. Also, as for the TD, they may be destroyed by a short 700-1000°C degree anneal.

It has been observed that the thermal history of a sample is extremely important and determines the PTIS spectrum observed. During heat treatment some interstitial oxygen is always lost to the growth of oxygen precipitates. The trends observed in the PTIS spectra of samples subjected to different heat treatments may be explained by differences in the STD growth rate correlated to differences in the interstitial oxygen concentration.

4.3.1 Photothermal Ionisation Spectroscopy: experimental results

Two samples from the same wafer of undoped n-type Cz-silicon were given the following heat treatments:

Sample A: 700°C preanneal, 1 hour at 450°C in oxygen

Sample B: 700°C preanneal, 3 hours at 450°C in oxygen,
10 mins at 1000°C, 1 hour at 450°C in oxygen.

The initial interstitial oxygen concentration was $10^{18}cm^{-3}$ in both samples. The previous thermal history of sample B reduces the available interstitial oxygen before the 1 hour anneal compared to sample A. After annealing for 1 hour at 450°C the net impurity concentrations estimated from the room temperature resistance were $4 \times 10^{13}cm^{-3}$ for sample A and $8 \times 10^{12}cm^{-3}$ for sample B. More donors have been formed in sample A than in sample B as expected from the TD formation kinetics. The P concentration in both samples is approximately $3.6 \times 10^{13}cm^{-3}$ from infrared transmission measurements. Hence by comparing the PTIS spectra of sample A and sample B after 1 hour annealing at 450°C as shown in Fig 4.6a and Fig 4.6b respectively the effect of the thermal history of sample B, assumed to be primarily the reduction in interstitial oxygen, can be studied. The measurements were carried out at 16K and 6.1V bias voltage at a resolution of $0.5cm^{-1}$.

Comparing the two spectra it is observed

- In a) the transitions of TD2, 3 and 4 are observed as strong minima in the photoionisation continuum.

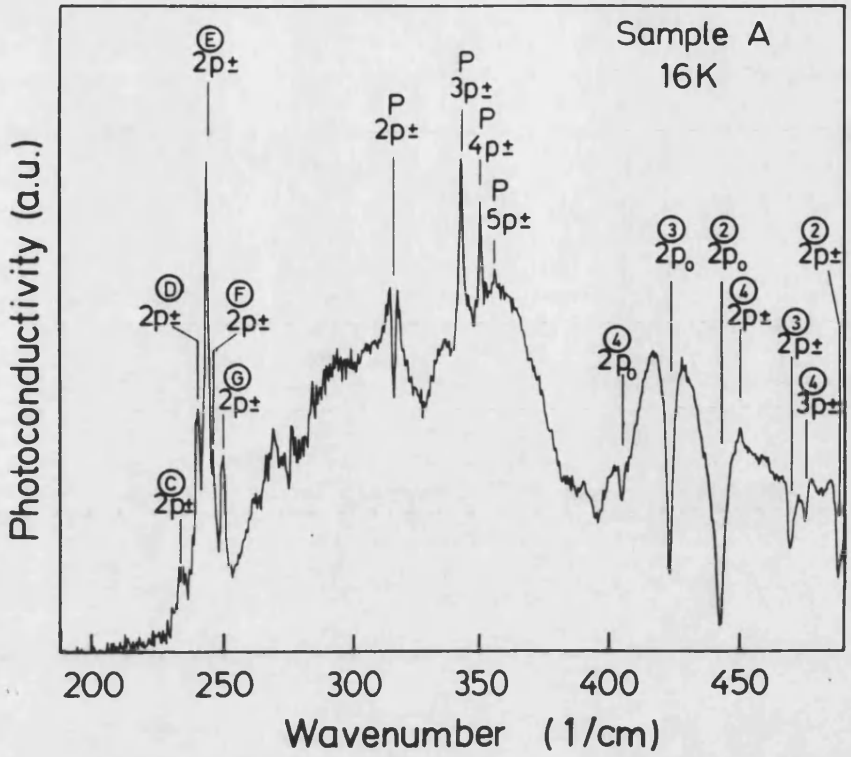

Fig 4.6a): The PTIS spectrum of an undoped oxygen-rich Cz-silicon sample after a heat-treatment: 700°C preanneal, 1 hour at 450°C in oxygen.

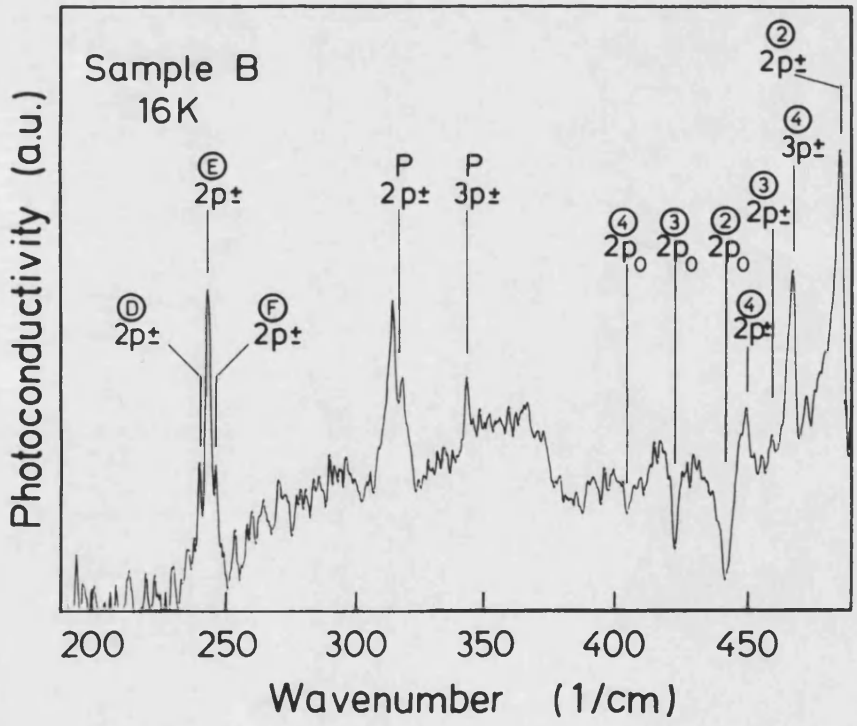

Fig 4.6b): The PTIS spectrum of an undoped oxygen-rich Cz-silicon sample after a heat-treatment: 700°C preanneal, 3 hours at 450°C in oxygen, 10 minutes at 1000°C (to destroy the TD activity), 1 hour at 450°C in oxygen.

- In b) the transitions TD2 $1s \rightarrow 2p_{\pm}$, TD4 $1s \rightarrow 3p_{\pm}$ and TD3 $1s \rightarrow 2p_{\pm}$ appear as peaks. The remaining transitions still appear as minima.
- The P $1s \rightarrow 2p_{\pm}$ transition appears as a minimum in a) and as a notched peak in b).
- In a) the STD continuum is well defined, in b) it is not.
- In a) the transitions of five STD are clearly distinguishable, in b) only three.

Taking these facts into account the two spectra may be explained in terms of the competing processes of photo-thermal ionisation and direct photo-ionisation within the three groups of donors, and their relative concentrations (see section 1.5.1).

4.3.2 The Thermal Donor transitions

The rate of growth of the TD is dependent on the fourth power of the initial interstitial oxygen concentration, therefore the concentration of TD1 to TD4 formed in sample A is expected to be higher than in sample B. A large concentration of TD gives rise to a large continuum in which the TD transitions appear as strong minima as seen for sample A. In sample B the lower concentration of TD gives rise only to a weak continuum and the strongest TD transitions emerge as peaks.

4.3.3 The phosphorus $1s \rightarrow 2p_{\pm}$ transition

Consider the model calculation presented in section 1.5.1 in which the competition of two donor species for the available photons was considered. The

effect of a shallow donor undergoing direct photo-ionisation on the $1s \rightarrow 2p_{\pm}$ transition of P was calculated. The model indicates that depending on the relative concentrations of the two donor species the P $1s \rightarrow 2p_{\pm}$ transition at $316cm^{-1}$ may appear as a peak or a minimum in the continuum.

In these samples the STD compete with the P for the available photons. In the case of sample A the relative concentrations are such that a minimum is observed at $316cm^{-1}$ and for sample B, a peak. A model calculation of the frequency spectrum around the $1s \rightarrow 2p_{\pm}$ transition at $316cm^{-1}$ relative to the background, is shown in Fig 4.7 for three different STD concentrations. At a STD concentration of $5 \times 10^{12}cm^{-3}$ a peak is predicted, at $1 \times 10^{13}cm^{-3}$ no feature is visible and at $5 \times 10^{13}cm^{-3}$ a minimum in the continuum is predicted. The absolute intensity of the continuum is related to the number of photons at each frequency. The continuum increases in intensity with increasing STD concentration and saturates beyond a certain critical concentration as shown in Fig 4.8.

In the model calculation the STD are treated as a single donor species. The STD concentrations given refer to the net STD concentration. The sample thickness is 2mm and the P concentration is $3.6 \times 10^{13}cm^{-3}$. The optical absorption cross-section for the P $1s \rightarrow 2p_{\pm}$ transition is $3 \times 10^{-14}cm^{2}$ (Baber, 1980) with a transition half-width of $3cm^{-1}$ and a Lorentzian lineshape. The optical absorption cross-section for the direct photo-ionisation of the STD is assumed to be $3 \times 10^{-14}cm^{2}$ and constant over the wavenumber range of the calculation.

The intensity of the P $1s \rightarrow 2p_{\pm}$ transition, normalised against the continuum, is shown in Fig 4.9 as a function of STD concentration. This figure shows that at STD concentrations less than $1 \times 10^{13}cm^{-3}$ a peak (ratio greater than one) is

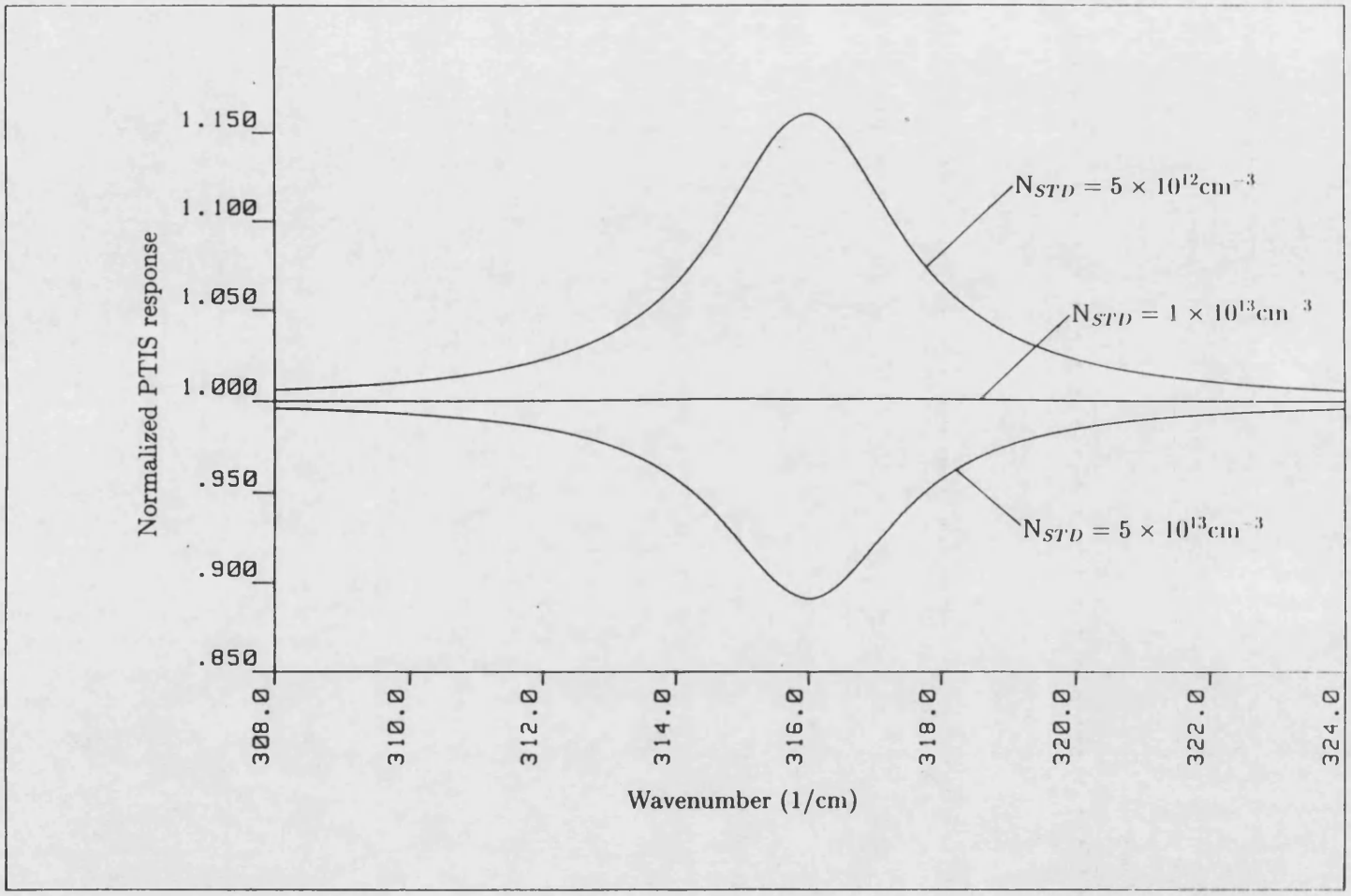

Fig 4.7: The PTIS response at the $1s \rightarrow 2p_{\pm}$ transition of P at 16K, normalized against the continuum for different concentrations of the STD (N_{STD}). $N_p = 3.6 \times 10^{13}cm^{-3}$, R=0.3, d=0.2cm and $\sigma_{STD} = \sigma_{P0} = 3 \times 10^{-14}cm^2$.

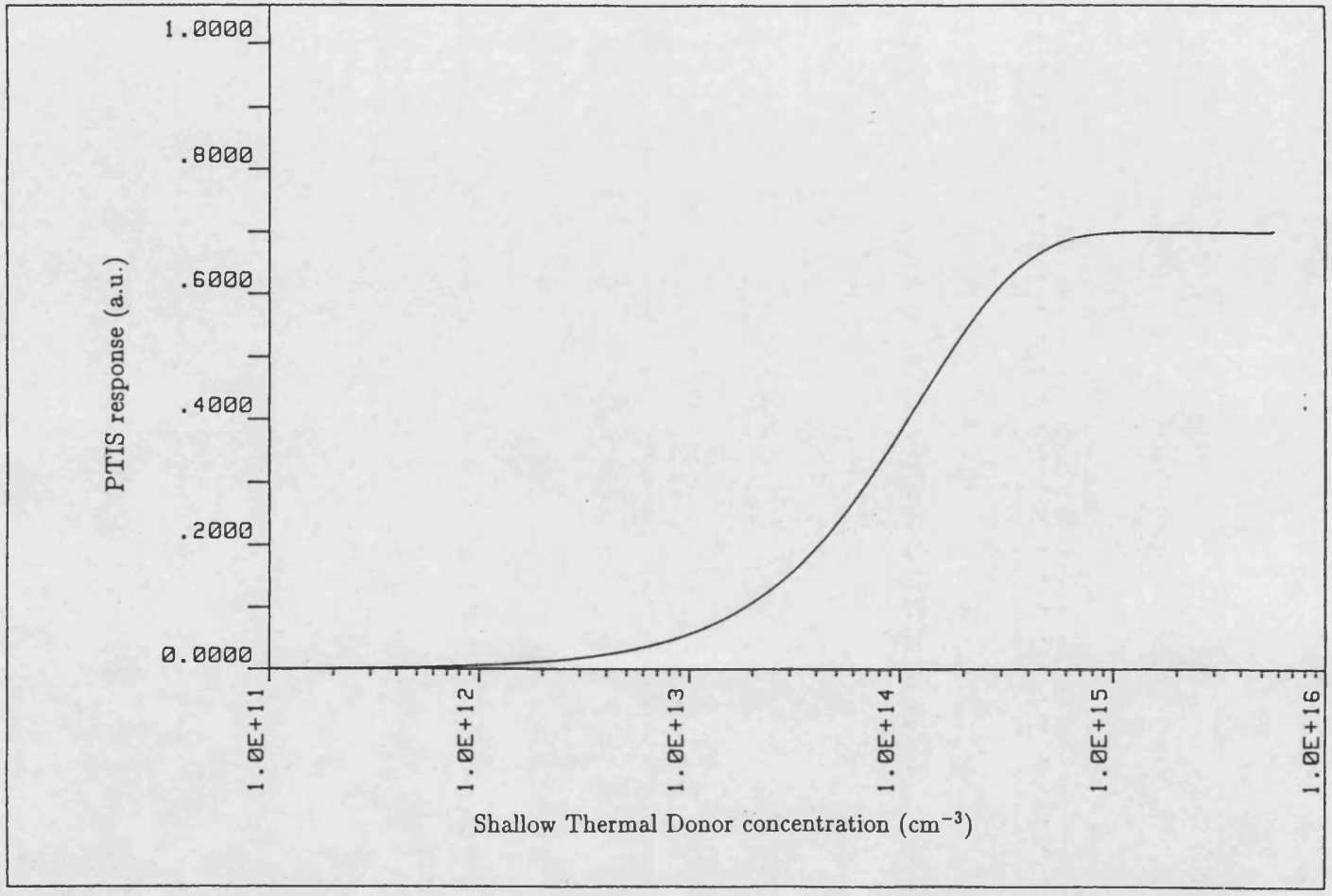

Fig 4.8: The calculated background PTIS response due to the direct photo-ionisation of the STD versus STD concentration.

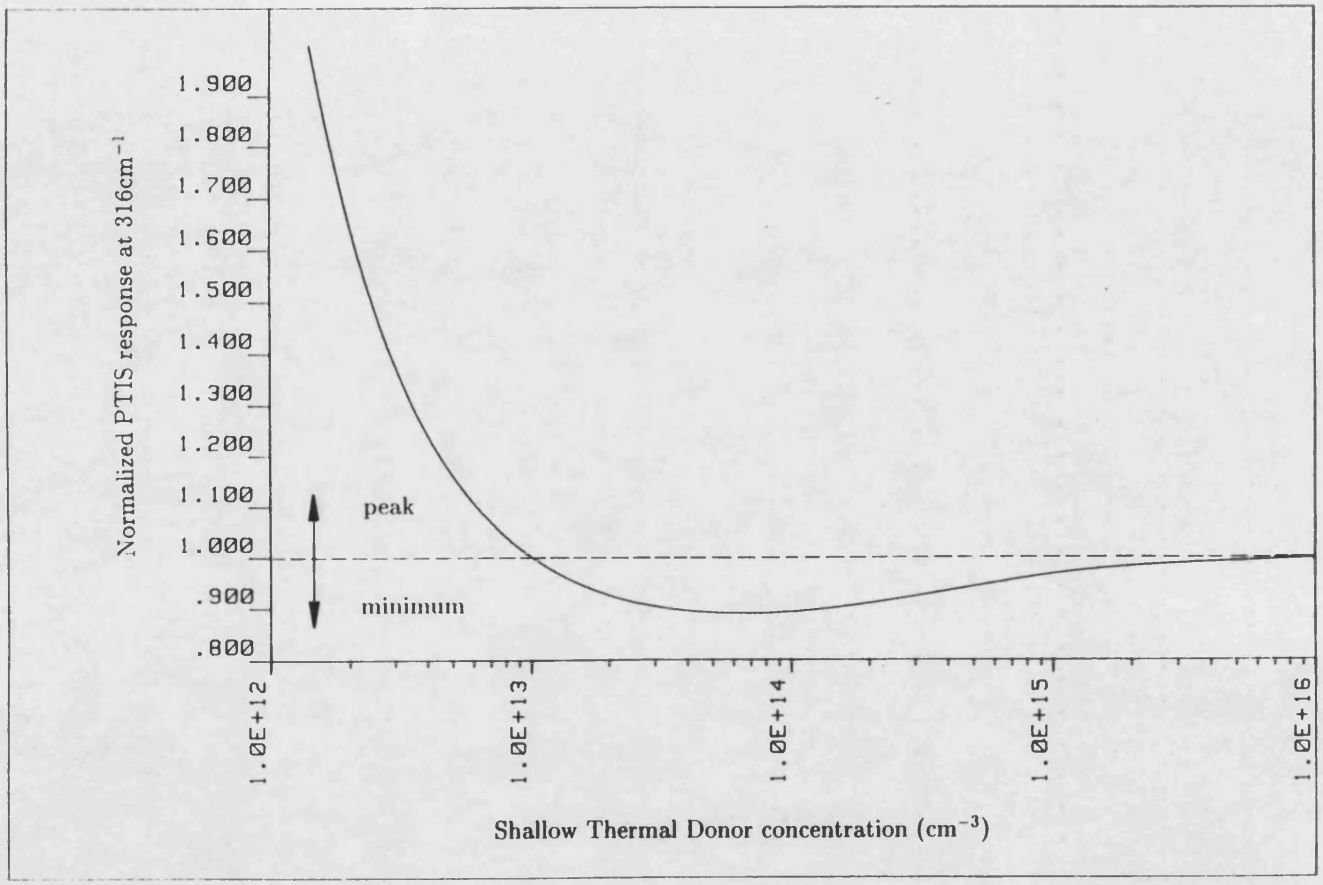

Fig 4.9: The ratio of the calculated magnitude of the PTIS response at the central frequency of the P $1s \rightarrow 2p_{\pm}$ transition (316cm^{-1}) to that of the background due to the STD, as a function of STD concentration. A ratio greater than one indicates a peak, a ratio less than one a minimum in the continuum in the PTIS spectrum.

expected at the transition frequency and at STD concentrations greater than $1 \times 10^{13}\text{cm}^{-3}$ a minimum (ratio less than one). Eventually the photo-ionisation of the STD becomes dominant and no feature is observed. This pinpoints the STD concentrations of samples A and B as of the order of 10^{13}cm^{-3} as indicated from the far infrared transmission measurements.

Further, at a total STD concentration of $1.009 \times 10^{13}\text{cm}^{-3}$ the predicted spectral response is a sharp minimum with positive shoulders similar to the form of the P transition in Fig 4.6a and at $1.002 \times 10^{13}\text{cm}^{-3}$ a notched peak is predicted similar to that observed in Fig 4.6b. The experimentally observed lineshapes are compared to the simulated PTIS response in Fig 4.10. The formation of such features can be seen to result from the shape of the oscillator describing the P transition. Although the qualitative features of the experimental lineshape are reproduced in detail, there are large differences in the predicted intensity. The model calculation predicts the features to be of very low intensity, less than 0.2% of the background intensity whereas the experimentally observed features are of the order of 100-200% compared to the continuum. Reconsidering the form of σ_P, the optical absorption cross-section for the $1s \rightarrow 2p_{\pm}$ transition of P, the experimental linewidth has been used in the Lorentzian lineshape. The total impurity concentration in these samples is high and therefore the transitions are broadened as discussed in section 2.8. The experimental lineshape results from photo-thermal ionisation and thus includes the absorption of a photon into a broadened excited state and the absorption of a phonon by an electron in such a state. However, for σ_P only the effect of the loss of sharpness of the excited state on photon absorption is significant. It is therefore suggested that the observed discrepancy of the intensities is linked to the fact that the mechanisms of concentration broadening and their relevance have not been considered. For example, describing σ_P with a sharper oscillator may be more

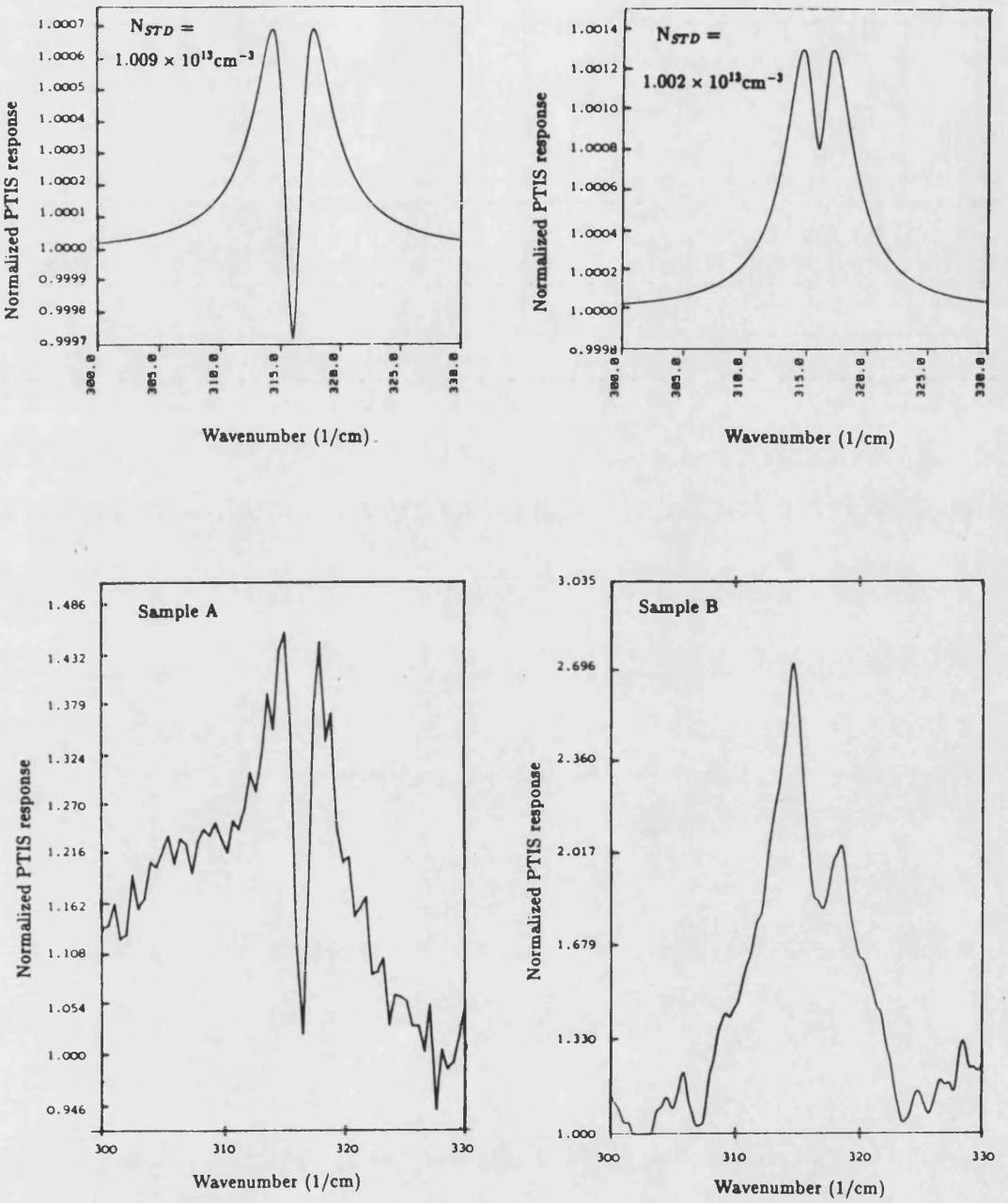

Fig 4.10: The lineshapes predicted by the PTIS model calculation at the changeover of the P $1s \rightarrow 2p_{\pm}$ transition from a peak to a minimum in the continuum compared to the experimentally observed lineshapes for samples A and B.

appropriate. Also, a more exact value for the optical absorption cross-section for the direct photo-ionisation of the STD should be found.

4.3.4 Conclusions

These calculations have demonstrated that assuming a constant P concentration the differences in the spectra in Fig 4.6 a) and b) may be attributed to a higher STD concentration in a) than in b). The model calculation predicts a total STD concentration of the order of $1 \times 10^{13}\text{cm}^{-3}$ and sets a lower limit for the difference in concentration between a) and b) of approximately $7 \times 10^{10}\text{cm}^{-3}$. The decrease in STD concentration between sample A and sample B is correlated to the decrease in available interstitial oxygen in the two samples, the same correlation is observed for the TD as expected. This supports the experimental data already presented which indicate that the STD are oxygen related donors.

These results also show that a simple model can successfully reproduce the experimentally observed features and is a great aid in understanding the complex interplay between different donor species giving rise to the resultant PTIS spectrum.

Applying this analysis to the original PTIS spectra of samples 1 and 2 it is seen that for sample 1 the peak at the $1s \rightarrow 2p_{\pm}$ transition frequency of P is less strong compared to the background than for sample 2. This indicates that more STD have been formed in sample 1 which had a longer heat treatment than in sample 2 as would be expected.

4.4 Summary

Phosphorus and boron do not appear to play a major role in the growth and formation of the STD. There is however considerable evidence that the STD are related to oxygen. The STD may be oxygen agglomerates similar to the TD. Although the concentration of P or B does not appear to be decisive for the formation of the STD it can not be excluded that either impurity might be contained in the STD core. This would not contradict the experimental results presented here if it is assumed that the growth process is oxygen-limited. The concentration of P or B required is only of the order of $10^{13}cm^{-3}$ and both elements are always present in all Cz-silicon at this order of magnitude. A study of the P concentration as determined from the P $1s \rightarrow 2p_{\pm}$ transition in infrared transmission and the STD concentration determined from the PTIS spectra and model calculations before heat-treatment at 450°C and after successive heat-treatments at 450°C using the same sample might answer this question for P.

Chapter 5

Investigation of the growth of the Shallow Thermal Donors with annealing time and temperature

The study of the development of the STD at different annealing temperatures determines whether their growth shows similarities to that of the TD. A similar dependence on annealing temperature would support the association of the STD with oxygen clustering. A study of the dependence of the STD growth on annealing time provides data for calculations on the kinetics of formation and for modelling the STD centres. The association of the TD with oxygen clusters of increasing size resulted primarily from such studies. Also the preparation of samples may be optimised by annealing at the temperature and for the duration most favourable for STD growth. If samples can be grown containing higher concentrations of STD it will be possible to apply other characterisation methods such as DLTS and photoluminescence for their study.

The dependence of the STD development on annealing temperature has been studied from the PTIS spectra of three similar samples annealed at 420°C, 450°C and 470°C respectively. Also the dependence of the STD concentration

on duration of annealing at 450°C has been studied from the PTIS spectra of eight similar samples annealed for different periods of time between 15 minutes and 15 hours. Comparison is made to the formation kinetics of the TD.

5.1 Sample Preparation

For the annealing temperature study three samples 10mm×10mm×2mm were cut from a single Cz-wafer 2/321, supplied by Wacker Heliotronic. This undoped, low carbon, material is n-type and contains $10^{18}cm^{-3}$ interstitial oxygen. The samples were polished and then annealed for 1 hour at 420°C, 450°C and 470°C respectively in a nitrogen atmosphere.

For the annealing time study eight samples 8mm× 8mm × 2mm were cut from another single wafer of the same material as above. The samples were polished and then annealed for 20 minutes at 700°C in an oxygen atmosphere to destroy the TD formed during growth and bring them to a common initial state. Individual samples were then annealed for times between 15 minutes and 15 hours at 450°C in an oxygen atmosphere as listed in Table 5.1. It is known that the total concentration of TD created increases with annealing time (section 1.7). A corresponding decrease in the resistance of the samples was observed. The sample resistance as a function of annealing time is shown in Fig 5.1.

Ohmic contacts were achieved by depositing multiple-layer contacts consisting of 100Å Ni: 500Å Au: 130Å Sb: 3870Å Au in strips 1mm wide and 6.5 - 8mm apart onto a polished face of each sample and laser annealing with a Neodynium-YAG laser.

Sample	Annealing Time at 450C (hours)	Resistance (Ω)	Estimated net donor concentration (cm^{-3})
1	0.25	302.0	1.4×10^{13}
2	0.5	148.0	2.8×10^{13}
3	1.0	70.0	6.0×10^{13}
4	1.5	53.9	8.0×10^{13}
5	2.0	31.7	1.4×10^{14}
6	2.5	24.3	1.9×10^{14}
7	3.0	18.6	2.4×10^{14}
8	14.3	7.4	6.0×10^{14}

Table 5.1: The duration of the 450°C anneal for eight equivalent oxygen-rich undoped Cz-silicon samples. The room temperature resistance of the samples decreases with increasing annealing time as expected, due to TD formation. An estimate of the net donor concentration is given in each case.

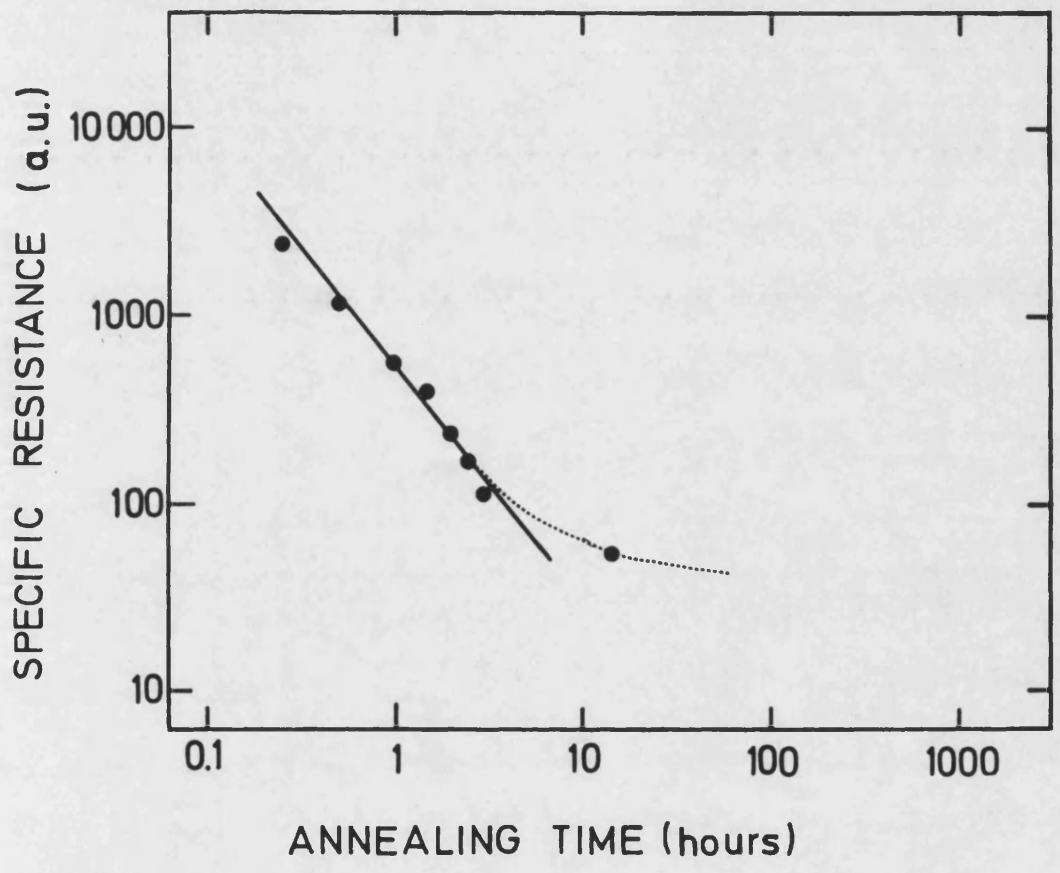

Fig 5.1: The specific resistance of the eight equivalent samples versus the duration of the 450°C anneal.

5.2 The dependence of the Shallow Thermal Donor concentration on annealing temperature

The PTIS spectra of the samples annealed at 470°C, 450°C and 420°C are shown in Fig 5.2 a), b) and c) respectively. This figure shows the spectral region 200-400cm^{-1} measured at a temperature of 15.5K, approximately 6V applied bias voltage and a resolution of 1cm^{-1}. All the spectra show transitions due to TD1, 2 and 3 in the region above 400cm^{-1} as expected after a 1 hour anneal. In the region below 400cm^{-1} the $1s \rightarrow 2p_{\pm}$ transitions of STD D, E and G are observed in all samples at 240.5cm^{-1}, 244.2cm^{-1} and 250cm^{-1} and the $1s \rightarrow 3p_{\pm}$ transitions at 266.9cm^{-1}, 270cm^{-1} and 273.2cm^{-1} respectively. Also the $1s \rightarrow 2p_{\pm}$ transition of P is observed as a minimum in the continuum at 316cm^{-1} and the $1s \rightarrow 2p_{\pm}$ transition as a peak at 342.8cm^{-1}. It is clear that the relative intensities of the STD transitions and P transitions are almost identical in all three spectra. It can therefore be concluded that within the range 420°C - 470°C there is no significant dependence of the growth of the STD on the annealing temperature.

The TD are observed after annealing between 300-500°C and formation is most rapid at 450-460°C. Further measurements on samples annealed over a wider range of temperatures are necessary to check the limiting temperatures for the STD growth. The initial experimental results suggest a temperature dependence of the growth similar to the TD.

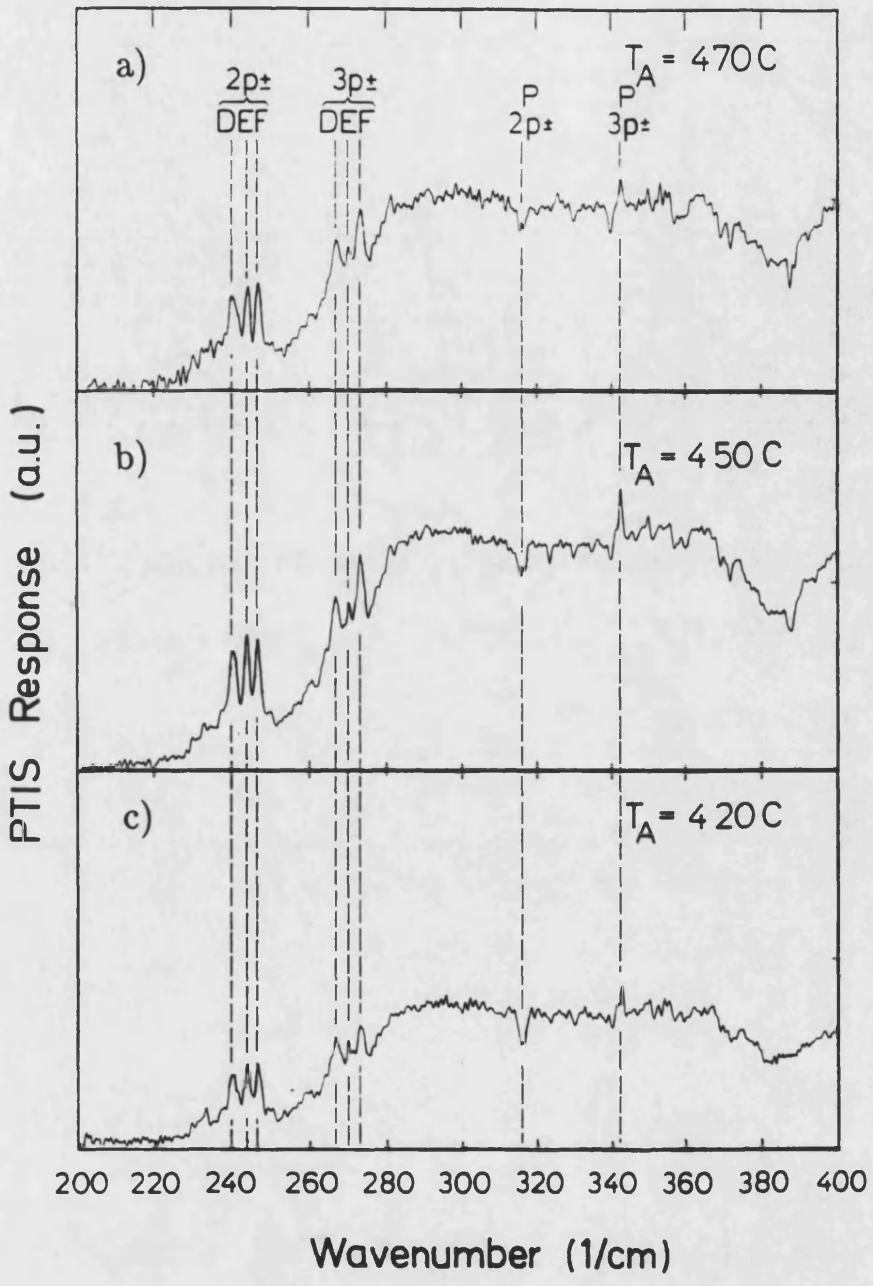

Fig 5.2: The PTIS spectra of three equivalent samples annealed for 1 hour at different annealing temperatures (T_A). Transitions associated with STD E, F and G and with P are indicated.

5.3 The dependence of the Shallow Thermal Donor concentration on annealing time

5.3.1 Infrared Transmission spectra

Infrared transmission spectra of the eight samples were taken at 5K and 0.25cm^{-1} resolution. In the spectral region 300cm^{-1} - 500cm^{-1} the transitions of the TD and P are observed. No features were observed in the spectral region below 300cm^{-1} up to three hours annealing time at 450°C. In the sample annealed for 14 hours and 20 minutes at 450°C large features are observed in this spectral region, but these could not be assigned to the STD.

The samples used for the annealing time study were carefully chosen to ensure a similar initial interstitial oxygen content and initial state before annealing. All samples were annealed under identical conditions and therefore the resultant spectra should show only the dependence of the donor growth on time. This is confirmed by a comparison to the results of Wagner et al (1984) for the TD in similar samples. The growth of the individual TD, in terms of the absorption coefficients of the $1s \rightarrow 2p_0$ transitions obtained from infrared transmission spectra, is shown in Fig 5.3. The experimental points are indicated by symbols and the dashed lines are given as a guide to the eye. The results of Wagner et al (1984) are indicated by solid lines. There is good qualitative agreement between the two measurements, and surprisingly close quantative agreement considering the strong dependence of the TD on the initial oxygen concentration and the somewhat higher annealing temperature of 460°C used by Wagner et al (1984).

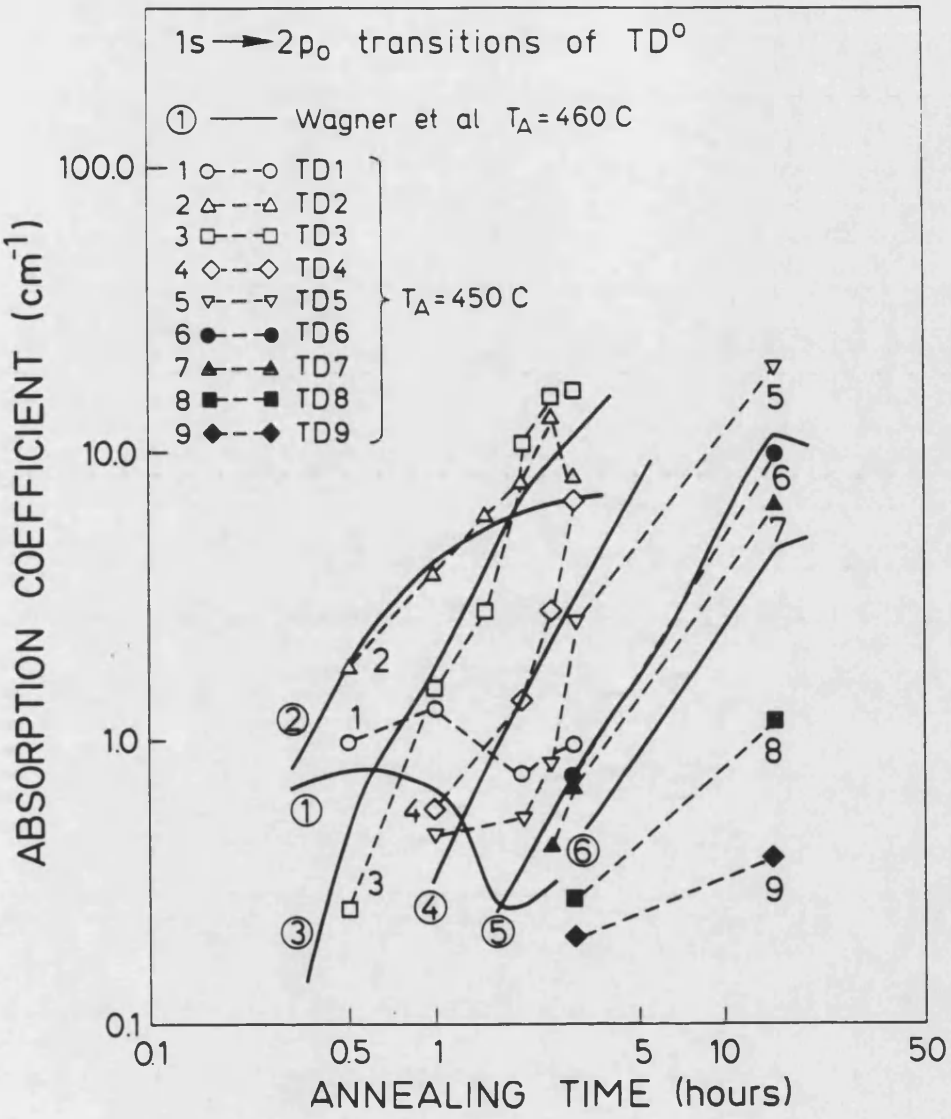

Fig 5.3: Absorption coefficients of the $1s \rightarrow 2p_0$ transitions of the TD^0 versus the duration of the 450° anneal (t_A). The experimental data from this study are shown as symbols connected by dashed lines as a guide to the eye with the notation TD1=1. For comparison the results of Wagner et al+ on similar samples are shown as solid lines with the notation TD1= ①.

+ P. Wagner, C. Holm, E. Sirtl, R. Oeder, W. Zulehner, Advances in Solid State Physics "Festkörperprobleme XXIV" (Vieweg, Braunschweig) 1984.

5.3.2 Photothermal ionisation spectra

The PTIS spectra of each sample was recorded at 15.5K ± 0.1K and 0.5cm^{-1} resolution with an applied bias voltage of approximately 6V. As seen in Fig 5.4 the development of the TD and STD concentrations with annealing time are clearly apparent. In the spectral region 350cm^{-1} - 500cm^{-1} a few TD transitions are visible after a 15 minute anneal, the number of transitions increase and become stronger with increasing annealing time. The transitions of the STD in the region 200cm^{-1} - 300cm^{-1} are present in all the spectra. These transitions are observed to increase in intensity up to 1.5 hours and then decline. The hydrogenic series due to P is also observed. The P $1s \rightarrow 2p_{\pm}$ transition changes from a peak at short annealing times to a minimum in the continuum after a 1 hour anneal. This phenomenon results from the interaction of the constant concentration of the P and the growing concentration of the STD as discussed in section 4.3.

5.3.3 The calibration of PTIS spectra

The absolute magnitude of the photoconductivity response in the PTIS spectra varies between samples and depends on the amplification factors used, the quality of the contacts, surface conditions and other factors. In order to compare the intensities of the transitions in the PTIS spectra a calibration must be made. Two methods of calibration have been used and both give effectively the same results when the intensities of transitions in the different spectra are compared.

The simplest method of calibration is to assume that the depths of the TD transitions in the background continuum in the PTIS spectra are proportional

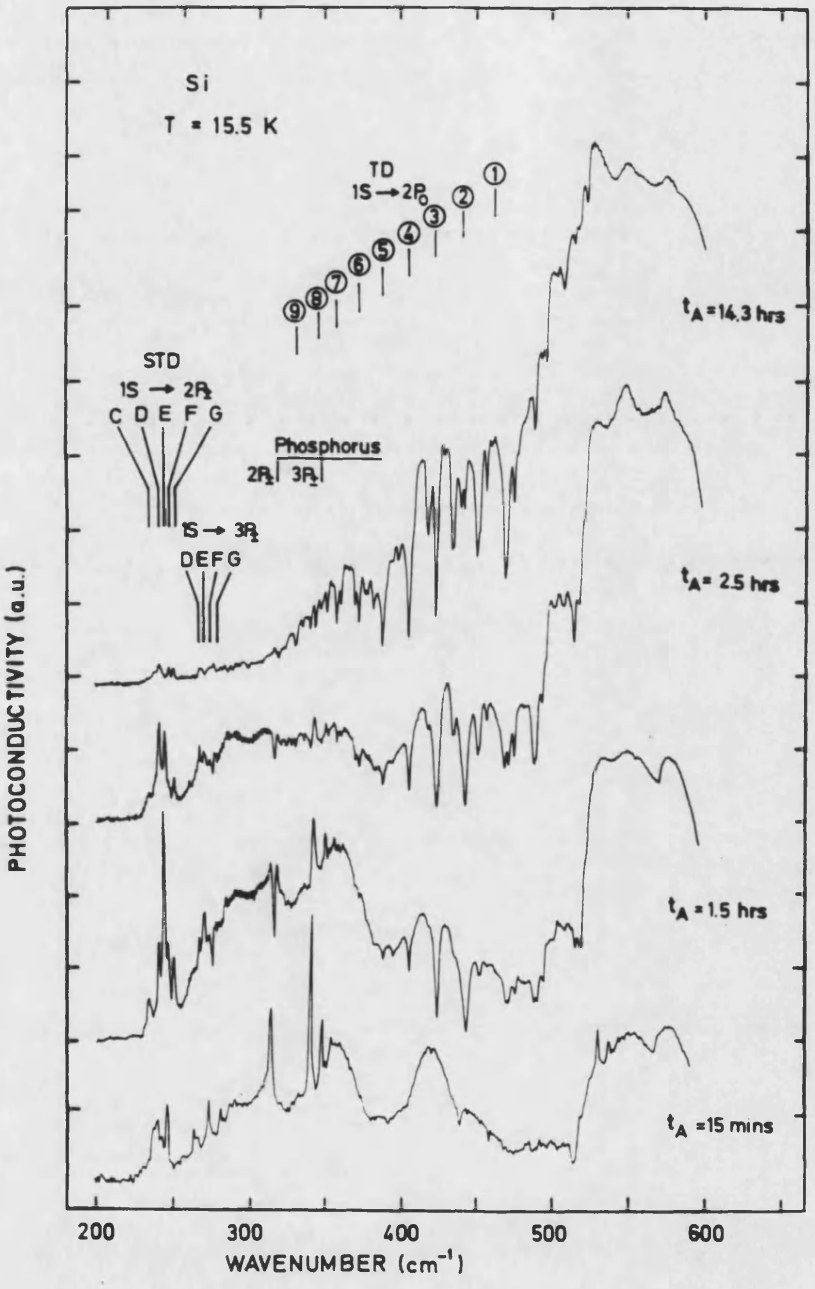

Fig 5.4: The PTIS spectra of equivalent samples as a function of annealing time (t_A) at 450°C. The STD and P transitions and the $1s \rightarrow 2p_0$ transitions of the TD^0 are indicated. A change in the transition intensities with duration of annealing time at 450°C is observed.

to the concentration of the relevant TD species. This calibration is of limited value since this approximation is not strictly true. The depth of a minimum in PTIS is known to depend on the concentration of the relevant donor species, here TD2 and the concentrations of shallower donor species, in this case TD9 - TD3, which are generating the continuum. The concentrations of these TD are also changing with annealing time.

An alternative calibration is based on the fact that the direct ionisation continua from all the TD give rise to a very large broad maximum between 520 - 600cm^{-1}. The observed response in this region is given by

$$R_{TD} = I\frac{(1-exp(-\sum_n \alpha(TD_n)\,d))(1-R)}{(1-Rexp(-\sum_n \alpha(TD_n)\,d))} \tag{5.1}$$

when $\sum \alpha d$ is large then the exponential term is small and R_{TD} is only determined by the intensity of the incoming radiation, I, which may be assumed to be the same in each spectrum, similar to Fig 4.8, section 4.3 for example. In the infrared transmission spectrum of sample 8 annealed for 14 hours and 20 minutes at 450°C total absorption is observed at 550cm^{-1}. The above condition ($\sum \alpha d$ large) is met and an absolute scale with a maximum of 1 at the peak of the continuum at 550cm^{-1} may be assigned to the corresponding PTIS spectrum. The remaining infrared transmission spectra show a residual transmission of 5 - 12% in this region. In this case the peak maxima observed at 550cm^{-1} in the PTIS spectra must represent the maximum possible intensity minus the relevant percentage of intensity observed in the transmission spectrum. In this way the remaining spectra may be calibrated. The intensities of transitions, according to the calibrated spectra, may now be compared.

5.3.4 Evaluation of the calibrated PTIS spectra

The intensities of the $1s \rightarrow 2p_{\pm}$ transitions of STD D, E, F and G are plotted as a function of annealing time at 450°C in Fig 5.5. The second calibration method described has been used in this case. The error in the intensities is of the order of ±5%. A similar figure based on the first calibration method is found in Appendix 1. The trend of these measurements indicates that the total STD concentration increases for annealing times up to 1.5 hours but then reaches a maximum and begins to decline, confirming the qualitative conclusion drawn from Fig 5.4. That no STD transitions were observed in the infrared transmission spectra indicates that the maximum concentration is of the order of $10^{13}cm^{-3}$ or less.

Unlike the TD no distinct clustering behaviour is observed for the STD. However the experimental difficulties associated with the measurements, for example obtaining "identical" samples, calibration of the PTIS spectra and the fact that the STD lines overlap make the trends of the individual STD difficult to follow. Qualitatively changes in the relative intensities of the STD are observed but these are very small compared to those observed for the TD. This study could be usefully extended by making measurements on a single sample after successive annealing stages at times between 30 minutes and 3 hours.

5.3.5 Compensation of the Shallow Thermal Donors and Phosphorus

The intensities of the STD transitions in Fig 5.4 and Fig 5.5 only indicate the neutral STD concentration. The spectrum of sample 8 shows very reduced STD transitions and also a very small positive peak at the $1s \rightarrow 2p_{\pm}$ transiton of P compared to the samples annealed for only 15 and 30 minutes. The P

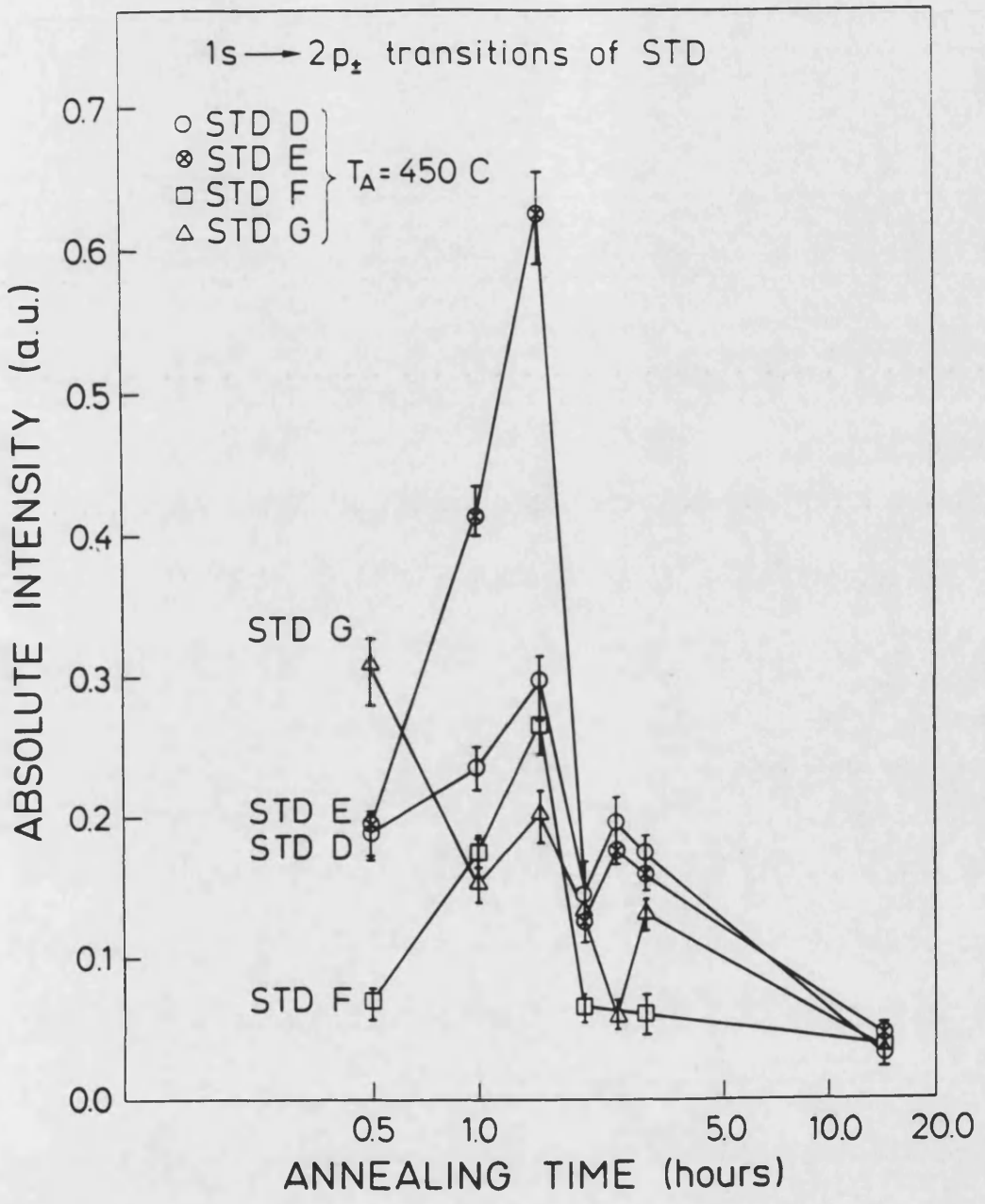

Fig 5.5: The relative intensities of the $1s \rightarrow 2p_{\pm}$ transitions of STD D, E, F and G obtained from the calibrated PTIS spectra of equivalent samples versus the duration of the 450°C anneal.

concentrations are similar in both cases and therefore the apparent decline of the P concentration observed in this spectrum is unexpected. Such behaviour can be understood if it is assumed that the STD and P are being compensated rather than decreasing in concentration.

Samples 1 and 2 were annealed at 1000°C to disperse the heat-treatment donors and reannealed at 450°C. The PTIS spectrum of these samples were measured by the author at Bruker Analytische Messtechnik, Karlsruhe, FRG using a Bruker IFS 113v at 16.5K with a resolution of $0.5cm^{-1}$. In the PTIS spectrum of sample 2 reannealed for 6 hours shown in Fig 5.6a) the STD are observed and a small mimumum is apparent at the P $1s \rightarrow 2p_{\pm}$ transition. In the PTIS spectrum of sample 1 reannealed for 12 hours in Fig 5.6b) no STD transitions are observed and no ionisation continuum from the STD is visible, the continuum first begins at $300cm^{-1}$. A small positive peak at the P $1s \rightarrow 2p_{\pm}$ transition is observed. This can again be understood on the assumption that the STD and P are being compensated.

The PTIS response function given in equation (1.22) will always give rise to a peak for the transitions of a single isolated donor species. In this regard we may consider the STD as a single donor species as there are no shallower donor species in competition with them for the available photons. If their concentration increases then the transition intensities will correspondingly increase. If the STD transition intensities decrease then

- either the STD are becoming electrically inactive or incorporated in larger clusters such that their absolute concentration is decreasing
- or they are being compensated so that their neutral concentration is decreasing.

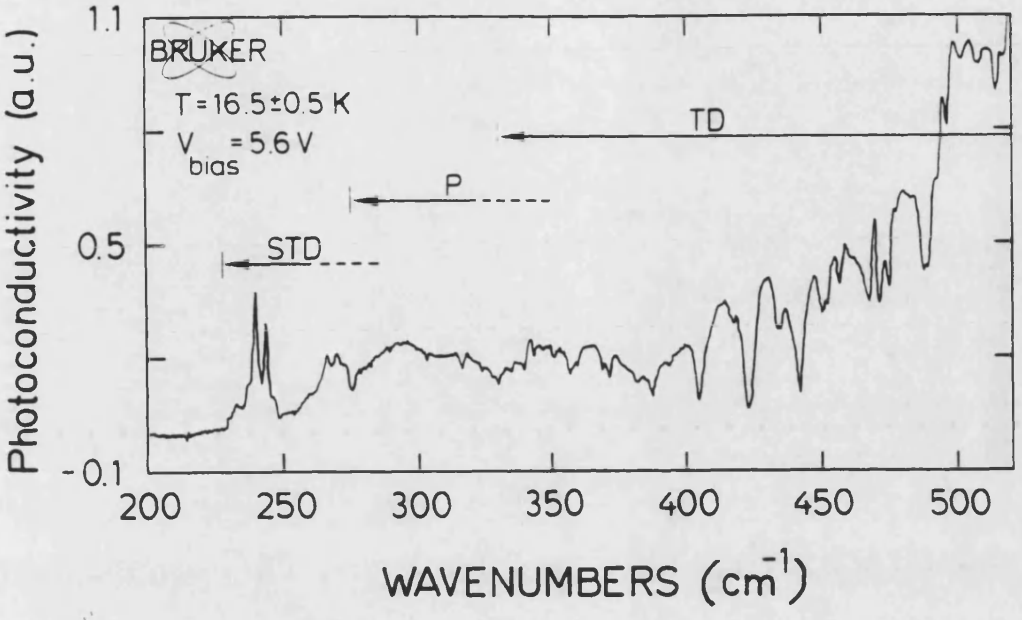

Fig 5.6a): The PTIS spectrum of sample 2 annealed for 10 minutes at 1000°C and subsequently reannealed for 6 hours at 450°C.

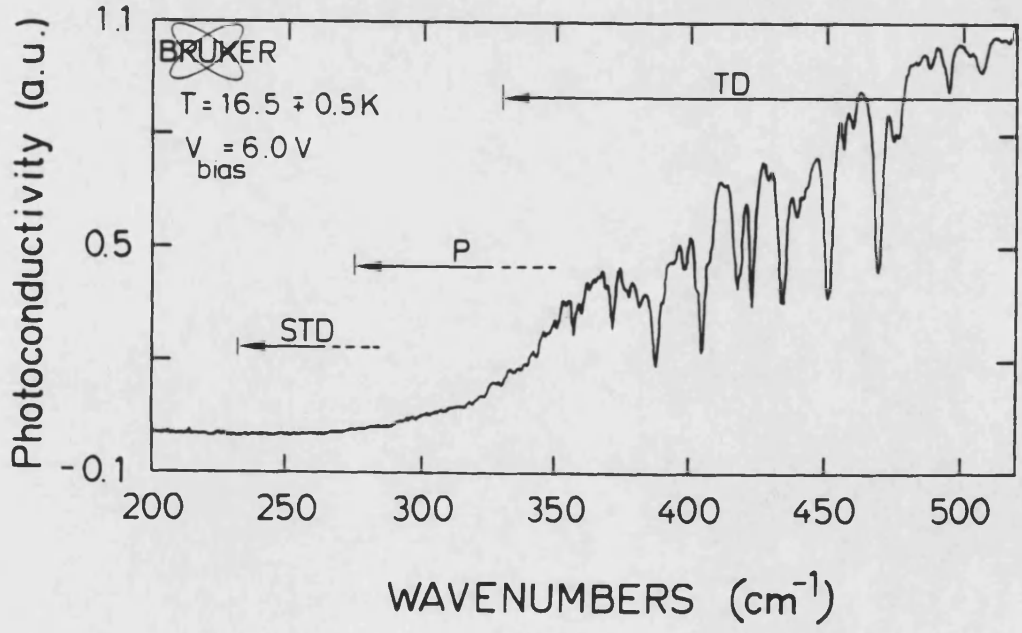

Fig 5.6b): The PTIS spectrum of sample 1 annealed for 10 minutes at 1000°C and subsequently reannealed for 12 hours at 450°C.

In the first case a decrease in the intensity of the STD transitions should be accompanied by an *increase* in the intensity of the P transitions since there is less competition for the available photons from the shallower donors. This is not observed experimentally. In the second case following a decrease in the STD transition intensities a decrease in the P transition intensities would be expected. This is similar to the actual experimental observation.

5.4 Summary

This study has confirmed that the STD concentration is dependent on duration of annealing at 450°C but not on the temperature of the anneal in the range 420°C - 470°C. The maximum concentration of the STD is estimated to be $\leq 10^{13}cm^{-3}$ and is reached after 1.5 hours compared to the maximum concentrations of $10^{15} - 10^{16}cm^{-3}$ reached by the TD after >10 hours (section 1.7.3). No clear indication of the successive growth and decay of the different STD, which would support cluster growth, is observed. In these samples STD D, E, F and G were always dominant, and although changes in the relative intensities were observed these were small. The decline of all the STD and P simultaneously does not correspond to the expected response if only the STD concentration is decreased. It is therefore suggested that the observed decline in the intensities of the STD transitions is due to the compensation of these shallowest donors by an unknown acceptor or acceptors.

Chapter 6

The temperature dependence of the Photothermal Ionisation Spectroscopy spectra

PTIS is a temperature dependent technique. The choice of measurement temperature may be used to optimize the experimental conditions for different transitions and impurity species as seen in Chapter 3. The hydrogenic series of transitions observed in PTIS allow an exact determination of the energy separation of the groundstate and excited states of an impurity. The temperature dependence of the intensity of these transitions allows the estimation of the thermal activation energies from the excited states.

The temperature dependence of the line intensities in the PTIS spectra is first considered for the simple case of n-type float-zone silicon containing only phosphorus impurities. Secondly, the temperature dependence of the intensities of the STD transitions has been studied and interpreted. It is shown that the temperature dependence is not described by a simple Boltzmann factor. In both cases the experimental data are explained by the use of a more detailed expression for the thermal ionisation probability from an excited state and the EMT predicted energy positions of the excited states below the conduction band.

6.1 Sample preparation

The float-zone silicon sample used for this study is high resistivity material with an atomic concentration of $3 \times 10^{14}cm^{-3}$ phosphorus as calculated from infrared transmission measurements. The sample is 10mm×10mm×0.5mm and polished on both faces with a 1° wedge to avoid channel spectra. Two 1mm wide strip contacts were deposited onto the top face as described in section 5.1.

The temperature dependence of the STD transitions was studied using sample 2 described in section 3.1. This sample was heat-treated at 450C for 15 minutes and has an estimated total STD concentration of $1 \times 10^{13}cm^{-3}$.

6.2 Temperature dependence of the phosphorus transition intensities in the PTIS spectra of float-zone silicon

PTIS spectra of the float-zone silicon sample were recorded at temperatures betwen 10K and 28K. The Leybold-Hereaus cryostat described in section 2.10 was used. The temperature was carefully controlled using an Allan Bradley 100Ω carbon resistor adjacent to the sample. A temperature stability of ±0.3 to ±0.1K was achieved. The measurements were made at a resolution of $0.5cm^{-1}$ with a bias voltage of 6V. The full width at half-height was approximately $0.5cm^{-1}$ for all transitions over the given temperature range.

Typical PTIS spectra obtained in this temperature range are shown in Fig 6.1. The transition intensities must be considered relative to the ionisation conti-

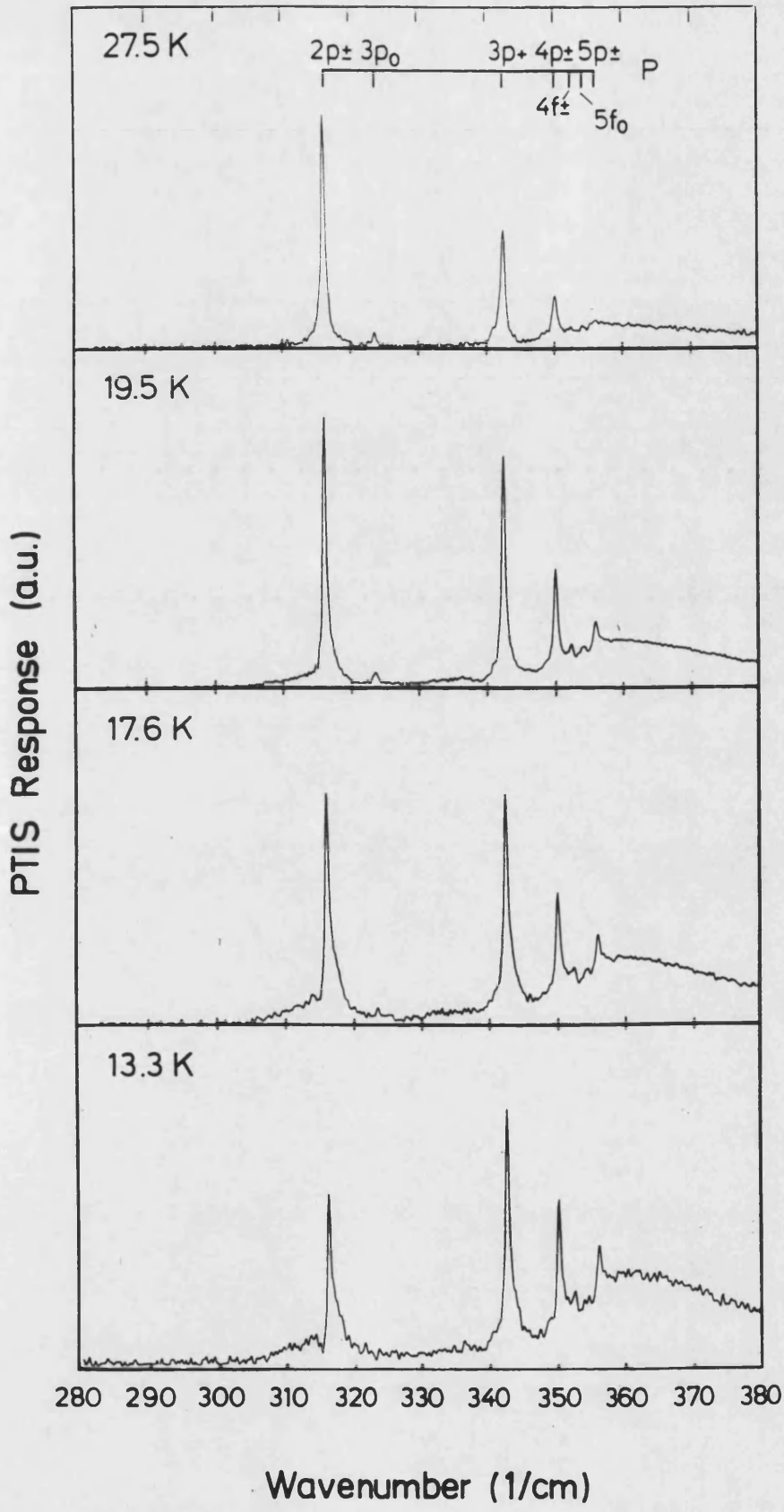

Fig 6.1: The temperature dependence of the intensities of the transitions of phosphorus in the PTIS spectra of float-zone silicon.

nuum (maximum at 360cm^{-1}). The continuum is not temperature dependent as it arises only from direct photo-ionisation from the groundstate. At lower temperatures the probability of photothermal ionisation is low and the intensity of the transitions is small compared to the ionisation continuum. This is more pronounced for the transitions associated with the deeper excited states. Due to the reduced signal strength the signal-to-noise ratio is smaller and the spectrum is more noisy. As the temperature increases the thermal ionisation probabilities from the excited states increases giving rise to higher line intensities relative to the continuum. Above 17K the P $1s \rightarrow 2p_{\pm}$ transition is more intense than the P $1s \rightarrow 3p_{\pm}$ transition indicating that the optical absorption cross-section is now dominant in the photothermal ionisation probability since thermal ionisation from the excited states is efficient in both cases.

6.3 Temperature dependence of the Shallow Thermal Donor transition intensities in the PTIS spectra of heat-treated Cz-silicon

The PTIS spectra of sample 2 were recorded at temperatures between 6K and 22K. The cryostat used and method of temperature sensing were identical to those of the previous experiment on float-zone silicon. Typical PTIS spectra obtained in this temperature range are shown in Fig 6.2. These spectra were recorded at a resolution of 1cm^{-1} with a bias voltage of approximately 6V. Only the relevant spectral region 200-380cm^{-1} containing the $1s \rightarrow 2p_{\pm}$ and $1s \rightarrow 3p_{\pm}$ transitions of STD E, F and G and the transitions of P is shown. The width at half-height of the transitions was 2-2.5cm^{-1} over the temperature range studied.

At low temperatures (<11K) the signal is weak and the resultant spectrum is

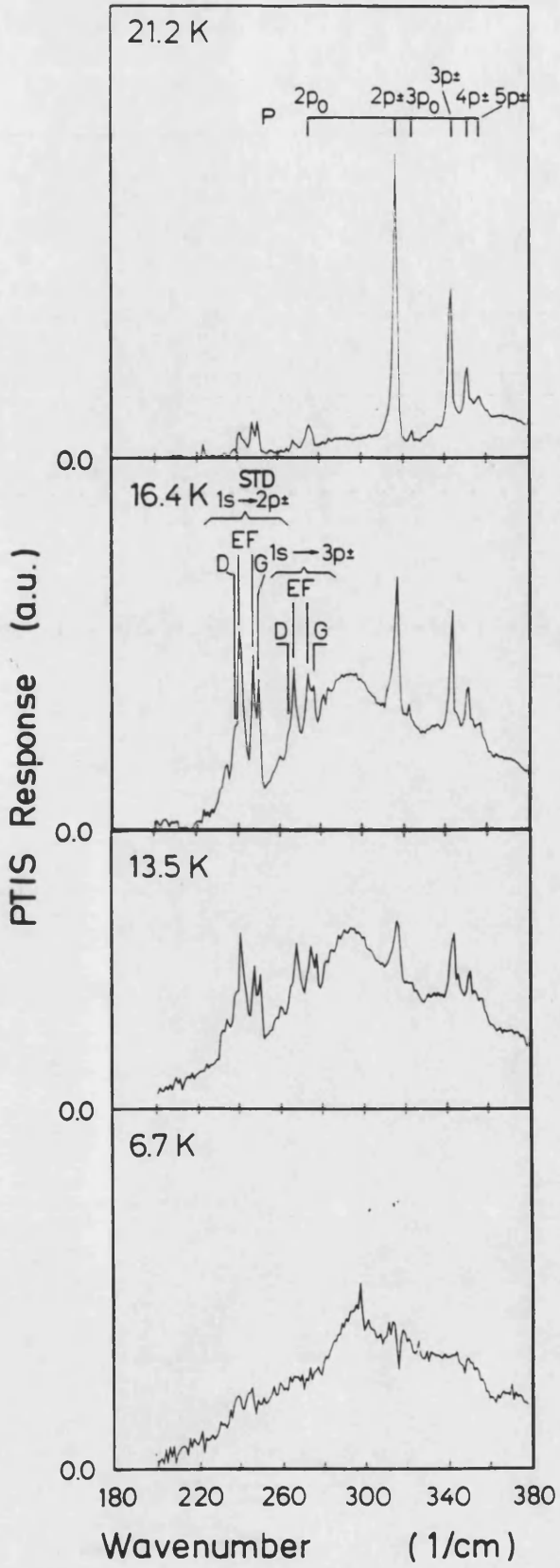

Fig 6.2: The temperature dependence of the intensities of the transitions of the STD E, F and G and phosphorus in the PTIS spectra of heat-treated Cz-silicon.

noisy. Thermal ionisation from the excited states is very low and therefore the intensity of the transitions arising from photothermal ionisation is very low compared to the continuum. As the temperature increases the STD transitions and also those due to P increase in intensity, reflecting the increase in the thermal ionisation probabilities from the excited states. At higher temperatures (>19K) the P transitions, by virtue of their higher concentration, dominate the spectrum. In comparison the STD transitions are small although they are now far more intense than their own continuum (maximum at 295cm^{-1}).

6.4 Temperature dependent factors in the PTIS response

The temperature dependence of the PTIS spectra stems principally from the temperature dependent thermal ionisation probability associated with the second stage of ionisation. A further factor is thermal ionisation from the groundstate which determines the equilibrium number of neutral donors available for PTIS. This factor will be treated first.

6.4.1 Direct Thermal Ionisation

In order to establish the neutral donor concentration at any given temperature an expression for the thermal ionisation from the groundstate must be derived. Consider the case of a single monovalent donor species in a semiconductor as shown in Fig 6.3 (Blakemore, 1962, Smith, 1964). The system contains N_d donor levels per cubic centimeter at an energy $E_c - E_d$, where E_d is the activation energy from the donor groundstate into the conduction band. The levels have spin degeneracy $\beta = 1/2$. It is assumed that the Fermi level, ϕ is

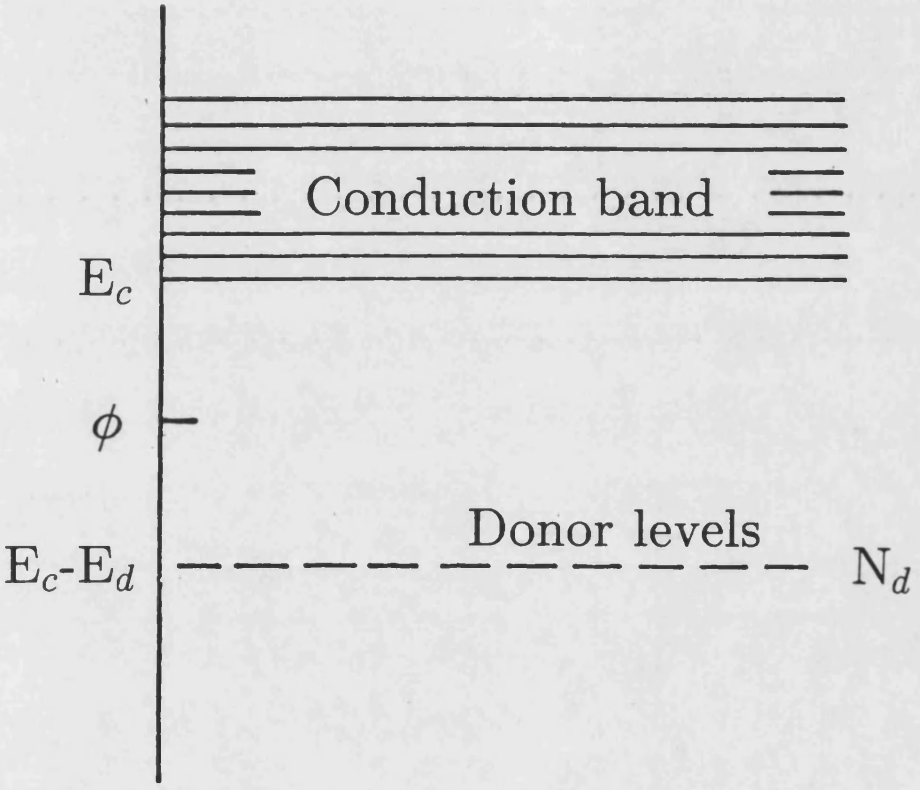

Fig 6.3: The simplest case of an extrinsic n-type semiconductor. Only a single monovalent donor is considered. (J. S. Blakemore, Semiconductor Statistics (Oxford, Pergamon) 1962.)

always several kT below the conduction band so that

$$exp\frac{E_c - \phi}{kT} \gg 1.$$

The number of electrons in the conduction band, n_o due to thermal ionisation is given by

$$n_0 = N_c f_{\frac{1}{2}} \left[\frac{\phi - E_c}{kT}\right] \tag{6.1}$$

where N_c is the effective density of states in the conduction band which is $6 \times 1.21 \times 10^{-15} T^{3/2} \mathrm{cm}^{-3}$ for silicon (Sze, 1981) and $f_{\frac{1}{2}}$ is the occupation probability given by the Fermi integral. This may also be expressed as

$$n_0 = N_d - N_d^0 \tag{6.2}$$

where N_d is the total donor concentration and N_d^0 is the concentration of neutral donors. This may be written in the form

$$n_0 = \frac{N_d}{1 + \beta^{-1} exp(E_d + \phi - E_c/kT)}. \tag{6.3}$$

The approximate solution of equation (6.1) is

$$n_0 \approx N_c \, exp - \frac{(E_c - \phi)}{kT} \tag{6.4}$$

Substituting for $exp - (E_c - \phi)/kT$ in equation (6.3) and rearranging gives a quadratic in n_0 with one real solution such that

$$n_0 = \frac{2 N_d}{1 + \sqrt{\frac{4 N_d}{\beta N_c} exp\left(\frac{E_d}{kT}\right)}}. \tag{6.5}$$

Knowing the value of n_0 the number of neutral donors at a given temperature may be obtained from equation (6.2).

In reality a semiconductor always contains acceptors and donors of more than one species. The effect of compensation has been discussed by Blakemore (1962). It has the effect of decreasing the fraction of ionised impurities at any given temperature.

Since the most shallow occupied donor species in the semiconductor determine the position of the Fermi level at low temperatures then for the two systems under consideration, where the P and the STD respectively are known to be the shallowest donors from PTIS, then equation (6.4) allows a good estimation of the significance of direct thermal ionisation on the neutral donor population over the temperature range of interest.

The ratio of the concentration of thermally ionised donors to the total donor concentration, n_o/N_d as calculated from equation (6.4) is shown in Fig 6.4 as a function of inverse temperature, for the two systems of interest.

For the P donor in float-zone silicon $E_d = 45\text{meV}$ and $N_d = 3 \times 10^{14}\text{cm}^{-3}$. It can be seen that up to 35K less than 5% of the donors are thermally ionised. For the thermal ionisation of the STD the value of n_o/N_d for the shallowest donor STD E with $E_d = 36.2\text{meV}$ and an estimated concentration $N_d = 3 \times 10^{12}\text{cm}^{-3}$ (total STD concentration estimated to be approximately $1 \times 10^{13}\text{cm}^{-3}$) is shown. Up to 25K less than 5% of the neutral donors are ionised.

Therefore, in both investigations carried out the temperature range was such that thermal ionisation from the groundstate is expected to be less than 5% and may be neglected.

6.4.2 Thermal ionisation probability from an excited state

If the temperature dependence of the neutral donor concentration is neglected then the thermal ionisation probability, P(T) from an excited state is the sole temperature dependent factor in the PTIS response (excepting the mobility of the carriers once in the conduction band which will not be considered here).

The simplest approximation for this probability is a Boltzmann factor such

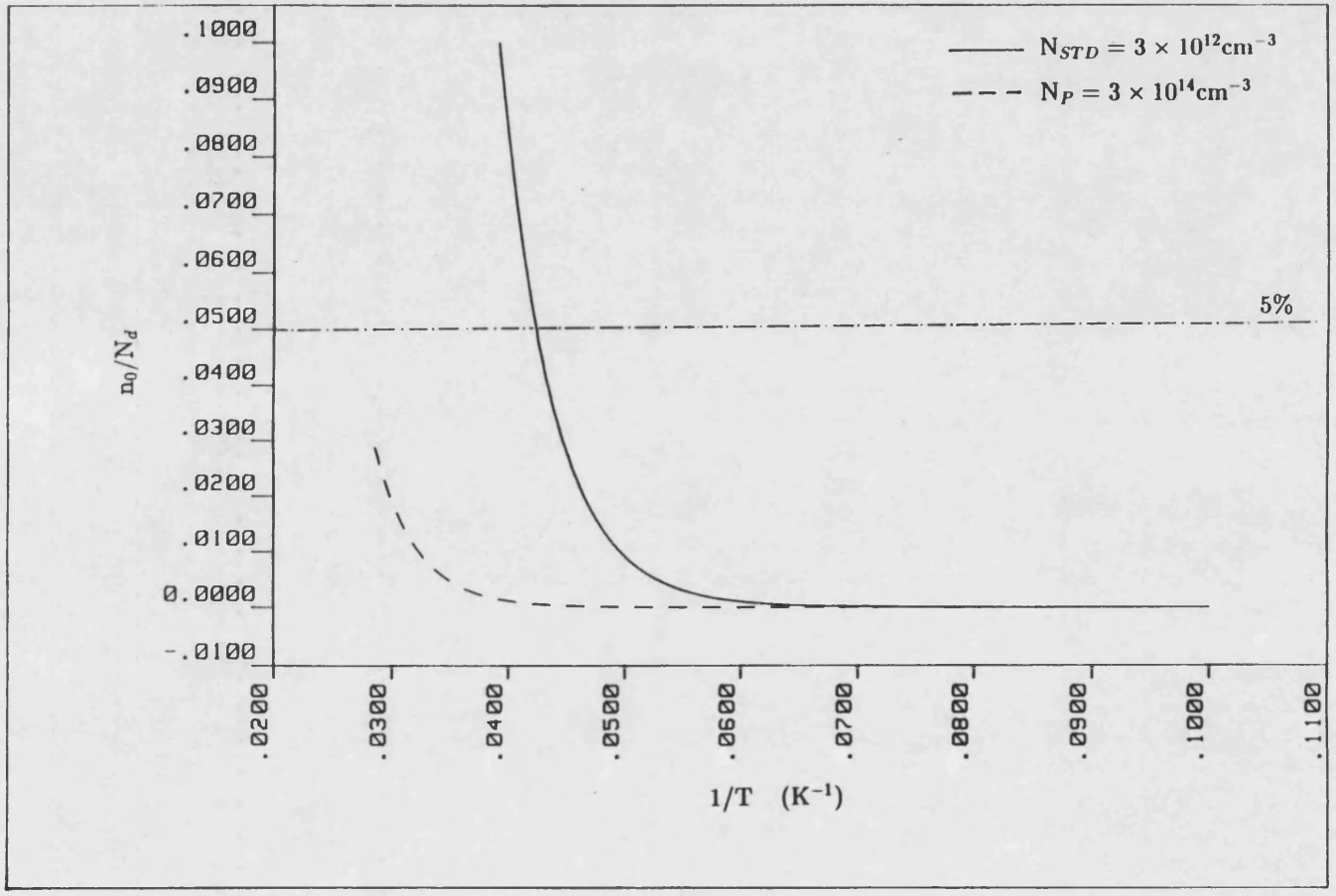

Fig 6.4: The ratio of the concentration of thermally ionised donors (n_0) to the total donor concentration (N_d) as a function of temperature calculated for the phosphorus donor in the float-zone silicon sample and the STD in the heat-treated Cz-silicon sample 2.

that

$$P(T) = exp - \frac{\Delta E}{kT} \tag{6.6}$$

where ΔE is the thermal activation energy. In general ΔE is taken to be the energy of the excited state below the conduction band.

However, it is known from temperature dependent PTIS studies of Ge (Jongbloets et al, 1979) that a better fit to the data is achieved if a more detailed expression is used. They describe the ionisation from the excited states using

$$P(T) = \frac{1}{1 + \frac{1}{g\,g'} exp\left[\frac{\Delta E}{kT}\right]} \tag{6.7}$$

where g is the degeneracy of the excited state and g' is the degeneracy of the conduction band.

An alternative expression for P(T) has been derived by Abakumov and Yassievich (1976) from an evaluation of the cross-section for recombination of an electron at an impurity. In this case

$$P(T) = \left(1 + \frac{\Delta E}{kT}\right) exp - \frac{\Delta E}{kT} \tag{6.8}$$

as quoted in section 1.5.

6.5 The Franck-Condon effect

The thermal activation energy ΔE of an excited state is generally taken as the energy of the excited state below the conduction band. However, this is a simplified approach since the bound electrons of the defect couple to some extent to the lattice. The excitation of a bound carrier into an excited state may result in the relaxation of the lattice in the neighbourhood of the defect for example (Bourgin and Lanoo, 1983). That is, the minimum of the excited state potential lies at a different atomic configuration than that of

the groundstate. This is shown schematically as a co-ordinate configuration diagram in Fig 6.5 for a donor groundstate localised at Q_0 and the first excited state and conduction band. Following the ionisation of the electron by the absorption of a photon the system relaxes by the emission of phonons through the vibrational states to its preferred potential minimum at a new lattice co-ordinate Q_1. The optically measured ionisation energy is given by $\epsilon_i(optical)$. If the donor is thermally ionised a lower ionisation energy $\epsilon_i(thermal)$ is observed.

Similarly, an optical transition into the first excited state is achieved by the absorption of a photon of energy $\hbar\omega$. By the absorption of a phonon of energy $\hbar\Omega$ the electron may be lifted into the conduction band. The thermal activation energy will not be the energy of the excited state below the conduction band (6.4meV for a $2p_{\pm}$ excited state) in this case, but a smaller value determined by the Franck-Condon parameter d_{FC}.

The magnitude of the Franck-Condon parameter depends on the strength of the coupling between the electron and lattice. For shallow donors the Franck-Condon parameter is usually insignificant and therefore the thermal activation energies are expected to be the same as the energies of the excited states below the conduction band. For deeper centres a measureable Franck-Condon shift is observed, for example the EL2 centre in GaAs ($\epsilon_i(optical)$=0.86eV) exhibits a Franck-Condon shift of 0.12eV.

6.6 Analysis of the experimental data

Consider the experimental data available from the PTIS spectra. The line intensities due to the transitions of each donor species may be measured relative to its own ionisation continuum. The intensity of the continuum results

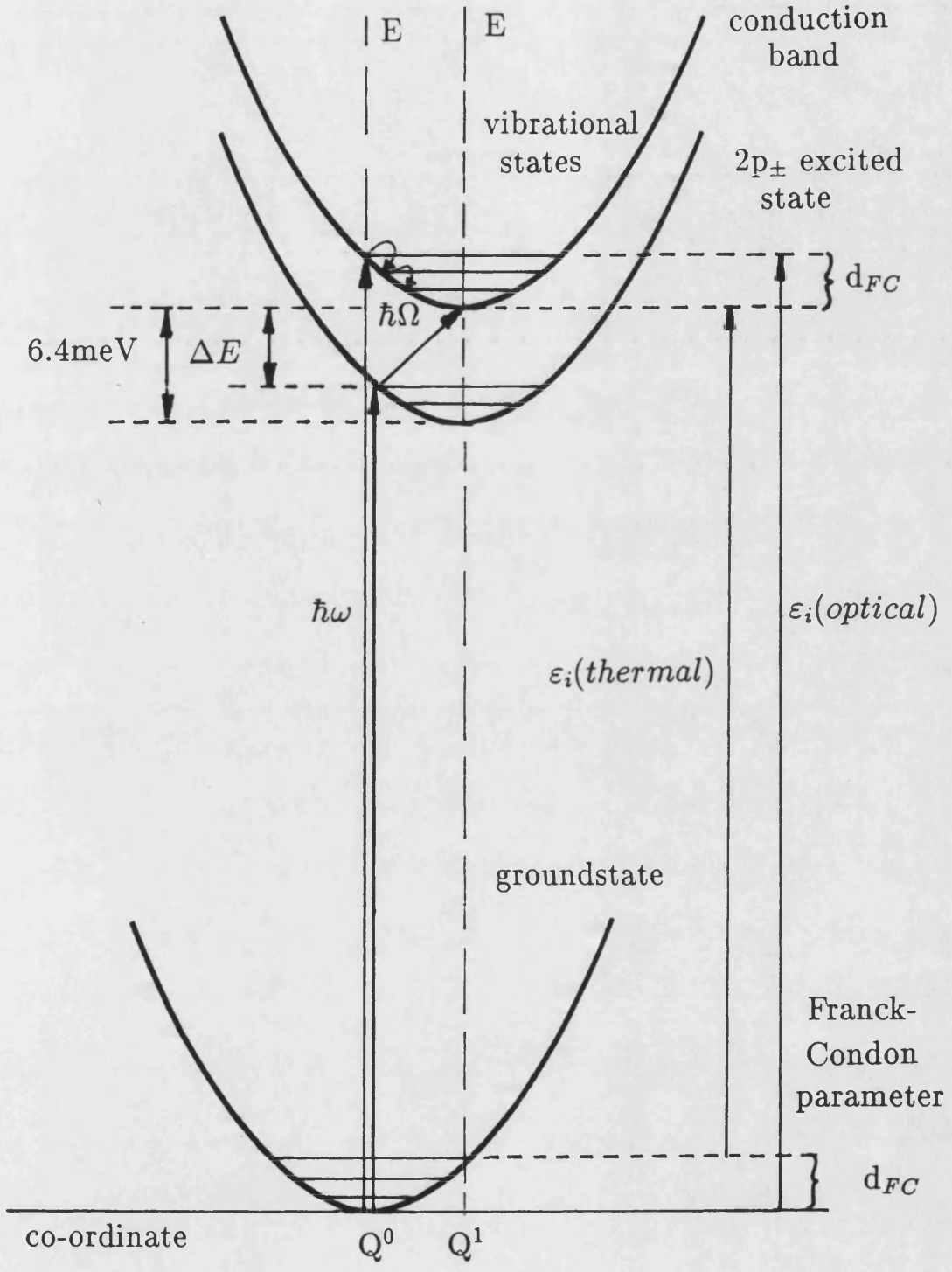

Fig 6.5: Co-ordinate configuration diagram for a donor with a Franck-Condon shift, d_{FC}.

only from direct photo-ionisation from the groundstate and is independent of temperature.

6.6.1 Phosphorus in float-zone silicon

The ratio of the P $1s \rightarrow 2p_{\pm}$ transition intensity (at 316cm^{-1}) to the intensity at the maximum of the ionisation continuum (at 360cm^{-1}) is plotted on a logarithmic scale as a function of inverse temperature in Fig 6.6. For comparison to the experimental data a least squares fit using a Boltzmann factor with $\Delta E = 6.4$meV is shown by the dashed line. It is clear that this does not explain the experimental data. A least squared fit to the experimental data with ΔE as the fit parameter, shown by the solid line, gives ΔE=4.45meV which deviates strongly from the expected EMT value.

Considering the full expression for the thermal ionisation probability from the excited state and the expected PTIS response at the two frequencies one expects

$$\frac{I(1s \rightarrow 2p_{\pm})}{I(continuum)} = \left[\frac{(1-e^{-N_d \sigma_{ptis}\, d})(1-Re^{-N_d \sigma_{dir}\, d})}{(1-Re^{-N_d \sigma_{ptis}\, d})(1-e^{-N_d \sigma_{dir}\, d})}\right] \times \left(1+\frac{\Delta E}{kT}\right) exp - \frac{\Delta E}{kT} \qquad (6.9)$$

where σ_{ptis} is the optical absorption cross-section for excitation into the excited state and σ_{dir} is the optical absorption cross-section for direct optical excitation into the conduction band.

The first term in equation (6.9) is a constant of proportionality, K and is not temperature dependent. The second term determines the shape of the curve when the data is plotted as a function of inverse temperature. There are only two variable parameters, the temperature and the thermal activation energy.

In order to determine the slope either ΔE or T may be treated as a fit parameter

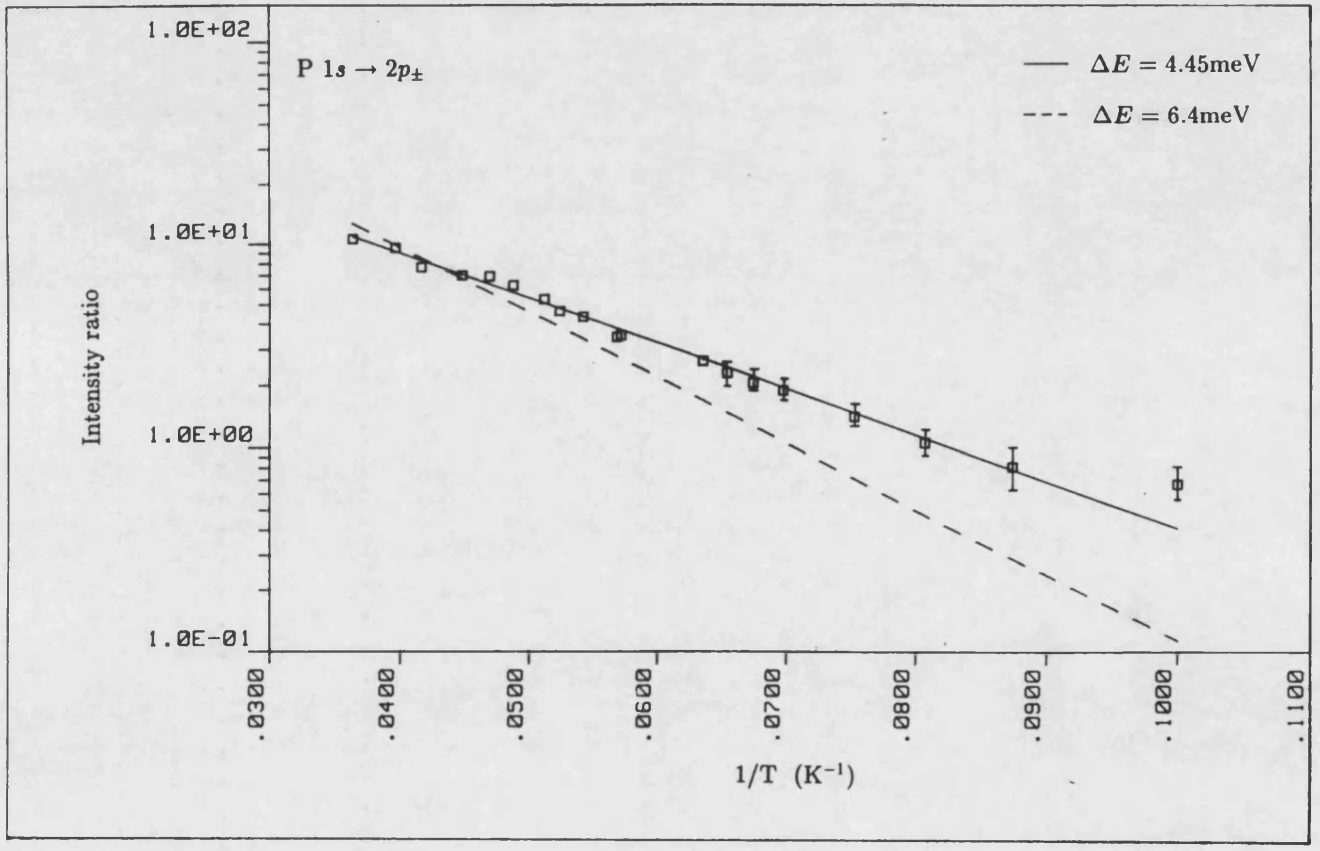

Fig 6.6: The ratio of the intensity of the $1s \rightarrow 2p_{\pm}$ transition of P to the maximum of the P photo-ionisation continuum in the float-zone silicon sample. Least-squares fits to the data using a Boltzmann factor with only a constant of proportionality (dashed line) as a fit parameter and the EMT value for the thermal activation energy (ΔE) and with ΔE as a fit parameter (solid line) are shown.

in order that a least squares fit may be made to the data. For a shallow donor only a weak Franck-Condon shift is expected and the observed thermal activation energies are expected to be the EMT energies of the excited states below the conduction band. Therefore, in the first instance a temperature shift of ΔT will be considered.

For the P $1s \rightarrow 2p_{\pm}$ transition a least squares fit to the experimental data using equation (6.9) gives values of K=40.39 and ΔT = 1.084K. Calculating K using $\sigma_{pti_s} = 1.35 \times 10^{-13}\text{cm}^2$ from Baber (1980) and $\sigma_{dir} = 1.7 \times 10^{-15}\text{cm}^2$ from Landolt and Börenstein (1982) with d = 0.05cm and $N_d = 3 \times 10^{14}\text{cm}^{-3}$ results in a value of 25.4. Since K is very sensitive to the exact values of N_d and the optical absorption cross-sections there is surprisingly good agreement between the fit value and the predicted value of K.

A temperature shift of the order of 1.084K could arise if the carbon resistor and sample are not at the same temperature. This is a well-know experimental difficulty. Here the carbon resistor is not in thermal contact with the sample due to the difficulty of maintaining its electrical isolation and such a temperature difference cannot be ruled out.

The experimental data of the P $1s \rightarrow 3p_{\pm}$ and $1s \rightarrow 4p_{\pm}$ transitions were fitted in the same way and give rise to values K=8.385 and ΔT = 1.40K and K=2.43 and ΔT=4.12K respectively. The fit values are in reasonable agreement with the expected values of K=10.5 for the $1s \rightarrow 3p_{\pm}$ transition and K=5.0 for the $1s \rightarrow 4p_{\pm}$ transition. These values are calculated by scaling the optical absorption cross-section for the $1s \rightarrow 2p_{\pm}$ transition by the oscillator strength of the relevant transition as given by Stillman et al (1977).

The temperature shift obtained from the best fit to the $1s \rightarrow 3p_{\pm}$ data is in

good agreement to that obtained from the $1s \rightarrow 2p_{\pm}$ data but the value obtained from the $1s \rightarrow 4p_{\pm}$ data is considerably larger. However, both the $1s \rightarrow 3p_{\pm}$ and $1s \rightarrow 4p_{\pm}$ transitions are mounted on the background continuum making the determination of their intensities more difficult and therefore the $1s \rightarrow 2p_{\pm}$ data is expected to give a more reliable value for ΔT.

In Fig 6.7 the experimental data for the P $1s \rightarrow 2p_{\pm}$, $1s \rightarrow 3p_{\pm}$ and $1s \rightarrow 4p_{\pm}$ transitions, corrected for a temperature offset of +1.0836K against the carbon resistor as obtained from the P $1s \rightarrow 2p_{\pm}$ fit, are plotted as function of inverse temperature. A least squared fit to the corrected data using only the constant of proportionality as a fit parameter is shown by the solid lines in each case. The fits give values of K'=40.39, 8.33 and 2.68 respectively. The fits are in good agreement with experiment for all three sets of data.

The alternative explanation of the experimental data is to assume that the thermal activation energies are different from the EMT predicted values, which are observed optically, due to a Franck-Condon shift. A least squared fit to the experimental data gives fit values of $\Delta E(2p_{\pm})$=5.085meV, $\Delta E(3p_{\pm})$=2.726meV and $\Delta E(4p_{\pm})$=1.494meV compared to the effective mass values of 6.4meV, 3.12meV and 2.19meV respectively. It is known from optical measurements that the energy separation of the excited states are in excellent agreement with the EMT values. In order to be consistent with this observation a configuration diagram in which all the excited states and the conduction band are associated with the same lattice co-ordinate compared to the groundstate is required. It would then still be expected that the separation between the thermal activation energies is also the EMT separation. However, the values obtained from the fits give $\Delta E(2p_{\pm}) - \Delta E(3p_{\pm})$=3.079meV compared to 3.28meV and $\Delta E(3p_{\pm}) - \Delta E(4p_{\pm})$=1.232meV compared to 0.93meV.

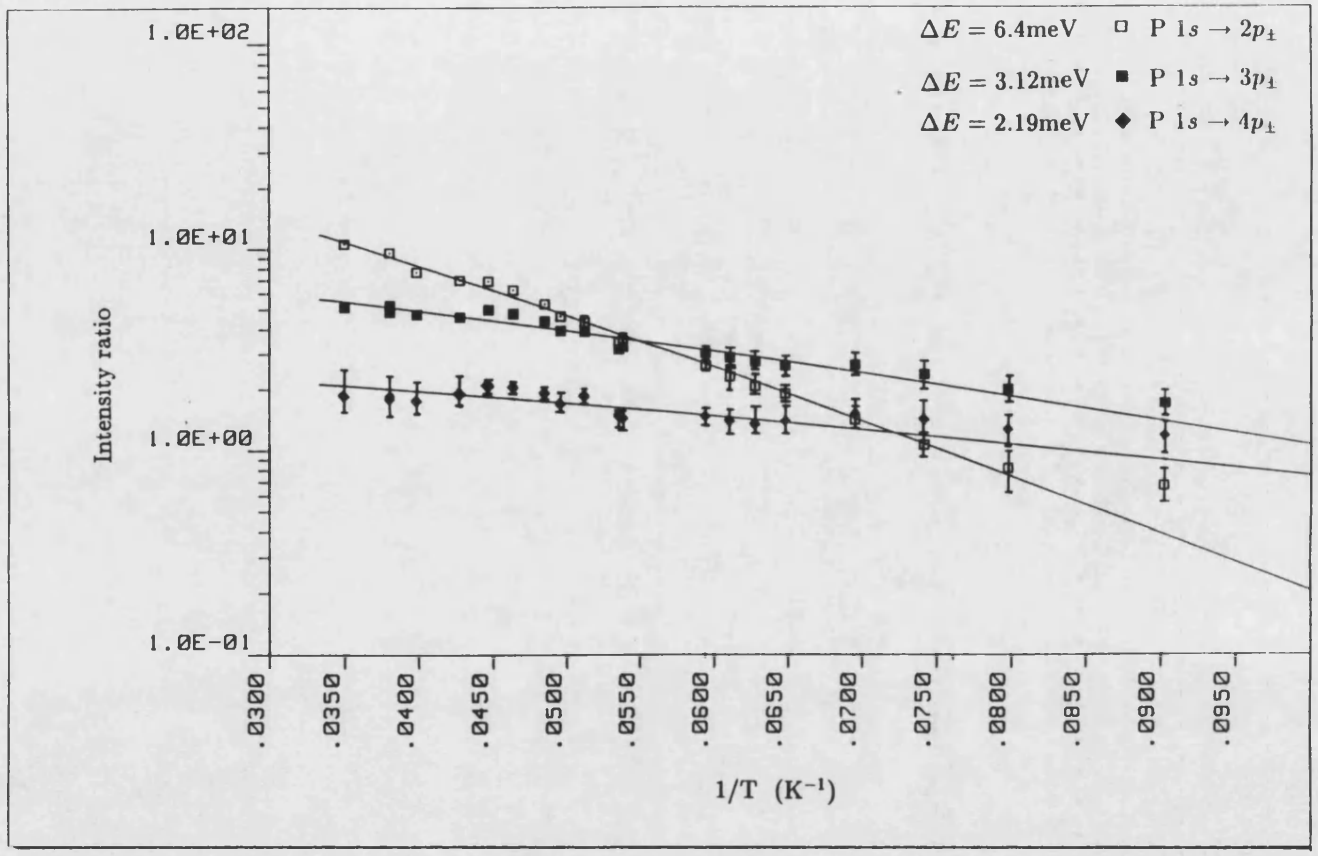

Fig 6.7: The intensities of the $1s \rightarrow 2p_{\pm}$, $3p_{\pm}$ and $4p_{\pm}$ transitions of P relative to the maximum of the P photo-ionisation continuum versus temperature. The experimental data have been adjusted for a discrepancy of -1.0836K in the originally recorded temperatures. The solid lines show the least-squares fits to the data using the EMT thermal activation energies (ΔE) and the constant of proportionality as the fit parameter in a full model of the PTIS response.

It is concluded that the thermal activation energies obtained from a fit to the energy can not be explained in a straight-forward manner in terms of a Franck-Condon model and therefore the simplest explanation, that the recorded temperature was slightly lower than that felt by the sample, is favoured. Fitting the data in this way the temperature dependence of the intensities of the P transitions observed by PTIS is consistent with the thermal ionisation from an excited state as described by Abakumov and Yassievich (1976) when the effective mass energies of the excited states below the conduction band are used.

Plotted on a logarithmic scale as a function of inverse temperature the experimental data can easily be fitted to a straight line using a Boltzmann factor, as is standard practice. It has been shown that the value of ΔE obtained from such an analysis is seriously in error. A simple Boltzmann factor does not sufficiently describe the thermal ionisation from the excited states in this case. The full analysis gives rise to a slightly curved fit to the data, without needing to evoke a departure from the effective mass energies of the excited states below the conduction band.

6.6.2 The Shallow Thermal Donor transitions in Cz-silicon

The STD are shallower than P and from previous PTIS measurements they are known to deviate only slightly from an ideal EMT donor centre. In the PTIS spectra of sample 2 the $1s \rightarrow 2p_{\pm}$ and $1s \rightarrow 3p_{\pm}$ transitions of STD E, F, and G are predominant at all temperatures. The individual maxima of the ionisation continua of these donors are not resolved, rather one continuum with a maximum at 298cm^{-1} is observed due to direct photo-ionisation from all three species.

The intensity of the $1s \rightarrow 2p_{\pm}$ transition of STD E referenced to the continuum is shown in Fig 6.8 as a function of inverse temperature. The dashed line shows a least squared fit to the data using a Boltzmann factor with ΔE= 6.4meV. The solid line shows a least squared fit using a Boltzmann factor with ΔE as a fit parameter resulting in ΔE=3.62meV which is considerably different to the expected value.

Again the data must be interpreted using a more exact expression for the thermal excitation probability from the excited state. Due to the strong EMT-like nature of the STD it is assumed that the thermal activation energies will be consistent with the energies of the excited states below the conduction band. Therefore, the gradient of the fit was determined by a temperature shift as for the P data in float-zone silicon. Below 11K the spectra are very noisy and above 19K the spectra are dominated by the P transitions resulting in a large error in the experimental data in these regions. Therefore the least squared fits were performed only using the data between 11K and 19K. The fit parameters obtained for the $1s \rightarrow 2p_{\pm}$ transitions of STD E, F and G after equation (6.9) with the constant of proportionality, K and the temperature shift ΔT as the fit parameters are shown in Table 6.1. The values obtained for K are smaller than for the P $1s \rightarrow 2p_{\pm}$ transitions but of the same order of magnitude confirming their similar shallow donor nature. An evaluation of the expected value of K is difficult since σ_{pti_s}, σ_{dir} and N_d are unknown for the STD. Also the continuum is now the sum of the contributions from all three donor species and K is given by

$$K = \frac{(1 - e^{-N_d \sigma_{pti_s} d})}{(1 - Re^{-N_d \sigma_{pti_s} d})} \frac{(1 - Re^{-(3N_d)(3\sigma_{dir})d})}{(1 - e^{-(3N_d)(3\sigma_{dir})d})}. \qquad (6.10)$$

In order to estimate the expected value of K the values of σ_{pti_s} and σ_{dir} of P were used and the individual STD concentrations were estimated to be 3×10^{12}cm^{-3}

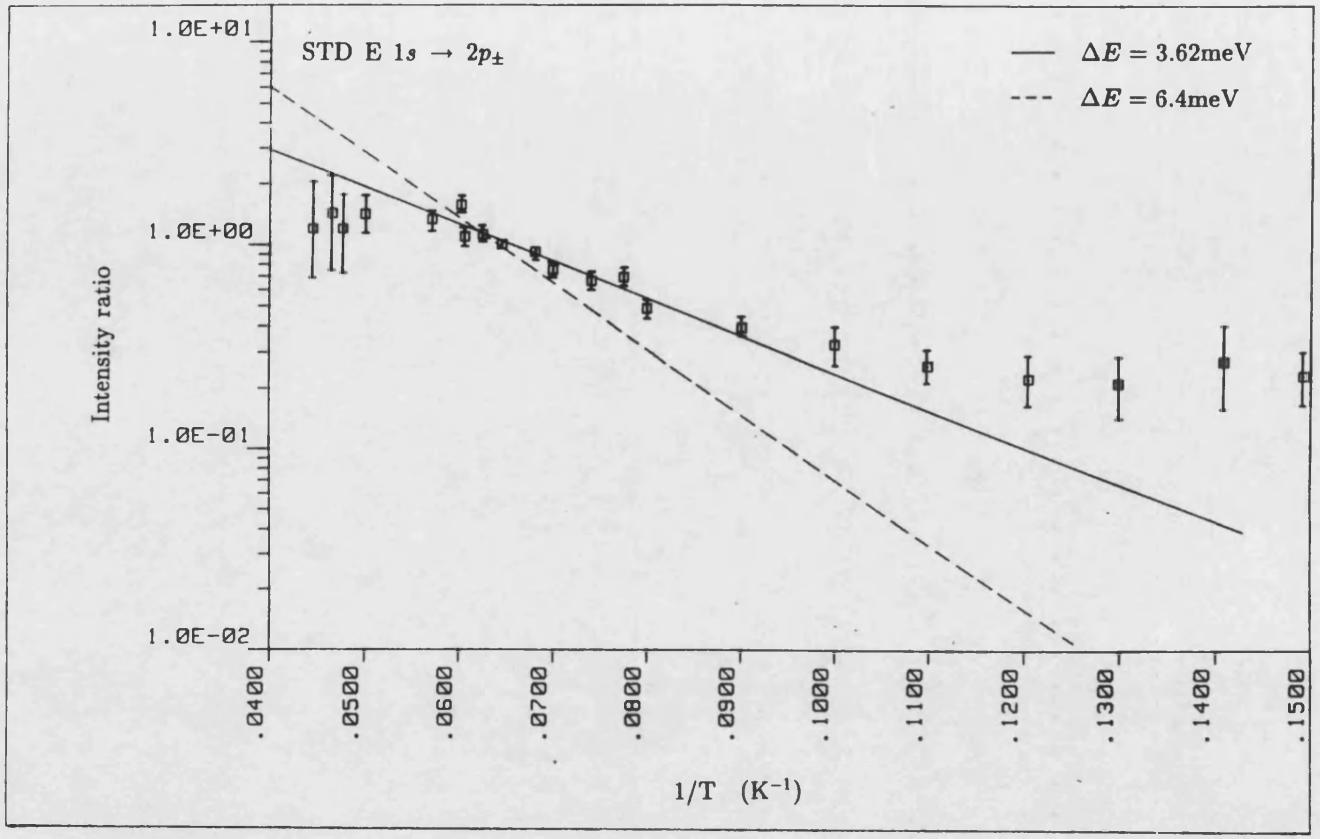

Fig 6.8: The ratio of the intensity of the $1s \rightarrow 2p_{\pm}$ transition of STD E to the maximum of the photo-ionisation continuum of the STD in heat-treated Cz-silicon sample 2. Least-squares fits to the data using a Boltzmann factor with only a constant of proportionality (dashed line) as a fit parameter and the EMT value for the thermal activation energy (ΔE) and with ΔE as a fit parameter (solid line) are shown.

$1s \rightarrow 2p_{\pm}$ transition	STD E	STD F	STD G
Fit parameter			
ΔT (Kelvin)	2.852	2.780	1.722
K	11.805	9.159	9.372
K′	12.678	9.714	8.159

Table 6.1: The parameters obtained from the least-squares fits to the data for the STD $1s \rightarrow 2p_{\pm}$ transitions. Fit parameters in the model of the PTIS response are the constant of proportionality, K and the temperature offset, ΔT. K′ are the new constants of proportionality obtained by fitting the experimental data adjusted by the average value of ΔT. The EMT value for the thermal activation energy $\Delta E = 6.4\text{meV}$ is used.

giving a total STD concentration of $9 \times 10^{12}cm^{-3}$. The sample thickness was 0.2cm. Under such conditions K=1.26 for all STD. The fit values are a factor of approximately five larger, indicating that the values for the optical absorption cross-sections or N_d are possibly slightly low.

The values obtained for fit parameter ΔT indicate a temperature discrepancy between the carbon resistor and the sample of approximately 2.5K. This difference although larger than for the float-zone silicon sample is still a realistic value. That a larger temperature difference is observed might be associated with the fact that the Cz-silicon sample is 0.2cm thick compared to the 0.05cm thick float-zone silicon sample.

In Fig 6.9 the experimental data for the $1s \rightarrow 2p_{\pm}$ transitions of STD E, F and G, corrected for a temperature shift of 2.451K obtained from the average ΔT obtained from the fits, are plotted as a function of inverse temperature. Least squared fits to the corrected data using only K as a fit parameter are shown by the solid lines in each case. The adjusted K parameters, K′ obtained from these fits are shown in Table 6.1. The experimental data are in good agreement with the fits in the range 25 - 13K for STD F and G but diverge at lower temperatures. This is probably attributable to the large noise in the spectra in this temperature range due to the weak signal strength. For STD E the same divergence is observed at low temperatures. Also, above 22K the experimental data are low compared to the fit. This difference at higher temperatures could be due to a saturation of the optical absorption process since the number of photons available is finite and this factor has not been incorporated in the fit.

It is therefore concluded that the temperature dependence of the intensity of the STD transitions may be interpreted using the effective mass theory pre-

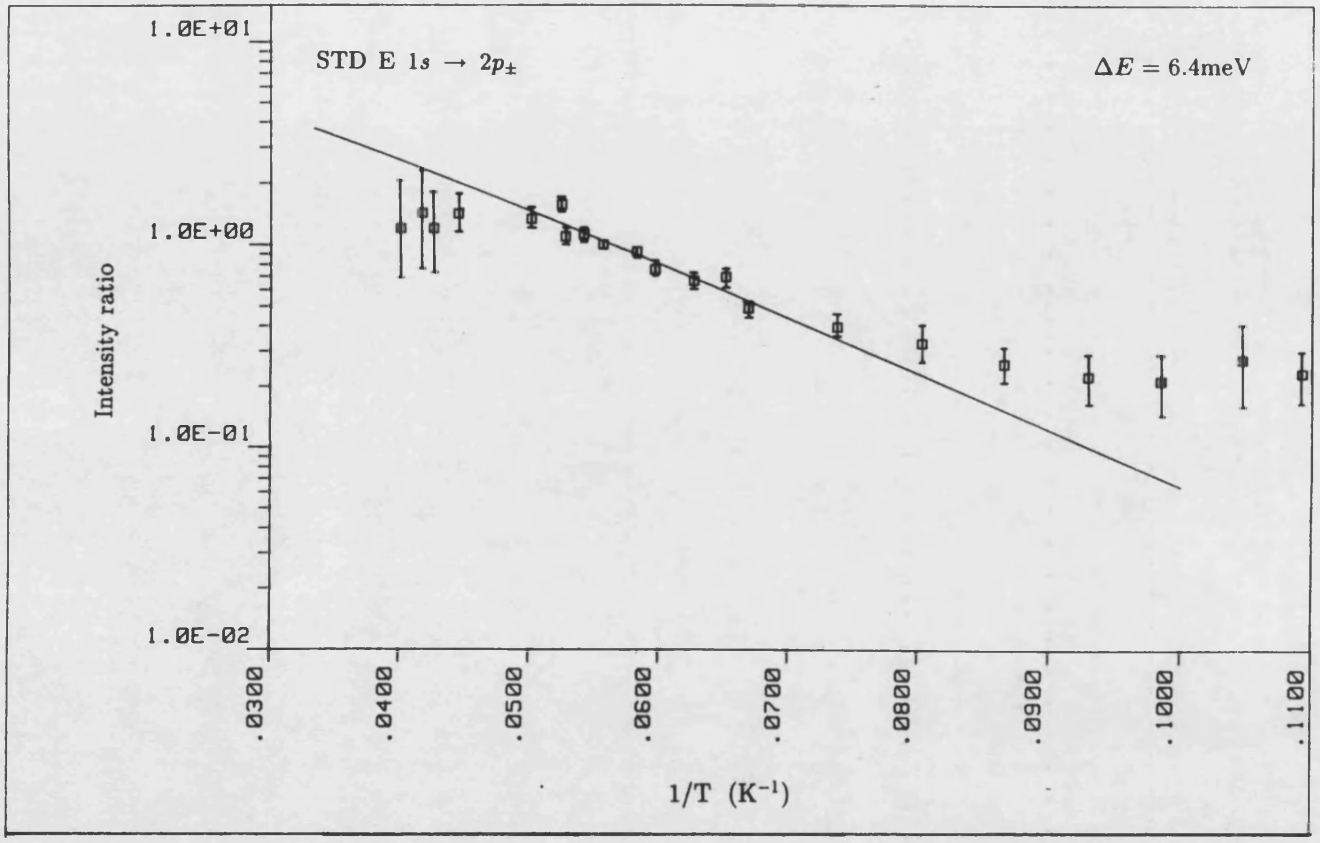

Fig 6.9a): The intensity of the $1s \rightarrow 2p_{\pm}$ transition of STD E relative to the maximum of the STD photo-ionisation continuum versus temperature. The experimental data have been adjusted for a discrepancy of -2.451K in the originally recorded temperatures. The solid line shows the least-squares fit to the data using the EMT thermal activation energy (ΔE) and the constant of proportionality as the fit parameter in a full model of the PTIS response.

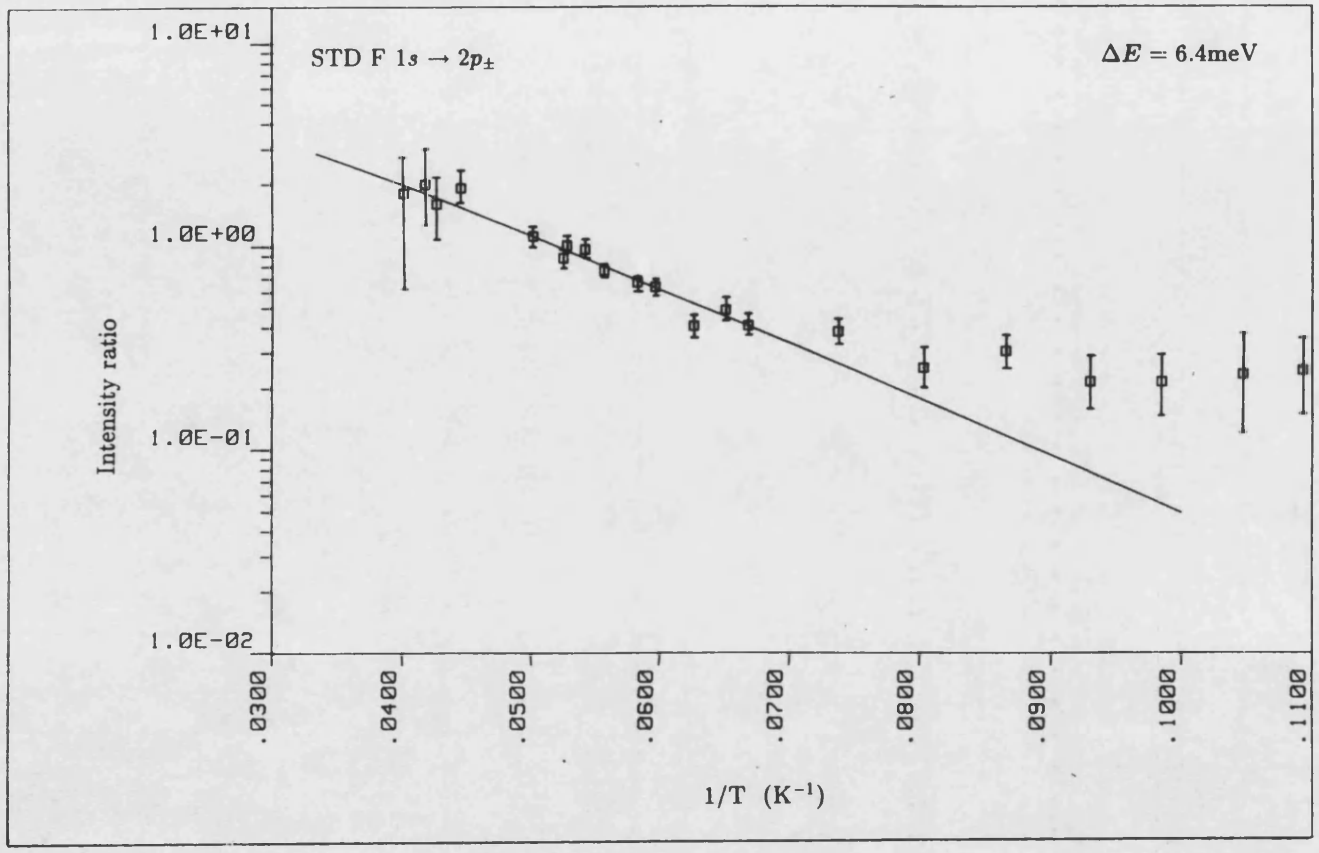

Fig 6.9b): The intensity of the $1s \rightarrow 2p_{\pm}$ transition of STD F relative to the maximum of the STD photo-ionisation continuum versus temperature. The experimental data have been adjusted for a discrepancy of -2.451K in the originally recorded temperatures. The solid line shows the least-squares fit to the data using the EMT thermal activation energy (ΔE) and the constant of proportionality as the fit parameter in a full model of the PTIS response.

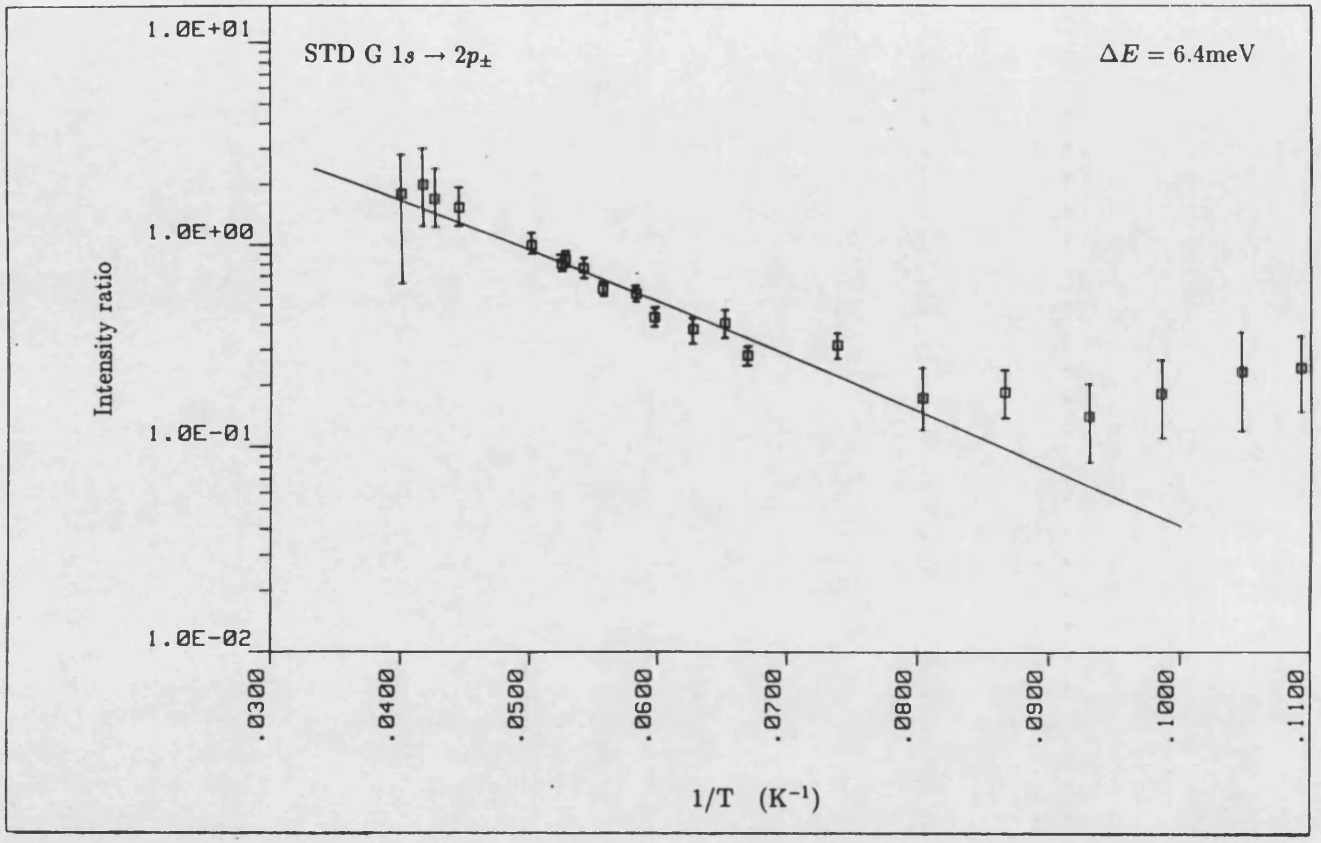

Fig 6.9c): The intensity of the $1s \rightarrow 2p_{\pm}$ transition of STD G relative to the maximum of the STD photo-ionisation continuum versus temperature. The experimental data have been adjusted for a discrepancy of -2.451K in the originally recorded temperatures. The solid line shows the least-squares fit to the data using the EMT thermal activation energy (ΔE) and the constant of proportionality as the fit parameter in a full model of the PTIS response.

dicted energies of the excited states below the conduction band and a thermal ionisation probability of the form given by Abakumov and Yassievich (1976) if a temperature difference of approximately 2.5K exists between the temperature measured by the temperature sensor and the actual temperature of the sample. Such a difference is possible in the present experimental set-up.

6.7 Conclusion

The temperature dependence of the intensities of the transitions observed in PTIS spectra has been studied in two cases. It has been shown that for shallow impurities in silicon the gradient of an Arrhenius plot may not be used to determine the energy of an excited state below the conduction band. It has already been shown by Jongbloets et al (1979) that the use of a more exact expression for the thermal ionisation energy improves the values of ΔE obtained for the P donor and B and Al acceptors in germanium. It has also been reported that in GaAs a Boltzmann factor gives a value of ΔE that is much smaller than that expected from the known ionisation energy and transition energies of the impurities (Stillman et al, 1977). Therefore, for the evaluation of the thermal activation energies of an impurity from the intensities of the transitions in the PTIS spectra it is clear that a more exact expression for the thermal ionisation probability of a carrier from an excited state, for example that of Jongbloets et al (1979) or Abakumov and Yassievich, (1976) must be used.

The two sets of experimental data studied here, for the P donor in float-zone silicon and the STD donors in Cz-silicon have been interpreted in this way. Both sets of data have been fitted using a least-squares fit program with the constant of proportionality and a temperature shift as the fit parameters. For

the P donor in float-zone silicon a value of approximately 1.08K was obtained for the difference between the recorded temperature and the actual sample temperature and for the STD donors in Cz-silicon a value of approximately 2.5K was obtained for this difference. Such discrepancies between the temperature of the sensing element and sample are well-known and may not be ruled out in these cases where the carbon resistor was not in direct thermal contact with the sample. The values for the constant of proportionality obtained were very similar to those expected from the known or estimated donor concentrations and optical absorption cross-sections. Taking account of this temperature offset the experimental data is explained using the EMT energies of the excited states below the conduction band. It has been shown that the intensities of the transitions of the STD donors depend on temperature in a way which confirms their single donor nature.

A fit to the data of P in float-zone silicon assuming no temperature offset but a deviation of the thermal activation energies from the EMT energy values of the excited states below the conduction band yielded results inconsistent with the Franck-Condon model. However, the possibility that such effects exist for the P and STD in silicon cannot be ruled out.

Further experiments, in which the true sample temperature is monitored are required to confirm this analysis. In the present apparatus this could be achieved by placing the temperature sensor in direct thermal contact with the sample in such a way as to avoid electrical contact which might lead to increased noise in the PTIS signal.

Chapter 7

Summary

7.1 Photothermal ionisation spectroscopy

The establishment of two systems to carry out PTIS spectroscopy on either a stepping FT spectrometer or a fast-scan FT spectrometer have been described in this thesis and the important experimental problems have been discussed. It has been shown from PTIS measurements on ultra-pure Ge that these systems match the sensitivity achieved by other groups. The investigation of the Shallow Thermal Donors in silicon presented in this thesis illustrates the application of this technique for the study of low concentrations of impurities in semiconductors in the presence of other impurity species.

7.2 The future of photothermal ionisation spectroscopy

The technique of PTIS has the advantage over other routine spectroscopic techniques such as infrared transmission spectroscopy and photoluminescence in that the sensitivity for the detection of shallow impurities in semiconductors is far higher. However, it has the disadvantage of being a more complicated

technique to use, the appropriate applied bias voltage and temperature range must be determined for each new material and high quality ohmic contacts must be achieved at low temperatures. Also, PTIS measurements do not allow a determination of the concentrations of the impurities observed.

In the future semiconductor materials will continue to be grown with increasing purity and new applications will reveal new problems related to trace impurities. In this environment PTIS can be expected to become an increasingly important spectroscopic method not only in research but also in industry. As experience is gathered on a wide range of materials a knowledge base is established and PTIS measurements will become more routine. As the model calculations in this thesis have demonstrated, calculations of the PTIS response as a function of impurity concentration and temperature in conjunction with experimental results can be used to obtain estimates of the impurity concentrations involved. Further study of the quantative interpretation of the PTIS spectra would be an extremely valuable contribution to the technique.

7.3 The Shallow Thermal Donors

The Shallow Thermal Donors were first discovered through the high sensitivity of photothermal ionisation spectroscopy as described in this thesis. This remains one of few methods available for their study since they occur in concentrations of 10^{13} atoms per cubic centimeter or less. These seven donors are found in heat-treated oxygen-rich silicon in which the TD are present. The experimental data presented in this thesis show that the STD are not an extension of the TD series but a distinct group of shallow donors. The STD are effective mass-like single donors unlike the TD, which are double donors.

The results presented in this thesis of studies on the dependence of the STD growth on annealing temperature and time and also on the effect of the thermal history of a sample indicate the STD may represent an alternative kinetic pathway for oxygen aggregation. Indeed, the perturbation model, which successfully describes the change in ionisation energy of the TD with increasing cluster size in Si and Ge, indicates that the STD may be grouped into two overlapping series of oxygen aggregates based on two different donor cores.

It is speculated that the STD are oxygen or oxygen-impurity complexes. These possibilities have been examined in this thesis and an association of the STD to oxygen is found. It has been shown that the two obvious impurities for complexing, boron and phosphorus, do not play a significant role in the STD development. However, it is possible that they are present in the STD in a passive role, for example in the core, such that very low concentrations of the order of 10^{13} or less are involved.

The results of a study of the development of the STD with annealing time have been presented in this thesis and shows that the STD concentration initially increases with increasing annealing time at 450°C but decreases again after $\approx$ 1.5 hours at 450°C, unlike the TD this is not the consecutive growth and decay of individual species indicative of clustering but a decrease of all the transition intensities of the STD and P. This behaviour may be understood if the STD and P are being compensated by an unknown acceptor species formed during annealing.

7.4 Future work

The STD have been extensively documented by PTIS and studies of their growth with annealing time have been made. It is now necessary that models are developed to try and determine the atomic stucture of these defects and that kinetics of formation calculations are made. Two further experiments would be significant for such modelling. Firstly, the determination of the groundstate symmetry of the STD by uniaxial stress measurements in PTIS. Secondly, the investigation of samples annealed for times greater than 1.5 hours by PTIS using illumination with band-edge light to determine whether the actual STD concentration decreases or whether they are compensated at this stage.

Acknowledgements

I would like to thank Prof. Dr. L. Genzel for giving me the opportunity to undertake my PhD at the Max Planck Institute for Solid State Research in Stuttgart, FRG, for his supervision of this work and many interesting and enlightening discussions.

I would also like to thank Dr W. C. Clark of the University of Bath, Avon, GB for his support as internal supervisor. The many discussions concerning the modelling of the PTIS response were very beneficial and his critical comments in completing this thesis were invaluable.

It is my pleasure to thank Dr. H. Navarro, University of Puebla, Mexico for the his collaboration in establishing PTIS at the Max Planck Institute and the interpretation of the STD results. I am very grateful for the many things he taught me in the laboratory and for our many discussions from which I learnt so much.

My thanks are also due to Dr. J. Weber for his interest and support and for many stimulating discussions. His collaboration in the interpretation of the PTIS spectra is much appreciated.

I would also like to thank Prof. E. E. Haller, Lawrence Berekely Lab., University of California, USA for his gift of several ultra-pure germanium samples. It was very educative and enjoyable to collaborate with him during his sabbatical leave at the Max Planck Institute investigating the low-field Zeeman effect of the D(H,O) donor in ultra-pure Ge by PTIS.

Special thanks are due to Dr. P. Wagner at Wacker Heliotronic, Burghausen, FRG for the gift of many high quality silicon samples which made this work

possible. It was his work on the Thermal Donors in silicon which stimulated interest in this problem.

Herr W. König is thanked for acquainting me with the Bruker IFS 113v spectrometer, his goodwill and support.

Ich möchte mich bei den Herren Rauscher, Böhme, Schlieter und Markewitz für die technische Unterstützung bedanken. Auch den Mitarbeitern der Servicegruppe Kristallpräparation sei gedankt. Schließlich geht mein Dank auch an alle Kollegen und Freunde des Max-Planck-Instituts für deren fachliche und moralische Unterstützung.

Bibliography

V. N. Abakumov and I. N. Yassievich, Sov. Phys. JETP 44, (2) (1976).

R. L. Aggarwal, Sol. Stat. Comm. 2, 163 (1964).

R. L. Aggarwal, P. Fisher, V Mourzine and A. K. Ramdas, Phys. Rev. 138, (3A), 882 (1965).

S. N. Artemenko, A. A. Kal'fa, Sh. M. Kogan and V. I. Sidorov, Sov. Phys Semicond. 8, (11) 1405 (1975).

S. C. Baber, Thin Solid Films 72, 201 (1980).

K. Bajaj, J. Birch, L. Eaves, R. Hoult, R. Kirkman, P. Simmonds and R. Stradling, J. Phys. C 8, 530 (1975).

A. Baldereschi and N. O. Lipari, Phys. Rev. B 9, (4) 1525 (1974).

G. Bambakidis and G. J. Brown, Phys. Rev. B 33, 8180 (1986).

A. R. Bean and R. C. Newman, J. Phys. Chem. Sol. 33, 255 (1972).

R. J. Bell, *Introductory Fourier Transform Spectroscopy* (Academic Press, New York, 1972).

L. V. Berman, Sh. M. Kogan, L. D. Saginov, V. I. Sidorov and A. A. Telegin, Sov. Phys. Semicond. 7, (11) 1398 (1974).

J. L. Benton, K. M. Lee, P. E. Freeland and L. C. Kimerling, *Proceedings of the 13th Int. Conf. on Defects in Semicond.*, edited by L. C. Kimerling and J.M. Parsey Jr. (The Metallurgical Soc. of AIME, N.Y. 1985), p639.

J. S. Blakemore, *Semiconductor Statistics* (Pergamon, Oxford, 1962).

J. T. Borenstein, D. Peak and J. W. Corbett, *Oxygen, Carbon, Hydrogen and Nitrogen in Crystalline Silicon*, MRS Symposia Proceedings 59, 1986a, edited by J. C. Mikkelsen, S. J. Pearton, J. W. Corbett and S. J. Pennycook (MRS, Pittsburgh, 1986) p173.

J. T. Borenstein and J. W. Corbett, *Oxygen, Carbon, Hydrogen and Nitrogen in Crystalline Silicon*, MRS Symposia Proceedings 59, 1986b, edited by J. C. Mikkelsen, S. J. Pearton, J. W. Corbett and S. J. Pennycook (MRS, Pittsburgh, 1986). p159

J. T. Borenstein, J. W. Corbett, M. Herder S. N. Sahu and L.C. Snyder, J. Phys. C: Sol. Stat. Phys. 19, 2893 (1986c).

J. Bourgoin and M. Lannoo, *Solid State Sciences 35: Point defects in semiconductors II* (Springer-Verlag, Berlin, 1983.), p89.

V Cazcarra and P. Zunino, J. App. Phys 51, (8), 4206 (1980).

T. C. Chandler, R. J. Spry, G. J. Brown, J. J. Rome and R. J. Harris, Phys. Rev. B 26, (12) 6588 (1982).

H. R. Chandrasekhar, L. Genzel and J. Kuhl, Optics Comm. 17, (1) 106 (1976).

P. Clauws, E. Simeon and J. Vennik, *13th Int Conf. on Defects in Semicond.*, edited by L. C. Kimerling and J. M. Parsey Jr. (Metallurgical Society of

AIME: Coronado, Claifornia, USA, 1984), p911.

P. Clauws and J. Vennik, Phys. Rev. B 30, (8) 4837 (1984).

P. Clauws and J. Vennik, *Proc. of 14th ICDS, Paris,* 1986, edited by H. J. Bardeleben (Trans. Tech. Pub., Switzerland, 1986), p941.

A. T. Collins and E. C. Lightowlers, Phys. Rev. 171, (3) 843 (1968).

L. Cook, M. Tashima N. Tabatabaie, T. Low and G. Stillman, Crystal Growth, 475 (1982).

R. Cooke, R. Hoult, R. Kirkman and R. Stradling, J. Phys. D: App. Phys. 11, 945 (1978).

J. W. Cooley and J. W. Tukey, Math. Comput. 19, 297 (1965).

J. W. Corbett, H. L. Frisch and L. C. Snyder, Materials Letters 2, 209 (1984).

L. S. Darken, J. App. Phys. 53, (5) 3754 (1982).

L. S. Darken, Phys. Rev. B 27, (10) 6564 (1983a).

L. S. Darken and S. A. Hyder, App. Phys. Lett. 42, (8) 731 (1983).

H. Y. Fan, *Light and Matter Ia, Encyclopedia of Physics XXV/2a,* edited by L. Genzel (Springer-Verlag, New York, 1967)

R. A. Faulkner, Phys. Rev. 184, (3) 713 (1969).

L. Genzel, H. R. Chandrasekhar and J. Kuhl, Optics Comm. 18, (3) 381 (1976).

L. Genzel and K. Sakai, Journal Opt. Soc. Am. 67, (7) 871 (1977).

L. Genzel and J. Kuhl, Infrared Physics 18, 113 (1978).

T. E. Gilmer Jr., R. K. Franks and R. J. Bell, J. Phys. Chem. Solids 26, 1195 (1965).

U. Gösele and T. Y. Tan, App. Phys. A 28, 79 (1982).

E. E. Haller and W. Hansen, Sol. Stat. Comm. 15, 687 (1974).

E. E. Haller, W. L. Hansen and F. S. Goulding, IEEE Trans on Nuc. Science NS22, 127 (1975).

E. E. Haller, G. Scott-Hubbard and W. L. Hansen, IEEE Trans on Nuc. Science NS24, (1) 48 (1977).

E. E. Haller, B. Joos and L. Falicov, Phys Rev B 21, (10) 4729 (1980).

E. E. Haller, R. E. McMurray Jr., L. Falicov, N. Haegel and W. L. Hansen, Phys. Rev. Lett. 51, (12) 1089 (1983a).

E. E. Haller and R. E. McMurray Jr., Physica 116B, 349 (1983b).

D. Helmreich and E. Sirtl, *"Semiconductor Silicon 1977"*, edited by H. R. Huff and E. Sirtl (The Electrochemical Soc. Inc., Princeton, N.J. 1977).

J. C. Hensel, H. Hasegawa and M. Nakayama, Phys. Rev. 138A, 225 (1965).

H. Herrmann, H. Herzer and E. Sirtl, *Advances in Solid State Physics "Festkörperprobleme XV"*, edited by H. J. Queisser (Vieweg, Braunschweig, 1975), p279.

L. T. Ho and A. K. Ramdas, Phys. Rev. B 5, (2) 462 (1972).

R. G. Humphreys, P. Migliorato and G. Fortunato, Sol. Stat. Comm. 40, 819 (1981).

C. Jagannath, Z. W. Grabowski and A. K. Ramdas, Phys. Rev. B 23, (5) (1981).

E. Janzén, R. Stedman, G. Grossman, H. G. Grimmeiss, Phys. Rev. B 29, (4) 1907 (1984).

R. L. Jones and P. Fisher, J. Phys. Chem. Solids 26, 1125 (1965).

H. Jongbloets, J. Stoelinga, M. van de Steeg and P. Wyder, Phys. Rev. B 20, (8) 3328 (1979).

W. Kaiser, H. L. Frisch, H. Reiss, Phys. Rev. 12, 1546 (1958).

L. C. Kimerling and J. L. Benton, App. Phys. Lett. 39, (5) 410 (1981).

R. Kirkman and R. Stradling, J. Phys. C: Sol. Stat. Phys. 6, L324 (1973).

Sh. M. Kogan and B. I. Sedunov, Sov. Phys. Sol. Stat. 8, (8) 1898 (1967).

Sh. M. Kogan and T. M. Lifshits, Phys. Stat. Sol.(a) 39, 11 (1977).

Sh. M. Kogan and N. Van Lien, Sov. Phys. Semicond. 15, (1) 26 (1981).

W. Kohn and J. M. Luttinger, Phys. Rev. 98, (4) 915 (1955).

B. O. Kolbesen, App. Phys. Lett. 27, (6) 353 (1975).

Landolt-Börenstein New Series, *Semiconductors* 117A (Springer Verlag, Berlin 1982).

K. M. Lee, G. D. Watkins and J. Trombetta, *"Microscopic identification of electronic defects in seminconductors"*, MRS Symposium Proc. 46, edited by N. M. Johnson, S. G. Bishop and G. D. Watkins (MRS Society, Pittsburgh, 1985), p263.

T. M. Lifshits and F. Ya. Nad', Sov. Phys. Dokl. 10, 532 (1965).

N. O. Lipari and A. Baldereschi, Sol. Stat. Comm. 25, (9) 665 (1978).

N. O. Lipari, M. Thewalt, W. Andreoni and A. Baldereschi, *Proc. 15th Int. Conf. Phys. Semicond., Kyoto*, 1980, J. Phys. Soc. Japan 49, Suppl. A 165 (1980a).

N. O. Lipari, A. Baldereschi and M. L. W. Thewalt, Sol. Stat. Comm. 33, 277 (1980b).

T. Low, G. Stillman, A. Cho, H. Morkoc and A Calawa, App. Phys. Lett. 40, (7) 611 (1982).

L. Mertz, *Transformations in Optics* (Wiley, New York, 1965).

R. McMurray Jr., PhD thesis, Lawrence Berkeley Lab., University of California, USA. (1984).

R. C. Newman *Oxygen, Carbon, Hydrogen and Nitrogen in Crystalline Silicon*, MRS Symposia Proceedings 59, 1986, edited by J. C. Mikkelsen, S. J. Pearton, J. W. Corbett and S. J. Pennycook (MRS, Pittsburgh, 1986) p205.

R. Oeder, P. Wagner, *Defects in Semiconductors II, MRS Symposium Proceedings* 14, edited by S. Mahajan and J. W. Corbett (North Hollandm, New York, 1983) p171.

G. S. Oehrlein, J. App. Phys. 54, 5453 (1983).

G. S. Oehrlein and J. W. Corbett, *Defects in Semiconductors II, MRS Proceedings* 14, edited by S. Mahajan and J. Corbett (North Holland, New York, 1983), p107.

A. Ourmazd, W. Schröter and A Bourret, J. App. Phys. 56, (6) 1670 (1984).

B. Pajot, H. Compain, J. Lerouille and B. Clerjaud, *Proceedings of 16th Int. Conf. on the Phys. of Semicond, Montpellier*, 1982.

B. Pajot, H. Compain, J. Lerouille and B. Clerjaud, Physica 117B & 118B, 110 (1983).

J. I. Pankove, *Optical Processes in Semiconductors* (Prentice-Hall Inc., New Jersey, 1971).

A. K. Ramdas and S. Rodriquez, Rep. Prog. Phys. 44 1297 (1981).

S. C. Shen, T. Welker, J. Kuhl and L. Genzel, Infrared Physics 20, 277 (1980).

M. S. Skolnick, L. Eaves, R. A. Stradling, J. C. Portal and S. Askenazy, Sol. Stat. Comm. 15, 1403 (1974).

B. Skromme, T. Low and G. Stillman, Inst. Phys. Conf. Ser. 65, 485 (1982).

B. Skromme, T. Low, T. Roth, G. Stillman, J. Kennedy and J. Abrokwah, Journal of Electronic Materials 12, (2) 433 (1983).

R. A. Smith, *Semiconductors* (Cambridge University Press, London, 1964).

K. Smith, Thin Solid Films 84, 171 (1981).

M. Stavola and L. C. Snyder, *Proc. Symp. "Defects in Silicon"*, edited by L. C. Kimerling and M. Bullis (The Electrochemical Society Inc., Pennington, N.Y., 1983.), p61.

M. Stavola, K. M. Lee, J. C. Nabity, P. E. Freeland and L. C. Kimerling, Phys. Rev. Lett. 54, (24) 2639 (1985a).

M. Stavola, K. M. Lee, J. C. Nabity, P. E. Freeland and L.C. Kimerling, *Microscopic identification of electronic defects in seminconductors*, edited by N.

M. Johnson, S. G. Bishop and G. D. Watkins (MRS Society, Pittsburgh, 1985b).

M. Stavola and K. M. Lee, *Oxygen, Carbon, Hydrogen and Nitrogen in Crystalline Silicon*, MRS Symposia Proceedings 59, 1986, edited by J. C. Mikkelsen, S. J. Pearton, J. W. Corbett and S. J. Pennycook (MRS, Pittsburgh, 1986), p95.

G. Stillman, C. Wolfe and D. Korn, *Proceedings of the XI Int. Conf. Semicond. Phys, Warsaw*, 1972, (Elsevier Pub. Com. New York, 1972), p863.

G. Stillman, C. M. Wolfe and J.O. Dimmock, *Semiconductors and Semimetals* 12, edited by R. K. Willardson and A. C. Beer (Academic Press, New York, 1977), p169.

G. Stillman, T. Low and B. Lee, Sol. Stat. Comm. 53, (12) 1041 (1985).

M. Suezsawa and K. Sumino, Phys. Stat. Sol. a 82, 235 (1984).

S. Sze, *Physics of semiconductor devices*, (Wiley, New York, 1981).

F. Szmulowicz and R. Baron, Infrared Physics 20, 385 (1980).

T. Y. Tan, R. Kleinhenz and C. P. Schneider, *Oxygen, Carbon, Hydrogen and Nitrogen in Crystalline Silicon*, MRS Symposia Proceedings 59, 1986, edited by J. C. Mikkelsen, S. J. Pearton, J. W. Corbett and S. J. Pennycook (MRS, Pittsburgh, 1986) p195.

M. Van de Steeg, PhD Thesis, Catholic University of Nijmegen, The Netherlands (1982).

P. Wagner, C. Holm, E. Sirtl, R. Oeder and W. Zulehner, *Advances in Solid State Physics, "Festkörperprobleme XXIV"* (Vieweg, Braunschweig, 1984), p191.

J. Weber and H. J. Queisser, *Oxygen, Carbon, Hydrogen and Nitrogen in Crystalline Silicon*, MRS Symposia Proceedings 59, 1986, edited by J. C. Mikkelsen, S. J. Pearton, J. W. Corbett and S. J. Pennycook (MRS, Pittsburgh, 1986) p195.

J. J. White, Canadian Journal of Phys. 45, 2797 (1967).

C. Wolfe, D. Korn and G. Stillman, App. Phys. Lett. 24, (2) 78 (1974).

C. Wolfe, G. Stillman and D. Korn, Inst. Phys. Conf. Ser. 33b, 120 (1977).

D. Wruck and P. Gaworzewski, Phys. Stat. Sol.(a) 56, 557 (1979).

Appendix A: Publications

Papers published by the author and collaborators relating to this work:

"New oxygen related shallow thermal donor centres in Czochralski-grown silicon", H. Navarro, J. Griffin, J. Weber and L. Genzel, Solid State Comm., 58, (3) 151 (1986).

"The new shallow thermal donor series in silicon", J. A. Griffin, H. Navarro, J. Weber, L. Genzel, J. T. Borenstein, J. W. Corbett and L. C. Snyder, J. Phys. C, 19, L579 (1986).

Papers appearing in conference proceedings:

"The study of oxygen thermal donors in silicon by photothermal ionisation spectroscopy", J. A. Griffin, H. Navarro and L. Genzel, *Oxygen, Carbon, Hydrogen and Nitrogen in Crystalline Silicon*, MRS Symposia Proceedings 59, 1986, edited by J. C. Mikkelsen, S. J. Pearton, J. W. Corbett and S. J. Pennycook (MRS, Pittsburgh, 1986), p139.

"Properties of the Shallow Thermal Donors in Cz-silicon as studied by photothermal ionisation spectroscopy (PTIS)", J. A. Griffin, H. Navarro, J. Weber and L. Genzel, *Proceedings of the 14th ICDS, Paris*, 1986, edited by H. J. Bardeleben (Trans. Tech. Pub., Switzerland, 1986), p997.

As a result of collaboration with Prof. E. E. Haller studying the ultra-pure germanium by PTIS the following papers have been accepted for publication:

"The Zeeman spectra of phosphorus and the D(H,O) donor complex in ultra-pure Ge", H. Navarro, J. Griffin and E. E. Haller. (to be published in J. Physics C.)

"Experimental study of three groundstate components of the hydrogen-oxygen donor in Ge", H. Navarro, J. Griffin and E. E. Haller. (to be published in Solid State Comm.)

Solid State Communications, Vol.58,No.3, pp.151-155, 1986.
Printed in Great Britain.

0038-1098/86 $3.00 + .00
Pergamon Press Ltd.

New Oxygen Related Shallow Thermal Donor Centres in Czochralski-grown Silicon

H. Navarro*, J. Griffin+, J. Weber and L. Genzel

Max-Planck-Institut für Festkörperforschung, Heisenbergstr. 1, D-7000 Stuttgart 80, FRG

(Received: Nov. 29, 1985 by M. Cardona)

A series of previously undetected effective-mass like oxygen related donor centres is observed in Czochralski-grown silicon (Cz-si) by means of Photothermal Ionization Spectroscopy. The new set of donors is shallower in energy than any of the known series of nine oxygen thermal donors reported in Cz-Si. The ionization energies of the new set of donors are between 34.7 and 37.4 meV. The new donor centres also appear as a result of thermally annealing the samples at 450°C.

This paper reports the observation of a set of new shallow donor states in two thermally treated Czochralski (Cz) grown, oxygen-rich, silicon crystals. The observations were performed by means of Photothermal Ionization Spectroscopy (PTIS)[1]. In Cz-Si there is always a high concentration of oxygen[2,3], up to 10^{18} cm^{-3}. During heat treatment at 450°C interstitial oxygen has been found to aggregate and form a series of nine different donor centres[4,5], the so-called "Thermal Donors" (TD). There is no theoretical constraint to believe that these nine TD are the only possible set of oxygen donor centres in Si. In particular, in oxygen-rich germanium up to 16 oxygen donor centres have been reported[6]. Due to its high sensitivity, PTIS is very well suited to the study of samples where several mutually competitive species of donor or acceptor centres coexist. In such a situation some species might appear in such small concentrations as to escape detection by more conventional techniques.

In high purity float-zone (FZ) silicon, PTIS has already been applied successfully to the study of some of the elemental centres, mainly phosphorus[7], indium[8] and sulphur[9]. In this paper we are presenting the application of PTIS to thermally treated Cz-silicon.

The Cz-Si starting material was of high resistivity and n-type. The net free carrier concentration was estimated from room temperature resistivity measurements to be $|N_d - N_a| \sim 4 \times 10^{12}$ cm^{-3}. Here N_d and N_a denote donor and acceptor concentrations. Two identical discs 12 mm in diameter and 2 mm thick were cut out of this material. Prior to the heat treatment at 450°C we subjected them to an annealing in nitrogen at 770°C for 10 min. Afterwards sample 1 was annealed for 4.5 hours at 450°C , whereas sample 2 was subjected 10 min. to the same annealing. The final donor concentrations were of the order of 8×10^{14} for sample 1 and 5×10^{13} cm^{-3} for sample 2. These estimates were obtained from the change in the electrical resistivity after the annealings.

It was necessary to prepare good ohmic contacts to monitor the photothermal conductivity. We used two stripes of gold-antimony evaporated on the samples which were subjected to short pulses of a high power Nd-YAG laser.

The experimental set-up consisted of a Fourier Transform Spectrometer (FTS), Bruker FTS-113, set-up to work between 100 to 900 cm^{-1}. The samples were mounted in a He contact gas Leybold-Heraus cryostat. The temperature was controlled within ± 0.1 K by means of a heater and the He gas flow rate. The temperature was measured by means of a calibrated Allen-Bradley carbon resistor, placed next to the sample. The lamp and enviromental radiations were filtered by a white polyethylene and a foil window and by a 190 um thick warm black polyethylene filter. The FTS used was calibrated by comparing the measured phosphorous lines in Si with the same spectrum measured with the double-beam FTS described in ref.[10], which in turn was calibrated with respect to the water absorption lines. Our energy positions for the phosphorous lines agreed well with the results reported by Ramdas and Rodriguez[11].

Figure 1 shows the PTI spectrum of sample 1, in the spectral region between 360 and 580 cm^{-1}, at 15.5K. This spectrum has been corrected to remove the absorption of the windows.

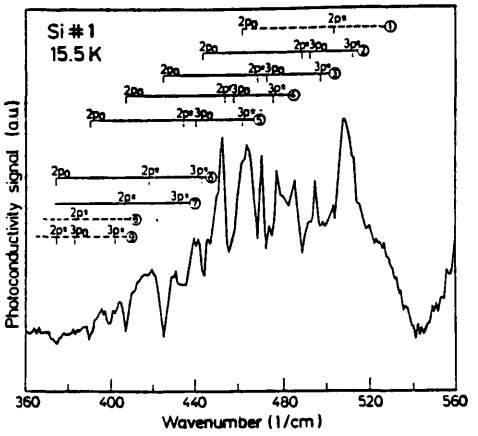

Fig. 1. Photoconductivity spectrum of sample 1, annealed at 450°C for 4.5 hours. The positions of the various transitions of the TD 1-9 are marked.

* Alexander von Humboldt Stipendiat. On leave of absence from Universidad Autonoma de Puebla, Puebla, México.

\+ Jointly at University of Bath,Bath,Avon, U.K.

All measured photoconductivity (PC) spectra presented similar characteristics: a photoionization continuum that starts in the neighbourhood of 210cm^{-1} (~26meV) and extends up to the maximum frequency observed (900) cm^{-1}, and discrete positive or negative peaks in the PC response between 220 and 520 cm^{-1} as discussed below. It is striking in Fig.1 that the expected TD transitions appear as negative peaks in the photoconductivity (PC) continuum. Normally PTIS shows up as positive photoconductive peaks. In this sample all nine well-characterized TD lines are visible. In Fig. 2 we show the normalized transmission spectrum of the same sample, recorded at 5K with a resolution of 0.25 cm^{-1} for comparison. This spectrum and the previous one indicate a typical intrinsic line half-width of 3-4 cm^{-1}. There is a very good qualitative agreement for the TD absorption lines between the two spectra in the common spectral region. In this sample the TD numbered 2, 3 and 4 are the most abundant[5] after an anneal of 4.5 hours. Table I summarizes the energy positions and the assignments of the observed TD lines. In this sample the TD lines always appear as negative peaks in the PCC for all temperatures observed (4.2 - 25K). The photoionization continuum underlying the sharp lines in Fig. 1 is due to shallower donors as we will show later.

In sample 2 at temperatures between 14 and 22K only transitions corresponding to the TD 1, 2 and 3 are observed, but as well defined, positive peaks. The line intensities increase with increasing temperature.

Negative peaks on the PCC of the type found in sample 1 were already reported in the PTIS of a positively charged acceptor in Ge[13]. They were explained as due to deeper lying energy states of other neutral acceptors with absorption coefficients between 1 to 10 cm^{-1}. An internal absorption within the neutral acceptors produced the dips in the PCC of the positively charged acceptors. From the transmission curve of sample 1 in Fig. 2 we deduce absorption coefficients for the TD in the order of 1-10 cm^{-1}. Hence we believe that the same internal absorption phenomenon is taking place in the PTIS of this sample. We believe that the appearance of the TD 1,2, and 3 as positive photoconductivity peaks in the PTIS of sample 2, is a consequence of the fact that these TD are expected to be close to their maximum attainable concentration[5], and hence they are in a higher relative concentration with respect to any of the shallower donors that produce the PCC.

In Figs. 3 and 4 it is possible to observe a series of peaks between 220 and 360 cm^{-1}, on top of the PCC, for samples 1 and 2 respectively. The resolution is 1 cm^{-1}. The spectra have not been corrected for the spectral background of the instrument.

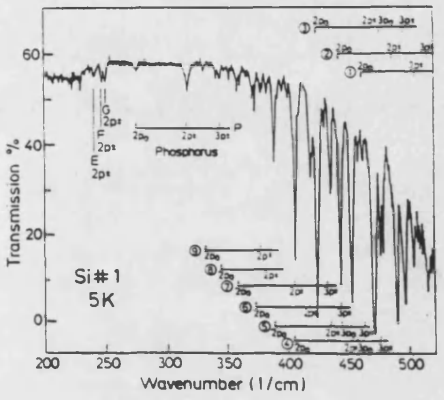

Fig. 2. Far infrared transmission spectra of sample 1, annealed at 450°C, for 4.5 h. The positions of IR transitions of the TD, STD and P are marked.

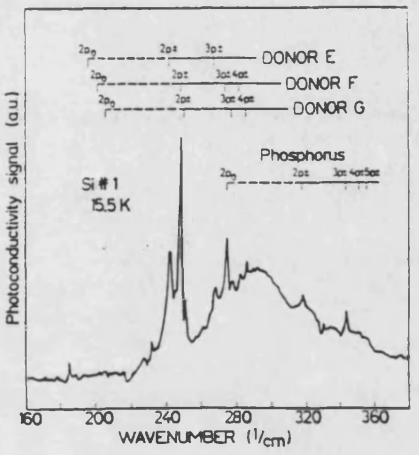

Fig. 3. Photoconductivity spectrum of sample 1, showing the STD transitions. The positions of the STD and P are marked.

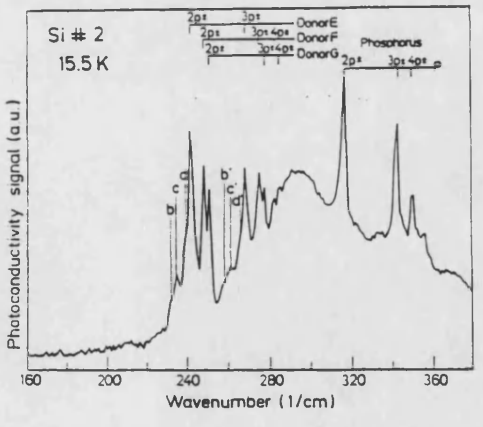

Fig. 4. Photoconductivity spectrum of sample 2, annealed at 450°C for 15 min, showing the STD transitions.

Table I

Thermal Donor and Phosphorus transitions observed by PTIS and FIRT in this work. The Cz-Si samples were subjected to a thermal annealing at 450°C as described in the text. The identification of the thermal donor and phosphorus transitions was carried out after ref 5 and 11. The small p and m in front of the PTIS transitions energy denotes either a peak on the PC or a sharp minimum,(negative peak).

Sample 1 Energy Position (cm^{-1}) PTIS (15.5K)		FIRT (6K)	Sample 2 Energy Position (cm^{-1}) PTIS (15.5K)		Donor	Assigned Transitions (from 1S to)
316.7 ±0.5	p	316.0 ±1.0	316.7 ±0.5	p	P	2P±
-		332.0	335.0	p	TD9	2Po
343.7	p	341.0	343.7	p	P,TD8	3P±,2Po
-		348.0	-		-	-
353.4	p	351.5	352.4	p	P	4P±
357.0	p	357.5	357.0	p	P,TD7	5P±,2Po
-		361.0	-		-	-
-		369.0	-		-	-
372.7	m	373.5	-		TD6	2Po
-		377.5	-		TD9	2P±
-		382.5	-		TD8,TD9	2P±,3Po
388.1	m	388.7	-		TD5	2Po
-		394.5	-		-	-
399.0*	m	399.0*	-		-	-
405.5		405.7	-		TD4,TD7	2Po,2P±
416.1	m	417.0	-		TD6	2P±
423.8	m	424.0	-		TD3	2Po
-		429.0	-		TD7	3P±
434.5	m	435.0	-		TD5	2P±
440.3	m	-	-		TD5	3Po
443.2	m	443.2	-		TD2,TD6	2Po,3P±
454.7	m	452.0	-		TD4	2P±
-		456.0	-		TD4	2Po
463.0	m	462.0	-		TD1,TD5	2Po,3P±
468.3	m	470.0	470.0	p	TD3	2P±
475.0	m	476.0	-		TD4	3P±
478.9	m	478.7	-		TD4	3P±
482.7	m	-	-		TD4	4P±
489.5	m	490.7	489.5	p	TD2	2P±
497.2	m	497.5	496.3	p	TD3	3P±
503.4	m	502.0	-		TD3	4P±
507.0	m	507.0	507.8	p	TD1	2P±
-		514.0	514.6	p	TD2	3P±

* coincides with a strong sharp absorption line of the cryostat window.

The lines visible in these figures can be grouped into two sets, one set that appears between 220 and 290 cm^{-1}, and a second set of lines between 315 and 360 cm^{-1}. The first group is dominated by the strong lines denoted E, F and G between 242 and 251 cm^{-1}, and what we assign as higher series transitions of the same donor centres between 268 and 284 cm^{-1}. These lines are common to both samples. The positions of the observed peaks are given in Table II. In this table can be seen that the first set of E, F and G lines can be identified as transitions between the Effective Mass Theory (EMT) donor levels 1S→2P±. The dipolar transitions 1S→3P± of the E, F and G donor are also visible. There are also 1S→4P± transitions visible for the F and G donors. That of the E donor overlaps with that 1S→3P± of the G donor. The transitions to the 2Po EMT level from the ground state, that appear very strongly in transmission spectroscopy, are obscured in the PTIS of phosphorus[9,10,11]. We find this transition to be less than 4% of the intensity of the 1S→2P± in P at 22K, a temperature close to the optimum for its PTIS transitions. The corresponding 2Po lines are not visible for these E, G and F donors at any temperature, because of the same phenomenon.

Four other sets of weaker lines appear in both samples in this region. They are denoted a, b, c, d and a', b', c', d' in Fig. 3 and 4. Only the lines b and b' are common to the two samples. The energy separation between a, a' as well as the separation of the other pairs fit the proper sequence for the energy difference between the ground state transitions to 2P± and 3P± EMT states. The lines are very weak and usually appear as poorly resolved shoulders of the most intense PT lines.

The two thermally annealed Cz-Si samples investigated show in total the existance of seven new different donor centres, shallower than the TD. From here on we will refer to them as the Shallow Thermal Donors (STD). They may correspond to different stages of aggregation of oxygen associated centres. The TD have ionization energies between 53.0 and 69.3 meV. However, the seven STD have ionization energies between 34.7 and 37.4 meV, close to the theoretical value of an EMT donor of 31.27 meV[11]. These large energy differences between the two sets of ionization energies points towards a different nature for the STD than that of the TD.

A very interesting feature in the spectral region of the STD is the photoionization continuum that starts above 210 cm^{-1} (~26meV) which is identical for both samples. It rises rapidly in intensity and has a local maximum at 295 cm^{-1} (36.6 meV). The energy position of this local maximum comes very close to the ionization energy of almost all the series of STD (34.7 to 37.4 meV). By determination of the instrumental background, it has been completely ruled out that

Table II

Energy positions of the observed as photoconductivity peaks in PTIS and of the absorption lines in FIRT corresponding to new shallower donor EMT centres in Czochralski grown Si See text.

Sample 1 Energy Position (cm^{-1}) PTIS (15.5K)	FIRT (6K)	Sample 2 Energy Position (cm^{-1}) PTIS (15.5K)	Donor	Assigned Transitions (from 1S to)
228.0 ±0.5	229.5 ±1.0	-	a	2P±
232.5	-	232.0 ±0.5	b	2P±
-	-	234.0	c	2P±
-	-	239.5	d	2P±
242.3	241.0	241.0	E	2P±
247.2	248.0	247.2	F	2P±
250.5	251.0	250.1	G	2P±
255.0 (a')	-	-	a	3P±
258.0 (b')	-	257.5 (b')	b	3P±
-	-	260.0 (c')	c	3P±
-	-	265.0 (d')	d	3P±
267.5	-	267.4	E	3P±
273.2	-	274.2	F, Phosphorus	3P±, 2Po
276.0	276.0	277.1	G,E	3P±, 4P±
283.0	-	282.5	F	4P±
286.5	-	285.0	G	4P±

this maximum is related to any instrumental effect. The PCC is already present at 4.2K, where the photothermal process for the STD is still not apparent. After a subtraction of the STD, the PCC is found to be almost independent of temperature. At approximately 20K, where the STD start to disappear very rapidly with rising temperature, the low energy tail of the PCC shrinks towards the 295 cm^{-1} maximum. The PCC disappears just before the onset of the corresponding ionization PCC of the phosphorus at 360 cm^{-1}, at 22K for sample 2 and at 25K for sample 1. The disappearance of the PCC at different temperatures in the two samples is an indication that the level or levels responsible could easily be present at concentrations different by an order of magnitude. In this case, the movement of the Fermi-level to lower energies with increasing temperature would depopulate the levels responsible for this PCC at different temperatures in the different samples. As no features were manifest in any careful observation in the spectral region between 30 and 210 cm^{-1} at any temperature, either in PTIS or FIR transmission, it is very difficult to argue about the physical nature of the PCC. However, it cannot be ruled out that it may be revealing the existence of a shallower donor state, non-EMT for instance, with either non- excited states or at least, states so shallow as to escape our detection. Also it is possible that as its maximum appears correlated with the ionization energy of the STD and it disappears almost simultaneously with them at the same temperature, that they have a common physical origin.

The observation of the new series of shallower thermally formed donors poses the question of their physical origin. That they are indeed oxygen associated and thermally formed is deduced from the following facts: firstly the previously reported experiments of PTIS on pure silicon[7,9] had enough sensitivity to detect the existence of these new centres. Secondly, PTIS performed by us in high resistivity unannealed Cz-silicon only showed the phosphorous transitions. Thirdly, samole 1 showed the STD in transmission, see Fig 2. Following a heat treatment at 770°C for 20 min., after the spectra shown were recorded, the transmission spectrum failed to show any trace of the existence of the TD, as expected, and also of the STD, or for that matter, of the phosphorus, all of which is now used for compensating the residual acceptors, once the STD have been destroyed.

The possibility of the STD transitions arising from either the shallower lying 1S(E) or any other 1S states can be ruled out for the following reasons: for any of the observed donor states, either the P or the TD, the relative thermal population factor for these 1S states is so overwhelmingly insignificant, that transitions from any of these shallower lying 1S states would not be observed even by the high sensitivity of the PTIS at any of the examined temperatures. On the other hand, it was found that the TD are centres of C_{2v}-Symmetry and, as a consequence, their 1S states are constructed from just a single pair of conduction band valleys[14]. Hence, the six-fold conduction band symmetry associated with T_d sites which gave rise to the higher lying 1S states has vanished. The phosphorus 1S(E) is well identified at 32.5 meV[7]. An apparently trivial, but also important argument, is that in sample 2 there is evidence of six STD and there are only four deeper lying donors: the P and TD 1, 2 and 3.

A possibility for the nature of these centres is that there might be different stages of aggregation of oxygen atoms around a residual impurity such as lithium. Li forms a series of six Li-oxygen complexes[15,16]. However, none of the observed transitions corresponds exactly to the known 1S→2P± transitions[15,16] of the different Li-O complexes. Only the donors a,b and G of the STD come within 0.3 meV of any of the Li-O series, as can be seen in table III, where the ionization energies of both the STD and of the Li-O of ref.[15] are summarized.

To summarize, our PTI spectroscopic data clearly show the existence of a series of new shallower thermally formed, oxygen related donors in Cz-grown silicon. These donors have EMT-like 1S ground states, comparable in energy to those of the Li-O centres of Stavola et al[14] and Aggarwal et al[16]. The STD ionization energies lie between 34.7 and 37.4 meV. The total concentration of STD seems to increase with annealing time for the two samples observed.The STD might correspond to higher aggregation stages of the same oxygen-related well-known

Table III

Ionization energies of the Shallow Thermal Donors in Cz Silicon. For comparison the ionization energies of the reported Li-O Complexes of ref. 15 are also included. The E_i was calculated by adding the binding energy of the 2P± level to the observed 1S→2P± transitions.

STD	Observed in Sample	Ionization Energy E_i(meV)
a	1	34.7 ±0.1
b	1 & 2	35.2
c	2	35.4
d	2	36.1
E	1 & 2	36.3
F	1 & 2	37.0
G	1 & 2	37.4
Li-O Complexes		
A		39.2
B		38.8
C		38.2
D		37.7
E		35.1
F		34.9

TD[8]. However, to establish this it will be necessary to find out if they also show the same C_{2v} site symmetry, for instance. The photoionization continuum starting around 26 meV observed in these samples remains as an unexplained feature, because the FIRT and the PTIS spectra failed to show any additional related features.

Acknowledgments- We thank P. Wagner, Wacker Heliotronic, Burghausen, FRG, for supplying us with the samples and some discussions. We particularly want to acknowledge H.J. Queisser for very enlightening discussions and his interest on this subject. We thank W. König for his assistence with the initial use of the FTS-113 Bruker Spectrometer. We also thank E. Kisela for the surface polishing of the samples and H. U. Habermeier for the evaporation of the contacts.

REFERENCES

1. Sh.M. Kogan and T.M. Lifshits, Phys. Stat. Sol. a 39, 11 (1977)
2. J.R. Patel in "Semiconductor Silicon 1977". Eds. H.R. Haff and E. Sirtl, pg. 521, Electrochem. Soc., Princeton (1977)
3. H. Herrmann, H. Herzer and E. Sirtl, in Festkörperprobleme (Advances in Solid State Phys.) XXV, p. 279, Vieweg, Braunschweig 1975. Ed. H.J. Queisser.
4. B. Pajot, H. Compain, J. Lerouille and B. Clerjaud, Proc. of the "16th Int. Conf. on the Physics of Semiconductors", Montpellier France, Ed. M. Averous, North Holland, Amsterdam (1982).
5. R. Oeder and P. Wagner, in "Defect in Semiconductors II, MRS Symposia Proceedings". Vol.14, Eds. S. Mahajan and J.W. Corbett., North Holland, New York 1982.
6. P. Claws, J. Broeckx, E. Simoen and J. Vennik, Solid State Commun., 44, 1011 (1982).
7. L.S. Darken and S.A. Hyder, Appl. Phys. Letters 42, 731 (1983). Also M. Skolnick, L. Eaves, R.A. Straddling, J.C. Portal and S. Askenazy, Solid State Commun.,15, 1403 (1974).
8. For Sulphur: C.T. Sah, T.H. Ning, L.L. Rosier and L. Forbes. Solid State Commun.,9, 917, (1971). For indium: T.C. Chandler, R.J. Harris, R.J.Spry, G.J.Brown and J.J. Rome, Phys. Rev. 26,6588,(1982).
9. R.A. Faulkner, Phys. Rev.,184,713 (1969). Also: E. Janzen, R. Stedman, G. Grossmann, and H.G. Grimmeiss, Phys. Rev. 29, 1907 (1984).
10. L. Genzel, H.R. Chandrasekhar and J. Kuhl, Optics. Commun.,18, 381 (1976).
11. A.K. Ramdas and S. Rodriguez, Rep. Prog. Phys., 44, 1297 (1981).
12. P. Wagner, C. Holm, E. Sirtl, R. Oeder and W. Zulehner, "Chalcogens as Point Defects in Silicon", Festkörperprobleme (Advances in Solid State Physics) XXIV, pg.191, Vieweg 1984. Ed. P. Grosse.
13. E.E. Haller, R.E. McMurray, N.M. Haegel and L.M. Falicov. Proceedings of the XVII Int. Conf. on the Physics of Semiconductors, San Francisco, Calif. USA (1984). Eds. J.D. Chadi and W.A. Harrison, Springer New York (1985), p. 679.
14. M. Stavola, K.M. Lee, J.C. Nabity, P. Freland and L.C. Kimerling, Phys. Rev. Lett. 54, 2639 (1985).
15. T.E. Gilmer, R.K. Franks and R.J. Bell, J. Phys. Chem. Solids 26, 1195 (1965).
16. R.L. Aggarwal, P. Fisher, V. Mourzine and A.K. Ramdas, Phys. Rev. 138, A882 (1965).

J. Phys. C: Solid State Phys. 19 (1986) L579–L584. Printed in Great Britain

LETTER TO THE EDITOR

The new shallow thermal donor series in silicon

J A Griffin†‡, H Navarro†§, J Weber†, L Genzel†, J T Borenstein‖, J W Corbett‖ and L C Snyder††

† Max Planck Institut für Festkörperforschung, Heisenbergstrasse 1, 7000 Stuttgart 80, Federal Republic of Germany

‖ Physics Department, SUNY/Albany, Albany, NY 12222, USA

†† Chemistry Department, SUNY/Albany, Albany, NY 12222, USA

Received 18 July 1986

Abstract. The electronic structure of a new series of shallow thermal donors (STD) recently observed by photo-thermal ionisation spectroscopy, as well as its relationship to the standard hierarchy of oxygen-related thermal donors, are discussed. It is concluded that the STD series are single donors.

In the thirty years since the discovery of oxygen-related thermal donors produced by annealing Czochralski silicon at 450 °C, a detailed picture of the electronic structure of these defects has emerged. Recent infrared electronic absorption spectroscopic studies (Graff *et al* 1973, Gaworzewski and Schmalz 1979, Pajot *et al* 1983, Oeder and Wagner 1983, Suezawa and Sumino 1983) have revealed that the thermal donors comprise a hierarchy of double donor defects with successively shallower energy levels. Kinetic models have ascribed this series of defects to a set of oxygen aggregates (Kaiser *et al* 1958, Oehrlein 1983, Suezawa and Sumino 1984, Ourmazd *et al* 1984 and Borenstein *et al* 1986b), each containing a thermal donor core (of unknown structure) which gives rise to electrical activity (Lindström *et al* 1985). The ladders of ground states for the neutral (TD^0) and singly ionised (TD^+) donors have been explained by a perturbation model (Corbett *et al* 1984 and Borenstein *et al* 1986a) which assumes that oxygen atoms successively agglomerating about the donor core introduce a repulsion with the shallow electrons.

Recent photo-thermal ionisation spectroscopy (PTIS) studies (Griffin *et al* 1986 and Navarro *et al* 1986) of Cz–Si heat-treated at 450 °C for 4.5 h have observed the hierarchy of thermal donors originally seen in the IR measurements. In addition, seven other donor states were observed, with effective-mass-like (EMT) excited state spectra and binding energies near 37 meV. This has been labelled the shallow thermal donor (STD) series (Griffin *et al* 1986), in the light of its shallow position in the band gap relative to the TD^0 series (53–69 meV) and the TD^+ series (119–155 meV). It is the purpose of this Letter to investigate the electronic structure of the STD relative to that of the thermal donor series, and to discuss the possible chemical structure of the STD centres.

‡ Jointly at University of Bath, Bath, Avon, UK.

§ On leave from Universidad Autonoma de Puebla, Puebla, Mexico.

0022-3719/86/260579 + 06 $02.50

The thermal donor series exhibits a hierarchy of ground states for both TD^0 and TD^+, with the defects associated with the shallower levels becoming more dominant as the annealing time is increased. The previously mentioned perturbation model explains the shift in ground-state energy (with reference to the deepest, or core, level) by assuming that the successive aggregation of oxygen atoms about the donor core introduces a repulsion with the shallow electrons. The repulsive interaction, which can be treated as a small perturbation to the attractive Coulombic well of the core, will increase the electron orbit sizes and thus reduce their binding energies. The simplest approximation is to assume that the repulsive interaction V_p between the agglomerating oxygen atoms and the shallow electrons is a constant over the (spherical) volume of the aggregate:

$$V_p = \begin{cases} V_0 & r < Rn^{1/3} \\ 0 & r > Rn^{1/3} \end{cases} \tag{1}$$

where R is the radius of an oxygen atom in silicon and n represents the number of oxygen atoms in the aggregate surrounding the core. The impact of assuming a spherical cluster is discussed extensively by Borenstein *et al* (1986a) and does not change the qualitative success of the model.

Matrix elements for the ground-state energy shifts can be found by first-order perturbation theory using the appropriate hydrogen-like (TD^+) and helium-like (TD^0) EMT wavefunctions. Comparison between the experimental binding energies (Pajot *et al* 1983, Oeder and Wagner 1983) and the predictions of the model (Borenstein *et al* 1986a) reveals that the ladder of donor states proceeds by the addition of single oxygen atoms into a thermal donor core. The results of this model are in excellent agreement with the experimental data.

The perturbation model argues that the thermal donor ground-state level is controlled by two opposing mechanisms: an attractive central cell correction originating from the core and a repulsive perturbing potential arising from a growing oxygen aggregate. The attractive correction causes the ground state of the first defect in the hierarchy to have a level deeper than that predicted by EMT (Kohn and Luttinger 1955). The repulsive perturbation gives rise to the ladder of ground states, and causes these levels to move toward the predicted EMT value. Insight into the nature of the STD may be gained by comparing the relative magnitudes of these two mechanisms in the thermal donor series.

The magnitude of the central cell correction for the deepest donor in the hierarchy is easily found for the singly ionised charge state; since the centre is doubly charged the attractive force is enhanced by a factor of four and thus the resulting EMT-predicted ground state is at $E_c - 125$ meV, four times deeper than for a single donor (Kohn and Luttinger 1955). For the neutral donor, the ground state cannot be directly compared to the EMT value for single donors because of the phenomenon known as incomplete nuclear screening. This behaviour is observed in the helium atom ground state (Bethe and Salpeter 1957) and in chalcogen defect levels in silicon (Lee *et al* 1975, Grimmeiss *et al* 1981, Kozlov 1982 and Singh *et al* 1983). Incomplete nuclear screening arises because two electrons in the same ground-state orbital do not completely screen one nuclear charge from another. The effective nuclear charge Z^* is constrained by $1 < Z^* < 2$, and can be calculated for a helium atom (Bethe and Salpeter 1957) or a double donor in a semiconductor (Borenstein *et al* (1986a) and Glodeanu (1967)). The EMT prediction for the ground state of a neutral double donor (E_B^*) can be estimated by analogy to incomplete screening in the helium atom (Ho and Ramdas 1972):

$$E_B^* = E_B[E_B(He^0)]/[E_B(H^0)] = 56\,meV \quad (2)$$

where E_B represents the EMT value for the single donor (31.3 meV) (Faulkner 1969) and $E_B(He^0)$ and $E_B(H^0)$ are the binding energies of a neutral helium and hydrogen atom, respectively. Since the deepest donors in the TD^0 series and the TD^+ series have binding energies of 69 meV and 156 meV, respectively, the central cell corrections are found to be 13 meV in the neutral donor case and 31 meV for the ionised defect.

The PTIS measurements find the STD to have ground states approximately 37 meV below the conduction band. If these states are part of the thermal donor series (TD^0) then comparison with (2) shows that the repulsive perturbing correction must far outweigh the central cell correction for these states. The predictions of the perturbation model demand that the number of oxygen atoms necessarily associated with the STD must be of the order of 18 in order to yield the necessary repulsive correction. The perturbation model calculates the binding energies for the TD^0 containing 16, 17 and 18 added oxygen atoms to be 38.3, 36.6 and 34.9 meV, respectively. The predicted spacings for these levels are much larger than those observed by Griffin *et al* (1986). In addition, if the STD are neutral double donors, then a set of corresponding singly ionised STD must exist. These are not observed as the PTIS or IR measurements of Griffin *et al* (1986) and Navarro *et al* (1986), and a recent systematic search of the PTIS spectra at temperatures between 10 and 30 K and in the spectra region up to 120 meV has failed to reveal any feature related to the STD. The singly ionised STD, if existing, should present observable transitions under such conditions.

In the light of these considerations, a more likely assumption is that the STD are *single* donors, with binding energies near the EMT value of 31.3 meV (Kohn and Luttinger 1955, Faulkner 1969). The large gap between the shallowest ground state in the old donor series and the STD levels is not due to a large difference in the central cell correction or the repulsive perturbation affecting these states, but rather to the difference in effective nuclear charge between a single donor and a neutral double donor. The deepest STD, with a binding energy of 37.4 meV, is thus seen to have a central cell correction of about 6 meV. The central cell corrections for the deepest levels in the TD^0, TD^+ and STD series are shown in figure 1.

The perturbation model predicts the spacing between single donors in a ladder similar to that observed for the thermal donor series to be of the order of 0.8 meV. Analysis of the ladder observed in (Navarro *et al* (1986)) indicates that it does not represent one evenly spaced series of donors. The spacing between the STD ranges from 0.2–0.7 meV. It is possible that the STD comprise more than one series of donors, each series having a different donor core. If two series are assumed to exist, each with a different donor core, one finds that each comprises an approximate ladder with an energy spacing of 0.9 meV, as shown in table 1. The results of the perturbation model for singly ionised double donors, neutral double donors and single donors (assuming that two STD series exist) are plotted versus the experimental data in figure 2. Further experiments will be required in order to determine both the number of series present in the STD, and the energy spacing of the ground-state ladder of each series.

The assignment of single donor status to the STD indicates that the core of these defects differs significantly from the core structure of the thermal donor series. The fact that the STD are produced by 450 °C annealing indicates that they are related to the thermal donor series, but Griffin *et al* (1986) find that the thermal donor formation kinetics are different from the growth behaviour of the STD. The low concentration of STD relative to the levels of the thermal donors found in the Griffin samples suggest that

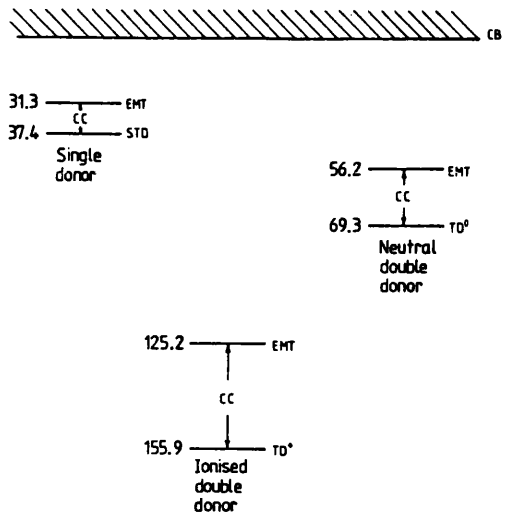

Figure 1. Experimental values for the ground-state energies of the deepest donors in the STD, TD^+ and TD^0 series referenced to the conduction band (CB), as compared with the effective mass theory (EMT), predictions for these states. Numbers adjacent to the levels are the binding energies in meV; the central cell correction (CC) equals the difference between the measured value and the prediction of EMT.

the STD are coupled to impurities in the host. One possibility is that the STD are coupled to a background concentration of boron in the material; the concentration of boron may be close to that of the phosphorus in the high-resistivity material used: ($N_D - N_A = 4 \times 10^{12}\,cm^{-3}$). The incorporation of the boron in a boron–oxygen ylid as the core of the STD series might result in the single donor behaviour of the STD. Early results, however, do not strongly support boron as a candidate for involvement in the STD core. Another possible explanation for the STD series is that there are multiple kinetic pathways for donor formation, and that the STD, by virtue of a reaction-limiting barrier, saturate at concentrations far below the levels typically reached by thermal donors.

Table 1. Experimental values for the ground-state energies (εi) of the STD referenced to the conduction band (CB) and the increase in ground-state energy ($\Delta\varepsilon i$) from the nth to the $(n + 1)$th donor assuming two overlapping donor series.

STD	εi (meV)	Interval	$\Delta\varepsilon i$ (meV)
Series 1			
G	37.4 ± 0.1	G–E	1.1 ± 0.2
E	36.3	E–c	0.9
c	35.4	c–a	0.7
a	34.7		
Series 2			
F	37.0 ± 0.1	F–d	0.9 ± 0.2
d	36.1	d–b	0.9
b	35.2		

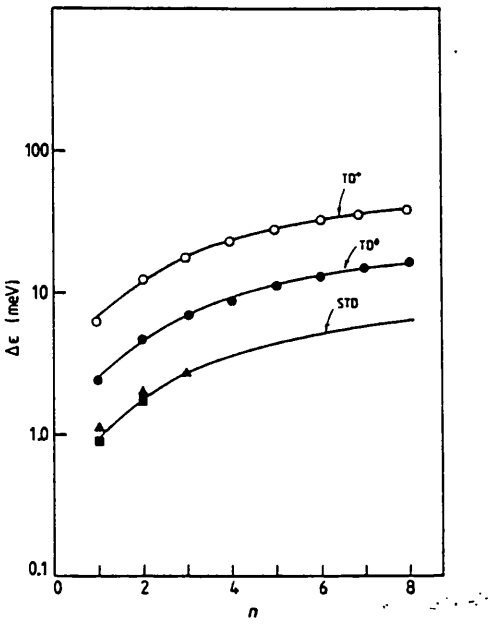

Figure 2. Shift ($\Delta\varepsilon$) in ground-state energy for the nth thermal donor referenced to the deepest thermal donor (TD-1) ground state, versus the number of oxygen atoms added to TD-1 (n), for both thermal donor charge states in silicon and for the STD. The full circles, open circles, triangles and squares represent the experimental values [3, 4, 15] for the TD^0, TD^+ and the two STD series, respectively and the full curves indicate the predictions of the perturbation model.

In summary, we may conclude that the STD are single donors which likely arise from an aggregation process similar to that for thermal donor formation. More experiments will be needed to further clarify the nature of the STD, as well as their relationship to the well known double donor series.

This work was supported in part by the Department of Energy–Jet Propulsion Laboratory Flat-Plate Solar Array Project, the United States Army Research Office and the Mobil Foundation.

References

Bethe H A and Salpeter E E 1957 *Quantum Mechanics of One- and Two-Electron Atoms* (Berlin: Springer)
Borenstein J T, Corbett J W, Herder M, Sahu S N and Snyder L C 1986a *J. Phys. C: Solid State Phys.* **19** 2893
Borenstein J T, Peak D and Corbett J W 1986b *Oxygen, Carbon, Hydrogen and Nitrogen in Silicon* ed. S J Pearton, J W Corbett, J C Mikkelsen Jr and S J Pennycook (Pittsburgh: Materials Research Society)
Corbett J W, Frisch H L and Snyder L C 1984 *Mater. Lett.* **2** 209
Faulkner R A 1969 *Phys. Rev.* **184** 713
Gaworzewski P and Schmalz K 1979 *Phys. Status Solidi* a **55** 699
Glodeanu A 1967 *Phys. Status Solidi* **19** K43
Graff K, Gallrath E, Ades S, Goldbach G and Tolg G 1973 *Solid State Electronics* **16** 887

THE STUDY OF OXYGEN THERMAL DONORS IN SILICON BY PHOTOTHERMAL IONISATION SPECTROSCOPY

JENNIFER A. GRIFFIN*, H NAVARRO**, L GENZEL
Max Planck Institut für Festkörperforschung, Heisenbergstrasse 1, 7000 Stuttgart 80, Federal Republic of Germany.
*jointly at University of Bath, Bath, Avon, Great Britain.
**Alexander Von Humboldt Stipendiat, on leave from Universidad Autonoma de Puebla, Puebla, Mexico.

ABSTRACT

It is well known that Czochralski-grown silicon contains up to $2x10^{18}cm^{-3}$ oxygen atoms. When this silicon is annealed at 450°C a series of "thermal" donors are formed. In this work we present the results of a study of annealed Czcochralski-silicon samples by Photothermal Ionisation Spectroscopy and IR transmission measurements. All previously reported thermal donors, which occur in the spectral region above $330cm^{-1}$, and have ionisation energies 53-69.3 meV, are observed by us. Also, our experimental results show the presence of at least three previously unreported thermally formed donor transition series below $330cm^{-1}$. Our results indicate that the ionisation energies of these new shallow thermal donors would be 36.3, 37.0 and 37.4 meV. Assignments are made by comparison of the energy differences between excited states to those predicted by the Effective Mass Theory.

INTRODUCTION

This paper reports on the observation of three new shallow donor centers in annealed Czochralski (Cz) silicon. These donor centers are observed by Photothermal Ionisation Spectroscopy (PTIS) [1] which has a very high sensitivity to low concentrations of impurity centers in semiconductors. PTIS involves the two stage ionisation of an impurity. Firstly, a photon is absorbed exciting the bound carrier into an excited state. Secondly, a phonon is absorbed thus ionising the impurity. The change in photocurrent due to the ionisation of the impurities is monitored. Impurity concentrations of the order of 10^7 atoms/cm^3 have been observed and identified in ultra-pure Ge [2,3] by this method. PTIS has previously been applied to the study of some elemental impurities in silicon such as phosphorus [4], indium [5], selenium and sulphur [6] but this is the first study of oxygen-rich silicon by this technique.

EXPERIMENTAL PROCEDURE

High-ohmic n-type Cz-silicon samples were studied. The free carrier concentration was known to be $|N_d-N_a| \sim 4x10^{12}$ cm^{-3} before heat treatment. Two samples, 1 and 2, were first subjected to 10 minutes of annealing at

Mat. Res. Soc. Symp. Proc. Vol. 59. ©1986 Materials Research Society

770°C. Secondly, sample 2 was annealed for 15 minutes and sample 1 for 4.5 hours at 450°C. This resulted in a donor concentration of ~$5x10^{13}$ cm^{-3} for sample 2 and ~$8x10^{14}cm^{-3}$ for sample 1 as determined from resistivity measurements.

Each sample, a disc 12mm in diameter and 2mm thick, was prepared for contacting by chemically polishing the circular faces. Then two strips of gold-antimony were evaporated onto the surface, 6mm apart. For PTIS it is important that ohmic contacts are achieved. It was found that laser annealing of the evaporated contacts using a pulsed Neodymium-YAG laser to create a local highly-conductive layer of alloyed Si produced good results.

The PTIS system consisted of a rapid scan Fourier Transform Spectrometer (FTS), the Bruker FTS 113, operating in the spectral region 100-900cm^{-1}. A voltage was applied across the sample using a constant current source and the photoconductive response of the sample was amplified using a PAR 124A ac-coupled band-pass amplifier before being applied to the Bruker signal input channel.

The sample was mounted in a continuous-flow He cryostat with a He contact gas sample chamber. The temperature was monitored by a calibrated Allen-Bradley resistor placed close to the sample. The temperature could be controlled within ±0.1K in the range 6K-30K.

The PTIS system was calibrated in photon energy by comparing the phosphorus series observed by PTIS to that of the same PTIS spectrum recorded on the Double Beam FTS described by Genzel et al [9]. This intrument had in turn been calibrated against the absorption lines of water. The energy positions of the phosphorus series were in good agreement with those reported by Ramdas and Rodriguez [10].

RESULTS

The IR transmission spectrum for Si 1 is shown in Fig. 1 at a resolution of 0.25cm^{-1}. Nine thermal donors have been reported from IR transmission measurements [7,8] with binding energies 53-69.3 meV. Lines arising from all nine known thermal donors [7] are observed. In addition the presence of phosphorus as a residual donor is identified. Most importantly there is an indication of several unidentified lines at lower energies labelled E, F and G. Indications of further lines a, b, c and d at much weaker intenstities have been seen in PTIS only and

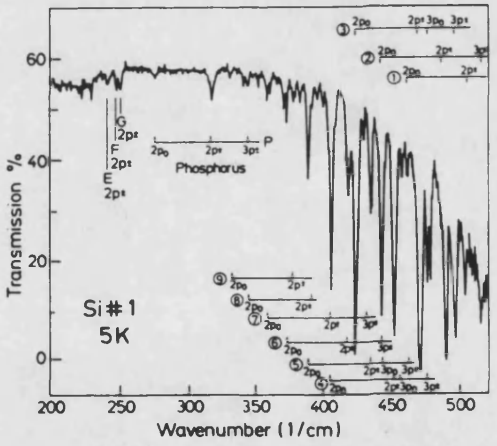

Fig. 1: IR transmission spectrum of Si 1 after annealing at 450°C for 4.5 hours. Thermal donors 1 to 9, phosphorus and the three new shallow thermal donors, labelled E, F and G, are observed.

are discussed elsewhere [11].

The PTIS spectrum of Si 1 in the spectral region 360-560cm^{-1}, where the majority of the TD transitions appear, is shown in Fig.2. The absorption of the plastic foil window of the cryostat disturbed the true form of the spectrum in this region. Therefore, this spectrum has been corrected for the instrumental background, excepting beamsplitter absorption at 540cm^{-1}, as measured with a commercial Ge bolometer (Infrared Lab. Inc. HD2). The donor transitions observed in transmission are also very clear in the PTIS spectrum even at a lower resolution of 1cm^{-1}. They appear as negative peaks in a continuum although PTIS lines are usually positive-going. This striking effect may only be explained when the presence of other lower energy donors is considered. Then, it can be shown that the peaks appear negative as a result of the competing ionisation processes of the photothermal ionisation of the thermal donors, and the direct ionisation of the lower energy donors. This effect is later discussed in more detail.

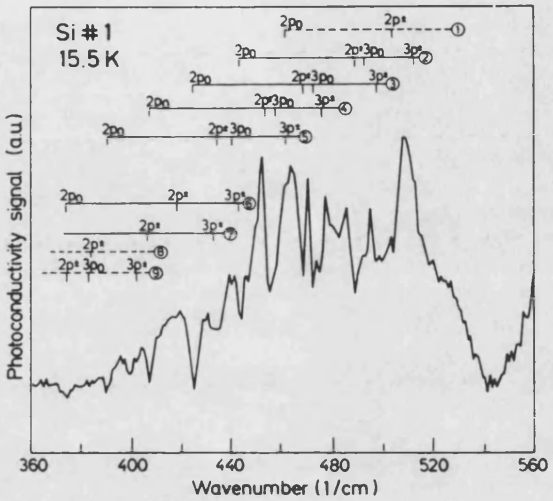

Fig. 2: The Photothermal Ionisation spectrum of Si 1 after annealing at 450°C for 4.5 hours. The transitions arising from the thermal donors 1 to 9 appear as absorptions in the photoionisation continuum.

In sample 2 only TD numbers 1, 2 and 3 were observed. This is consistent with the known formation rates of the TD [7]. In the PTIS spectrum of Si 2 the TD transitions are seen as positive peaks on the continuum. This can be explained from the fact that the concentrations of the different donors are at least one order of magnitude less in Si 2 than in Si 1, but the thermal donors are present in a much higher relative concentration in Si 2 compared to the concentration of lower energy donors.

In addition to the known thermal donors a series of peaks were, for the first time, observed at lower energies in both samples. The PTIS spectrum of Si 1 showing these positive-going lines is shown in Fig 3 with a resolution of 1cm^{-1}. It was not necessary to correct the spectrum for the instrumental background. The lines observed can be divided into two groups, those lying on the lower energy side of the maximum in the continuum at 295 cm^{-1} (36.6 meV) and those lying on the higher energy side. The group of higher energy transitions were identified as due to residual phosphorus from comparison to the values of Ramdas and Rodriguez [10] with an ionisation energy of 45.31 meV [1].

The lines newly observed at lower energies have not yet been identified. Three transitions take place at 241.4, 247.2 and 250.1 cm^{-1} and a second group of three at 267.4, 273.2 and 276.1 cm^{-1}. Comparing to the Effective Mass Theory (EMT) [6,12] the first set of three lines are identified as transitions between the EMT donor levels 1s→2p± and the second set of three lines as the transitions between the 1s→3p± EMT donor levels. Hence three different EMT-like new shallow thermal donors (STD)

are being observed, labelled E, F and G in Fig. 3. The 1s→4p± transitions of F and G are also observed, that for E lying under the 1s→3p± of donor G. The ionisation energies of the new STD, calculated by adding the 2p± level binding energy to the energies of the 1s→2p± transitions, are 36.3, 37.0 and 37.4 meV. The relative intensities of the 1s→2p±, 1s→3p± and 1s→4p± lines are consistent with these assignments. The 1s→$2p_0$ transitions are not observed. In Table I the observed transitions for the new STD are summarized.

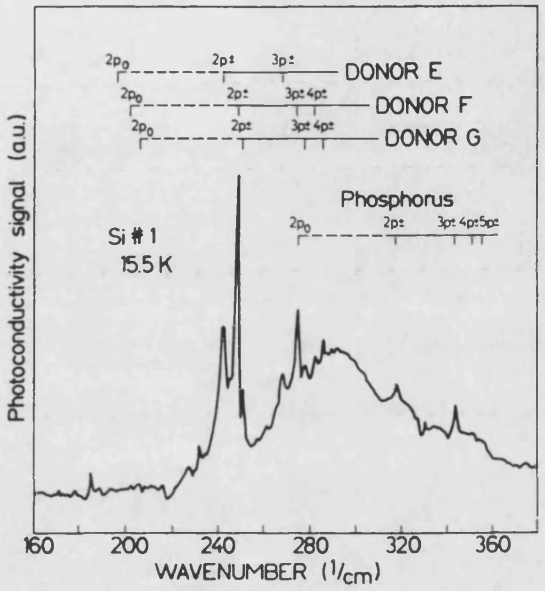

Fig. 3: The Photothermal Ionisation spectrum of Si 1 showing the transitions arising from the new shallow thermal donors, labelled E, F and G, as positive peaks on a continuum.

The 1s→$2p_0$ EMT donor level transition appears very strongly in transmission but always appears only weakly in PTIS spectra [4,6]. This transition for phosphorus was observed in our samples at 22K with 4% of the intensity of the 1s→2p± transition. This is the temperature which is optimum for the PTIS of phosphorus. No 1s→$2p_0$ transition was observed for either donor E, F or G in the temperature range 6K-22K studied. The expected intensity of these transitions is such that they would barely be distinguishable in the noise level of the measurements.

Another interesting spectral feature is the broad continuum on which the lines lie. This continuum begins at approximately 220 cm^{-1} and increases exponentially with increasing photon energy to a well defined maximum at 295 cm-1 (36.6 meV) which is identical in both samples and is independent of temperature. The origin of this continuum is as yet

Transitions (cm^{-1})	EMT donor[6]	Donor E	Donor F	Donor G
1s→2p±	200.51	241.37±0.5	247.16±0.5	250.06±0.5
1s→3p±	226.98	267.43	273.23	276.12
1s→4p±	234.51	-	280.95	284.81
Intervals(cm^{-1})				
1s→3p± - 1s→2p±	26.47	26.06	26.07	26.06
1s→4p± - 1s→3p±	7.52	-	7.72	8.69
Ionisation(cm^{-1}) energy,	252.13	292.78	298.42	301.65
ϵ_i (meV)	31.26	36.3±0.1	37.0±0.1	37.4±0.1
Central Cell Correction, $\Delta\epsilon_i$ (meV)	-	5.0±0.1	5.7±0.1	6.1±0.1

Table I: Energy positions of transitions from the 1s ground state to excited levels for the new STD E, F and G compared to those calculated for the EMT donor in silicon.

unknown. The ionisation energies of the new STD are 36.3 to 37.4 meV which suggests the maximum may be due to direct ionisation of these centers. However, this alone can not explain all the observed phenomenology of the photoionisation continuum.

The intensity of lines observed by PTIS is highly temperature dependent. When considering the temperature dependence it must be remembered that if the sample temperature is too low then no phonons are available for the photo-thermal ionisation process and only a continuum, arising from the direct ionisation of donor centers, will be observed. Similarly, if the sample temperature is too high, all the donors will be thermally ionised and no PTIS signal will be generated. Within the temperature window, where photo-thermal ionisation is possible, this process and direct ionisation compete.

The temperature dependence of the new STD and phosphorus donor centers is shown in Fig. 4. The intenstiy of the new STD lines increases with temperature to a maximum and then decreases again. The increase in intensity is explained by the increase in the thermal ionisation probability, for an electron already in an excited state, with temperature. The following decrease in intensity is explained as a depopulation of the ground state of the donor centers due to the shifting of the Fermi level with temperature.

The phosphorus lines show a particularly complex temperature behavior. At 12K the $1s \rightarrow 2p^{\pm}$ transition appears as a negative-going line in the continuum, while at 17K it is emerging as a positive-going line and increases continuously in intensity in the temperature range studied.

A negative line can arise when there are lower energy donor centers present. A photon of energy greater than or equal to the ionisation energy of the shallower donor, but also corresponding in energy to a transition from the ground state to an excited state of the phosphorus may be used for either process. If the phosphorus was not present such photons would directly ionise the shallower centers to give a continuum intensity. However, the presence of the phosphorus means that some of these photons are absorbed by the phosphorus. If the thermal ionisation probability of the excited electron bound to the phosphorus is low, due to the low temperature of the sample, few of these photons will succeed in promoting a carrier to the conduction band. The net result is a decrease in the photoconductivity at this photon energy, i.e. a negative peak.

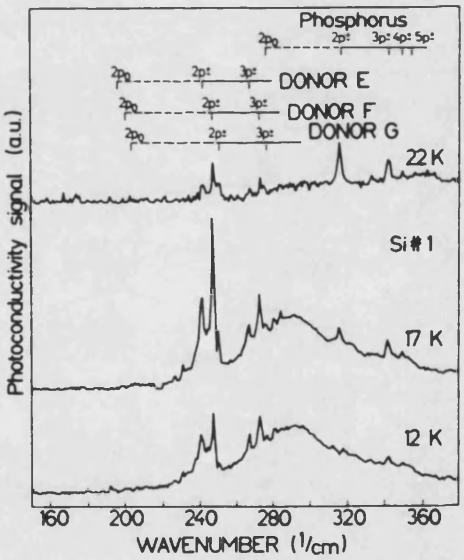

Fig. 4: The temperature dependence of line intensities in the Photothermal Ionisation spectra for Si 1 between 12K and 22K. The temperature behavior of the lines is related to the competition between different ionisation processes with different ionisation probabilities.

At higher temperatures the probability of two stage ionisation is much greater for both the shallow centers and the phosphorus and the resultant is a positive peak for the phosphorus transition. Finally, when the shallower donor levels begin to be depopulated the phosphorus is the major agent absorbing such photons, and the two stage ionisation probability is still increasing, and so the intensity of the positive peak will continue to increase. The phosphorus line intensities will only decrease once the ground state of the phosphorus itself begins to be depopulated. In the case of phosphorus it is known that there exist the new STD which are playing the role of the shallower donor centers described above.

This explanation may also be applied to explain the presence of the TD as positive or negative peaks if the concentration of the different donor centers are taken into account. In the case of the TD, both the new STD, phosphorus and shallower TD in the series may be considered as the shallower donor centers depending on which TD is being analysed. Similar absorption processes have been observed in PTIS in Germanium [13].

DISCUSSION

The presence of three new shallow thermal donors has been reported in this paper. The nature and origin of these donors is still under discussion. The three STD E, F and G are EMT-like and have very small central cell corrections 5.0, 5.7 and 6.1 meV respectively. These donor centers are thermally formed. Previous PTIS studies [4,5,6] of unannealed silicon, although having the sensitivity to detect these centers, did not detect them. Also, the new STD centers were not observed in the unannealed Cz-silicon used by us, only residual phosphorus was observed in PTIS.

A recently proposed model and experimental results for the TD indicate that the TD have C_{2v} symmetry [14], in which the ground state remains unsplit. Hence it is not expected that the E, F and G transitions arise from a 1s(E) or other 1s ground states of the TD. Phosporus has T_d symmetry and the 1s(E) state is well identified at 32.58 meV [10] ruling out the possibility that the observed new STD arise from transitions from this state. Also, the same three donors are identified in two samples in which the thermal donors present are very different. Although the TD and STD are both theramlly formed in Cz-silicon by annealing at 450°C there appears to be no direct correlation between the two groups of transitions.

The only type of donor centers which have been reported in Cz-silicon in the same spectral region as the new STD are the Li-O complexes [15,16]. However the STD transitions do not coincide with any of the six reported series of the Li-O complexes. The previous experiments which identified the Li-O complexes were carried out on samples where Li had been diffused into the Si by immersion in reactor grade Li [15] or being coated in Li [16] and being subjected to strenuous heat treatment, conditions which were in no way fulfilled for our samples.

CONCLUSIONS

The existence of three new shallow thermal donors is proposed from the results of PTIS measurements on Cz-silicon annealed at 450°C. The new STD are EMT-like thermally formed shallow donor centers with small central cell corrections comparable in order only to the Li-O complexes. However, it is not expected that the new STD are previously unobserved Li-O complexes. It is also ruled out that the new STD arise from a higher 1s state of any of

the observed TD or phosphorus. The fact that the relative concentrations of the new STD differ between the two samples annealed for different times suggests that these STD could be complexes which are formed at different rates during annealing.

The temperature dependence of the observed lines is explained in terms of competing ionisation processes with different ionisation probabilities and the combination of different concentrations of higher and lower energy donor centers.

The underlying photoionisation continuum beginning at 220 cm^{-1} with a local maximum at 295cm^{-1} is an interesting spectral feature which is expected to be associated with the onset of the ionisation continuum of the new STD at 292 cm^{-1}. However its exponential rise from at 220 cm^{-1} remains unexplained.

ACKNOWLEDGEMENTS

We thank Dr P Wagner for the Cz-silicn samples and useful discussions. We particularly want to thank Prof. H J Queisser for his continued interest and involvement in this work and for many useful and productive discussions. We also thank Dr J Weber for assistance with the sample preparation and very helpful discussions. We thank Mr W König for his guidance in the use of the Bruker FTS 113 Spectrometer. Thanks are also due to Mr E Kisela for sample polishing and the Technology Group for evaporation of the contacts onto the samples.

REFERENCES

1. Sh M Kogan and T M Lifshits, Phys Stat Sol a 39, 11 (1977)
2. E E Haller, W L Hansen, F S Goulding, IEEE Transactions on Nuclear Science NS-22, 127 (1975)
3. E E Haller, R E McMurray, Jr., Physica 116 B, 349 (1983)
4. M S Skolnick, L Eaves, R A Stradling, Solid State Communications 15, 1403 (1974)
5. T C Chandler, R J Spry, G J Brown, J J Rome, Phys Rev B 26 (12), 6588 (1982)
6. E Janzén, R Stedman, G Grossman, H G Grimmeiss, Phys Rev B 29 (4),1907 (1984)
7. P Wagner, C Holm, E Sirtl, R Oeder, W Zulehner, Festkörperprobleme XXIV Advances is Solid State Physics (Vieweg, Braunschweig, 1984) p191
8. R Oeder and P Wagner, in Defects in Semiconductors II, MRS Proceedings 14, edited by S Mahajan and J W Corbett (North Holland, 1982)
9. L Genzel, H R Chandrasekhar, J Kuhl, Optics Communications 18, 381 (1976)
10. A K Ramdas and S Rodriguez, Rep Prog Phys 44, 1297 (1981)
11. H Navarro, J Grffin, J Weber, L Genzel, to be published.
12. R A Faulkner, Phys Rev 184 713 (1969).
13. E E Haller, R E McMurray, Jr., N M Haegel, L M Falicov, Proceedings of the XVII International Conference of Semiconductors, edited by D J Chadi and W A Harrison (Springer, New York, 1985) p679
14. M Stavola, K M Lee, J C Nabity, P E Freeland, L C Kimerling, Phys Rev Lett 54, 2639 (1985)
15. T E Gilmer, R K Franks, R J Bell, J Phys Chem Solids 26, 1195 (1965)
16. R L Aggarwal, P Fisher, V Mourizine, A K Ramdas, Phys Rev 138, A 882 (1965)

Defects in Semiconductors - Edited by H. J. von Bardeleben.
Materials Science Forum Volumes 10-12 (1986), pp. 997-1002.

PROPERTIES OF THE SHALLOW THERMAL DONORS IN CZ-SILICON AS STUDIED BY PHOTOTHERMAL IONIZATION SPECTROSCOPY (PTIS)

J.A. Griffin[1], H. Navarro[2], J. Weber and L. Genzel
Max-Planck Institut für Festkörperforschung, Heisenbergstr. 1
7000 Stuttgart 80, Federal Republic of Germany

The development of the Shallow Thermal Donor series has been studied with respect to annealing time using the highly sensitive Photothermal Ionisation Spectroscopy technique. The seven reported Shallow Thermal Donors are formed by a 450C anneal in Czochralski-silicon together with the deeper Thermal Donor series. The formation of the Thermal Donors as recorded by PTIS and IR absorption spectroscopy is discussed in relationship to the Shallow Thermal Donors.

INTRODUCTION

The Shallow Thermal Donors (STD) are formed in Czochralski(Cz)-silicon in the same annealing process as the well-known Thermal Donors (TD). Seven STD (G→A) have recently been reported [1,2] with ionisation energies 34.7 - 37.4 meV. We have made a study of the formation of the STD at 450C as function of annealing time between 15 minutes and 15 hours. Also, samples with different thermal histories have been compared.

Photothermal Ionisation Spectroscopy (PTIS) has been used for this study for its high sensitivity (concentrations of impurities as low as $10^7 cm^{-3}$ can be detected)[3]. This technique involves a two stage ionisation process: firstly a photon is absorbed lifting the electron into an excited state, secondly, a phonon is absorbed lifting the electron into the conduction band. The appropriate far infrared photons are supplied using a Fourier Transform Spectrometer with the sample acting as the infrared(IR) detector [4].

The STD were investigated by PTIS and the TD by both PTIS and IR absorption spectroscopy in the spectral range 50 - $600 cm^{-1}$.

Infrared spectrascopic studies have shown the TD to be a hierarchy of nine interdependent double donor defects with ionisation energies 69.3 - 53.0 mev (TD1 → TD9) [5,6,7]. With increasing annealing time oxygen seems to agglomerates on an (as yet unknown) TD core to form successive donors in the series [8,9,10]. The donor ionisation energy decreases with increasing

defect size. This behaviour was described by the agglomerating oxygen introducing a repulsion to the potential seen by the shallow electrons [11,12]. The growth of the individual TD as a function of annealing time has been studied by Wagner et al [7]. They observed that the individual TD form at different rates and and after reaching a maximum start to decay.

EXPERIMENTAL PROCEDURE

For the investigation of the development of the STD with annealing time a series of identical samples was required. The TD growth is known to be dependent on the initial oxygen concentration [8,9]. Eight samples 8mmx8mmx2mm were cut from the same slice of undoped n-type Cz-silicon. All samples were preannealed at 700C for 20 minutes in an oxygen atmosphere. Individual samples were then annealed at 450C in an oxygen atmosphere for times between 15 minutes and 15 hours as shown in table 1.

	Sample 1	2	3	4	5	6	7	8
Preanneal	20 minutes at 700C							
First anneal at 450C in hours	0.25	0.5	1.0	1.5	2.0	2.5	3.0	14.3
Preaneal	30 minutes at 1000C							
Second anneal at 450C in hours	12.3	6.0	-	3.0	-	2.0	1.0	2.0

Table 1: Heat treatment of 8 samples cut from the same undoped n-type CZ-silicon slice.

The total number of TD created increases with annealing time and a corresponding decrease in the resistance of the samples was observed. The sample resistance as a function of annealing time is shown in figure 1 and linear dependence observed indicates that the initial oxygen concentrations in the samples were not significantly different.

We evaporated two stripe contacts (Au:Sb:Ni) on to each sample surface ~7mm apart and laser annealed them with a Nd-YAG laser to create good ohmic

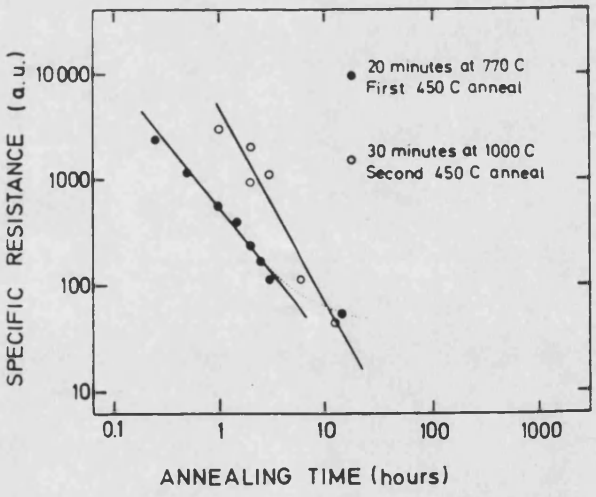

Fig. 1: Specific resistance as a function of annealing time at 450C.

contacts. A Bruker FTS 113 Fourier Transform Spectrometer was used to obtain the PTIS spectra. The samples were held in a stress free mount in a Leybold-Hereaus flow-through contact gas cryostat. The temperature was maintained at 15.5K±0.1K by the helium gas flow and a heater, as measured by a 100Ω Allen-Bradley resistor mounted close to the sample. A bias voltage of -6V was applied to the samples across a variable load resistor.

The Bruker FTS 113 was also used to record the IR transmission spectra taken at 5K using an Oxford Instruements cold finger cryostat and an Infrared Laboratories Germanium Bolometer.

In the second stage of the study several samples were reannealed at 1000C for 30 minutes to redisperse the oxygen and subsequently reannealed at 450C between 1 hour and 13 hours as shown in table 1. It is known that the oxygen available for donor formation is reduced after each anneal due to the formation of precipitates. The increased resistances of the samples after the second anneal therefore reflects the reduction in the available oxygen and hence the slower TD formation rate.

RESULTS AND DISCUSSION

In figure 2 the development of the STD and TD with annealing time is presented. Let us consider sample 1 annealed for 15 minutes as shown in figure 2 at a resolution of $1cm^{-1}$. The STD and TD may be described within the effective mass theory as a hydrogen-like and helium-like system respectively. In the PTIS spectra in figure 2 the Rydberg series of transitions from the groundstate to the excited states of each donor is observed and hence the ionisation energies may be calculated. This sample contains the STD D,E,F and G with ionisation energies 36.1, 36.3, 37.0 and 37.4meV and TD1, TD2 and TD3 with ionisation energies 69.3, 66.9 and 64.7 meV respectively.

The 1S→2P±, 3P± and 4P± transitions of Phosphorus (P) are observed at $316.8cm^{-1}$, $343.7cm^{-1}$ and $351.5cm^{-1}$ respectively and are in good agreement with the values given by Ramdas and Rodriquez[13].

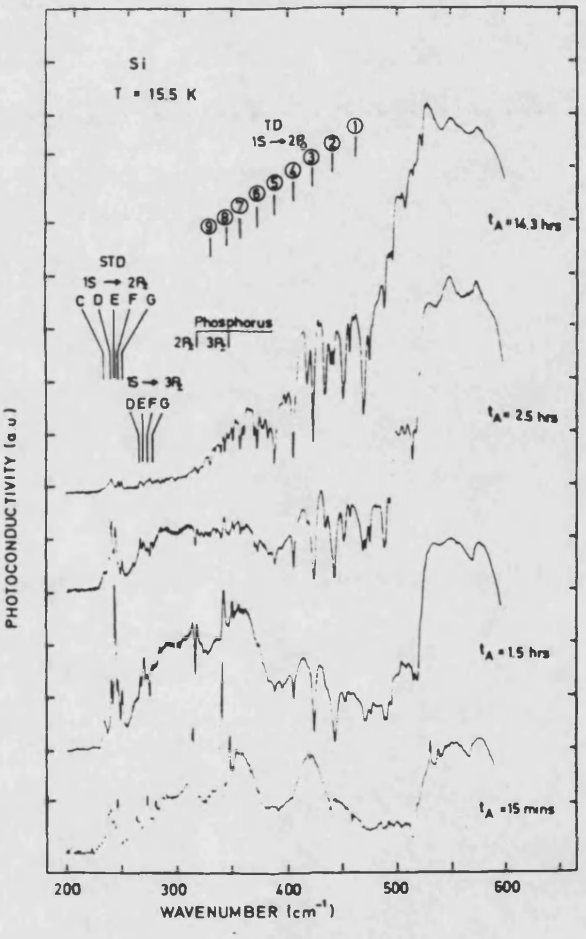

Fig. 2: A comparison of spectra obtained at increasing annealing times. The positions of the most important transitions are indicated.

The transition intensities observed are dependent on the concentration of the donors and the population of their groundstates. The population of the groundstates is determined by the position of the Fermi level which itself depends on the groundstate energies of the donors in the system and the donor concentrations. At the relative concentrations of low lying and deeper lying donor species present in sample 1 it seems the Fermi level lies above the groundstates of the STD. Thermal ionisation from the excited states at 15.5K is efficient for the STD and P donor but not for the TD. Hence the net photo-response from the TD is a reduction in the number of photons contributing to the ionisation continuum of the lower lying donors and so the TD transitions are seen as absorption lines in the continuum. The net photo-response from the STD and P donor is positive.

Next we consider the development of the TD as a function of annealing time. At shorter annealing times the transitions of the deeper donor complexes (e.g. TD1 and TD2) are predominant whereas after longer anneals transitions arising from the complete series of nine donors may be seen. This behaviour is observed very clearly in our PTIS spectra as shown in figure 2 (at $0.5cm^{-1}$ resolution except for the 15 minutes anneal at $1cm^{-1}$ resolution). The transitions lie between $330cm^{-1}$ ($1S \rightarrow 2P_0$ of TD9) and $533cm^{-1}$ ($1S \rightarrow 3P\pm$ of TD1) but only the positions of the $1S \rightarrow 2P_0$ transitions are indicated.

If we now trace the behaviour of the individual TD we observe, from the PTIS spectra and the IR transmission spectra, that the successive donors in the series are formed in increasing concentrations with increasing annealing time, and their development corresponds well with the description given by Wagner et al[7]. It should be noted that the background continuum of the TD increases correspondingly with annealing time.

The behaviour of the P transitions appears more complicated at first glance. The net photo-response at the $1S \rightarrow 2P\pm$ transition frequency is positive at short annealing times and negative at longer annealing times ≥ 1.5 hours. A similar effect is observed when the temperature of the sample is varied [14] and arises from the coexistance of differently populated donor species. In figure 2 the temperature and P concentration (from the IR transmission measurements) was found to be constant over the samples so we conclude that this indicates that at 1.5 hours annealing the concentration of the STD has increased relative to that of the P and the continuum due to the direct ionisation of the STD is reduced due to competition from the P donor. After 2.5 hours annealing the P $1S \rightarrow 2P\pm$ absorption line decreases in intensity and after 14 hours it is no longer observed.

THE DEVELOPMENT OF THE SHALLOW THERMAL DONORS WITH ANNEALING TIME

The STD occur in the samples in low concentrations and are only detectable by PTIS. A disadvantage of PTIS is that the spectra must be calibrated as the intensity scale is arbitrary in each case. The depths of the TD absorptions in IR transmission are proportional to the concentration of the centres. Therefore we applied the following calibration: from the IR transmission data the ratio of the depths of the TD3 $1S \rightarrow 2P\pm$ transitions were calculated relative to the TD3 $1S \rightarrow 2P\pm$ transition at 1.5 hours annealing time. The PTIS spectra were then adjusted to give the same ratios relative to the PTIS spectrum at 1.5 hours annealing time. (For sample 2 the TD2 $1S \rightarrow 2P_0$ transition was used and for sample 1 no suitable transition was found.) A $1S \rightarrow 2P\pm$ transition of the TD was used as the $1S \rightarrow 2P_0$ is known to be less strong in PTIS than in IR transmission.

After this calibration the intensities of the STD which are proportional to the concentrations can be calculated from the different spectra. In figure 3 the intensities of the $1S \rightarrow 2P\pm$ transitions for each individual STD and the total

intensity due to all the STD is plotted as a function of annealing time. This figure presents the trend seen qualitatively in figure 2 in a more exact fashion. The total STD concentration increases up to ~1.5 hours annealing time but then decreases. We believe this effect arises from a downward shift of the Fermi level which causes the STD and also the P groundstates to become less populated. The number of deeper-lying TD increases enormously with annealing time and therefore the relative concentrations of the different donor species which determine the position of the Fermi level are continuously changing [15]. This system is particularly complicated since it consists of many donor species. Qualitatively it is reasonable to assume that the Fermi Level is pulled down very close to the STD groundstates by the increasing concentration of the TD. In this way the decrease in the intensity of the P 1S→2P± and its higher transitions is also explained.

The development of the individual STD was more difficult to follow as the transitions overlap. The general trend seems similar to that of the total STD intensity. In these samples STD D, E, F and G were always most predominant. However, qualitatively one can see from figure 2 that there is a significant change in the relative intensities of the STD with annealing time.

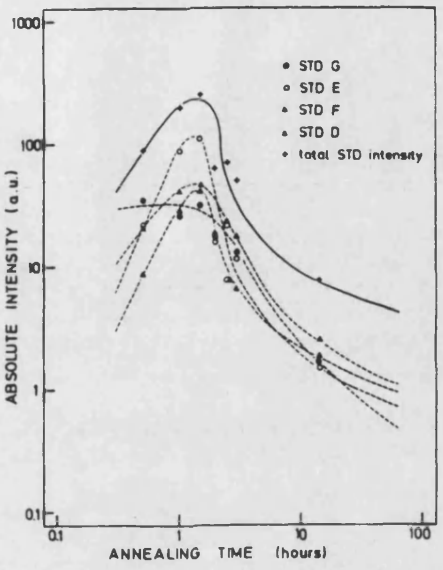

Fig. 3: The total intensity of the STD 1S→2P± transitions is shown in comparison to the individual 1S→2P± transition intensities. The error on the relative intensities is ~5% but the error in the absolute intensities is of the order of 30%.

THE RELEVANCE OF THE THERMAL HISTORY OF THE SAMPLES

The PTIS and IR transmission results for those samples reannealed at 1000C and then reannealed at 450C show qualtitatively similar results. However the thermal history of each sample is different and no quantative analysis could be made. Comparing the samples which were preannealed at 700C with those reannealed at 1000C reveals that fewer TD were created in the same time after the 1000C anneal as is to be expected. The slower TD formation rate is observed for all reannealed samples as shown by the resistances of the samples in figure 1. Our results show that the STD also form more slowly after the 1000C anneal. This suggests that the STD are also sensitive to initial oxygen concentration in the samples. Other samples measured by us [1,2] of different initial oxygen concentrations have also shown very different concentrations of the total STD concentration and different relative concentrations, supporting this view.

SUMMARY

We believe the STD are single donor complexes which are related to oxygen. The STD are always observed when the TD are observed but always in lower

concentrations (~10^{13} cm^{-3} at maximum concentrations) so that they are only occasionally detected in IR transmission measurements.

The concentration of STD increases with annealing time at 450C up to ~1.5 hours in the samples studied. At annealing times longer than ~1.5 hours the transition strengths decrease. This effect is most likely due to a downward shift of the Fermi level caused by the rapidly increasing concentration of the deeper-lying TD reducing the population of the shallower donors.

The Fermi level effect is dependent on the relative concentrations of the STD and TD and therefore the time after which the STD begin to be depopulated may vary between samples. It is not certain which parameters determine the observed concentration of STD although the initial oxygen concentration seems to play a vital role.

Further more detailed studies will be required if the growth of the individual STD is to be accurately traced.

ACKNOWLEDGEMENTS

We would like to thank H J Queisser for his continuing interest and support in this project. We thank P Wagner, Heliotronic, Burghausen, FRG for the Cz-silicon samples. We also thank W König for assistance with the IR transmission measurements, E Kisela and H U Habermeier for sample preparation and contacting respectively.

REFERENCES

1) Griffin,J.A., Navarro,H., Genzel,L.:in Oxygen, Carbon, Hydrogen and Nitrogen in Silicon,1986,139,edited by S.J. Pearton, J.W. Corbett, J.C. Mikkelsen Jr., and S.J. Pennycook (Materials Research Society, Pittsburgh).
2) Navarro,H., Griffin,J.A., Weber,J., Genzel,L.:Solid State Comm.,1986, 58, 151.
3) Haller,E.E., Hansen,W.L., Goulding,F.S.:IEEE Transactions on Nuclear Science,1975, NS-22, 127.
4) Kogan,Sh.M. and Lifshits,T.M.:Phys. Stat. Sol. a,1977, 39, 11.
5) Oeder,R. and Wagner,P.:in Defects in Semiconductors II,1982, Materials Research Society Proceedings 14 edited by S.J. Mahajan and J.W. Corbett (Elsevier, New York).
6) Pajot,B., Compain,H., Lerouille,J., Clerjaud,B.:Proc. of the "16th Int. Conf. on the Physics of Semiconductors", Montpellier, France,1982, edited by M. Averous (North Holland).
7) Wagner,P., Holm,C., Sirtl,E., Oeder,R., Zulehner,W.:Advances in Solid State Physics,1984, Festkörperprobleme XXIV, 191, (Vieweg, Braunschweig).
8) Kaiser,W., Frisch,H.L., Reiss,H.:Phys. Rev.,1958, 112, 1546.
9) Oehrlein,G., Corbett,J.W.:in Defects in Semiconductors II,1982, Materials Research Society Proceedings 14, 107, edited by S.J. Mahajan and J.W. Corbett (Elsevier, New York).
10) Ourmazd,A., Schröter,W., Bourret,A.:J. App. Phys.,1984, 56, 1670.
11) Corbett,J.W., Frisch,H.L., Snyder,L.C.:Materials Letters,1984, 2, 209.
12) Borenstein,J.T., Corbett,J.W., Herder,M., Sahu,S.N., Snyder,L.C.:J. Phys. C,1986, 19, 2893.
13) Ramdas,A.K. and Rodriquez,S.:Rep. Prog. Phys.,1981, 44, 1297.
14) Bambakidis,G. and Brown,G.J.:Phys. Rev. B,1986, B33, 8180.
15) Blakemore,J.S.:Semiconductor Statistics,1962 (Pergamon Press, Oxford).